Proceedings of I. Javakhishvili Tbilisi State University

ივ. ჯავახიშვილის სახელობის თბილისის
სახელმწიფო უნივერსიტეტის შრომები

357

ISSN 1512-1461

PHYSICS

ფიზიკა

39

Proceedings of I. Javakhishvili Tbilisi State University

ივ. ჯავახიშვილის სახელობის თბილისის
სახელმწიფო უნივერსიტეტის შრომები

357

ISSN 1512-1461
http://gesj.internet-academy.org.ge

PHYSICS

ფიზიკა

39

TBILISI UNIVERSITY PRESS

თბილისის უნივერსიტეტის გამომცემლობა

Tbilisi 2004 თბილისი

უაკ (UDC) 53(082)

ფ 505

MOUNTAIN-CANYON CIRCULATION AND THE LOCAL ATMOSPHERE PROCESSES

N. Ramishvili, Z. Khvedelidze, R. Aplakov, G. Erkomaishvili, T. Shalamberidze

Accepted for publication January, 2004

ABSTRACT. **Investigation of canyon winds, created by microcirculation processes, orographic and thermal factors have always been actual. In the known equations system of hydro-thermo dynamic a new parameter, which describes micro-regional peculiarity, has been brought. Corresponding solution has been obtained. The parameter has been specified, observed and the results have been calculated. Specification has been done in (30-40)% interval.**

In Georgia mountain-canyon type of winds is registered almost everywhere. This kind of wind is created with the help of the Sun radiation and local orographic, direction of which during the day is from foot to top along the mountain slope and at night it blows from top to the foot.

Local wind changes not only air streams field, it also changes regional temperature and dampness regime, weather and ecological conditions.

As local winds from the point of climate have not been studied completely, [1-5] their theoretical and experimental investigations are still actual.

Not equally warmed surface at a corner to horizon is considered. System of coordinates (x,y,z) on the foot of the slope is taken.

Axis ox is directed along the slope, oy – parallel to horizontal plane (all characteristics along oy are considered to the constant). Temperature of the air is changed only along the slope. Because of the small territory Coriolis forces could be ignored. We assume that the process time development is so small, that the process could be considered as a stationary. According to the above-said with the atmosphere balance continuity, motion and thermal-transport equations will be [1-3, 9]:

$$-\frac{1}{\rho}\frac{\partial P}{\partial x} - g\sin\alpha + \nu\frac{\partial^2 U}{\partial z^2} = 0, \quad (1)$$

$$-\frac{1}{\rho}\frac{\partial P}{\partial z} = g\cos\alpha, \quad (2)$$

$$\frac{\partial U}{\partial x} + \frac{\partial W}{\partial z} = 0, \quad (3)$$

$$\nu\frac{\partial^2 T}{\partial z^2} = U\frac{\partial \Theta}{\partial x} + W\frac{\partial \Theta}{\partial z}. \quad (4)$$

T is an air temperature; ρ - density; P - atmosphere pressure; g- acceleration of gravity; ν- coefficient of turbulent diffusion; t- time; U, V, W-components of velocity to the *x*, y, z axes accordingly. The problem is to find small declination of f (*x*, y, z) of meteorological components of phonic f (*x*) values.

After using above-mentioned coordinates (see Fig.1) we will have [4, 5]

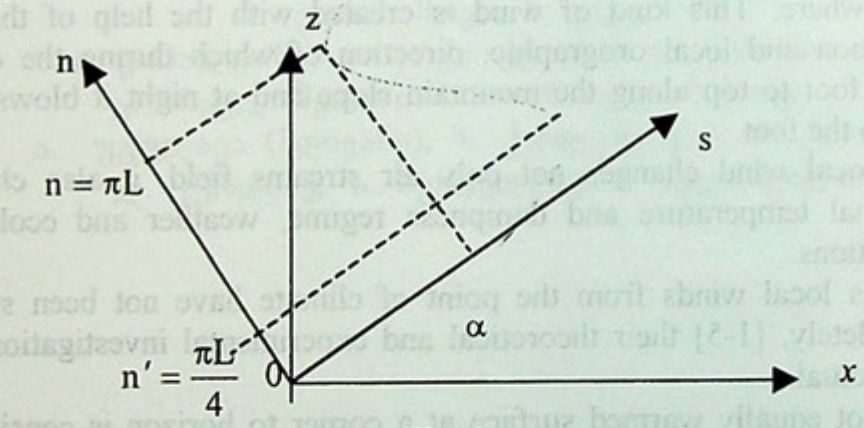

Fig. 1.

$$\left.\begin{aligned} s' &= x\cos\alpha + z\sin\alpha \\ n' &= z\cos\alpha - x\sin\alpha \end{aligned}\right\}. \quad (5)$$

In the new coordinates (1, 2, 3, 4) equation system will be [1, 2]

$$\nu \frac{\partial^2 U_1}{\partial n^2} + g \rho T_1 \sin \alpha - \frac{1}{\rho} \frac{\partial P_1}{\partial s} = 0, \quad (6)$$

$$\frac{1}{\rho} \frac{\partial P_1}{\partial n} + g \rho T_1 \cos \alpha = 0, \quad (7)$$

$$\frac{\partial U_1}{\partial \rho} + \frac{\partial W_1}{\partial n} = 0, \quad (8)$$

$$\nu \frac{\partial^2 T_1}{\partial n^2} + U_1 T_1 \sin \alpha - W_1 T_1 \cos \alpha = 0. \quad (9)$$

In equations (6) and (9) unknowns should satisfy boundary requirements. When $n_1=0$; $U_1=W_1=0$; $T_1=F_1(x)$; in these conditions after solution of equation system (6) and (9) we obtain equations:

$$U_1 = i\sqrt{\frac{2\beta}{\Theta_z}} F_1 e^{-\sigma z} \sin \sigma n, \quad (10)$$

$$T_1 = F_1 e^{-\sigma z} \cos \sigma n. \quad (11)$$

Here β is an air coefficient of thermal expansion. Θ_z - vertical gradient of potential temperature; and for vertical component air streams velocity we get equations:

$$W = \Theta'_0 \sqrt{\frac{g\beta a^2}{\nu\beta}} e^{-n/L} \sin \frac{n}{L}, \quad (12)$$

$$L = \sqrt[4]{\frac{4\nu a^2}{g\beta B \sin^2 \alpha}}, \quad (13)$$

where a is heat conduction coefficient, B is value of temperature gradient. From (12), (13) equations it is seen, that wind velocity is equal to 0 on the slopes surface (n = 0). It increases according to the altitude and gets maximum on $n = \frac{\pi L}{4}$ (Fig.1).

Basically maximal velocity depends on atmosphere stratification and on daily time. Theoretical and practical values are very near to each other, but sometimes there are significant declinations [7]. In [3] it is given that the winds velocity does not depend on α angle (eq.12). Experiments in Dusheti district show, that according to changing of angle α winds vertical velocity has changed sharply. Along the canyons, several times winds direction has been changed [7].

Let us consider new approach of circulation of mountain-canyon and describe this motion with the help of velocity potential (φ).

$$U = \frac{\partial \varphi}{\partial x},$$

$$W = \frac{\partial \varphi}{\partial z}. \qquad (14)$$

In continuity equation we shall account dependence of density only on z and get:

$$\frac{\partial^2 \varphi}{\partial x^2} + \frac{\partial^2 \varphi}{\partial y^2} = \frac{\partial \varphi}{\partial z}\left(q \frac{\partial \varphi}{\partial z}\right), \qquad (15)$$

where $q = \frac{g}{RT_0}$ is constant.

Solution of (15) with the boundary requirements, when $z \to \infty$; U=V, W=0 we get:

$$\varphi = V\left[x - b \cos mx e^{-nz}\right]. \qquad (16)$$

It is obvious that:

$$U = V\left[1 + bm \sin mx e^{-nz}\right], \qquad (17)$$

$$W = Vbn \cos nx e^{-nz}. \qquad (18)$$

Here m and n are wave numbers. The following dependence is true:

$$m^2 + n^2 = nq. \qquad (19)$$

Designate

$$r = n + \frac{q}{2}, \text{ than } r^2 = m^2 + \frac{q^2}{4}. \qquad (20)$$

Let us integrate continuity equation on x from 0 to x on z from z_1 to z_2; and foresee that point $x = z = 0$ is on the line of current which coincides with the slopes profile, i.e. $z_2 \approx e^{qz}$, that will be:

$$e^{-nz} \sin mx = -\frac{m}{bq} + \frac{m}{bq} e^{qz}, \qquad (21)$$

or taking into account (19) and (20) the (21) will be rewritten as:

$$e^{-nz} \sin mx = \frac{B}{q}\left[e^{\frac{qz}{2}} - e^{-\frac{qz}{2}} \right]. \qquad (22)$$

It means that slopes hillocks maximal height is defined by condition:

$$e^{-nz} \sin mx = \frac{B}{q}\left[e^{\frac{qz}{2}} - e^{-\frac{qz}{2}} \right], \qquad (23)$$

$$\left(\frac{1}{2} qz\right) \prec\prec 1.$$

To express profile of current line, right part of equation (22) will be put into series and then define z. We shall get:

$$z = \frac{b}{m} e^{-rz} \sin mx. \qquad (24)$$

From inequality (23)

$$z = \frac{2}{q} \cong 2 \cdot 10^3. \qquad (25)$$

It means that thermal influence along the slope is extended on 2-3 kilometers height. (In fact: in the Caucasus above 3 kilometers, the current is conditioned by western transfer [1]). Micro-relief peculiarities of mountain-canyon circulation should be taken into account. *a*) Using Kibel parameter [1, 4, 9]

$$Z' = \frac{Z - \xi(x, y)}{H - \xi(x, y)} H . \tag{26}$$

H is height of mountain; $\xi(x, y)$ describes shape of the slope relief. With the help of this parameter slope relief will be more real and will be presented as a combination of small torsions.

After dead-ripe stage instead of (15) it will be:

$$\frac{\partial^2 \varphi}{\partial x^2} + a^2 \frac{\partial^2 \varphi}{\partial z^2} = qa \frac{\partial \varphi}{\partial z},$$

where $a = \frac{H}{H - \xi}$ is constant for some specific cases. For profile of current line we get:

$$Z = \frac{ab}{m} e^{-\frac{r}{a} z} \sin mx . \tag{27}$$

And for maximal height:

$$Z_{max} = \frac{2a}{q} . \tag{28}$$

As $a = (0.8 - 1.2)$, it means $Z_{max} = 2.4 \cdot 10^3$ m. This value is more near with observed z = 3nm value than calculated by equation (28), so introduction of parameter *a* is expedient.

b) If the winds potential field is considered as three-dimensional, i.e.:

$$\frac{\partial^2 \varphi}{\partial x^2} + \frac{\partial^2 \varphi}{\partial y^2} + \frac{\partial^2 \varphi}{\partial z^2} = q \frac{\partial \varphi}{\partial z} . \tag{29}$$

Solution will be:

$$\varphi = V\left[x - b\cos mx \cdot e^{-(ny+kz)}\right]. \quad (30)$$

We will have:

$$r^2 = m^2 - n^2 + \frac{q}{2}, \quad \text{here } k = r - \frac{q}{2}. \quad (31)$$

Other results are not changed.

c) Consider combination of two (*a* and b) cases. We get equation:

$$\frac{\partial^2\varphi}{\partial x^2} + \frac{\partial^2\varphi}{\partial y^2} + a^2\frac{\partial^2\varphi}{\partial z^2} = aq\frac{\partial\varphi}{\partial z}. \quad (32)$$

In this case:

$$ak = r - \frac{q}{2} \text{ and } k = \frac{2r-q}{2a}. \quad (33)$$

The (27) dependence remains valid. So, quite new point of view confirms that during mountain-canyon circulation parallel to the slope meteorological values deflection is too small which is given in [3. 4] without any confirmation.

Equation (24) shows, that wind velocity depends on the thermal condition of the air stream. It greatly increases during the day, changes direction according to the height and rotates. (Fig.1) [1,7]. If the slopes have multiple torsions (Caucasus, Elbrus territory, Surami mountain ridge), then microcirculation turbulences are observed. Especially anomalous conditions are in Kutaisi district and Alazani valley [1,2]. Passing through canyon, wind is dispersed and decreased. Because of this $\Delta T = T_{day} - T_{night}$ above the mountains is bigger than on the valleys. For example: in the Caucasus on the height $Z = 3\,km$, in the mornings $\Delta T = 2.5^\circ$, or during the days $\Delta T = 1.1^\circ$.

We have tried to explain with our theory daily temperature gradients increasing and availability of ecological "shock" during the last ten years in the cities (Tbilisi example). Tbilisi occupies canyon of the river "Mtkvari", between to the south-east mountain "Mtatsminda"

(with an altitude 760 m) and to the north-west Mountain "Makhata" (with an altitude 520 m).

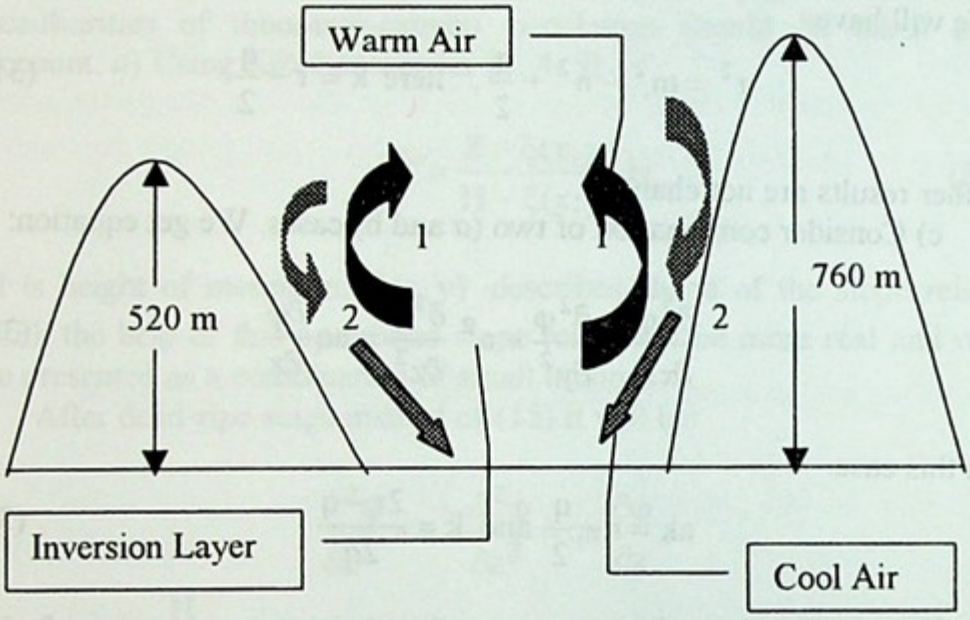

Fig. 2.

Tbilisi local circulation. 1-during the day
2-during the night.

In winter there is sunny, quiet, anticyclone weather; very often, temperature on the mountain "Mtatsminda" is 5-9 degrees higher than in the observatory (450 m). Transported air to the river "Mtkvari" canyon, with the emanations loses temperature, and because of the bad conductivity stays there. That's why the temperature appreciably is low in the nights and daily amplitude increases. It's paradox, but fact (our theory shows the same), on "Mtatsminda" in winter period, during the day it is warmer than in the center of the city (in summer period temperature is less). Dampness increases in the center and very often there is mist (visibility is less than 1 kilometer) [12]. Wind in the center of the city is less (in January $V_{average}$=2.2 m/sec, in July –2.1 m/sec) than in the suburb (in Digomi accordingly 3.7 m/sec and 5.2 m/sec or in airport 5.4 m/sec and 7.2 m/sec). There is not vertical mixture of air, except of slope type of wind (Fig.2). Because of this,

dusts and other admixtures are accumulated in inversion layer and air pollution is increased. This issue promotes decreasing of suns ray energy on 20-30%. It is observed, pollution air is good conductor for the long waves and bad for ultra-violet radiation. This is too dangeous for life. Over ground ozone concentration increases (this year in August average concentration of ozone was 58 mg/m^3, standard is (15-20) mg/m^3), which is very undesirable. Increasing of air pollution promotes decreasing of the Earth effect emanation, which embarrasses cooling of air. All this promotes global increasing of temperature in the centers of cities and not be in suburban places. In Tbilisi in January and July average temperature is 0.6-1.2 degrees more than in Digomi and Samgori.

Studies of local atmosphere dynamics processes of mountain-canyon winds general theory gives possibility to calculate winds vertical height value of the mountains slopes. In the work it is explained the fact of air pollution increasing in the over ground layer and increasing on 2-2.5 degrees of daily temperature amplitude for the last ten years in comparison with the 70 s of the last century.

REFERENCES

1. Z.Khvedelidze. Dinamikuri meteorologia. Tbilisi, 2002, (Georgian).
2. D.Laikhtman. Fizika pogranichnogo sloia atmosferi. M., 1970, (Russian).
3. L. Prandtl. Gidromechanika. M., 1951, (Russian).
4. A. Khrgiai. Fizika atmosferi. L., 1978, (Russian).
5. O. Settoi. Mikrometeorologia. L., 1958, (Russian)
6. Z. Khvedelidze, N. Ramishvili. The nature of Changes of Meteorological Values in the Earth Surface Lager of Atmosphere of Georgia Region. Bull. Georg. Acad.of Sci., 1999, **159**, 3, 421.
7. A. Asitashvili, K. Sapitskii, Z.Khvedelidze. Meteorologia i gidrologia. **5**, 1976, 91, (Russian).
8. Z.Khvedelidze. Sinoptikuri meteorologiis mokle kursi. Tbilisi, 1998, (Georgian).
9. E.Dobrinin. O vetre sklonov nad termicheski neodnorodnoi podstilaiushei poverkhnostiu. Trudi TSIP, **7**, 1956, 370, (Russian).

10. Modeling of atmosphere flow fills. Scientific theoretical physics. Editors Demetri P. Lalas, Corrado F. Ratto, 1996, 775.
11. E. Burman. Mestnie vetri. M., 1969, (Russian).
12. A. Kotaria. Zogadi meteorologia da klimatologia. II, Tbilisi, 1973, (Georgian).
13. N. Fabrikant. Aerodinamika. M., 1964, (Russian).

Tbilisi State University

ნ. რამიშვილი, ზ. ხვედელიძე, რ. აპლაკოვი, გ. ერქომაიშვილი, თ. შალამბერიძე

მთა-ხეობის ცირკულაცია და ლოკალური ატმოსფერული პროცესები

დასკვნა

მიკროცირკულაციური პროცესებიდან ოროგრაფიისა და თერმული ფაქტორის გავლენით წარმოშობილი ხეობის ქარის შესწავლა იყო და არის აქტუალური. ჰიდროთერმოდინამიკის ცნობილ განტოლებათა სისტემაში შემოტანილია ახალი პარამეტრი, რომელიც ახასიათებს მიკრორეგიონალურ თავისებურებებს. მიღებულია შესაბამისი ამოხსნა და გაკეთებულია სათანადო ანალიზი. აღნიშნული პარამეტრის შემოტანამ დააზუსტა პრაქტიკაში შესწავლილი და გამოთვლილი შედეგები; დაზუსტება მოხდა დაახლოვებით (30-40)%-ის ფარგლებში.

ON THE QUESTION OF DEPOLARIZATION OF LIGHT IN NONSTATIONARY ABSORBING OBJECTS

A.Purtseladze

Accepted for publication February, 2004

ABSTRACT. **The change of the polarization state of light in passing through nonstationary anisotropic medium with complex birefringence which is described by the sinusoidally changing square function of time has been considered. It has been shown that with definite meanings of characteristics the medium causes a full depolarization of originally fully polarized light.**

The passing of light through the nonstationary anisotropic medium results in the factor that the originally fully polarized light becomes partially polarized [1,2]. In those works the nonstationary anisotropic medium was characterized by nonstationary birefringence $\Delta n(t)$ (in a general case complex) and nonstationary angle of orientation of the axis of anisotropy $\rho(t)$, in this case the axis of anisotropy was considered with respect to the laboratory coordinate system if we admit that the axes of birefringence and anisotropic absorption coincide. [1,2] contains information about the degree of polarization of the field which has passed through the nonstationary medium in the most general way without concretizing the kind of temporal dependence the of $\Delta\hat{n}(t)$ and $\rho(t)$. As an example in the work [3] there has been considered the nonstationary medium with a sinusoidal change of coefficient of birefringence with linear change of $\rho(t)$.

In this work we consider the nonstationary anisotropic medium which is characterized by complex birefringence (taking absorption into consideration) in the form of sinusoidally changing square function of time. In this case it is admitted that $\rho(t)$ is the linear function of time. This admission is due to little change of $\rho(t)$ with change of $\Delta\hat{n}(t)$ [4]:

$$\begin{cases} \hat{n}_x + \hat{n}_y \approx 2\hat{n}_o, \\ \Delta\hat{n}(t) = \hat{n}_o A \cos^2 \omega t, \quad \rho(t) = kt, \quad t < T', \\ \Delta\hat{n}(t) = 0, \quad \rho(t) = 0, \quad t > T', \end{cases} \tag{1}$$

where $\hat{n}_o = \hat{n}_o - in\tau_o$ is the initially complex refraction coefficient; $\hat{n}_x = n_x - in\tau_x$, $\hat{n}_y = n_y - in\tau_y$ are complex refraction coefficients according to the respective axes (n_o, n_x, n_y are real refraction coefficients, τ_o, τ_x, τ_y are extinction coefficients); A, ω, k are characteristics of the nonstationary medium depending on the kind of the medium; T' in the time of observation.

Here $\Delta\hat{n}(t)$ and $\rho(t)$ are sufficiently quick functions of time which are comparable with optical frequency.

Let the fully elliptically polarized wave E with frequency ω_o with the orientation of the major axis of the ellipse along the axis X of the laboratory coordinate system which is spreading along the axis Z be incident on the nonstationary anisotropic medium. When passing through this medium the wave is partially depolarized and the degree of the polarization of the past field is defined by the ratio [5]

$$V = \frac{I_{pol}}{I_{pol} + I_{nonpol}}, \qquad 0 \le V \le 1, \tag{2}$$

when I_{pol} is the intensity of the polarized part, I_{nonpol} is the intensity of the nonpolarized part.

The expression of the degree of polarization in the most general way without taking into consideration the apparent kind of temporal dependence for the characteristics of the nonstationary medium has the form [2]:

$$V = \frac{\int_{-\infty}^{+\infty} \sin^2 2\rho(t) \left[sh^2\left(\frac{æ_o d}{2}\Delta n\tau(t)\right) + \sin^2\left(\frac{æ_o d}{2}\Delta n(t)\right)\right] dt}{\int_{-\infty}^{+\infty} \left(1 + 2sh^2\left(\frac{æ_o d}{2}\Delta n\tau(t)\right)\right) dt + \frac{1-\varepsilon^2}{1+\varepsilon^2} \int_{-\infty}^{+\infty} sh\left(æ_o d \Delta n\tau(t)\right) \cos 2\rho(t) dt}, \tag{3}$$

where $E = E_x \exp i(\omega_o t - æ_o z)\begin{pmatrix} 1 \\ \pm i\varepsilon \end{pmatrix}\left(0 \le \varepsilon = \frac{E_y}{E_x} \le 1\right)$ is a wave which is incident on the medium, E_X, E_y are components of electrical vector according to the respective axis: $æ_o = \frac{2\pi}{\lambda_0}$, λ_O is a wavelength; d is the thickness of the medium.

Substituting into (3) the evident kind of the function $\Delta\hat{n}(t)$ and $\rho(t)$ from (1) we shall receive

$$V = \frac{\int_0^{+\infty} \sin^2(2kt)\left[\mathrm{sh}^2\left(\frac{æ_o d}{2} n\tau_o A\cos^2\omega t\right) + \sin^2\left(\frac{æ_o d}{2}\right) n_o A\cos^2\omega t\right]dt}{\int_0^{+\infty}\left(1 + 2\mathrm{sh}^2\left(\frac{æ_o d}{2} n\tau_o A\cos^2\omega t\right)\right)dt - \frac{1-\varepsilon^2}{1+\varepsilon^2}\int_0^{+\infty} \mathrm{sh}\left(æ_o dn\tau_o A\cos^2\omega t\right)\cos(2kt)dt} \tag{4}$$

Having solved the integrals which enter into (4) for the degree of polarization we shall receive

$$V = \frac{I_1 - I_2 - I_3 + I_4}{4\left(I_1 - \frac{1-\varepsilon^2}{1+\varepsilon^2} I_5\right)}, \tag{5}$$

where I_1, I_2, I_3, I_4, I_5 is the solution of the integrals:

$$I_1 = \int_0^{+\infty} \mathrm{ch}\left(æ_o dn\tau_o A\cos^2\omega t\right)dt =$$

$$= \frac{\pi}{8\omega}\left[e^{-\frac{æ_o dn\tau_o A}{2}} H_o^{(1)}\left(\frac{iæ_o dn\tau_o A}{2}\right) - e^{\frac{æ_o dn\tau_o A}{2}} H_o^{(2)}\left(\frac{iæ_o dn\tau_o A}{2}\right)\right], \tag{6}$$

$$I_2 = \int_0^{+\infty} \cos\left(æ_o dn_o A\cos^2\omega t\right)dt =$$

$$= \frac{\pi}{8\omega}\left[e^{\frac{i\text{æ}_o dn_o A}{2}} H_o^{(1)}\left(\frac{\text{æ}_o dn_o A}{2}\right) - e^{-\frac{i\text{æ}_o dn_o A}{2}} H_o^{(2)}\left(\frac{\text{æ}_o dn_o A}{2}\right)\right], \quad (7)$$

$$I_3 = \int_0^{+\infty} \cos(4kt)\,\mathrm{ch}\left(\text{æ}_o dn\tau_o A\cos^2\omega t\right)dt =$$

$$= (-1)^{k/\omega}\frac{\pi}{8\omega}\left[e^{-\frac{\text{æ}_o dn\tau_o A}{2}} H_{2k/\omega}^{(1)}\left(\frac{i\text{æ}_o dn\tau_o A}{2}\right) - \right.$$

$$\left. - e^{\frac{\text{æ}_o dn\tau_o A}{2}} H_{2k/\omega}^{(2)}\left(\frac{i\text{æ}_o dn\tau_o A}{2}\right)\right], \quad (8)$$

$$I_4 = \int_0^{+\infty} \cos(4kt)\cos\left(\text{æ}_o dn_o A\cos^2\omega t\right)dt =$$

$$= (-1)^{k/\omega}\frac{\pi}{8\omega}\left[e^{\frac{i\text{æ}_o dn_o A}{2}} H_{2k/\omega}^{(1)}\left(\frac{\text{æ}_o dn_o A}{2}\right) - \right.$$

$$\left. - e^{-\frac{i\text{æ}_o dn_o A}{2}} H_{2k/\omega}^{(2)}\left(\frac{\text{æ}_o dn_o A}{2}\right)\right], \quad (9)$$

$$I_5 = \int_0^{+\infty} \cos(2kt)\,\mathrm{sh}\left(\text{æ}_o dn\tau_o A\cos^2\omega t\right)dt =$$

$$= -(-i)^{k/\omega}\frac{\pi}{8\omega}\left[e^{-\frac{\text{æ}_o dn\tau_o A}{2}} H_{k/\omega}^{(1)}\left(\frac{i\text{æ}_o dn\tau_o A}{2}\right) + \right.$$

$$\left. + e^{\frac{\text{æ}_o dn\tau_o A}{2}} H_{k/\omega}^{(2)}\left(\frac{i\text{æ}_o dn\tau_o A}{2}\right)\right], \quad (10)$$

where $H_p^{(1)}, H_p^{(2)}$ (Hankel function) are cylindrical functions of the 3rd kind of order p [6].

Substituting into (5) the solution of the integrals in the apparent kind (6)-(10) we shall receive:

$$V = \frac{E}{4F}, \qquad (11)$$

where

$$E = e^{-\frac{æ_o dn\tau_o A}{2}}\left[H_0^{(1)}\left(\frac{iæ_o dn\tau_o A}{2}\right) - \right.$$

$$- e^{\frac{æ_o dn\tau_o A}{2}}\left[H_0^{(2)}\left(\frac{iæ_o dn\tau_o A}{2}\right) - (-1)^{k/\omega} H_{2k/\omega}^{(2)}\left(\frac{iæ_o dn\tau_o A}{2}\right)\right] -$$

$$- e^{\frac{iæ_o dn_o A}{2}}\left[H_0^{(1)}\left(\frac{æ_o dn_o A}{2}\right) - (-1)^{k/\omega} H_{2k/\omega}^{(1)}\left(\frac{æ_o dn_o A}{2}\right)\right] -$$

$$- e^{-\frac{iæ_o dn_o A}{2}}\left[H_0^{(2)}\left(\frac{æ_o dn_o A}{2}\right) - (-1)^{k/\omega} H_{2k/\omega}^{(2)}\left(\frac{æ_o dn_o A}{2}\right)\right] \qquad (12)$$

$$F = e^{-\frac{æ_o dn\tau_o A}{2}}\left[H_o^{(1)}\left(\frac{iæ_o dn\tau_o A}{2}\right) + (-i)^{k/\omega}\frac{1-\varepsilon^2}{1+\varepsilon^2} H_{2k/\omega}^{(1)}\left(\frac{iæ_o dn\tau_o A}{2}\right)\right] - \qquad (13)$$

$$- e^{\frac{æ_o dn\tau_o A}{2}}\left[H_o^{(2)}\left(\frac{iæ_o dn\tau_o A}{2}\right) - (-i)^{k/\omega}\frac{1-\varepsilon^2}{1+\varepsilon^2} H_{2k/\omega}^{(2)}\left(\frac{iæ_o dn\tau_o A}{2}\right)\right].$$

If we know characteristics of the anisotropic nonstationary medium and the wavelength of the incident light λ_o then the expressions (11)-(13) allow the numerical value of the degree of the partial polarization of the light which has passed through the medium to be found with the help of Tables of cylindrical function (1).

With sufficiently big values of the argument $H_p^{(1)}$ and $H_p^{(2)}\left(\frac{æ_o dn\tau_0 A}{2} >> 1, \frac{æ_o dn_0 A}{2} >> 1\right)$, we can make use of an asymptotic approximation [6] and under these conditions (6)-(10) are simplified.

$$I_1 \approx \frac{\pi i}{2\omega\sqrt{\pi i æ_o dn\tau_o A}} \sin\left(i æ_o dn\tau_o A - \frac{\pi}{4}\right), \qquad (6_1)$$

$$I_2 \approx \frac{\pi i}{2\omega\sqrt{\pi æ_o dn_o A}} \sin\left(æ_o dn_o A - \frac{\pi}{4}\right), \qquad (7_1)$$

$$I_3 \approx \frac{(-1)^{k/\omega}\pi i}{2\omega\sqrt{\pi i æ_o dn\tau_o A}} \sin\left(i æ_o dn\tau_o A - \frac{\pi}{4} - \frac{k}{\omega}\pi\right), \qquad (8_1)$$

$$I_4 \approx \frac{(-1)^{k/\omega}\pi i}{2\omega\sqrt{\pi æ_o dn_o A}} \sin\left(æ_o dn_o A - \frac{\pi}{4} - \frac{k}{\omega}\pi\right), \qquad (9_1)$$

$$I_5 \approx \frac{-(-i)^{k/\omega}\pi}{2\omega\sqrt{\pi i æ_o dn\tau_o A}} \cos\left(i æ_o dn\tau_o A - \frac{\pi}{4} - \frac{k}{2\omega}\pi\right). \qquad (10_1)$$

In this case for the degree of polarization from (5) we shall receive:

$$V \approx \frac{\sin\left(i æ_o dn\tau_o A - \frac{\pi}{4}\right) - (-1)^{k/\omega}\sin\left(i æ_o dn\tau_o A - \frac{\pi}{4} - \frac{k}{\omega}\pi\right)}{\sin\left(i æ_o dn\tau_o A - \frac{\pi}{4}\right) + (-i)^{k/\omega+1}\frac{1-\varepsilon^2}{1+\varepsilon^2}\cos\left(i æ_o dn\tau_o A - \frac{\pi}{4} - \frac{k}{2\omega}\pi\right)} -$$

$$-\sqrt{\frac{in\tau_o}{n_o}}\,\frac{\sin\left(æ_o dn_o A - \frac{\pi}{4}\right) - (-1)^{k/\omega}\sin\left(æ_o dn_o A - \frac{\pi}{4} - \frac{k}{\omega}\pi\right)}{\sin\left(i æ_o dn\tau_o A - \frac{\pi}{4}\right) + (-i)^{k/\omega+1}\frac{1-\varepsilon^2}{1+\varepsilon^2}\cos\left(i æ_o dn\tau_o A - \frac{\pi}{4} - \frac{k}{2\omega}\pi\right)} \qquad (14)$$

If $\frac{k}{\omega} \to 0$ then from (14) V = 0 which suggests the fully polarized light which has passed through the medium (1) is fully depolarized.

The analog of the medium which is described in (1) can be the device of the Kerr cell type.

In conclusion we shall note that later the experimental test of the results received in this work with the purpose of creating a device, which fully depolarizes polarized radiation, is expected.

Acknowledgment. The author thanks B. Kilosanidze for useful discussions.

REFERENCES.

1. Sh. Kakichashvili. The Journal of Technical Physics, 1995, **65**, 200, (Russian).
2. Sh. Kakichashvili, A. Purtseladze. Letter to Journal of Technical Physics, 1999, **25**, 74, (Russian).
3. A. Purtseladze. Proceedings to I. Javakhishvili Tbilisi State University, 2002, **38**, 15.
4. Sh. D. Kakichashvili. Optics and Spectrocopy. 1984, **56**, 6, 977.
5. U. Sherkliff. Polarized light. M., 1969.
6. T.A.Rozet. Elements of the theory of cylindrical functions with the supplement to radio engineering. M., 1956, 224.

Georgian Academy of Sciences
Institute of Cybernetics

ა. ფურცელაძე

არასტაციონარულ მშთანთქმელ ობიექტებში სინათლის დეპოლარიზაციის შესახებ

დასკვნა

განხილულია სინათლის პოლარიზაციის მდგომარეობის ცვლილება არასტაციონარულ ანიზოტროპულ არეში გავლის შემდეგ. ორმაგი სხივთტეხის კომპლექსური კოეფიციენტი აღწერილია დროში სინუსოიდალური ცვლილების კვადრატული ფუნქციით. ნაჩვენებია, რომ მახასიათებლების გარკვეული მნიშვნელობებისათვის მოცემული არე იწვევს თავდაპირველად სრულად პოლარიზებული სინათლის სრულ დეპოლარიზაციას.

BOUND $q\bar{q}$ SYSTEMS IN THE FRAMEWORK OF TWO-BODY DIRAC EQUATIONS OBTAINED FROM DIFFERENT VERSIONS OF 3D-REDUCTIONS OF THE BETHE-SALPETER EQUATION

T. Babutsidze, T. Kopaleishvili, D. Kurashvili

Accepted for publication March, 2004

ABSTRACT. The two-body Dirac equations for bound $q\bar{q}$ systems are obtained from the different (five) versions of the 3D-equations derived from Bethe-Salpeter equation with the instantaneous kernel in the momentum space using the additional approximations. There are formulated the normalization conditions for the wave functions satisfying the obtained two-body Dirac equations. The spin structure of the confining $q\bar{q}$ interaction is taken in the form $x\gamma_1^0 \otimes \gamma_2^0 + (1-x)I_1 \otimes I_2$, with $0 \le x \le 1$. It is shown that the two-body Dirac equations obtained from the Salpeter equation does not depend on x. As to other four versions such dependence is left. For the systems $(u\bar{s})$, $(c\bar{u})$, $(c\bar{s})$ the dependence of the stable solutions of the Dirac equations obtained in the different version on the mixture parameter x is investigated. Results are compared with such dependence of 3D-equations derived from Bethe-Salpeter equations without the additional approximation and some new conclusions are obtained.

1. INTRODUCTION

The Bethe-Salpeter (BS) equation provides natural basis for the relativistic treatment of bound $q\bar{q}$ systems in the framework of the constituent quark model. But due to fact that the BS wave function (amplitude) has not probability interpretation, three-dimensional (3D) reduction is necessary. Review of investigations of bound $q\bar{q}$ systems (mesons) on basis of equations for the wave function obtained in

different versions of 3D-reduction of BS equation in the instantaneous (static) approximation for kernel of BS equation is given in Ref. 1. In literature there are known five such versions formulated in Refs. \cite{b1}-\cite{b7}, below noted as SAL 2, GR 3, MW 4, CJ 5 and MNK 6, 7, versions. The last four 3D-equations have correct one-body limit (the Dirac equation) when the mass of one of the particles tends to infinity. As it is well-known the Salpeter has not such a limit. Note that Gross equation is obtained only for $m_1 \neq m_2$ case, while other versions work for the equal masses ($m_1 = m_2$) too.

In our previous papers [7-9] the dependence of the existence of the stable solutions of above mentioned 3D-equations on the Lorentz (spin) structure of $q\bar{q}$-confining interaction potential was investigated. In the literature (see e.g [10,11]) this problem was considered in the framework of two-body Dirac equation (TBDE). There arises the problem, what kind of Lorentz (spin) structure must be used in the TBDE. It seems theoretically natural to begin from the above mentioned 3D-relativistic equations obtained from BS equation and use some additional kinematical approximations. Below such approach is used for derivation of the TBDE for wave function of bound $q\bar{q}$ systems and the corresponding normalization conditions for wave function are formulated.

Then these equations are used for investigation of some aspects of the problem connected to the mass spectra of $q\bar{q}$ bound systems (mesons), namely, dependence of the existence of the stable solutions of these equations and mass spectra on the Lorentz (spin) structure of $q\bar{q}$ interaction potential.

2.THE TWO BODY DIRAC EQUATION FOR BOUND $q\bar{q}$ SYSTEMS AND NORMALIZATION CONDITIONS FOR THE CORRESPONDING WAVE FUNCTION

To derive such an equation note that all 3D-equations given in Ref.1 can be written in the common form (c.m.f.)

$$[M - h_1(p) - h_2(-p)]\tilde{\Phi}_M(p) =$$

$$= \Pi(M;\mathbf{p})\gamma_1^0 \otimes \gamma_2^0 \int \frac{d^3\mathbf{p}'}{(2\pi)^3} V(\mathbf{p},\mathbf{p}')\tilde{\Phi}_M(\mathbf{p}') \qquad (2.1)$$

where

$$\Pi(M;p) = \begin{cases} \frac{1}{2}\left(\frac{h_1}{\omega_1} + \frac{h_2}{\omega_2}\right), & \text{(SAL)} \\ \frac{1}{2}\left(1 + \frac{h_1}{\omega_1}\right), & \text{(GR)} \\ \frac{1}{2}\left(\frac{h_1}{\omega_1} + \frac{h_2}{\omega_2}\right) + \frac{M}{\omega_1+\omega_2}\left(1 + \frac{h_1}{\omega_1} \otimes \frac{h_2}{\omega_2}\right), & \text{(MW)} \\ \frac{1}{2}\left[\frac{M + h_1 + h_2}{\omega_1+\omega_2}\right], & \text{(CJ)} \\ \frac{1}{2}\left[\frac{M\left(a - p_0^{(+)2}\right) - p_0^{(+)}M\left(h_1 - h_2\right) + B\left(h_1 + h_2\right)}{BR}\right], & \text{(MNK)} \end{cases} \qquad (2.2)$$

$$a = E_1^2 - E_2^2 = \frac{1}{4}\left(M^2 + b_0^2 - 2(\omega_1^2 - \omega_2^2)\right), \quad b_0 = E_1 - E_2,$$

$$E_{\binom{1}{2}} = \frac{M}{2}\left(1 \pm d_{12}\right)$$

$$d_{12} = \frac{m_1^2 - m_2^2}{M^2}, \qquad p_0^{(+)} = \frac{R-b}{2y}, \qquad y = \frac{m_1 - m_2}{m_1 + m_2},$$

$$R = \sqrt{b^2 - 4y^2 a}, \qquad b = M + b_0 y, \quad B = a + p_0^{(+)} b_0 + p_0^{(+)2}.$$

$$h_i = \alpha_i p_i + m_i \gamma_i^0, \quad \omega_i = \sqrt{m_i^2 + p_i^2}, \quad O_1 = O_1 \otimes I_2, \quad O_1 = I_1 \otimes O_2.$$

Note that from the eq.(2.1) with the operators Π (2.2) immediately the system of equations (3.61) in Ref.1 follows with

definition (3.62,63), if eq. (2.1) is multiplied from left by projection operator $\Lambda_{12}^{(\alpha_1\alpha_2)}$ and their properties are used:

$$\Lambda_{12}^{(\alpha_1\alpha_2)} = \Lambda_1^{(\alpha_1)} \otimes \Lambda_2^{(\alpha_2)}, \Lambda_i^{(\alpha_i)} = \frac{\omega_i + \alpha_i h_i}{2\omega_i}, \Lambda_i^{(\alpha_i)}\Lambda_i^{(\beta_i)} = \delta_{(\alpha_i\beta_i)}\Lambda_i^{(\alpha_i)}$$

$$\Pi^{SAL} = \Lambda_{12}^{(++)} - \Lambda_{12}^{(--)} = \frac{1}{2}\left(\frac{h_1}{\omega_1} + \frac{h_2}{\omega_2}\right),$$

$$\Pi^{GR} = \Lambda_{12}^{(++)} + \Lambda_{12}^{(+-)} = \frac{1}{2}\left(1 + \frac{h_1}{\omega_1}\right) \qquad (2.3)$$

Now if in the operator Π^{SAL} we use the approximation

$$\frac{h_i}{\omega_i} \Rightarrow \frac{h_i}{\omega_i}\Bigg|^{p_i \to 0} = \gamma_i^0 \qquad (2.4)$$

then the TBDE is obtained:

$$\left[M - h_1(\mathbf{p}) - h_2(-\mathbf{p})\right]\Psi_M(\mathbf{p}) =$$

$$= \Pi_0^{SAL}\gamma_1^0 \otimes \gamma_2^0 \int \frac{d^3\mathbf{p}'}{(2\pi)^3} V(\mathbf{p},\mathbf{p}')\Psi_M(\mathbf{p}'), \qquad (2.5)$$

$$\Pi_0^{SAL} = \frac{1}{2}\left(\gamma_1^0 + \gamma_2^0\right) \qquad (2.6)$$

This has already been used in coordinate space for bound $q\bar{q}$ systems in Refs.10, 11 and corresponds to Lorentz (spin) structure of confining potential (see below(2.14)).

In approximation (2.4) from (2.2) it follows

$$\Pi_0^{GR} = \frac{1}{2}\left(1 + \gamma_1^0\right). \qquad (2.7)$$

As to MW, CJ and MNK versions for derivation of corresponding TBDE the additional to (2.4) approximation is need, namely,

$$\Pi(M;0) \Rightarrow \Pi(m_1 + m_1;0) \equiv \Pi_0, \tag{2.8}$$

which is quite natural because it corresponds to zero approximation in iteration procedure for solving nonlinear over M eq. (2.1) for the MW, CJ and MNK versions. As a result from (2.2) it follows

$$\Pi_0^{MW} = \frac{1}{2}\left[\gamma_1^0 + \gamma_2^0 + (1 - \gamma_1^0 \otimes \gamma_2^0)\right] \tag{2.9}$$

$$\Pi_0 = \frac{1}{2}\left[1 + \mu_1\gamma_1^0 + \mu_2\gamma_2^0\right] \qquad \begin{matrix} \mu_i = \dfrac{m_i}{m_1 + m_2}, & \text{(CJ)} \\ \mu_i = \dfrac{m_i^2}{m_1^2 + m_2^2}. & \text{(MNK)} \end{matrix} \tag{2.10}$$

Thus, we have the following TBDE obtained from, (2.1), (2.2)

$$\left[M - h_1(p) - h_2(-p)\right]\Psi_M(p) = $$

$$= \Pi_0\gamma_1^0 \otimes \gamma_2^0 \int \frac{d^3p'}{(2\pi)^3} V(p,p')\Psi_M(p'), \tag{2.11}$$

where the operator Π_0 is given by the formulae (2.6), (2.7), (2.9), (2.10).

Note that there is the another approach for formulation the TBDE, namely, generation of the one-body Dirac equation to two-body one, using constrain dynamics and relation to quantum field theory. Review of such an approach is given in Ref.12.

Representing the wave function $\Psi_M(\mathbf{p})$ as sum of "frequency" components

$$\Psi_M(\mathbf{p}) = \sum_{\alpha_1\alpha_2} \Lambda_{12}^{(\alpha_1\alpha_2)}(\mathbf{p})\Psi_M(\mathbf{p}) = \sum_{\alpha_1\alpha_2} \Psi_M^{(\alpha_1\alpha_2)}(\mathbf{p}) \tag{2.12}$$

from the eq. (2.11) the system of the equation for the functions $\Psi_M^{(\alpha_1\alpha_2)}(\mathbf{p})$ follows

$$\left[M-(\alpha_1\omega_1+\alpha_2\omega_2)\right]\Psi_M^{(\alpha_1\alpha_2)}(\mathbf{p})=\Lambda_{12}^{(\alpha_1\alpha_2)}\Pi_0\gamma_1^0\otimes\gamma_2^0$$

$$\int\frac{d^3\mathbf{p}'}{(2\pi)^3}V(\mathbf{p},\mathbf{p}')\sum_{\alpha_1'\alpha_2'}\Psi_M^{(\alpha_1'\alpha_2')}(\mathbf{p}'). \qquad (2.13)$$

Taking the $q\bar{q}$ interaction operator V in the form 1 (combination of one-gluon exchange and confining part of potential)

$$V=\gamma_1^0\otimes\gamma_2^0V_{OG}+\left[x\gamma_1^0\otimes\gamma_2^0+(1-x)I_1\otimes I_2\right]V_C \qquad (2.14)$$

and representing the function $\Psi_M^{(\alpha_1\alpha_2)}(\mathbf{p})$ as

$$\Psi_M^{(\alpha_1\alpha_2)}(\mathbf{p})= \qquad (2.15)$$

$$=N_{12}^{(\alpha_1\alpha_2)}(p)\left[\begin{pmatrix}1\\ \dfrac{\alpha_1\sigma_1\mathbf{p}}{\omega_1+\alpha_1m_1}\end{pmatrix}\otimes\begin{pmatrix}1\\ \dfrac{-\alpha_2\sigma_2\mathbf{p}}{\omega_2+\alpha_2m_2}\end{pmatrix}\equiv f_{12}^{(\alpha_1\alpha_2)}(\mathbf{p})\right]\chi_M^{(\alpha_1\alpha_2)}(\mathbf{p}),$$

where

$$N_{12}^{(\alpha_1\alpha_2)}(p)=\sqrt{\frac{\omega_1+\alpha_1m_1}{2\omega_1}}\sqrt{\frac{\omega_2+\alpha_2m_2}{2\omega_2}}, \qquad (2.16)$$

then for the wave functions $\chi_M^{(\alpha_1\alpha_2)}(\mathbf{p})$ from (2.13) can be obtained the following system of equations

$$\left[M-(\alpha_1\omega_1+\alpha_2\omega_2)\right]\chi_M^{(\alpha_1\alpha_2)}(\mathbf{p})=$$

$$= \sum_{\alpha_1'\alpha_2'} \int \frac{d^3p'}{(2\pi)^3} V_{eff}^{(\alpha_1\alpha_2\alpha_1'\alpha_2')}(\mathbf{p},\mathbf{p}') \chi_M^{(\alpha_1'\alpha_2')}(\mathbf{p}') \qquad (2.17)$$

where

$$V_{eff}^{(\alpha_1\alpha_2\alpha_1'\alpha_2')}(\mathbf{p},\mathbf{p}') = N_{12}^{(\alpha_1\alpha_2)}(\mathbf{p}) B^{(\alpha_1\alpha_2\alpha_1'\alpha_2')}(\mathbf{p},\mathbf{p}') N_{12}^{(\alpha_1'\alpha_2')}(\mathbf{p}'), \quad (2.18)$$

$$B^{(\alpha_1\alpha_2\alpha_1'\alpha_2')}(\mathbf{p},\mathbf{p}') =$$

$$\left[1 - \frac{\alpha_1\alpha_2\alpha_1'\alpha_2'(\boldsymbol{\sigma}_1\mathbf{p})(\boldsymbol{\sigma}_2\mathbf{p})(\boldsymbol{\sigma}_1\mathbf{p}')(\boldsymbol{\sigma}_2\mathbf{p}')}{(\omega_1+\alpha_1 m_1)(\omega_2+\alpha_2 m_2)(\omega_1'+\alpha_1' m_1)(\omega_2'+\alpha_2' m_2)}\right] V_1(\mathbf{p},\mathbf{p}'), \quad \text{(SAL)} \qquad (2.19)$$

$$B^{(\alpha_1\alpha_2\alpha_1'\alpha_2')}(\mathbf{p},\mathbf{p}') =$$

$$= \left[V_1(\mathbf{p},\mathbf{p}') + \frac{\alpha_2\alpha_2'(\boldsymbol{\sigma}_2\mathbf{p})(\boldsymbol{\sigma}_2\mathbf{p}')}{(\omega_2+\alpha_2 m_2)(\omega_2'+\alpha_2' m_2)} V_2(x;\mathbf{p},\mathbf{p}')\right], \quad \text{(GR)} \qquad (2.20)$$

$$B^{(\alpha_1\alpha_2\alpha_1'\alpha_2')}(\mathbf{p},\mathbf{p}') =$$

$$= \left[1 - \frac{\alpha_1\alpha_2\alpha_1'\alpha_2'(\boldsymbol{\sigma}_1\mathbf{p})(\boldsymbol{\sigma}_2\mathbf{p})(\boldsymbol{\sigma}_1\mathbf{p}')(\boldsymbol{\sigma}_2\mathbf{p}')}{(\omega_1+\alpha_1 m_1)(\omega_2+\alpha_2 m_2)(\omega_1'+\alpha_1' m_1)(\omega_2'+\alpha_2' m_2)}\right] V_1(\mathbf{p},\mathbf{p}') +$$

$$\left[+\frac{\alpha_1\alpha_1'(\boldsymbol{\sigma}_1\mathbf{p})(\boldsymbol{\sigma}_1\mathbf{p}')}{(\omega_1+\alpha_1 m_1)(\omega_1'+\alpha_1' m_1)} + \right.$$

$$\left. + \frac{\alpha_2\alpha_2'(\boldsymbol{\sigma}_2\mathbf{p})(\boldsymbol{\sigma}_2\mathbf{p}')}{(\omega_2+\alpha_2 m_2)(\omega_2'+\alpha_2' m_2)}\right] V_2(x;\mathbf{p},\mathbf{p}'), \quad \text{(MW)} \qquad (2.21)$$

$$B^{(\alpha_1\alpha_2\alpha_1'\alpha_2')}(\mathbf{p},\mathbf{p}') = V_1(\mathbf{p},\mathbf{p}') + \left[\frac{\alpha_1\alpha_1'(\boldsymbol{\sigma}_1\mathbf{p})(\boldsymbol{\sigma}_1\mathbf{p}')}{(\omega_1+\alpha_1 m_1)(\omega_1'+\alpha_1' m_1)}\mu_2 + \right.$$

$$+\frac{\alpha_2\alpha_2'(\sigma_2\mathbf{p})(\sigma_2\mathbf{p}')}{(\omega_2+\alpha_2 m_2)(\omega_2'+\alpha_2' m_2)}\mu_1\Bigg]V_2(x;\mathbf{p},\mathbf{p}'), \qquad (2.22)$$

$$(CJ, MNK)$$

$$\omega_i'=\sqrt{m_i^2+\mathbf{p}'^2},\ V_1(\mathbf{p},\mathbf{p}')=V_{OG}(\mathbf{p},\mathbf{p}')+V_C(\mathbf{p},\mathbf{p}'),$$

$$V_2(x;\mathbf{p},\mathbf{p}')=V_{OG}(\mathbf{p},\mathbf{p}')+(2x-1)V_C(\mathbf{p},\mathbf{p}'). \qquad (2.23)$$

It is very important that the TBDE (2.17) with effective potential (2.18) with (2.19) obtained from the equation (2.1), corresponding to SAL version (2.2) does not depend on parameter x interned in the interaction operator (2.14), which means that from this equation no information can be obtained on the Lorentz (spin) structure of the confining $q\bar{q}$ interaction potential (2.14). Second interesting result is that the wave functions satisfying the TBDE (2.17) with effective potentials defined by formulae (2.18) with expression(2.19), (2.20), obtained for SAL and GR versions (2.2) of the 3D-relativistic equations have all nonzero "frequency components" whereas two components of the wave functions satisfying the equation (2.1) with projection operators (2.2), are zero, namely:

$$\tilde{\Phi}_M^{(\pm\mu)}=\Lambda_{12}^{(\pm\mu)}\tilde{\Phi}_M=0 \quad (SAL)$$
$$\tilde{\Phi}_M^{(-\pm)}=\Lambda_{12}^{(-\pm)}\tilde{\Phi}_M=0 \quad (GR) \qquad (2.24)$$

which directly follows (and is well known) from the eq.(2.1) if it is multiplied (from left) by the operators $\Lambda_{12}^{(\pm\mu)}$, $\Lambda_{12}^{(-\pm)}$ and used the formulae (2.3).

For formulation of normalization condition for the wave function (2.12) which satisfies the equation (2.11), we note that normalization condition for Salpeter wave function obtained in Ref.1 (see (3.14)) can be written in the form

$$\left\langle\tilde{\Phi}_M\left|\Pi^{SAL}\right|\tilde{\Phi}_M\right\rangle=2M. \qquad (2.25)$$

The analogous condition can be derived for wave function satisfying Gross equation (2.1) (2.2) if we use equation for full Green operator corresponding to the equation (2.1).

$$\widetilde{G} = g_0 \Pi \Gamma_0 + g_0 \widetilde{U} \widetilde{G}, \qquad g_0 = [M - h_1 - h_2]^{-1},$$

$$\Gamma_0 = \gamma_1^0 \otimes \gamma_2^0, \qquad \widetilde{U} = \Pi \Gamma_0 V. \tag{2.26}$$

Assuming that the operator $\widetilde{G}^{-1}$ exists (being natural at any rate in the bound states, we need) from eq. (2.26) after some transformations the following relation can be obtained

$$\widetilde{G}\Gamma_0 \Pi \left[g_0^{-1} - \widetilde{U} \right] \widetilde{G}\Gamma_0 = \widetilde{G}\Gamma_0 \Pi\Pi . \tag{2.27}$$

Noting that $\Pi_{GR}\Pi_{GR} = \Pi_{GR}$ from (\ref{eq.20}) we have

$$\widetilde{G}\Gamma_0 \Pi^{GR} \left[g_0^{-1} - \widetilde{U} \right] \widetilde{G}\Gamma_0 \Pi^{GR} = \widetilde{G}\Gamma_0 \Pi^{GR} . \tag{2.28}$$

Now using the spectral representation of Green operator $\widetilde{G}$

$$\widetilde{G}(p) = \sum_B \frac{\left|\widetilde{\Phi}_{P_B}\right\rangle \left\langle\widetilde{\bar{\Phi}}_{P_B}\right|}{P^2 - M_B^2} + \widetilde{R}(P), \left\langle\widetilde{\bar{\Phi}}_{P_B}\right| = \left\langle\widetilde{\Phi}_{P_B}\right| \Gamma_0, \tag{2.29}$$

from (2.28) it can be obtained the relation

$$\left\langle\widetilde{\Phi}_M\right| \Pi^{GR} \left|\widetilde{\Phi}_M\right\rangle \Pi^{GR} = 2M\Pi^{GR} . \tag{2.30}$$

It means that the normalization condition analogous to (2.25)

$$\left\langle\widetilde{\Phi}_M\right| \Pi^{GR} \left|\widetilde{\Phi}_M\right\rangle = 2M \tag{2.31}$$

holds only in corresponding subspace of the Gilbert space. Note that the condition (2.31) can be obtained from the formula (3.28) of ref.1, which was not derived, but supposed with an analogy to (3.14).

Now, noting that the TBDE (2.11) for the SAL and GR versions of the 3D-relativistic equation (2.1) were obtained in the approximation (2.4) for the projection operators Π^{SAL} and Π^{GR}, the corresponding condition for wave function can be obtained from (2.25), (2.31) by replacement $\Pi^{SAL} \Rightarrow \Pi_0^{SAL}$ (2.6) and $\Pi^{GR} \Rightarrow \Pi_0^{GR}$ (2.7). Thus we have

$$\langle \Psi_M | \Pi_0^{SAL,GR} | \Psi_M \rangle = 2M , \tag{2.32}$$

where Π_0^{SAL} and Π_0^{GR} are given by formulae (2.6), (2.7).

Further, noting that the projection operator Π_0^{MW} (2.9) satisfies condition $\Pi_0^{MW}\Pi_0^{MW} = 1$, from relation (2.27) can be obtained the normalization condition analogous to (2.32) i.e.

$$\langle \Psi_M | \Pi_0^{MW} | \Psi_M \rangle = 2M. \tag{2.33}$$

As to normalization conditions for wave functions satisfying the TBDE (2.11), corresponding to the CJ and MNK versions, they can not be derived analogously because the corresponding projection operators Π_0 (2.10) does not satisfy the conditions $\Pi_0\Pi_0 = \Pi_0$ or $\Pi_0\Pi_0 = 1$. But bellow we assume (suppose) that the condition analogous to (\ref{eq.25}) can be written in common form

$$\langle \Psi_M | \Pi_0 | \Psi_M \rangle = 2M , \tag{2.34}$$

where operator Π_0 is given by the formulae (2.6), (2.7), (2.9), (2.10) for all versions. As a result with an account of the formulae (2.12), (2.15), (2.16) the normalization condition for the components of the wave functions $\chi_M^{(\alpha_1\alpha_2)}$ takes the form

$$\sum_{\alpha_1\alpha_2\beta_1\beta_2} \left\langle \chi_M^{(\alpha_1\alpha_2)} \middle| N_{12}^{(\alpha_1\alpha_2)} f_{12}^{(\alpha_1\alpha_2)+} \Pi_0 f_{12}^{(\beta_1\beta_2)} N_{12}^{(\beta_1\beta_2)} \middle| \chi_M^{(\beta_1\beta_2)} \right\rangle = 2M \quad (2.35)$$

from which follows

$$\int \frac{d^3p}{(2\pi)} \sum_{\alpha_1\alpha_2\beta_1\beta_2} \frac{1}{4} [E_{12}^{(\alpha_1\alpha_2\beta_1\beta_2)} \begin{pmatrix} 1 \\ 1 \\ 1 \\ 1 \end{pmatrix} +$$

$$+\alpha_1\beta_1 E_{12}^{(-\alpha_1\alpha_2-\beta_1\beta_2)} \begin{pmatrix} 0 \\ 0 \\ 1 \\ \mu_2 \end{pmatrix} + \alpha_2\beta_2 E_{12}^{(\alpha_1-\alpha_2\beta_1-\beta_2)} \begin{pmatrix} 0 \\ 1 \\ 1 \\ \mu_1 \end{pmatrix} - \quad (2.36)$$

$$-\alpha_1\alpha_2\beta_1\beta_2 E_{12}^{(-\alpha_1-\alpha_2-\beta_1-\beta_2)} \begin{pmatrix} 1 \\ 0 \\ 1 \\ 0 \end{pmatrix}] \chi_M^{(\alpha_1\alpha_2)*}(\mathbf{p}) \chi_M^{(\beta_1\beta_2)}(\mathbf{p}) = 2M, \begin{pmatrix} SAL \\ GR \\ MW \\ CJ, MNK \end{pmatrix},$$

where

$$E_{12}^{(\alpha_1\alpha_2\beta_1\beta_2)} = \sqrt{(1+\alpha_1 \frac{m_1}{\omega_1})(1+\alpha_2 \frac{m_2}{\omega_2})(1+\beta_1 \frac{m_1}{\omega_1})(1+\beta_2 \frac{m_2}{\omega_2})}. \quad (2.37)$$

Now we use the partial-wave expansion for the function $\chi_M^{(\alpha_1\alpha_2)}(\mathbf{p})$ [1]

$$\chi_M^{(\alpha_1\alpha_2)}(\mathbf{p}) = \sum_{LSJM_J} \langle \hat{\mathbf{n}} | LSJM_J \rangle R_{LSJ}^{(\alpha_1\alpha_2)}(p) \equiv \sum_{JM_J} \chi_{JM_J}^{(\alpha_1\alpha_2)}(\mathbf{p}); \left(\hat{\mathbf{n}} = \frac{\mathbf{p}}{p} \right). \quad (2.38)$$

where $R_{LSJ}^{(\alpha_1\alpha_2)}(p)$ are corresponding radial wave functions. And the potential functions $V_{OG}(\mathbf{p},\mathbf{p}')$, $V_C(\mathbf{p},\mathbf{p}')$ are represented in form (local potentials)

$$V(\mathbf{p}-\mathbf{p}') = (2\pi)^3 \sum_{\bar{L}SJM_{\bar{J}}} V^{\bar{L}}(p,p')\left\langle \mathbf{n}\middle|\bar{L}S\bar{J}M_{\bar{J}}\right\rangle\left\langle \bar{L}S\bar{J}M_{\bar{J}}\middle|\mathbf{n}'\right\rangle, \quad (2.39)$$

where

$$V^{\bar{L}}(p,p') = \frac{2}{\pi}\int_0^\infty j_{\bar{L}}(pr)V(r)j_{\bar{L}}(p'r)r^2dr, \quad (2.40)$$

$j_{\bar{L}}(x)$ being the spherical Bessel function. Then from the system of equations (2.17), the effective potentials of which are defined by the formulae (2.18)-(2.23) we obtain the following system of equations for the radial functions $R^{(\alpha_1\alpha_2)}_{LSJ}(p)$

SAL version

$$\left[M-(\alpha_1\omega_1+\alpha_2\omega_2)\right]R^{(\alpha_1\alpha_2)}_{J(^0_1)J}(p) =$$

$$= \sum_{\alpha_1'\alpha_2'}\int_0^\infty p'^2dp'[(N^{(\alpha_1\alpha_2)}_{12}(p)N^{(\alpha_1'\alpha_2')}_{12}(p') -$$

$$-\alpha_1\alpha_2\alpha_1'\alpha_2'N^{(-\alpha_1-\alpha_2)}_{12}(p)N^{(-\alpha_1'-\alpha_2')}_{12}(p'))V^J_1(p,p')]R^{(\alpha_1'\alpha_2')}_{J(^0_1)J}(p') \quad (2.41)$$

$$\left[M-(\alpha_1\omega_1+\alpha_2\omega_2)\right]R^{(\alpha_1\alpha_2)}_{J\pm11J}(p) =$$

$$= \sum_{\alpha_1'\alpha_2'}\int_0^\infty p'^2dp'\{[N^{(\alpha_1\alpha_2)}_{12}(p)N^{(\alpha_1'\alpha_2')}_{12}(p')V^{J\pm1}_1(p,p') - \quad (2.42)$$

$$-\alpha_1\alpha_2\alpha_1'\alpha_2'N^{(-\alpha_1-\alpha_2)}_{12}(p)N^{(-\alpha_1'-\alpha_2')}_{12}(p')V_{1(J\pm1)}(p,p')]R^{(\alpha_1'\alpha_2')}_{J\pm11J}(p') -$$

$$-[\alpha_1\alpha_2\alpha_1'\alpha_2'N^{(-\alpha_1-\alpha_2)}_{12}(p)N^{(-\alpha_1'-\alpha_2')}_{12}(p')\frac{2}{2J+1}V_{1(-)J}(p,p')]R^{(\alpha_1'\alpha_2')}_{J\mp11J}(p')\}$$

GR version

$$\left[M-(\alpha_1\omega_1+\alpha_2\omega_2)\right]R^{(\alpha_1\alpha_2)}_{J(^0_1)J}(p) =$$

$$= \sum_{\alpha_1'\alpha_2'} \int_0^\infty p'^2 dp' \{ [N_{12}^{(\alpha_1\alpha_2)}(p) N_{12}^{(\alpha_1'\alpha_2')}(p') V_1^J(p,p') +$$

$$+ \alpha_2\alpha_2' N_{12}^{(\alpha_1-\alpha_2)}(p) N_{12}^{(\alpha_1'-\alpha_2')}(p') V_{2\oplus J}^{(1_1^0)}(x;p,p')] R_{J(1_1^0)J}^{(\alpha_1'\alpha_2')}(p') -$$

$$- [\alpha_2\alpha_2' N_{12}^{(\alpha_1-\alpha_2)}(p) N_{12}^{(\alpha_1'-\alpha_2')}(p') V_{2(-)J}^{(1_1^0)}(x;p,p')] R_{J(1_0^1)J}^{(\alpha_1'\alpha_2')}(p') \} \quad (2.43)$$

$$\left[M - (\alpha_1\omega_1 + \alpha_2\omega_2)\right] R_{J\pm 1 1 J}^{(\alpha_1\alpha_2)}(p) =$$

$$= \sum_{\alpha_1'\alpha_2'} \int_0^\infty p'^2 dp' [N_{12}^{(\alpha_1\alpha_2)}(p) N_{12}^{(\alpha_1'\alpha_2')}(p') V_1^{J\pm 1}(p,p') +$$

$$+ \alpha_2\alpha_2' N_{12}^{(\alpha_1-\alpha_2)}(p) N_{12}^{(\alpha_1'-\alpha_2')}(p') V_2^J(x;p,p')] R_{J\pm 1 1 J}^{(\alpha_1'\alpha_2')}(p') \quad (2.44)$$

MW, CJ and MNK versions

$$\left[M - (\alpha_1\omega_1 + \alpha_2\omega_2)\right] R_{J(1_1^0)J}^{(\alpha_1\alpha_2)}(p) =$$

$$= \sum_{\alpha_1'\alpha_2'} \int_0^\infty p'^2 dp' \{ [(N_{12}^{(\alpha_1\alpha_2)}(p) N_{12}^{(\alpha_1'\alpha_2')}(p') \begin{pmatrix} 1 \\ 1 \end{pmatrix} -$$

$$- \alpha_1\alpha_2\alpha_1'\alpha_2' N_{12}^{(-\alpha_1-\alpha_2)}(p) N_{12}^{(-\alpha_1'-\alpha_2')}(p') \begin{pmatrix} 1 \\ 0 \end{pmatrix}) V_1^J(p,p') +$$

$$+ (\alpha_1\alpha_1' N_{12}^{(-\alpha_1\alpha_2)}(p) N_{12}^{(-\alpha_1'\alpha_2')}(p') \begin{pmatrix} 1 \\ \mu_2 \end{pmatrix} +$$

$$+ \alpha_2\alpha_2' N_{12}^{(\alpha_1-\alpha_2)}(p) N_{12}^{(\alpha_1'-\alpha_2')}(p') \begin{pmatrix} 1 \\ \mu_1 \end{pmatrix}) V_{2\oplus J}^{(1_1^0)}(x;p,p')] R_{J(1_1^0)J}^{(\alpha_1'\alpha_2')}(p') +$$

$$+ [(\alpha_1\alpha_1' N_{12}^{(-\alpha_1\alpha_2)}(p) N_{12}^{(-\alpha_1'\alpha_2')}(p') \begin{pmatrix} 1 \\ \mu_2 \end{pmatrix} -$$

$$- \alpha_2\alpha_2' N_{12}^{(\alpha_1-\alpha_2)}(p) N_{12}^{(\alpha_1'-\alpha_2')}(p') \begin{pmatrix} 1 \\ \mu_1 \end{pmatrix}) V_{2(-)J}(x;p,p')] R_{J(1_0^1)J}^{(\alpha_1'\alpha_2')}(p') \} \quad (2.45)$$

$$\left[M - (\alpha_1\omega_1 + \alpha_2\omega_2)\right] R_{J\pm 1 1 J}^{(\alpha_1\alpha_2)}(p) =$$

$$= \sum_{\alpha_1'\alpha_2'} \int_0^\infty p'^2 dp' \{ [N_{12}^{(\alpha_1\alpha_2)}(p) N_{12}^{(\alpha_1'\alpha_2')}(p') \begin{pmatrix} 1 \\ 1 \end{pmatrix} V_1^{J\pm1}(p,p') -$$

$$-\alpha_1\alpha_2\alpha_1'\alpha_2' N_{12}^{(-\alpha_1-\alpha_2)}(p) N_{12}^{(-\alpha_1'-\alpha_2')}(p') \begin{pmatrix} 1 \\ 0 \end{pmatrix} V_{1(J\pm1)}(p,p') +$$

$$+(\alpha_1\alpha_1' N_{12}^{(-\alpha_1\alpha_2)}(p) N_{12}^{(-\alpha_1'\alpha_2')}(p') \begin{pmatrix} 1 \\ \mu_2 \end{pmatrix} + \qquad (2.46)$$

$$+\alpha_2\alpha_2' N_{12}^{(\alpha_1-\alpha_2)}(p) N_{12}^{(\alpha_1'-\alpha_2')}(p') \begin{pmatrix} 1 \\ \mu_1 \end{pmatrix}) V_2^J(x;p,p')] R_{J\pm1\,1J}^{(\alpha_1'\alpha_2')}(p') +$$

$$+[\alpha_1\alpha_2\alpha_1'\alpha_2' N_{12}^{(-\alpha_1-\alpha_2)}(p) N_{12}^{(-\alpha_1'-\alpha_2')}(p') \frac{2}{2J+1} V_{1(-)J}(p,p')] R_{J_\mu 1\,1J}^{(\alpha_1'\alpha_2')}(p') \},$$

where

$$V_{n\oplus J}^{\binom{0}{1}} = \frac{1}{2J+1}\left[\begin{pmatrix} J+1 \\ J \end{pmatrix} V_n^{J+1} + \begin{pmatrix} J \\ J+1 \end{pmatrix} V_n^{J-1}\right],$$

$$V_{n(-)J} = \frac{\sqrt{J(J+1)}}{2J+1}\left[V_n^{J+1} - V_n^{J-1}\right] \quad n=1,2, \qquad (2.47)$$

$$V_{n(J\pm1)} = \frac{1}{(2J+1)^2}\left[V_n^{J\pm1} + 4J(J+1)V_n^{J\mp1}\right]$$

Note that if only confining potential (2.14) and parameter $x = \frac{1}{2}$ are taken into account, then equations for MW (2.45), (2.46) and SAL versions (2.41), (2.42) versions are the same. As to versions GR and CJ, MNK equations (2.43), (2.44) and (2.45), (2.46) coincide with each other and what is more, dependence of these equations on total spin (S) disappears. Dependence of spin (S) appears only if V_{OG} is taken into account, what can be seen from formulae (2.20), (2.22) too.

It is interesting to compare the system of equations (2.41)-(2.46) with the system of equations obtained from (2.1) without the approximation (2.4), (2.8) (see eqs. (4.16, 17) in [1], ignoring the terms corresponding to t'Hooft interaction)

$$\left[M-(\alpha_1\omega_1+\alpha_2\omega_2)\right]R^{(\alpha_1\alpha_2)}_{J(^0_1)J}(p)=$$

$$=A^{(\alpha_1\alpha_2)}(M;p)\sum_{\alpha_1'\alpha_2'}\int_0^\infty p'^2dp'\{[(N^{(\alpha_1\alpha_2)}_{12}(p)N^{(\alpha_1'\alpha_2')}_{12}(p')+$$

$$+\alpha_1\alpha_2\alpha_1'\alpha_2'N^{(-\alpha_1-\alpha_2)}_{12}(p)N^{(-\alpha_1'-\alpha_2')}_{12}(p'))V^J_1(p,p')+$$

$$+(\alpha_1\alpha_1'N^{(-\alpha_1\alpha_2)}_{12}(p)N^{(-\alpha_1'\alpha_2')}_{12}(p')+$$

$$+\alpha_2\alpha_2'N^{(\alpha_1-\alpha_2)}_{12}(p)N^{(\alpha_1'-\alpha_2')}_{12}(p'))V^{(^0_1)}_{2\oplus J}(x;p,p')]R^{(\alpha_1'\alpha_2')}_{J(^0_1)J}(p')-$$

$$-[(\alpha_1\alpha_1'N^{(-\alpha_1\alpha_2)}_{12}(p)N^{(-\alpha_1'\alpha_2')}_{12}(p')-$$

$$-\alpha_2\alpha_2'N^{(\alpha_1-\alpha_2)}_{12}(p)N^{(\alpha_1'-\alpha_2')}_{12}(p'))V_{2(-)J}(x;p,p')]R^{(\alpha_1'\alpha_2')}_{J(^1_0)J}(p')\} \qquad (2.48)$$

$$\left[M-(\alpha_1\omega_1+\alpha_2\omega_2)\right]R^{(\alpha_1\alpha_2)}_{J\pm11J}(p)=$$

$$=A^{(\alpha_1\alpha_2)}(M;p)\sum_{\alpha_1'\alpha_2'}\int_0^\infty p'^2dp'\{[N^{(\alpha_1\alpha_2)}_{12}(p)N^{(\alpha_1'\alpha_2')}_{12}(p')V^{J\pm1}_1(p,p')+$$

$$+\alpha_1\alpha_2\alpha_1'\alpha_2'N^{(-\alpha_1-\alpha_2)}_{12}(p)N^{(-\alpha_1'-\alpha_2')}_{12}(p')V_{1(J\pm1)}(p,p')+$$

$$+(\alpha_1\alpha_1'N^{(-\alpha_1\alpha_2)}_{12}(p)N^{(-\alpha_1'\alpha_2')}_{12}(p')+ \qquad (2.49)$$

$$+\alpha_2\alpha_2'N^{(\alpha_1-\alpha_2)}_{12}(p)N^{(\alpha_1'-\alpha_2')}_{12}(p'))V^J_2(x;p,p')]R^{(\alpha_1'\alpha_2')}_{J\pm11J}(p')+$$

$$+[\alpha_1\alpha_2\alpha_1'\alpha_2'N^{(-\alpha_1-\alpha_2)}_{12}(p)N^{(-\alpha_1'-\alpha_2')}_{12}(p')\frac{2}{2J+1}V_{1(-)J}(p,p')]R^{(\alpha_1'\alpha_2')}_{J\mp11J}(p')\},$$

where

$$A^{(\pm\pm)}=\pm1,\ A^{(\pm\mp)}=0,\ \text{(SAL)};\ A^{(+\pm)}=\pm1,\ A^{(-\pm)}=0,\ \text{(GR)};$$

$$A^{(\pm\pm)}=\pm1,\ A^{(\pm\mp)}=\frac{M}{\omega_1+\omega_2},\ \text{(MW)};$$

$$A^{(\alpha_1\alpha_2)}=\frac{M+(\alpha_1\omega_1+\alpha_2\omega_2)}{2(\omega_1+\omega_2)},\ \text{(CJ)}; \qquad (2.50)$$

$$A^{(\alpha_1\alpha_2)}=\frac{1}{2BR}\Big[M(a-p_0^{(+)2})-p_0^{(+)}M(\alpha_1\omega_1-\alpha_2\omega_2)+B(\alpha_1\omega_1+\alpha_2\omega_2)\Big],$$

(MNK).

Note that the last expression in (2.50) is obtained from (3.62) in [1] after some transformation.

Main difference between the system of equations (2.41)-(2.46) and (2.48), (2.49) with the expression (2.50) is following: 1) In the wave functions $R_{LSJ}^{(\alpha_1\alpha_2)}(p)$ satisfying the system of equations (2.48), (2.49) for (SAL) and (GR) versions the nonzero functions are only $R_{LSJ}^{(\pm\pm)}(p)$ and $R_{LSJ}^{(+\pm)}(p)$ respectively (about this fact was mentioned above), whereas in the corresponding system of equations (2.41), (2.42), (2.43), (2.44) all components of wave functions $R_{LSJ}^{(\alpha_1\alpha_2)}(p)$ are nonzero; 2) The system of equations (2.48), (2.49) for the MW, CJ and MNK versions are nonlinear over M whereas the system of equations (2.45), (2.46) are linear one; 3) Dirac equations (2.41), (2.42) obtained from the Salpeter equation do not depend on mixture parameter x, what can be seen directly from (2.13), (2.14).

3. PROCEDURE FOR SOLVING THE OBTAINED EQUATIONS

For solving bound-state equations (2.41)-(2.46) or (2.48), (2.49), we need to specify the interaction potentials V_{OG} and V_C (2.14). Below for $V_C(r)$ we use the following form [1], [8]

$$V_C(r)=\frac{4}{3}\alpha_S(m_{12}^2)\left(\frac{\mu_{12}\omega_0^2r^2}{2\sqrt{1+A_0m_1m_2r^2}}-V_0\right) \tag{3.1}$$

$$\alpha_S(Q^2)=\frac{12\pi}{33-2n_f}\left[\ln\frac{Q^2}{\Lambda^2}\right]^{-1},\ m_{12}=m_1+m_2,\ \mu_{12}=\frac{m_1m_2}{m_{12}}, \tag{3.2}$$

where Q^2 is the momentum transferred and the 4/3 comes from the color-dependent part of the $q\bar{q}$ interaction, n_f is the number of flavors (n_f =3 for u, d, s quarks; n_f =4 for u, d, s, c; n_f =5 for u, d, s, c, b). ω_0, A_0, V_0 and Λ are considered to be the free parameters of the model. The potential given by expression (3.1) effectively reduces to the harmonic oscillator potential for the light quarks u, d, s and to the linear potential to the heavy c, b quarks is the dimensionless parameter A_0 is chosen small enough. Moreover, asymptotically, for a large r it is linear and almost flavor-independent. The one-gluon exchange potential is given by standard expression [1], [8]

$$V_{OG}(r) = -\frac{4}{3}\frac{\alpha_S(m_{12}^2)}{r^2}. \qquad (3.3)$$

Now we have to specify the numerical procedure for solution of the systems of radial equations (2.41)-(2.46), (2.48), (2.49). A possible algorithm looks as follows: we choose the known basic functions by $R_{nL}(p)$. The unknown radial wave functions are expanded in the linear combination of the basic functions

$$R_{LSJ}^{(\alpha_1\alpha_2)}(p) = \sqrt{2M(2\pi)^3}\sum_{n=0}^{\infty} C_{nLSJ}^{(\alpha_1\alpha_2)} R_{nL}(p), \qquad (3.4)$$

where $C_{nLSJ}^{(\alpha_1\alpha_2)}$ are the coefficients of the expansion. The integral equation for the radial wave functions is then transformed into the system of linear equations for these coefficients. If the transaction is carried out the finite system of equations is obtained that can be solved by using conventional numerical methods. The convergence of the whole procedure, with more terms taken into account in the expansion (3.4) depends on the successful choice of the basis. In case of the confining potential of form (3.1) it is natural to take as a basis the functions corresponding to oscillator potential, which is obtained from (3.1) at $A_0 = 0$, in non-relativistic limit of the system of

equations obtained from (2.41)-2.46), (2.48),(2.49). The radial wave functions in this case have the form [1] (the formula (4.52)).

$$R_{nL}(p) = p_0^{-3/2} R_{nL}(z), \quad p_0 = \sqrt{\mu_{12}\omega_0 \sqrt{\frac{4}{3}\alpha_S(m_{12}^2)}},$$

$$z = \frac{p}{p_0} \; R_{nL}(z) = c_{nL} z^L \exp(-\frac{z^2}{2}) {}_1F_1(-n, L+\frac{3}{2}, z^2),$$

$$c_{nL} = \sqrt{\frac{2\Gamma(n+L+\frac{3}{2})}{\Gamma(n+1)}} \frac{1}{\Gamma(L+\frac{3}{2})},$$

where ${}_1F_1$ denotes the confluent hypergeometric function.

Now, satisfying the expression (3.4) into the system of equations (2.41)–(2.46) gebraic equations for the coefficients $C_{nLSJ}^{(\alpha_1\alpha_2)}$ can be obtained

$$MC_{nLSJ}^{(\alpha_1\alpha_2)} = \sum_{\alpha_1'\alpha_2'} \sum_{n'L'S'} H_{nLSJ;n'L'S'J'}^{(\alpha_1\alpha_2;\alpha_1'\alpha_2')}(M) C_{nLSJ}^{(\alpha_1'\alpha_2')} . \qquad (3.5)$$

It is necessary to note that the matrix $H_{\alpha\beta}(M)$ depends on meson mass M only for MW, CJ and MNK versions as it can been seen from equations (3.6) for M is not linear one and therefore should be solved, e.g. by iteration. As to the system of Dirac equations (2.41)–(2.46) such a problem does not exist.

4. THE NUMERICAL RESULTS AND ADDITIONAL CONCLUSIONS

The main problem we have investigated at first stage is dependence of the existence of stable solutions of the eq. (3.6) i.e. the equations (2.41)–(2.46), (2.48), (2.49) on Lorentz (spin) structure of

the confining $q\bar{q}$ interaction potential, i.e. on the parameter x. This will be done taking as examples the $u\bar{s}$, $c\bar{u}$ and $c\bar{s}$, bound states with constituent quark masses $m_u = m_d = 280\,\text{MeV}$, $m_s = 400\,\text{MeV}$, $m_c = 1470\,\text{MeV}$ and the free parameters of the confining potential (3.1), (3.2) - $\omega_0 = 710\,\text{MeV}$, $V_0 = 525\,\text{MeV}$, $A_0 = 0.0270$, $\Lambda = 120\text{MeV}$

Note, that in [8] only the SAL version of 3D-reduction of Bethe-Salpeter equation was considered as to MW, CJ and MNK without additional approximation (2.4) with oscillator like potential ($A_0 = 0$ in (3.1)) were considered in Refs.7, 9.

The results of the calculations are given for states $^{2S+1}L_J$ (note, that for cases $^3S_1, ^3P_2$ are ignored additional corresponding terms $^3D_1, ^3F_2$ because they give small contribution in the calculated mass).

The additional conclusions (to pure theoretical results obtained in the section 2), which can be obtained from the Tables 1, 2 are the following:

1. The area of changing of parameters x, for which stable solutions of two-body Dirac equations exist, is a little enlarged compared for all versions of 3D-equations.
2. For $c\bar{u}$ and $c\bar{s}$ bound systems Gross version works better what is related to the large difference of constituent masses.
3. The area of existence of the stable solutions is enlarged with increasing of the constituent masses which is theoretically understandable.
4. Masses of the bound $q\bar{q}$ systems obtained from solutions of Dirac equations are bigger then masses corresponding to 3D-equations obtained from BS equation for all versions except GR version case.
5. It is very important, that for x=0.5 (i.e. the equal mixture of scalar and 4th-component of vector confining $q\bar{q}$-interaction potential) the stable solutions of considered relativistic equations always exist and can be used for investigations the mass spectrum and properties of bound $q\bar{q}$ systems.

Table 1. The dependence of the $q\bar{q}$ system mass for light constituent quarks on the mixing parameter x in the different 3D-reductions of Bethe-Salpeter equations and corresponding Dirac equations. "*" denotes the absence of the stable solutions. Masses are given in MeV.

x	0.0	0.1	0.3	0.5	0.7	0.9	1.0
	$u\bar{s}$ $^3S_1$ (892)						
SAL	*	812	870	914	950	980	993
SALD	979						
GR	839	859	897	934	967	*	*
GRD	944	947	954	962	975	*	*
MW	863	877	907	943	983	*	*
MWD	879	887	905	928	957	*	*
CJ	878	893	924	959	998	*	*
CJD	924	930	942	955	972	*	*
MNK	814	830	861	891	*	*	*
MNKD	923	929	941	955	972	*	*
	$u\bar{s}$ (1350)						
SAL	1189	1204	1213	1210	1202	1189	1182
SALD	1349						
GR	1233	1232	1229	1223	1218	*	*
GRD	1304	1302	1300	1298	1298	*	*
MW	1255	1253	1249	1250	*	*	*
MWD	1278	1274	1267	1260	1257	*	*
CJ	1268	1267	1263	1260	1264	*	*
CJD	1296	1294	1290	1287	1284	1285	*
MNK	1217	1212	1202	1190	*	*	*
MNKD	1295	1293	1289	1286	1284	*	*
	$u\bar{s}$ $^3P_2$ (1430)						
SAL	*	*	1189	1289	1367	1430	1458
SALD	1318						
GR	1119	1159	1237	1310	1381	*	*

GRD	1278	1284	1297	1314	1336	*	*
MW	1184	1209	1262	1326	1384	*	*
MWD	1185	1200	1234	1275	1326	*	*
CJ	1181	1211	1276	1345	1421	*	*
CJD	1254	1264	1286	1310	1337	1369	1388
MNK	1137		1223	1282	1344	1408	*
MNKD	1254	1264	1285	1309	1388	1372	*

Table 2. The dependence of the $q\bar{q}$ system mass for heavy constituent quarks on the mixing parameter x in the different 3D-reductions of Bethe-Salpeter equations and corresponding Dirac equations. "*" denotes the absence of the stable solutions. Masses are given in MeV.

x	0.0	0.1	0.3	0.5	0.7	0.9	1.0
	$c\bar{u}\ {}^1S_0$ (1863)						
SAL	1881	1895	1920	1943	1965	1985	1994
SALD	1983						
GR	1883	1896	1921	1944	1966	1986	1995
GRD	1979	1979	1978	1978	1978	1978	1979
MW	1915	1922	1935	1951	1972	*	*
MWD	1924	1929	1942	1958	1979	*	*
CJ	1921	1928	1943	1960	1982	*	*
CJD	1932	1937	1948	1961	1978	2003	*
MNK	1928	1934	1946	1961	1978	*	*
MNKD	1927	1932	1944	1958	1977	*	*
	$c\bar{u}\ {}^3S_1$ (2010)						
SAL	1883	1897	1922	1946	1968	1988	1988
SALD	1981						
GR	1886	1899	1924	1947	1969	1989	1999
GRD	1977	1977	1978	1979	1981	1982	1983
MW	1918	1924	1938	1955	1977	*	*

MWD	1921	1926	1939	1955	1975	*	*
CJ	1923	1930	1948	1963	1981	*	*
CJD	1932	1937	1948	1961	1978	2003	*
MNK	1930	1935	1948	1963	1981	*	*
MNKD	1927	1932	1944	1958	1977	*	*
	$c\bar{s}$ $^1S_0$ (1971)						
SAL	2020	2031	2055	2070	2088	2105	2113
SALD	2106						
GR	2023	2033	2052	2071	2089	2106	2114
GRD	2106	2100	2100	2100	2100	2100	2100
MW	2044	2050	2062	2077	2094	2118	*
MWD	2052	2058	2070	2084	2101	2126	*
CJ	2051	2057	2071	2087	2105	2126	*
CJD	2063	2067	2077	2087	2100	2116	2127
MNK	2052	2057	2069	2082	2097	2116	*
MNKD	2059	2063	2073	2085	2100	2120	*
	$c\bar{s}$ $^3S_1$ (2107)						
SAL	2023	2033	2054	2073	2091	2108	2116
SALD	2104						
GR	2025	2035	2055	2074	2092	2110	2118
GRD	2098	2099	2100	2102	2103	2105	2106
MW	2047	2053	2065	2080	2098	2124	*
MWD	2049	2054	2066	2080	2097	2121	*
CJ	2053	2060	2074	2089	2108	*	*
CJD	2063	2067	2077	2089	2108	2116	2127
MNK	2054	2059	2071	2084	2100	2119	*
MNKD	2059	2063	2073	2085	2100	2120	*

5. ACKNOWLEDGMENTS

The authors thank A. Khelashvili and A. Rusetsky for useful discussions and comments.

REFERENCES

1. T. Kopaleishvili, Phys. Part. Nucl. 32, 2001, 560.
2. E. E. Salpeter, Phys. Rev. 87, 1952, 328.
3. F. Gross, Phys. Rev. 186, 1969, 1448; C26, 1982, 2203.
4. V. B. Mandelzweig, S. J. Wallace, Phys. Lett. B197, 1987, 469.
5. E. D. Cooper, B. K. Jennings, Nucl. Phys. A500, 1989, 551.
6. K. M. Moung, J. W. Norbury, D. E. Kahana, J. Phys. G. Nucl. Part. Phys. 22, 1996, 315.
7. T. Babutsidze, T. Kopaleishvili, A. Rusetsky, Phys. Lett. B426, 1998, 139.
8. A. Archvadze, M. Chachkhunashvili, T. Kopaleishvili, A. Rusetsky, Nucl. Phys. A581, 1995, 460.
9. T. Babutsidze, T. Kopaleishvili, A. Rusetsky Phys. Rev. C59, 1999, 976.
10. Z. K. Silagadze, A. A. Khelashvili, Theor. Math. Phys. 61, 1984, 431.
11. C. Semay, R. Cenleneer, Phys. Rev. D48, 1993, 4361.
12. H. W. Crater, P. Van Alstine invited paper presented at a conference on September 12th, 1997 at the University of Georgia in honor of Professor Donald Robson on his 60th birthday.

Tbilisi State University

თ. ბაბუციძე, თ. კოპალეიშვილი, დ. ყურაშვილი

ბმული $q\bar{q}$ სისტემები ორ-სხეულოვან დირაკის განტოლებების ფარგლებში, რომლებიც მიღებულია ბეტე-სოლპიტერის განტოლების 3-განზომილებიანი რედუქციის შედეგად სხვადასხვა ვარიანტებში მიღებულ განტოლებებიდან

კვარკ-ანტიკვარკის ($q\bar{q}$) სისტემებისათვის მიღბულია ორ-სხეულოვანი დირაკის განტოლებები, ბეტე-სოლპიტერის (ბს) განტოლებიდან 3-განზომილებიანი რედუქციის შედეგად მიღებული განტოლებებიდან ხუთ სხვადასხვა ვარიანტში, როცა ბს-განტოლების

გული განხილულია ერთდროულ (სტატიკურ) მღვარში იმპულსურ წარმოდგენაში, რისთვისაც გამოყენებულია დამატებითი ბუნებრივი მიახლოებები. ფორმულირებულია ნირმირების პირობები ტალღური ფუნქციებისათვის, რომლებიც აკმაყოფილებენ მიღებულ ორ-სხეულოვან დირაკის განტოლებებს. $q\bar{q}$ ურთიერთქმედების პოტენციალის კონფაინმენტის ნაწილისათვის ლორენც (სპინური) სტრუქტურა აღებულია შემდეგი ფორმით $x\gamma_1^0 \otimes \gamma_2^0 + +(1-x)\mathrm{I}_1 \otimes \mathrm{I}_2$, სადაც $0 \le x \le 1$. ნაჩვენებია, რომ სოლპიტერის განტოლებიდან მიღებული დირაკის ორ-სხეულოვანი განტოლებები არაა დამოკიდებული b-ზე. რაც შეეხება სხვა ვარიანტებს, ასეთი დამოკიდებულება ძალაში რჩება. ბმული სისტემებისათვის $u\bar{s}$, $c\bar{u}$, $c\bar{s}$ გამოკვლეულია განტოლებების სტაბილური ამოხსნების არსებობის დამოკიდებულება b-ზე და შედარებულია იმ შედეგებთან, რომელიც მიიღება ბს-განტოლების 3-განზომილებიანი რედუქციის შედეგად დამატებითი მიახლოების გარეშე და მიღებულია ზოგიერთი ახალი დასკვნა.

ON THE UNIVERSALITY AND ASYMPTOTIC BEHAVIOR OF THE MULTIPLICITY DISTRIBUTIONS OF CHARGED HADRONS IN THE COLLISIONS AT HIGH ENERGIES IN THE FRAMEWORK OF THE CLUSTER-CASCADING MODEL

L. Akhobadze, V. Garsevanishvili, T. Jalagania, Yu. Tevzadze

Accepted for publication April, 2004

ABSTRACT. Multiplicity distributions of charged hadrons created in the e^+e^-, PP($\bar{P}$) and A_iA_t (nucleus-nucleus) collisions at high energies are analyzed in the framework of the cluster-cascading model (CCM). It is shown that the average numbers of clusters <N> reach corresponding plateaus (it depends on the type of collision e^+e^-, PP($\bar{P}$), A_iA_t). Multiplicity distributions of particles inside cluster do not depend on the type of colliding objects and have universal character.

ITRODUCTION

Cluster-cascading model (CCM) is based on the Negative Binomial Distribution (NBD) which is of the form [1]

$$P_n(<n>,K) = \frac{\Gamma(n+K)}{n!\Gamma(K)}\left(\frac{<n>}{<n>+K}\right)^n\left(\frac{K}{<n>+K}\right)^K , \qquad (1)$$

where $<n>\equiv<n_\pm>$ is average multiplicity of charged secondary hadrons . Parameter K determines the form of the distribution.

Quantities K and <n> are related to the dispersion $D^2 (D = \sqrt{<n^2> - <n>^2})$ as follows:

$$K = \frac{<n>^2}{D^2 - <n>} . \qquad (2)$$

Recurrence relation between P_n and P_{n+1} is of the form

$$\frac{(n+1)P_n+1}{P_n} \equiv g(n) = \alpha + \beta n \qquad (3)$$

α and β are related to <n> and K in the following way:

$$\alpha = \frac{K < n >}{K + < n >}, \qquad \beta = \frac{< n >}{K + < n >} . \qquad (4)$$

According to CCM the process of multiple production is interpreted as follows: after the collision of high energy objects (leptons, hadrons, nuclei) an excited multiparticle compound system is created in the form of N-cluster state; Each cluster is produced from one particle (which is produced in the initial act of the collision) called "patriarch". One "patriarch" forms one cluster. It is assumed that "patriarch" (clusters) can be considered as resonances which formed and decaying independently from each other.

<N>- average number of clusters is given by the expression

$$< N >= \frac{< n >}{< n_c >} , \qquad (5)$$

where $<n_c>$ is the average number of particles in the cluster

$$< n_c >= - \frac{\beta}{(1-\beta)\ln(1-\beta)} . \qquad (6)$$

Multiplicity distribution of particles inside the cluster is given by

$$F(n_c) = \frac{-(\beta)^{n_c}}{n_c \ln(1-\beta)} . \qquad (7)$$

The dispersion of particles in clusters is given by the expression

$$D_c = \sqrt{< n_c^2 > - < n_c >^2} , \qquad (8)$$

where

$$< n_c^2 >= -\frac{< n_c >}{(1-\beta)} \qquad (9)$$

THE ANALYSIS OF EXPERIMENTAL DATA

In Refs. [2,3] multiplicity distributions at charged secondaries P_n in e^+e^--annihilation (in the energy range $14 \leq \sqrt{s} \leq 130$ GeV), $PP(\bar{P})$ - collisions (in the energy range $6 \leq \sqrt{s} \leq 900$ GeV) and A_tA_t-collisions (in the energy range $2.48 \leq E_L \leq 10$ AGeV) have been considered in the framework of the CCM.

It has been shown that the average number of produced clusters $< N >$ practically does not depend on the energy (in the energy interval considered) and on the atomic weights of colliding nuclei and is approximately equal to ~ 4.5.

Analysis of data for A_tA_t- collisions at 200 AGeV shows that the number of created clusters practically remains the same ($4.77 \pm 0.25 \div 5.98 \pm 0.35$) (see Table 1).

It has been shown [2,3] that in e^+e^- - annihilation average number of cluster <N> reaches the plateau with the value ~ 15. Analysis of data at higher energies ($\sqrt{s}$ >130 GeV) confirms the assumption on the plateau in <N> (see Table 2).

In $PP(\bar{P})$ – collisions the plateau value $<N> \approx 8$ is reached at $\sqrt{s} \approx 30$ Gev and this value practically does not change up to the energy $\sqrt{s} = 900$ GeV [2,3].

Properties of the multiplicity distributions are studied usually by the analysis of the behavior of their momenta and first of all D(<n>). It is known that the dispersion increases linearly with <n>. The dependence is approximated by the formula

$$D = a + b <n>, \qquad (10)$$

which is called Malhotra-Wroblewski formula [4]. Such a dependence takes place for different colliding objects ($\pi^{\pm}p$, $k^{\pm}p$, $PP(\overline{P})$, A_iA_t) [4,5].

Parametrs in Equation (10) weakly depend on the of colliding objects. For $PP(\overline{P})$ collisions in the energy interval ($3 \leq \sqrt{s} \leq 900$) GeV parameters in Eq (10) have the values: $a = -0.56 \pm 0.02$; $b = 0.58 \pm 0.01$ (Table 3, Fig.1.) [4,5,6].

For the additional check the D (<n>) – dependence has been approximated by the expresion

$$D(<n>) = a + b<n> + c<n>^2 \qquad (11)$$

It turned out that this fact does not make the discription better, the values of parameters a and b do not change, the value of the parameter c is practically zero ($c = 0.00015 \pm 0.00060$). Thus the eviation from the linearity is not observed. This is in agreement with data at lower energies [4].

In Refs [2,3] the dependences D (< n >) and $D_c(<n_c>)$ (D_c is the dispersion of the distribution of particles in the cluster, $<n_c>$ is the average number of hadrons in the cluster) for e^+e^-, $PP(\overline{P})$ and A_iA_t – collisions have been studied. It has been shown that in the energy interval studied $14 \leq \sqrt{s} \leq 130$ GeV for e^+e^- - collisions, for $PP(\overline{P})$ – collisions $6 \leq \sqrt{s} \leq 900$ GeV, and for A_iA_t – collisions $E_L \leq 10$ AGeV) the dependence D (<n>) are placed on three different curves.
But the dependence $D_c(<n_c>)$ is of the universal character – one curve for all types of interaction.

In the present paper the dependences D (< n >) and $D_c(<n_c>)$ are analyzed in a more wide interval of energy and for more heavy nuclei – for e^+e^- -interaction three points are added ($\sqrt{s}$ =161, 189 and 200 Gev), for A_iA_t –collisions 8 points are added p(Ag, Ar, Xe, Au), S(S,Cu) and O(Cu,Au) at 200 AGeV [7-14].
Results of the approximation by the formula (10) are given in Table 3 (see Fig.1).

The D(<n>) – dependence is again presented by three curves for e^+e^-, $PP(\overline{P})$ and A_iA_t –collisions (curves 1,2,3 respectively).

The values of the slope parameter b

Table 1

Average characteristics of multyplicity distribution of secondary charged hadrons in A_iA_t – collisions at 200 AGeV

Characteristics	SS	SCu	OCu	OAu
$\langle n \rangle$	75 ±4	97 ±5	70 ±3	98 ±5
D	72 ±3	94 ±4	69 ±4	96 ±5
K	1.1	1.08	1.05	1.05
$\langle n_c \rangle$	12.53 ±0.06	19.76 ±0.10	12.53 ±0.06	20.53 ±0.11
D_c	21.66 ±0.90	37.49 ±1.59	21.67 ±1.26	39.05 ±2.03
$\langle N \rangle$	5.98 ±0.35	4.91 ±0.30	5.56 ±0.36	4.77 ±0.25

Table 2

Characteristics of multiplicity distributions of secondary charged hadrons in e^+e^- - collisions in the energyinterval

$(14 \le \sqrt{s} \le 200)$ GeV

$(s)^{1/2}$	14	22	34	91	130	161	189	200
$\langle n \rangle$	9.40 ±0.40	11.3 ±0.4	13.50 ±0.50	20.74 ±0.81	23.46 ±0.70	24.46 ±0.80	27.47 ±0.50	27.58 ±0.64
D	3.22 ±0.15	3.77 ±0.16	4.47 ±0.20	6.28 ±0.35	7.55 ±0.50	7.68 ±0.71	8.71 ±0.25	8.64 ±0.33
$\langle n_c \rangle$	1.12 ±0.05	1.14 ±0.04	1.22 ±0.04	1.41 ±0.05	1.59 ±0.07	1.60 ±0.05	1.74 ±0.07	1.72 ±0.04
D_c	0.30 ±0.01	0.37 ±0.01	0.56 ±0.05	0.82 ±0.05	1.12 ±0.07	1.14 ±0.10	1.35 ±0.04	1.31 ±0.05
$\langle N \rangle$	8.40 ±0.36	9.65 ±0.34	11.06 ±0.41	13.06 ±0.48	14.99 ±0.63	15.29 ±0.44	15.79 ±0.29	16.12 ±0.37
K	90.91 ±3.4	43.48 ±2.1	27.78 ±1.2	22.73 ±1	17.13 ±0.80	17.33 ±0.85	15.26 ±0.60	16.16 ±0.65

Results of the approximation of D (< n >) – dependence be eq. (10) D =a + b <n >

Reaction	Energy Interval [GeV]	a	b
$PP(\overline{P})$	$3 \leq \sqrt{s} \leq 900$	-0.56±0.02	0.58±0.01
$\pi^+ p$	$7 \leq E_L \leq 100$	-0.61±0.06	0.55±0.02
$K^+ P$	$8 \leq E_L \leq 100$	-0.46±0.14	0.53±0.04
e^+e^-	$14 \leq \sqrt{s} \leq 200$	0.41±0.05	0.03±0.01
A_iA_t	$\langle n \rangle \leq 25$	-1.22±0.04	0.79±0.01

Results of the approximation of $D_c(\langle n_c \rangle)$ – dependence be eq. (10) $D_c = a + b \langle n_c \rangle$

pp(p), e^+e^-, A_iA_t	Summary Data	-1.62±0.02	1.72±0.02

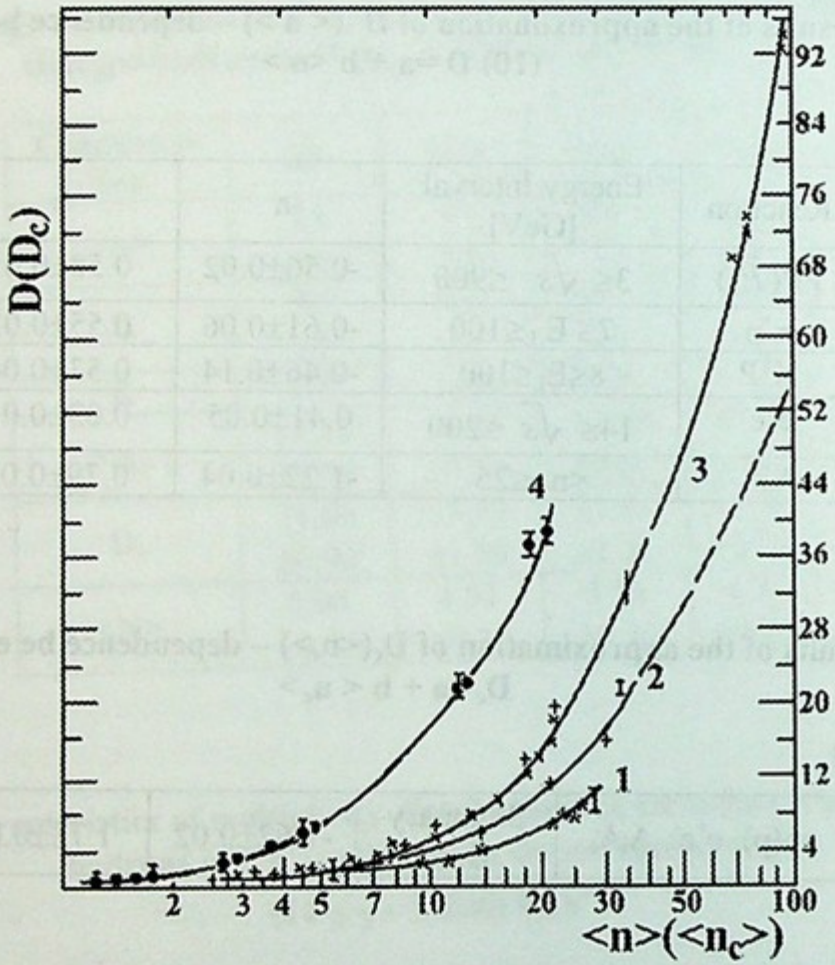

Fig.1. The dependence of the dispersion – D, on the <n> -average multiplicity - D(<n>)

Curve 1 – e^+e^- collision

Curve 2 – PP($\overline{P}$) collision

Curve 3 – A_iA_t collision

Curve 4 – the dependence $D_c(<n_c>)$ for e^+e^-, PP($\overline{P}$) and A_iA_t – collisions (summary data)

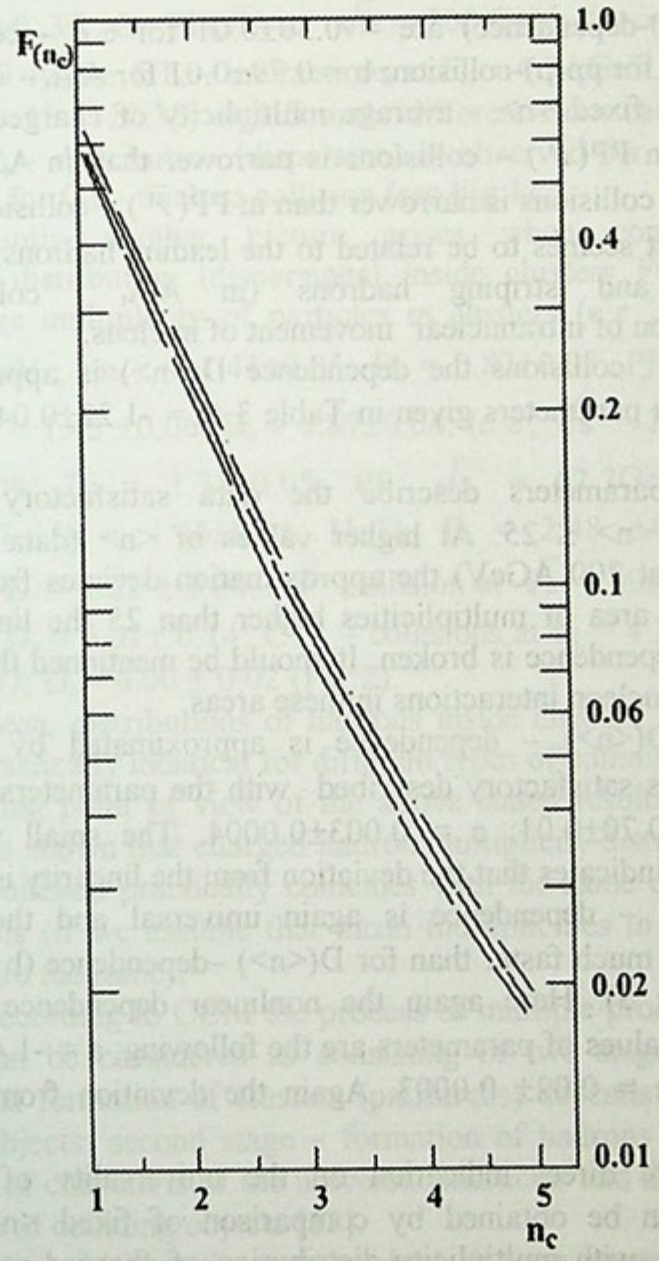

Fig.2. $F(n_c)$ – multiplicity distribution of particles (hadrons) inside clusters for fixed $\langle n_c \rangle$

HeTa(E_L = 2.48AGeV--); (PP ($\sqrt{s}$ = 62.2GeV- - -); (e^+e^-($\sqrt{s}$ = 200GeV —)). $\langle n_c \rangle$ = 1.70; D_c = 1.24

(for D(<n>)-dependence) are = 0.30±0.01 for e^+e^- - collisions; b = 0.58 ± 0.01 for pp(p)-collision; b = 0.79±0.01 for A_iA_t – collisions.

Thus at fixed <n> - average multiplicity of charged hadrons the dispersion in PP($\overline{P}$) – collisions is narrower than in A_iA_t - collisions and in e^+e^- - collisions is narrower than in PP($\overline{P}$) – collisions.

This fact seemes to be related to the leading hadrons (in PP($\overline{P}$) – collisions) and striping hadrons (in A_iA_t - collisions); or, intensification of intranuclear movement of nucleus.

In A_iA_t - collisions the dependence D(<n>) is approximated by Eq.(10) with parameters given in Table 3 (a = -1.22±0.04; b = 0.79 ± 0.01).

These parameters describe the data satisfactory up to the multiplicity <n> ≤ 25. At higher values of <n> (data on S(S,Cu), O(Cu, Au) at 200 AGeV) the approximation deviates from the data. Thus in the area of multiplicities higher than 25 the linearity of the D(<n>) – dependence is broken. It should be mentioned that there may arise multi nucleon interactions in these areas.

If the D(<n>) – dependence is approximated by Eq.(11) the experiment is satisfactory described with the parameters a = -0.94 ± 0.06; b = 0.70±0.01; c = 0.003±0.0004. The small value of the parameter c indicates that the deviation from the linearity is small.

$D_c(<n_c>)$ – dependence is again universal and the growth of dispersion is much faster than for D(<n>) –dependence (b = 1.72±0.02 Fig.1, Table 3). Here again the nonlinear dependence (11) works better. The values of parameters are the following: a = -1.49±0.03; b = 1.60±0.02; c = 0.02± 0.0003. Again the deviation from linearity is small.

The more direct indication on the universality of intracluster dynamics can be obtained by comparison of fixed <n> - average multiplicities, with multiplicity distribution of charged secondaries P_n (or with D - dispersion) for e^+e^-, pp(p) and A_iA_t - collisions . The results obtained have to be compared with the behavior of $F(n_c)$ – multiplicity distributions of particles inside clusters.

Experimental data show [2,3,7,8] that multiplicity distributions P_n (or dispersions D) for e^+e^-, PP($\overline{P}$) and A_iA_t – collisions at fixed <n>, for example $< n > \approx 2\,0$ (for e^+e^- at $\sqrt{s}$ = 91 GeV, <n> = 20.71±0.80;

D = 6.98±0.35; for PP($\overline{P}$) at $\sqrt{s}$ = 200 GeV, <n> =21.30 ±0.80; D = 10.90±0.40; for CT_a – interactions at E_L = 4.3AGeV, <n> = 19.75 ± 0.40; D = 15.71±0.35) significantly different from each other. The narrowest P_n - distribution (dispersion) is observed for e^+e^- collision, the widest – for CT_a- nucleus collision (see Fig.1).

Significantly another picture arises when considering the multiplicity distribution (dispersions) inside clusters $F(n_c)$, at fixed $\langle n_c \rangle$ average multiplicity of particles in clusters (e^+e^- - collision at $\sqrt{s}$ = 91GeV ; $\langle n_c \rangle$ = 1.41±0.05; D_c = 0.82±0.03. PP, $\sqrt{s}$ = 30.4 GeV; <nc> = 1.43 ±0.06; D_c = 0.87±0.04. (e^+e^-, $\sqrt{s}$ = 200GeV; $\langle n_c \rangle$ = 1.72±0.04. D_c = 1.31±0.05; PP, $\sqrt{s}$ = 62.2GeV; $\langle n_c \rangle$ = 1.69±0.07; D_c = 1.26±0.05; HeTa, E_L = 2.48 AGeV; $\langle n_c \rangle$ = 1.67±0.05; D_c = 1.22 ± 0.04. P$\overline{P}$ -collision at $\sqrt{s}$ = 900 GeV, $\langle n_c \rangle$ = 4.55±0.12; D_c = 6.01± 0.14; CTa – collisions at E_L = 4.3 AGeV, $\langle n_c \rangle$ = 4.50 ±0.07; D_c = 6.00 ± 0.02 (Fig.2).

As is seen, distributions of hadrons inside clusters $F(n_c)$, at fixed $\langle n_c \rangle$ are practically identical for different types of colliding objects.

Interesting point of view of the above stated results is mentioned in [13]. It is shown that charged hadron multiplicity distribution per jet for e^+e^- - collision practically coincides with the same distributions in pp collisions (if we assume that mean multiplicities in e^+e^- and pp-collisions are the same).

Thus according to CCM the process of multiple production at high energies can be considered as consisting of two stages: first stage-creation and formation of clusters (patriarchs) depends on the type of colliding objects; second stage – formation of hadrons inside clusters and decay of clusters is of the universal character and does not depend on the type of colliding objects [13].

It can be said, that the picture obtained is in accordance with the existing chromodinamical models of particle production at high energies.

According to this models the interaction process at high energy can be considered of consisting of two stages – first: partons are created (this stage depends on the type of interaction (strong, weak,

electromagnetic); second stage - hadronization of partons occurs [9,10].

The authors express their deep gratitude to D. Chokheli, D. Khubua and Z. Metreveli for help.

REFERENCES

1. A.Giovanini, L. Van Hove. Z. Phys. C. **30,** 1986, 391.
2. L. Akhobadze et al. Proceedings of I. Javakhishvili Tbilisi State University, **337,** Physics **35,** 2000, 152.
3. Sh. Esakia et al. On multiplicity distribution of charged secondaries in the collisions of relativistic nuclei. hep-ph/ 9704251 (IHEP, Tbilisi, Georgia).
4. V. S. Murzin, L. I. Saricheva. High Energy Hadrons Interactions., Moscow, 1983, (Russia).
5. T. Jalagania et al. Proceedings of I. Javakhishvili Tbilisi State University, **345,** Physics **36-37,** 2001,19.
6. N. Grigalashvili et al. Yad Phys. **48,** 1988, 476.
7. P. Alner et al. (UA5 Collaboration) Phys Lett B. **167,** 1986, 476.
8. P. Abreu et al. (DELPHI Collaboration) Z. Phys. C. **50,** 1991, 185.
9. V. Grishin, UFN **148,** 1988, 221, (Russia).
10. V. Grishin. Quarks and hadrons interactions at high energy., Moscow, 1988, (Russia).
11. D. Brick et al. Phys Rev. D, **39,** 1980, 2484 C. De Marzo et al. Phys Rev.D. 1982, **26,** 1019.
12. J. Bachler et al. Charge particle multiplicity's in nuclear collisions at 200AGeV (NA35 Collaboration) 1991.
13. K. Goulianos. Phys. Lett. B. **193,** 1987, 151.
14. N. Angelov et al. JINR, R1-12281, Dubna, Sov. J. Nucl. Physics. **30,** 1979, 1590

Tbilisi State University

ლ. ახობაძე, ვ. გარსევანიშვილი, ი. თევზაძე, თ. ჯალაღანია

მაღალ ენერგიებზე დაჯახებისას დაბადებული დამუხტული ნაწილაკების მრავლობითობების განაწილებების უნივერსალობისა და ასიმპტოტური ყოფაქცევის საკითხები კლასტერულ-კასკადური მოდელის ფარგლებში

დასკვნა

მაღალ ენერგიებზე კლასტერულ-კასკადური მოდელის ფარგლებში შესწავლილია ელექტრონულ-პოზიტრონული (e^+e^-), ნუკლონ-ნუკლონური (PP), ($P\bar{P}$) და ბირთვი-ბირთვულ (AlAt) დაჯახებებში დაბადებული დამუხტული ნაწილაკების მრავლობითობების განაწილებები. ნაჩვენებია, რომ კლასტერთა საშუალო რაოდენობები აღნიშნული ტიპის დაჯახებებში ენერგიის გაზრდით გადიან შესაბამის პლატოებზე. ნაჩვენებია აგრეთვე, რომ მრავლობითობების განაწილებები კლასტერის შიგნით არ არის დამოკიდებული ნაწილაკების ტიპზე და უნივერსალური ხასიათისაა.

AVERAGE MULTIPLICITY OF CHARGED SECONDARIES AS A FUNCTION OF THE NUMBER OF INTERACTING NUCLEONS IN THE COLLISIONS OF RELATIVISTIC NUCLEI IN THE ENERGY RANGE OF (0.250-200) AGEV

L. Akhobadze, V. Garsevanishvili, T. Jalagania, Yu. Tevzadze, G. Vanishvili

Accepted for publication April, 2004

ABSTRACT. Average multiplicity of charged secondaries (produced in collisions of light and intermediate mass nuclei with intermediate and heavy mass nuclei, in the energy range of (0.250-200) AGeV) as a function of the number N_A of nucleons participating in the interactions, have been analysed.

It is shown that at low (≤0.400 AGeV) and at very high (200 AGeV) energies the deviation from the linear $< n (N_A) >$ - dependence is observed. An attempt is undertaken to explain the breakdown of linearity by the absorption (in heavy targets) and small cascade multiplication (at low energies); by the growth of the contribution of neutral particles to the total multiplicity and by the certain role of multiparticle (collective) proceses, which cause the neutralization of negative particles (at 200 AGeV).

INTRODUCTION

In references [1-7] the dependence of the average multiplicity <n> of charged secondaries produced in $A_i A_t$ -nucleus-nucleus interactions (A_i - atomic number of incoming nucleus, A_t - atomic number of the target) as functions of R, R_n b N_A (R, R_n and N_A are numbers of interacting protons, neutrons and nucleons) are studied. Quantities R, R_n and N_A are defined as follows [1,2,3].

$$R = (Z_i A_t^{2/3} + Z_t A_i^{2/3}) / (A_i^{1/3} + A_t^{1/3})^2 \qquad (1)$$

Z_i (Z_t)- the charge of the incoming (target) nucleus.

$$R_n = (N_i A_t^{2/3} + N_t A_i^{2/3}) / (A_i^{1/3} + A_t^{1/3})^2 \quad (2)$$

N_i (N_t)- a number of neutrons in the incoming (target) nucleus

$$N_A = (A_i A_t^{2/3} + A_t A_i^{2/3}) / (A_i^{1/3} + A_t^{1/3})^2 \quad (3)$$

Expression for R, R_n and N_A is derived assuming that the nucleons have sharp radii [1,3]. They are introduced in the framefork of the geometrical approach and can be interpreted as the maximal number of nucleons from both nuclei, which can participate in the collision, provided the total overlapping of colliding ions [6].

It is evident that in the reality a less than N_A nucleons are participating.

However one can assume that in central collisions the number of interacting nucleons is growing and approaches N_A. Note, that N_A does not depend on criteria of the event selection and in contrast to average number of NN - collisions is not connected with the uncertainity in choice of cross-section, i. e. it is exactly definite.

The analysis of data has shown, that at any energy and any A_i and A_t the dependence of average multiplicity on the number of protons $\langle n(R) \rangle$ is linear. The equality $\langle n(R) \rangle = R$ (according to refs [1, 2, 4, 7]) corresponds to the geometrical picture of the interaction, when the contribution to the multiplicity is given by protons only (one active proton gives one charged particle). Such a picture is realized in (p, He, Ne, Ar) (Ca, U) - collisions at the energy of 0.250 AGeV.

At the energy 0.400 AGeV a deviation from the geometrical picture is observed. At the energy 1.04 AGeV (and higher) a significant deviation from the geometrical picture is observed, but, the linearity of the $\langle n(R) \rangle$ - dependence is preserved (Fig.1a).

The question arises: whether or not the linearity is preserved in $\langle n(R_n) \rangle$ and $\langle n(N_A) \rangle$ dependences and what causes the breakdown of linearity.

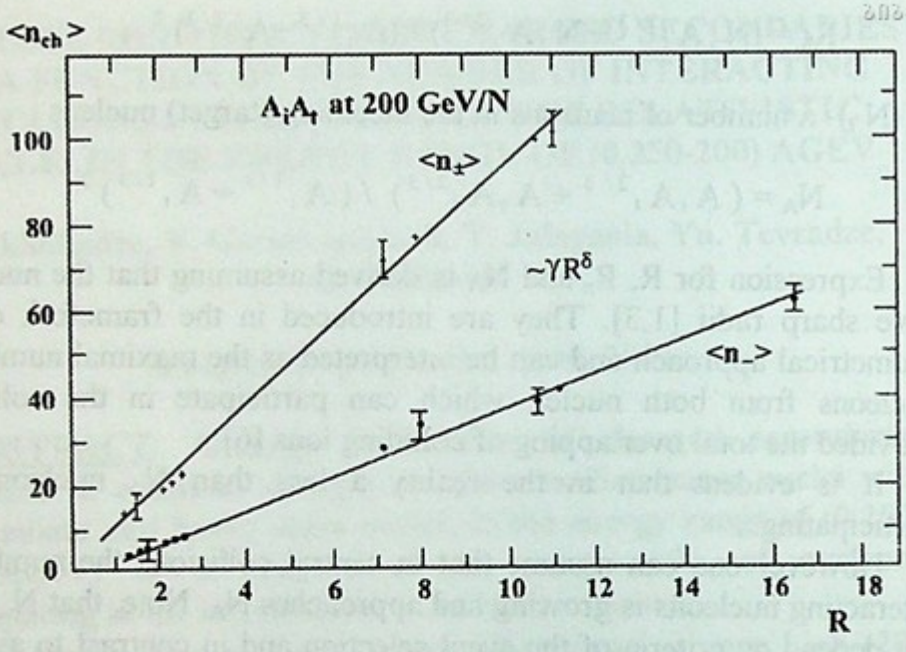

Fig.1a

Fig.1. $<n_{ch}>$ average hadrons multiplicity as a function of the number of interacting protons R, neutrons R_n and N_A – nucleons, for $A_i A_t$ -collisions at 200 AGeV.

„•" - negative hadrons for p(Mg,S,Ar,Ag,Xe,Au), O(Cu,Au), S(S,Cu,Pb) collisions.

„+"- total charged hadrons multiplicity for p(Mg,Ar,Ag,Xe,Au), O(Cu,Au), S(S,Cu)- collisions.

1a. $<n_{\pm}(R)>$ - dependence for all charged secondary hadrons, $<n_-(R)>$ - dependence for negatively charged secondary hadrons.

1b. The same as on Fig.1a, but only for R_n - the number of neutrons.

1c. The same as on Fig.1b, but only for N_A - the number of nuclons

ANALYSIS OF EXPERIMENTAL DATA ON $<N_i(R)>$, $<N_i(R_N)>$ AND $<N_i(N_A)>$ - DEPENDENCES AT 200 AGEV

In the present article the $<n_i(R)>$, $<n_i(R_n)>$ and $<n_i(N_A)>$ - dependences in p(Mg, S, Ar, Ag, Xe, Au), O(Cu, Au), S(S, Cu, Pb) - interactions at 200 AGeV [8, 9, 10] are analysed. Data at other energies [1-7], are used for comparison. $<(n_i)>$ - is the average multiplicity of charged hadrons; „i" = „±" - all charged hadrons; „i" = „-" negatively charged hadrons.

$<n_i(R)>$, $<n_i(R_n)>$ b $< n_i(N_A)$ - dependences for $A_i A_t$- collisions are approximated by the formula

$$< n_i >= \gamma \tilde{R}^{\delta} \qquad (\tilde{R} = R, Rn, N_A). \tag{4}$$

Results of the approximation are presented in Figs. 1a, 1b, 1c. $<n(R)>$ - dependence for p(Mg, S, Ar, Ag, Xe, Au), O(Cu, Au) and S(S, Cu, Pb) - interactions is linear for both $<n_{\pm}>$ ($\delta = 0.98 \pm 0.01$; $\gamma = 9.59 \pm 0.01$) and $<n_->$ ($\delta = 1.02 \pm 0.01$; $\gamma = 3.18 \pm 0.08$). However, the dependence $<n_i(R_n)>$ is clearly nonlinear ($\delta = 0.80 \pm 0.01$; $\gamma = 12.10 \pm 0.21$ for $<n_{\pm}>$; and $\delta = 0.86 \pm 0.01$; $\gamma = 4.02 \pm 0.07$ for $<n_->$).

The $<n(N_A)>$ dependence is also nonlinear ($\delta = 0.89 \pm 0.02$; $\gamma = 5.83 \pm 0.18$ for $<n_{\pm}>$. $\delta = 0.93 \pm 0.01$; $\gamma = 1.91 \pm 0.07$ for $<n_->$).

Note, that for $<n(N_A)>$ - dependence the deviation from linearity is not so strongly pronounced. It is natural, because the deviation from linearity in $<n(N_A)>$ - is caused by R_n only.

At the energies of 1.04 AGeV and 2.1 AGeV the dependences $<n(N_A)>$ and $<n(R_n)>$ are linear. But at lower energies (namely at 0.400 AGeV) the $<n(N_A)>$ -dependence is nonlinear (Fig.2). This is caused by the nonlinearity of $<n(R_n)>$ -dependence. Note that deviation from linearity is observed, starting from $N_A > 20$.

Thus, in $A_i A_t$ - collisions the $<n(N_A)>$ - dependence is nonlinear at 0.400 AGeV and 200 AGeV.

For the analysis of the situation at 0.400 AGeV and 200 AGeV consider first the $<n(N_A)>$ dependence for $A_i C$ and $A_i Ta$ collisions at 2.48 AGeV and 4.30 AGeV (Fig.3). As is shown the slope of $<n(N_A)>$ - dependence is increased with energy and at fixed energy (at 2.3 AGeV) the slope of curve is increased more in $A_i C \equiv$ (p, d, He, C)C -

collisions than in $A_iTa \equiv$ (p, d, He, C)Ta -collisions. So, for light target the avarage multiplicity <n> is growing faster than for heavy target [7].

In Refs. [2,7] such a picture is realized for <n(R)> dependence. The difference in slopes is explained by the absorption in heavy target (especially at low energy) which plays more significant role in heavy

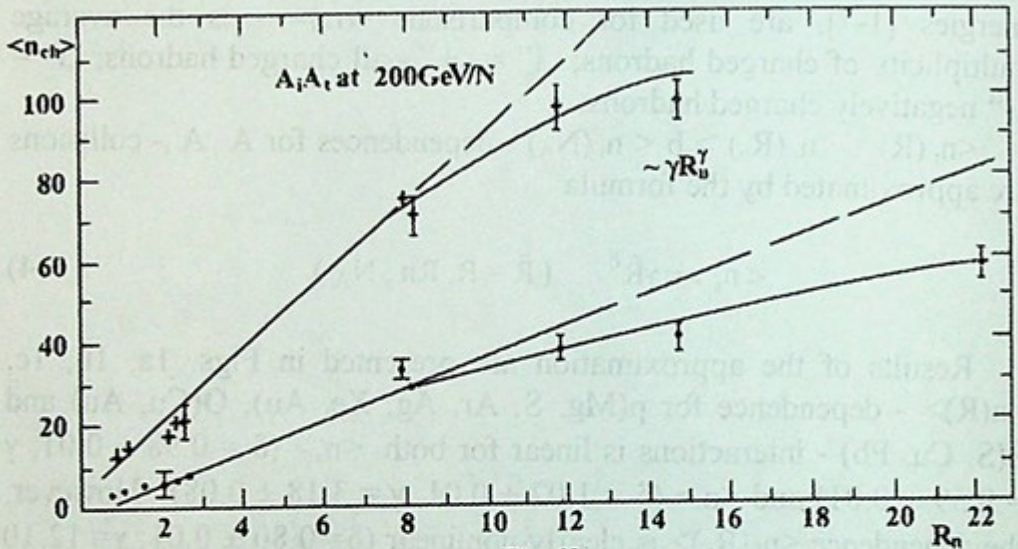

Fig.1b

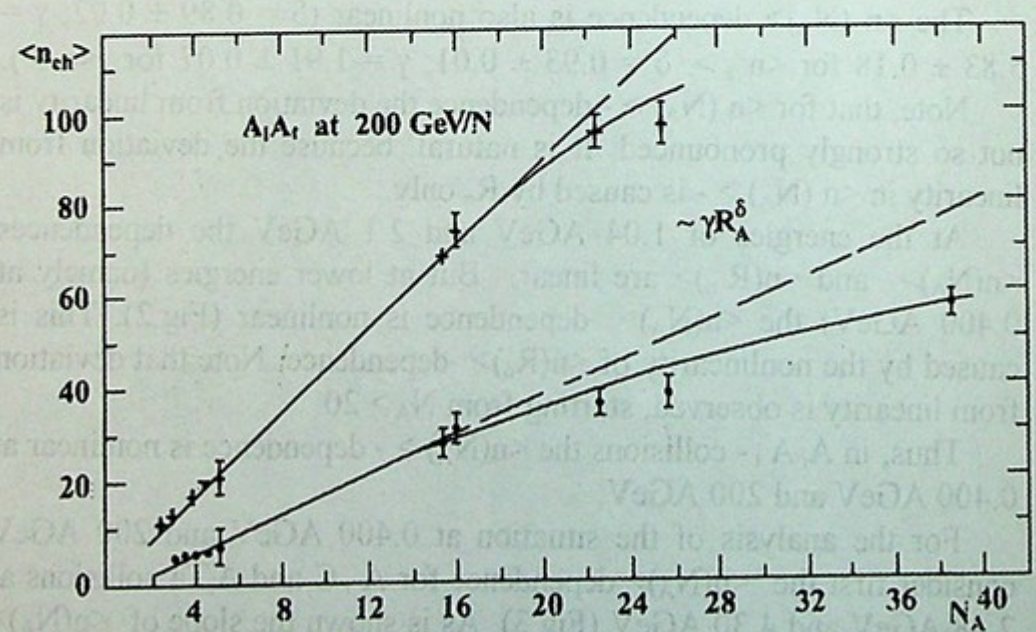

Fig.1c

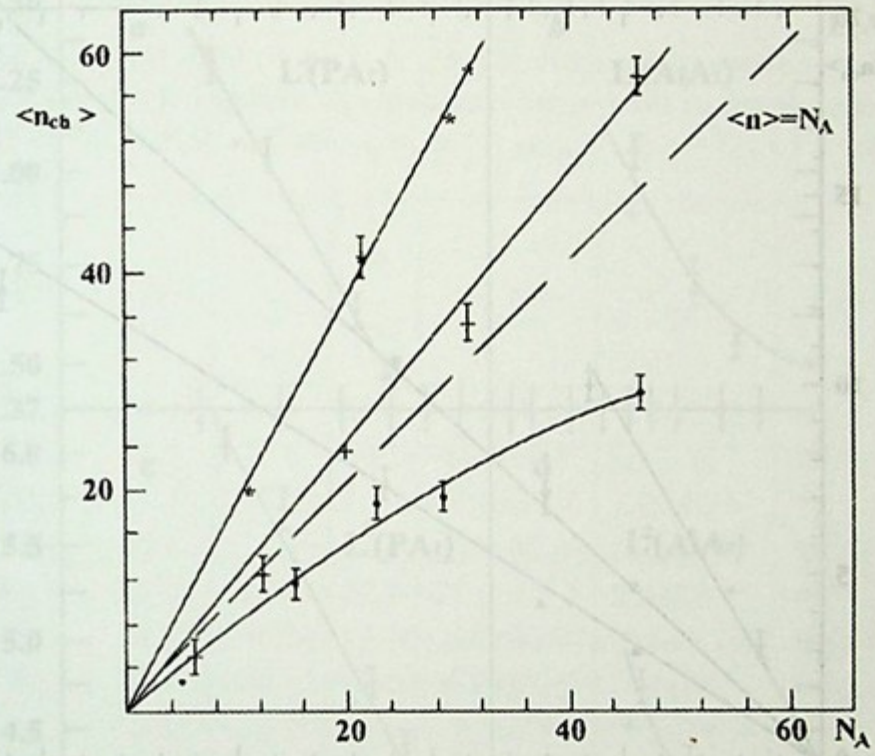

Fig.2. $\langle n_{\pm}(N_A)\rangle$ - dependence for $A_i A_t$ - collisions at 0.400; 1.040 and 2.100 AGeV
„•" - (He, Ne)Al, Ne(Ag, Au), ArU at 0.400 AGeV
„+" -(p, He, Ne, Ar)U, ArCa - at 1.040 AGeV
„*" - Ne(Al,Ag, Au,U) - at 2.100 AGeV
$\langle n_{\pm}(N_A)\rangle = N_A$ geometrical picture of interaction

target, than in the light one. Obviously, the similar explanation is valid for $\langle n(N_A)\rangle$ - dependences, which are considered here.

Return now to the Fig.2. The decrease of the slope of $\langle n(N_A)\rangle$ - dependence at 1.04 AGeV as compared to 2.1 AGeV is obviously caused by the decrease of intranuclear cascading and by the growth of the absorption effect. It is evident that at 0.400 AGeV cascading process is decreased (especially for heavy target). This leads to the fact, that the slope of the $\langle n(N_A)\rangle$ -dependence at 0.400 AGeV is even smaller than at 1.04 AGeV and 2.10 AGeV. For large N_A ($N_A > 20$) the linear dependence is broken.

Consider now $A_i A_t$ -collisions at 200 AGeV. Introduce the quantity

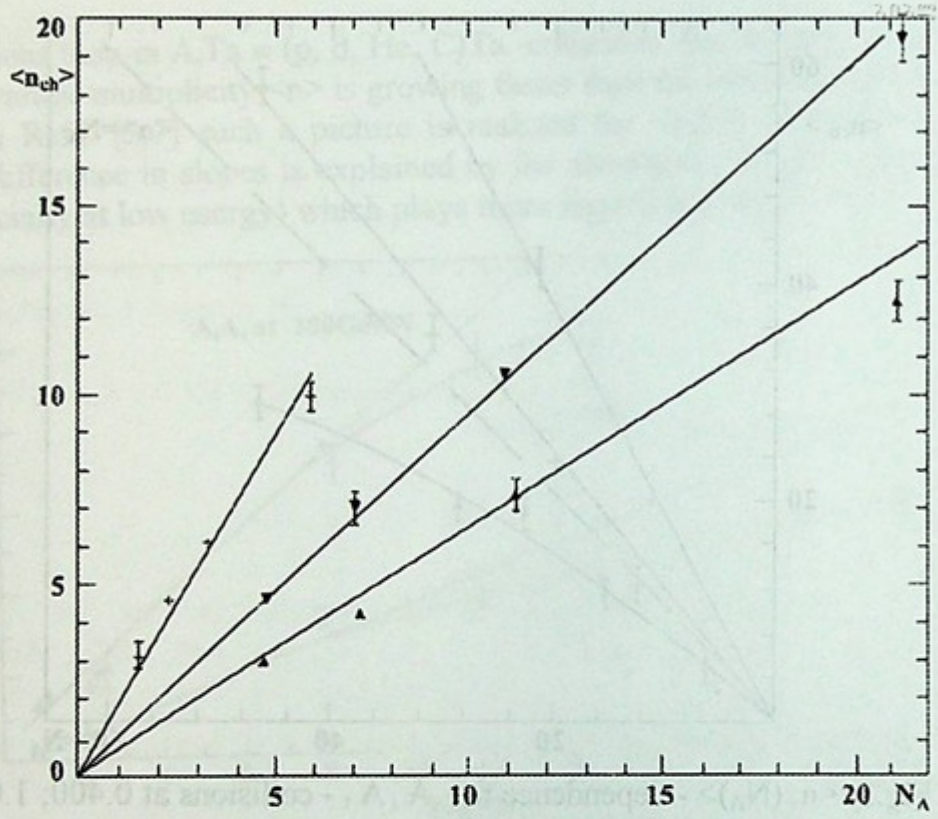

Fig.3. $<n_{\pm}(N_A)>$ - dependence for $A_i C$ $A_i Ta$ -collisions at 2.48 AGeV
($A_i C$ – "+", $A_i Ta$ -„▲"); and for $A_i Ta$ - collisions at 4.30 AGeV „▼"

$$L A_i A_t) = L^i(A_i A_t) = <n_i>_{A_i A_t} / N_A , \qquad (5)$$

where $L(A_i, A_t)$ - is the average number of the charged secondaries, corresponding to one (active) nucleon.

Consider the $L(A_i A_t)$ - dependence on N_A at 200 AGeV (Fig.4, Table 1). It is seen that $L(A_i A_t)$ decreases with increasing N_A.

This decrease is more pronounced for negative hadrons (in pA_t - collisions).

If we consider the same dependences for (p, d, He, C)Ta and (p, d, He, C, F, Mg)C -collisions at 2.48 AGeV and 4.30 AGeV a different picture arises (Fig.5).

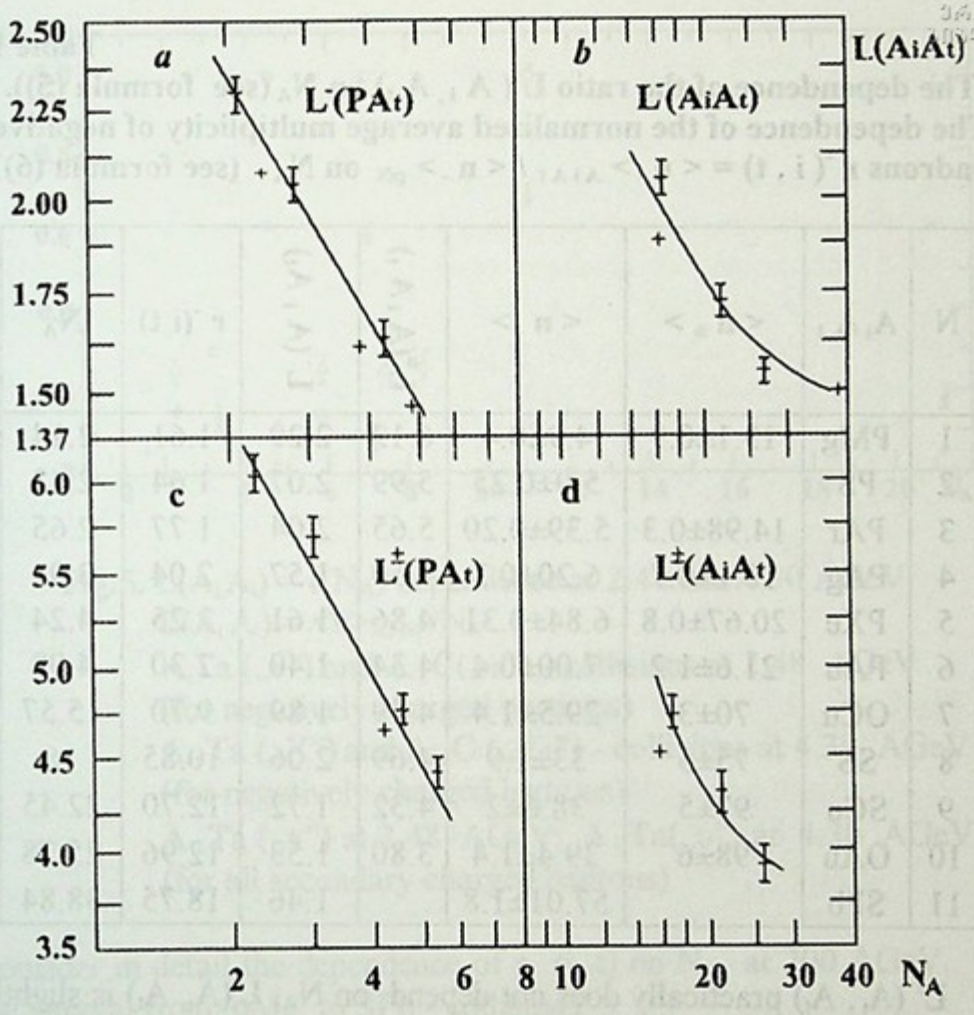

Fig.4. $L(A_i A_t) = f(N_A)$ - dependence for at 200 AGeV.
$L(A_i A_t) = \langle n \rangle_{Ai\,At} / N_A$ average number of particles corresponding to one active nucleon

4a. $L^-(P, A_t) = f(N_A)$ for negatively charged hadrons from p(Mg, S, Ar, Ag, Xe, Au) -collisions

4b. $L^-(A_i, A_t) = f(N_A)$ for negatively charged hadrons from S(S, Cu, Pb), O(Cu, Au) -collisions

4c. $L^{\pm}(P, A_t) = f(N_A)$ for all charged hadrons from p(Mg, Ar, Ag, Xe, Au) -collisions

4d. $L^{\pm}(A_i, A_t) = f(N_A)$ for all charged hadrons from S(S, Cu), O(Cu, Au) - collisions.

Table 1.

The dependence of the ratio $L(A_i, A_t)$ on N_A (see formula (5)). The dependence of the normalized average multiplicity of negative hadrons $r^-(i,t) = \langle n_- \rangle_{A_iA_t} / \langle n_- \rangle_{pN}$ on N_A (see formula (6))

N	A_iA_t	$\langle n_\pm \rangle$	$\langle n_- \rangle$	$L^\pm(A_iA_t)$	$L^-(A_iA_t)$	$r^-(i,t)$	N_A
1	PMg	13.1±0.9	4.9±0.4	6.12	2.29	1.61	2.14
2	PS		5.0±0.25	5.99	2.07	1.64	2.42
3	PAr	14.98±0.3	5.39±0.20	5.65	2.04	1.77	2.65
4	PAg	18.1±0.7	6.20±0.3	4.59	1.57	2.04	3.94
5	PXe	20.67±0.8	6.84±0.31	4.86	1.61	2.25	4.24
6	PAu	21.6±1.2	7.00±0.4	4.34	1.40	2.30	4.98
7	OCu	70±3	29.5±1.4	4.49	1.89	9.70	15.57
8	SS	75±5	33±1.9	4.69	2.06	10.85	16
9	SCu	97±5	38.6±2	4.32	1.72	12.70	22.45
10	OAu	98±6	39.4±1.4	3.80	1.53	12.96	25.78
11	SPb		57.01±1.8		1.46	18.75	38.84

$L^\pm(A_i, A_t)$ practically does not depend on N_A; $L^-(A_i, A_t)$ is slightly increasing with increasing N_A, especially for heavy target Ta.

The fact that $L^-(A_i, A_t)$ at 4.30 AGeV is significantly larger than at 2.48 AGeV is explained by small cascading at 2.48 AGeV [5,6].

For the analysis a A_iTa and A_iC -collisions at 2.48 AGeV and 4.30 AGeV in ref. [5] the dependence of the normalized average multiplicity of the negative hadrons

$$r^-(i,t) = \langle n_- \rangle_{A_iA_t} / \langle n_- \rangle_{pN} \qquad (6)$$

on the average number of nucleon-nucleon collisions $\langle \nu_{it} \rangle$ is considered. The quantity $r^-(i, t)$ can be called the multiplication coefficient of particles in the nucleus.

We consider here the dependence $r^-(i, t)$ on N_A, because $N_A \sim \langle \nu_{it} \rangle$ [2].

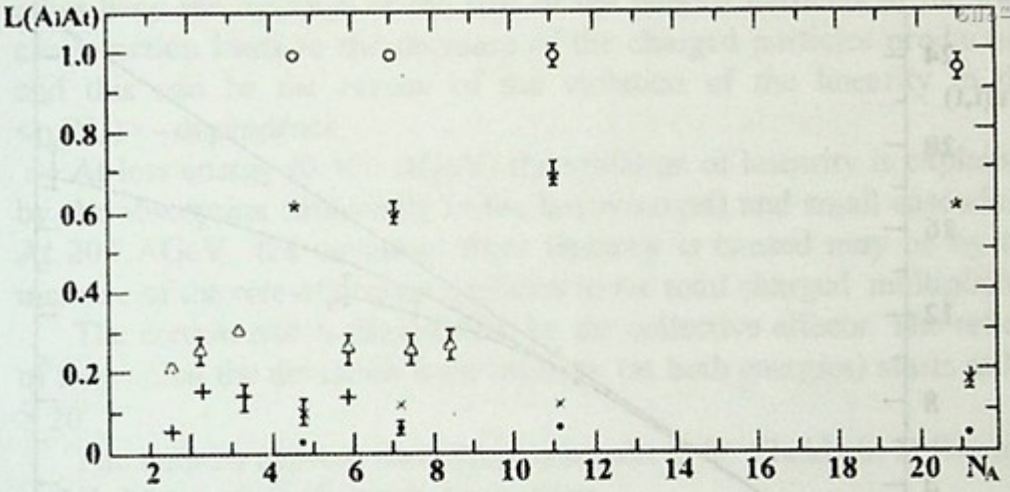

Fig.5. $L(A_i,A_t) = f(N_A)$ dependence at 2.48 and 4.30 AGeV
$L(A_i,A_t) = \langle n \rangle_{Ai\,At} / N_A$
A_iTa („•") and A_iC („+") - collisions at 2.48 AGeV (for negatively charged particles)
A_iTa („X") and A_iC („□") - collisions at 4.30 AGeV (for negatively charged hadrons)
A_iTa („*") at 2.48 AGeV; A_iTa („o") at 4.30 AGeV (for all secondary charged hadrons)

Consider in detail the dependence of $r^-(i, t)$ on N_A, at 200 AGeV, in the interval from pMg to SPb - collisions.

Let us devide this interval into two parts:
I - (pMg – OCu) and II - (OCu – SPb).

In the first interval the growth ΔN_A of the quantity N_A is 13.48; but the growth of the quantity $r^-(i, t)$, $\Delta r^-(i, t) = 8.09$ (Table 1).

It can be said that the slope of the dependence $r^-(i, t) = f(N_A)$ in the first interval is characterized by the quantity

$$\alpha_I = \Delta r^-(i, t) / \Delta N_A = 0.60 \qquad (7)$$

and in the second interval by the quantity

$$\alpha_{II} = 0.39. \qquad (8)$$

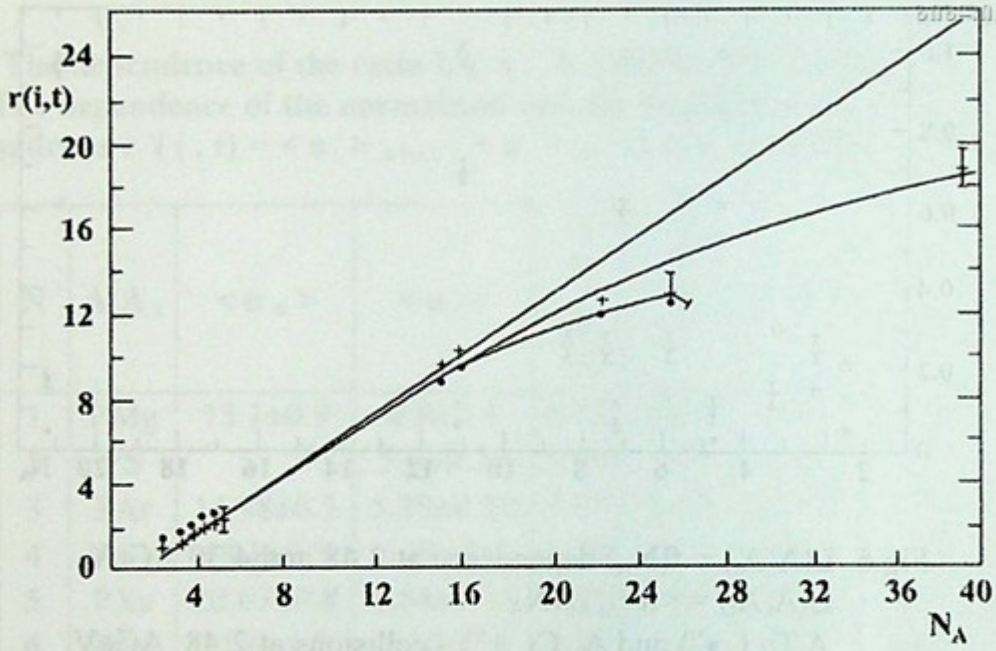

Fig.6. r (i , t) = f(N_A) – dependence. $r^{-}(i, t) = \langle n^{-} \rangle_{A_i A_t} / \langle n^{-} \rangle_{pN}$ „•" - for all secondary charged hadrons. „+" - for all negative charged hadrons for negative charged hadrons we have 11 points, at 200 AGeV p(Mg, S, Ar, Ag, Xe, Au), S(S, Cu, Pb), O(Cu, Au)) collisions. For $n_{\pm}$ we have 9 points) – there are does not exist data for SPb and PS collisions.

Comparing these two quantities, one can say that violation of the linear dependence $r^{-}(i, t) = f(N_A)$ (Fig. 6) takes place. In the same figure the dependence of $r^{\pm}(i, t)$ on N_A is presesnted. The deviation from the linearity takes place, but the effect is less pronounced, since the interval of variation of N_A is narrower (maximal value of $N_A \approx 26$ (OAu-collision).

Note, that the deviation from linearity (as, for $\langle n_i(N_A) \rangle$ dependence) starts at $N_A > 20$ (Figs.1-c, 2).

The deviation from linearity in the $r(i, t) = f(N_A)$ or in $\langle n_i (N_A) \rangle$ dependences in A_i, A_t . collisions at 200 AGeV, can be caused by the increase of the role of neutral particles to the total cross-section. Experiments show, that in pp-collisions the cross-section of the producton of the neutral particles increases with increase of energy and at 200 AGeV accounts 30% of the total inelastic cross-section. On the

other hand the increase of the role of the neutral particles in the total cross-section leads to the decrease of the charged particles production and this can be the reason of the violation of the linearity in the $<n_i(N_A)>$ - dependence.

At low energy (0.400 AGeV) the violation of linearity is explained by the absorption (especially in the heavy target) and small cascading. At 200 AGeV the deviation from linearity is caused may be by the increase of the role of neutral particles to the total charged multiplicity.

The certain role is played also by the collective effects. The reflect of this is that the deviation from linearity (at both energies) starts at $N_A \geq 20$.

The authors express their deep gratitude to D. Chokheli, D.Khubua and Z. Metreveli for helpfull discussions.

REFERENCES

1. H. Steiner. Preprint LBL - 6756, Berkeley, 1977. A.Sandoval. et al. Phys. Rev. C. **21,** 1980, 1321.
2. T. R. Djalagania. et al. Tbilisi State University. **230 (13),** 1982, 31. M. A. Dasaeva. et al. Yad. Fiz. **39,** 1984, 846.
3. S. Nagamia. Preprint LBL - 14034, Berkeley, 1982; **10956,** 1980; **10461,** 1980.
4. J. Gosset. et al. Preprint LBL - 5820, Berkley, 1977.
5. N. R. Grigalashvili et al. Yad. Fiz., **48,** 1988,_476.
6. N. Koutsidi, Yu. Tevzadze. Yad. Fiz., **41,** 1985, 1559.
7. B.Garsevanishvili et al. Physics of Atomic Nuclei, **61, 4,** 1998, 595.
8. C. De Marzo et al. Phys. Rev. D, **26,** 1982, 1019.
9. J. Bachler et al. Charge particle multilicities in nuclear collisions at 200 GeV/N (NA35 Collaboration) 1991.
10. D.H. Brick. et al. Phys. Rev. D, **39,** 1989, 2484.
11. V. C. Murzin and L. I. Saricheva. High energy hadrons interactions. Moscow, 1983, (Russian).
12. E.N. Kladnitskaya. Particles and Nuclei. Lettters. **13,** 1982, 669.

Tbilisi State University

ლ.ახობაძე, გ.ვანიშვილი, ვ.გარსევანიშვილი, თ.ჯალაღანია,
ი.თევზაძე

მეორადი დამუხტული ჰადრონების საშუალო მრავლობითობის დამოკიდებულება ურთიერთქმედებებში მონაწილე ნუკლონების რიცხვისაგან, რელატიური იონების დაჯახებებში, ენერგიების ინტერვალში (0.250-200) Aგევ

დასკვნა

ნაშრომში მსუბუქი, საშუალო და მძიმე ბირთვების დაჯახებებში დაბადებული მეორადი დამუხტული ჰადრონების $\langle n \rangle$ - საშუალო მრავლობითობების ანალიზი ჩატარებულია, დამოუკიდებლად ურთიერთქმედი ნუკლონების მოდელის საფუძველზე.

ნაჩვენებია, რომ დაბალ ენერგიებზე (≤ 0.400 A გევ) და ძალიან მაღალ ენერგიებზე (200 Aგევ) შეინიშნება $\langle n(N_A) \rangle$ დამოკიდებულების წრფივობიდან გადახრა.

N_A - ურთიერთქმედებაში მონაწილე ნუკლონების რაოდენობაა (N_A გამოთვლილია დამოუკიდებლად ურთიერთქმედი ნუკლონების მოდელის საფუძველზე).

$\langle n(N_A) \rangle$ - დამოკიდებულების წრფივობიდან გადახრა ახსნილია შთანთქმის პროცესებით (მძიმე სამიზნეებში) და მცირე კასკადური გამრავლებით (დაბალ ენერგიებზე), და ნეიტრალური ნაწილაკების წვლილის გაზრდით სრულ მრავლობითობაში; ამის გარდა გარკვეული მნიშვნელობა აქვს მრავალნაწილაკოვან (კოლექტიურ) პროცესებს, რაც შეიძლება იწვევს უარყოფითი ჰადრონების ნეიტრალიზაციას (ძალიან მაღალ ენერგიებზე - 200 Aგევ).

THE DETERMINATION OF TIME OF INITIAL CHAOTIZATION IN THE SYSTEM OF INTERACTING SPINS

A. Ugulava, T. Gvarjaladze, S. Chkhaidze

Accepted for publication May, 2004

ABSTRACT. **The paper considers the theoretical study of time of initial chaotization of phases in the spin system bound by anisotropic exchange interaction.**

The motion of separate spin at quite strong anisotropy of interacting is considered as nonlinear procession at the presence of initial transverse polychromatic field. At the same time upon the certain conditions resonance covering, yielding on initial chaotization of phases may occur. It is shown, that at that time the shape of EPR line receives Lorenz shape.

The investigations of irreversible phenomena in nonlinear systems [1-3] become more important. It is clear, that the statistical description of system behaviour is possible not only for macroscopic system, accepted earlier, but for nonlinear dynamical systems too with small number of freedom degree. The motion of nonlinear system of the end of some time, called the time of initial chaotization may be stochastic and can be described statistically. For example, the stochastic regimes exist in the motion of nonlinear oscillator, which has been undergone to periodical push [1,2] in the motion of nonlinear processing of magnetic momentum being under influence of periodical series of radio-frequency pulses [4] and in the motion of many various systems [1,5].

Presence of the stochastic regime of motion in the dynamical systems, which arises owing to the nonlinear character of the motion, gave birth to the idea of irreversibility of processes in macroscopic systems (ideal gas) [6]. The thread of this idea is that stochasticity in the motion of any system arises, when the interaction of resonances appears [2,8]. It should be noted that the above problem was considered in [7]. In this paper, the problem of the system of interacting phonons is reduced to the motion of nonlinear oscillator undergoing to the affect of periodical pushes, and kinetic equation is

formed without assumption of chaotic phases. At such approach it is possible to set a small scale of time, consequently, at the end of which a kinetic description is correct.

The aim of this paper is determination of initial chaotization time in the system of interacting spins. This time called the transverse relaxation time T_2 determines width of line of magnetic resonance.

2. Hamiltonian system of interacting spins can be written as

$$\mathscr{H} = \mathscr{H}_0 + \mathscr{H}', \tag{1}$$

where

$$\mathscr{H}_0 = \omega_0 \sum_{i=1}^{N} S_i^z + \frac{1}{2} \sum_{i \neq j} I_{ij}^{\parallel} S_i^z S_j^z,$$

$$\mathscr{H}' = \frac{1}{2} \sum_{i \neq j} I_{ij}^{\perp} (S_i^x S_j^x + S_i^y S_j^y). \tag{2}$$

Here S_i^z is z-component of effective spin ion put in i-junction, ω_0 Larmor frequency of precession, N - number of spins, $I_{ij}^{\parallel}$ and $I_{ij}^{\perp}$ are constants of anisotropic exchange interaction. It is known, that a exchange interaction between paramagnetic ions, expressed through effective spins, has an anisotropic appearance even in the case, when it was expressed through the real spins and was still isotropic.

By means of Hamiltonian (1) let us make operator equations of motion of transversal spin components:

$$\dot{S}_i^x = i[S_i^x, \mathscr{H}] = \omega_0 S_i^y + S_i^y \sum_{j \neq i} I_{ij}^{\parallel} S_j^z - S_i^z \sum_{j \neq i} I_{ij}^{\perp} S_j^y$$

$$\dot{S}_i^y = i[S_i^y, \mathscr{H}] = -\omega_0 S_i^x + S_i^x \sum_{j \neq i} I_{ij}^{\parallel} S_j^z - S_i^z \sum_{j \neq i} I_{ij}^{\perp} S_j^x. \tag{3}$$

Making a transition in the equations (3) by means of expressions

$$S_i^x = S_i^{\perp} \cos\varphi_i, \qquad S_i^y = S_i^{\perp} \sin\varphi_i \tag{4}$$

to the cylindrical variables $S_i^{\perp}$ and φ_i, we get

$$\dot{S}_i^{\perp} = -S_i^z (V_i \sin\varphi_i - W_i \cos\varphi_i),$$

$$\dot{\varphi}_i = \omega_i - \frac{S_i^z}{S_i^{\perp}} (V_i \cos\varphi_i - W_i \sin\varphi_i), \tag{5}$$

where

$$\omega_i = -(\omega_0 + \sum_{i \neq j} I_{ij}^{\parallel} S_j^z)$$

$$V_i = \sum_{j \neq i} I_{ij}^{\perp} S_j^{\perp} \cos\varphi_j, \qquad W_i = \sum_{j \neq i} I_{ij}^{\perp} S_j^{\perp} \sin\varphi_j. \tag{6}$$

The values V_i and W_i describe an interaction of i-spin with local transversal field, which was built with the other spins.

Like ref. [6] we consider action of i-spin in the local fields been averaged with the unperturbed wave function V_i and W_i reducing given task to the task of motion of one spin in the effective field.

To determine unperturbed wave functions $\mathscr{H}_0$ can be written as:

$$\mathscr{H}_0 = \omega_0 \sum_{\alpha=0}^{\infty} S_{\alpha}^z + N \sum_{\alpha=1}^{\infty} I_{\alpha}^{\parallel} S_0^z S_{\alpha}^z, \tag{7}$$

where $S_{\alpha}^z = \sum_{i=1}^{N_{\alpha}} S_i^z$ is z-component of full spin of α-coordination sphere, N_{α} is a number of ions on the α-coordination sphere, $I_{\alpha}^{\parallel}$ is longitudinal component of exchange interaction of some ions with ion, situated in the center of α-coordination sphere.

A fundamental function of Hamiltonian (7) can be written as:

$$\Psi = \prod_{\alpha=0}^{\infty} \Psi_{m_\alpha} , \tag{8}$$

where

$$S_\alpha^z \Psi_{m_\alpha} = m_\alpha \Psi_{m_\alpha} \tag{9}$$

m_α in the case of half-effective spin takes whole number value from $-\frac{1}{2}N_\alpha$ to $\frac{1}{2}N_\alpha$. A state with induced m_α has multiplication of degeneration

$$G_{N_\alpha}(m_\alpha) = \frac{N_\alpha!}{\left(\frac{1}{2}N_\alpha - m_\alpha\right)!\left(\frac{1}{2}N_\alpha + m_\alpha\right)!} . \tag{10}$$

Averaging the expressions for local fields (6) according to the wave functions (8) we get[1]:

$$\overline{V_i} = \sum_{j\neq i} I_{ij}^{\perp} \overline{S_j^{\perp} \cos\alpha_j} , \qquad \overline{W} = \sum_{j\neq i} I_{ij}^{\perp} \overline{S_j^{\perp} \sin\alpha_j} , \tag{11}$$

where

$$\alpha_j = \int_0^t \omega_j dt , \qquad \overline{A} = \prod_{\alpha=0}^{\infty} 2^{-N_\alpha} \sum_{m_\alpha=-\frac{1}{2}N_\alpha}^{\frac{1}{2}N_\alpha} A_{m_\alpha, m_\alpha} G_{N_\alpha}(m_\alpha) \tag{12}$$

A_{m_α, m_α} is diagonal matrix element according to the wave functions Ψ_{m_α}. If ω_i depends on time weakly enough $\dot{\omega}_i << \omega_i^2$, we may

---

[1] Here we ignore the perturbation in the expression for the phase (12), which is right for the time $t << 1/I^{\perp}$. We shall see below, that this limit is not of importance in the given consideration.

suppose $\varphi_i \approx \omega_i t$. Taking into account (9,10) we can get an averaged expression without any force:

$$\overline{S_j^{\perp} \cos\alpha_j} = \frac{1}{\sqrt{2}} F(t)\cos\omega_0 t\,, \quad \overline{S_j^{\perp} \sin\alpha_j} = \frac{1}{\sqrt{2}} F(t)\sin\omega_0 t\,, \qquad (13)$$

where

$$F(t) = \prod_{\alpha=1}^{\infty} \cdot \sum_{m_\alpha = -\frac{1}{2}N_\alpha}^{\frac{1}{2}N_\alpha} 2^{-N_\alpha} \cdot G_{N_\alpha}(m_\alpha) \cos I_\alpha^{||} m_\alpha t \qquad (14)$$

and equations of motion may be written as:

$$\dot{S}_i^{\perp} = -S_i^z \gamma h_{\ell oc}(t)\sin(\varphi_i - \omega_0 t),$$

$$\dot{\varphi}_i = \omega_i - \frac{S_i^z}{S_i^{\perp}} \gamma h_{\ell oc}(t)\cos(\varphi_i - \omega_0 t)\,, \qquad (15)$$

where

$$h_{\ell oc}(t) = h_{\ell oc} \cdot F(t)\,, \quad h_{\ell oc} = \frac{1}{\gamma}\sum_{\alpha=1}^{\infty} N_\alpha I_\alpha^{\perp}\,, \quad \gamma = g_\alpha \beta\,. \qquad (16)$$

$I_\alpha^{\perp}$ transverse component of exchange interaction with ions being in the α-coordination sphere, β Bohr magnetron.

4. Before beginning of investigation of spin motion on the basis of equations (15), we have to investigate expression (14) in detail. Assume, that interaction possesses effective radius of action in which it equals to $I_1^{||}$ and $N_1 >> 1$ number of spins fall in the region of interaction. Then in (14) we may suppose $I_\alpha^{||} = 0$ $(\alpha = 2,3,\ldots)$

$$G(m_1) = \left(\frac{2}{\pi N_1}\right)^{1/2} \cdot 2^{N_1} e^{-\frac{2m_1^2}{N_1}} \qquad (17)$$

and as usual making transition into (14) from summing to integrity according to m_α, we get for $\overline{S_j^x}$

$$\overline{S}_j^x = \frac{1}{\sqrt{2}} e^{-\frac{t^2}{2T_2^2}} \cos\omega_j t, \qquad (18)$$

where

$$\frac{1}{T_2} = \frac{1}{4} N_1 (I_1^{\parallel})^2 . \qquad (19)$$

Formula (19) coincides with usual expression of the second moment in approximation $I_1^{\parallel} >> I_1^{\perp}$, and T_2 plays the role of transverse relaxation.

However transition from summing to integrating in expression (14), which corresponds to the transition from discrete to continuous consideration of local field may be wrong because of the following reasons. It is known [1-3] that during the investigation of nonlinear oscillations (nonlinear precessions [4] also) in the polychromatic field different types of resonances may exist. One of them is "isolated resonance", which may occur if spin-system is in resonance with one harmonic of a variable field $h_{loc}(t)$ and nonlinearity is not strong enough to "tear off" the spin-system and shift the resonance frequency up to the other resonance harmonic.

The second type of resonance opposite to the first is "interacting resonance". It occurs when none of harmonics of variable field $h_{loc}(t)$ due to strong nonlinearity is able to hold the spin-system in the resonance. The second type of resonance, different from the first one leads to the stochastic motion. In this case limited transition from discrete imagination of field to continuous one being perfected in (14) leads to the wrong conclusion.

5. Let's investigate the system of equations (15) rejecting the above mentioned transition in (14) for continuous imagination. If exchange interaction possesses quite high effective radius of action, then we assume $I_\alpha = 0$ $(\alpha = 2,3,\ldots)$, $(N_1 >> 1)$ in the expression (14), the distribution function $G_{N_\alpha}(m_\alpha)$ may be replaced by the

rectangular one of width $(2/\pi N_1)^{1/2}$ and height $(2/\pi N_1)^{1/2}$. Taking into account this, summing harmonics we obtain

$$h_{loc}(t) = \sqrt{\frac{N_1}{2}} I_1^{\perp} \Phi(t), \tag{20}$$

where

$$\Phi(t) = \frac{\sin n_1 \pi \frac{t}{\tau_1}}{\sin \pi \frac{t}{\tau_1}} \tag{21}$$

n_1 is whole part of $(2N_1/\pi)^{1/2}$. It is clear, that function $\Phi(t)$ can be presented as periodical sequence of short pulses. In addition, the moments of pulse arising (or moments of maximums, reached by the functions $\Phi(t)$, which equal to one) are determined by the ratio $t_\ell = \ell\tau_1$, where ℓ - whole number, $\tau_1/\sqrt{N_1}$ - order of pulse duration. During the time interval of τ_1 between pulses $\Phi(t)$ fast oscillated with the period of $\tau_1/\sqrt{N_1}$, and at comparatively small amplitude.

Assuming smaller duration of pulse in comparison with the period of Larmor precession $\left(\tau_1/\sqrt{N_1}\right) << \left(2\pi/\omega_0\right)$, for jumps transversal component $\Delta S_i^{\perp(n)} = S_i^{\perp(n+1)} - S_i^{\perp(n)}$ and phase $\Delta\varphi_i^{\perp(n)} = \varphi_i^{(n+1)} - \varphi_i^{(n)}$ at the action of n-pulse we get

$$\Delta S_i^{\perp(n)} = -\sqrt{2}\pi \frac{I_1^{\perp}}{I_1^{\parallel}} S_i^{z(n)} \sin(\varphi_i^{(n)} - \omega_0 t_n),$$

$$\Delta\varphi_i^{(n)} = \omega^{(n)} + 2^{3/2}\pi^2 \frac{I_1^{\perp}}{I_1^{\parallel}} \sum_{j=1}^{N_1} S_j^{\perp(n)} \sin(\varphi_j^{(n)} - \omega_0 t_n), \tag{22}$$

where

$$\omega^{(n)} = -\left(\omega_0 + I_1^{\parallel} \sum_{i=1}^{N_1} S_i^{z(n)}\right), \qquad (23)$$

$S^{z(n)}$, $S^{\perp(n)}$ and $\varphi^{(n)}$ are values of longitudinal and transversal components and phase at the moment of acting of n-pulse.

To investigate the transversal relaxation we have to observe a correlation function

$$R_i^{(n)} = < S_i^{x(n)} S_i^{x(0)} + S_i^{y(n)} S_i^{y(0)} >, \quad < A > = \frac{1}{2\pi} \int_0^{2\pi} A d\varphi^{(0)} . \qquad (24)$$

Here we are confined only to the calculation of $R_i^{(1)}$, which may be written taking into account the relations (4)

$$R_i^{(1)} = (S_i^{\perp(0)})^2 \, Re < e^{i(\varphi_i^{(1)} - \varphi_i^{(0)})} > . \qquad (25)$$

Rejecting the suggestion of initial chaotic phases we assume them equal $\varphi_i^{(0)} = \varphi_j^{(0)}$ $(j = 1,2,\ldots)$.

Then from (22) for $\Delta\varphi_i^{(1)}$ we obtain

$$\Delta\varphi_i^{(1)} = \omega_0 \tau_1 + \mathrm{K}_1 \sin \varphi_i^{(0)}, \qquad (26)$$

where

$$\mathscr{K}_1 = 2\pi^2 N_1 \frac{I_1^{\perp}}{I_1^{\parallel}} \qquad (27)$$

Substituting expressions (26,27) in (25) we see that we have come to the known (1,2,5) expressions for the correlation function

$$R_i^{(1)} = \int_0^{2\pi} e^{i \mathscr{K}_1 \sin x} dx . \qquad (28)$$

In the presence of $\mathcal{K}_1 >> 1$ expression (28) gives us $R_i^{(1)} \sim exp\left(-ln\sqrt{\mathcal{K}_1}\right)$, which corresponds to exponential relaxation of transversal component with characteristic time

$$T_2 = \frac{\pi}{I_1^{||} ln \mathcal{K}_1}. \qquad (29)$$

Consequently, the motion of spin in the considered local field at $\mathcal{K}_1 >> 1$ becomes stochastic[2] and thus arising stochasticity is the main reason of transverse relaxation. If we assume, changeable interaction to cover $N_1 \geq 10$ spins at $N_1 \approx 10$ for velocity of transverse relaxation using the formulae (29) we get $T_2^{-1} \approx 1.8\, I_2^{||}$, which is less than corresponding expression ($\approx 3{,}2\, I_1^{||}$), obtained according to the theory of moments (19).

REFERENCES

1. G.M. Zaslavsky. Statisticheskaia neobratimost v nelineinikh sistemakh. 1970, (Russion).
2. G.M. Zaslavsky, B.V. Chirikov. Sov. Suc.of Phys.Sci., **105,** 1971, 3.
3. G.M. Zaslavsky. Phys. Rep. **80,** 1981, 157.
4. L. Buishvili, A. Ugulava. Sov. Phys. Solid State, 1983, 2370.
5. V.N. Gubankov, S.L. Ziglin et al. Sov. Phys. JETP. **86,** 1984, 343., A.Ugulava. Sov. Phys. JETP. **86,** 1984, 497., T. Katayama, Y.Yamaguchi, F. Furukaura, C. Jshii. Phys. Pev. **B27,** 1983, 3096.
6. N.S. Krilov. Raboti po obosnovaniu statisticheskoi fiziki. 1950, (Russion).
7. G.M. Zaslavsky, R.Z. Sagdeev. Sov. Phys. JETP. **52,** 1967, 1083.

[2] The condition $\mathcal{K}_1 >> 1$ is the criterion of stochasticity of Chirikov [3] for the given task.

8. R. Balescu. Equilibrium and Nonequilibrium Statistical Mechanics. 1975.
9. A. Abragam. The Principles of Nuclear Magnetism. 1961.
10. S.A. Altshuler, B.M. Kozirev. Elektronnii paramagnitni rezonans soedinenii promezhutochnikh grupp. 1972.
11. Abragam. B. Bleaney. Electron Paramagnetic Resonance of Transition ions. 1970.

Tbilisi State University

ა. უგულავა, თ. გვარჯალაძე, ს. ჩხაიძე

საწყისი ქაოტიზაციის დროის განსაზღვრა ურთიერთმოქმედ სპინთა სისტემაში

დასკვნა

ნაშრომში შესწავლილია სპინურ სისტემაში ფაზების საწყისი ქაოტიზაციის დრო, რომელიც დაკავშირებულია ანიზოტროპულ გაცვლით ურთიერთქმედებასთან. ცალკეული სპინის მოძრაობა საკმაოდ ძლიერი ანიზოტროპული ურთიერთქმედებისას წარმოდგენილია არაწრფივი პრეცესიის სახით შინაგანი განივი პოლიქრომატული ველის არსებობის დროს. ამასთან, გარკვეულ პირობებში შეიძლება განხორციელდეს რეზონანსის გაღაფარვაც, რაც განაპირობებს ფაზების საწყის ქაოტიზაციას. ნაჩვენებია, რომ ეპრ-ის ხაზს ამ დროს აქვს ლორენცის ხაზის ფორმა.

STATISTICAL STRUCTURE OF DIURNAL PRECIPITATION DISTRIBUTION ON THE TERRITORY OF EASTERN GEORGIA

Z. Khvedelidze, A Amiranashvili, J.Dolidze, D. Chitaladze, N. Pavlenishvili

Accepted for publication May, 2004

ABSTRACT. **Researching intensity and distribution of precipitations has always been the most actual problem among well-known atmospheric events. It became even more important on the background of the ongoing process of desertion. The work introduces the specially selected region of Eastern Georgia with all meteorological stations scattered on it. The presented research consists of 1982-1986 summer, spring data. The correlations between data from every single station are established, corresponding correlative matrix is built, and relevant analysis (including dividing the region) is done. The performed study gives ability to put apart new series that makes the quality of the picture of synoptic and statistical prognosis more accurate.**

Precipitation is a basic source for moistening earth's surface. It belongs to those meteorological elements, which play an active role in water-water vapor circulation. Precipitation study, statistical characterization and the proper analysis have always been an urgent problem. Based upon aforesaid we aimed to state the statistical structure of diurnal precipitation for such complex physico-geographical district as Eastern Georgia. Taking into consideration precipitation distribution seasonality and intensity [1-3] for Eastern Georgia, we selected spring-summer seasons (15.04-15.07). Using full (within the limits of the possible) data of Hydro Meteorological Database, spring-summer seasons, 1982-86 were selected. We chose 18 meteorological stations located on the territory of Eastern Georgia, which are distinguished by reliability of data. On the ground of statistical elaboration of the material we tried to state precipitation quantity, duration and intensity values and other statistical

characteristics for the given region; compare them with current specifications with the aid of the theory of mathematical statistics.

Diurnal observation data for the above-mentioned period of the given season has been processed separately according to years (92 data for a station) as well as in the form of five-season integrated series (455 data for a station).

We have processed separately daily precipitation, nightly precipitation and diurnal total data.

The driest from the given period turned spring-summer seasons of 1984, while the most abundant in precipitation that of 1983.

To solve our ultimate problem, to elaborate diurnal precipitation forecast, it is of interest to study autocorrelation relation for selected station data. Autocorrelation matrix computed by 1, 2, 3, 4, 5 days shifting shows that there is almost no relation between them; hence their use for practical aims is not reasonable, that is, it is unreasonable to draw up precipitation forecast for the following five days by today's precipitation in a given locality.

We have studied correlation relations between stations both for each year separately and five-year series. Some years were notable for high correlativity (1985). Generally, the results turned low for five-year series: in case of daily precipitation the mean value of correlation coefficient is 30%, for nightly precipitation 0.36%, and for diurnal total precipitation it equals to 0.38% (Table 1).

As one can see, in spite of small territory of Eastern Georgia, precipitation spatial distribution is not remarkable for high correlativity. The fact testifies complexity and peculiarity of the mentioned region. The correlations are higher for Western Georgia region [4] though it should be noted that in that case the terms of series are monthly total precipitation. Despite this, one can find in Tables such comparatively high correlation coefficients, according to which we can consider the territory division into districts on spatial distribution of diurnal precipitation. There are comparatively high correlations for diurnal total precipitation on the territory of Shida Kartly: Mukhrany – Dusheti - (0.80), Tskhinvali – Khashuri - (0.72), Khashuri – Borjomi - (0.73), Pasanauri – Dusheti - (0.73) (Table 1).

Table 1.

Correlation coefficient between diurnal totals of diurnal precipitation for meteorological stations of Eastern Georgia

	Telavi	Gurjaani	Lagodekhi	Dedoplistsk.	Sagarejo	Gardabani	Bolnisi	Manglisi	Tbilisi	Mukhrani.	Gori	Tskhinvali	Khashuri	Borjomi	Akhaltsikhe	Akhalkalaki	Pasanauri	Dusheti
	1	2	3	4	5	6	7	8	9	10	11	12	13	14	15	16	17	18
1	1.00																	
2	0.55	1.00																
3	0.37	0.63	1.00															
4	0.28	0.50	049.	1.00														
5	0.64	0.55	0.36	0.31	1.00													
6	0.52	0.47	0.32	0.35	0.59	1.00												
7	0.32	0.36	0.17	0.24	0.44	0.47	1.00											
8	0.40	0.34	0.15	0.26	0.41	0.43	0.57	1.00										
9	0.56	0.41	0.18	0.24	0.50	0.39	0.49	0.47	1.00									
10	0.52	0.29	0.15	0.23	0.47	0.41	0.44	0.53	0.47	1.00								
11	0.46	0.20	0.13	0.13	0.37	0.38	0.39	0.48	0.40	0.60	1.00							
12	0.46	0.18	0.09	0.11	0.40	0.38	0.35	0.40	0.42	0.59	0.65	1.00						
13	0.34	0.15	0.07	0.14	0.30	0.31	0.26	0.31	0.28	0.50	0.59	0.72	1.00					
14	0.29	0.14	0.06	0.12	0.26	0.29	0.27	0.36	0.27	0.43	0.54	0.55	0.73	1.00				
15	0.28	0.13	0.01	0.08	0.23	0.27	0.31	0.43	0.30	0.38	0.40	0.46	0.41	0.57	1.00			
16	0.28	0.20	0.06	0.10	0.29	0.29	0.34	0.42	0.27	0.38	0.42	0.39	0.40	0.49	0.52	1.00		
17	0.49	0.22	0.15	0.16	0.46	0.40	0.36	0.44	0.41	0.66	0.59	0.66	0.55	0.42	0.39	0.37	1.00	
18	0.54	0.37	0.24	0.26	0.52	0.46	0.48	0.57	0.52	0.80	0.63	0.62	0.51	0.48	0.42	0.41	0.72	1.00

Considering the mean square error of correlation coefficients calculated by us for case n = 455 [5] that equals to $\sigma = 0.05$, one can say according to the Table that correlation coefficient values vary within $(0.6 \div 0.8) \pm 0.05$. Daily and nightly precipitation correlations taken individually per given region are characterized by comparatively high values.

Kakheti region is comparatively low correlation according to the same material. Maximum of correlation coefficient here does not exceeds 0.64 (Sagarejo-Telavi). Only in two cases there was obtained greater than 0.60. The low correlations between the stations of this region can be explained by the fact, that in most cases in Kakheti in spring-summer seasons precipitation occurs in the result of convectional process development; the precipitation is characterized by locality; very often this precipitation is in the form of hail. Comparing with Europian data, one sees that convection clouds in Europe are 10% from the total, whereas on the East Caucasioni mountain ridge their index runs up to 90% [6]. The Tables show that it is low correlation relation between stations of Southern Georgia and that of Kakheti region. Akhalkalaki region has similar low correlation dependence with all other regions but Akhaltsikhe. Hence, when forecasting it would be reasonable to discuss Southern Georgia region individually. Lagodekhi station is notable for low correlation even among Kakheti stations, except Gurjaani, to which it is territorially near. Evidently the reason is that Lagodekhi region is climatically distinguished zone.

We have studied separately Tbilisi station precipitation correlations with the rest stations. We are giving correlation coefficient data as well as stations' distances from Tbilisi (Table 2). Graphs (linear, exponential, polynomial) have been plotted using the above mentioned data; we have obtained regression equations too. We are citing as an example a graph for diurnal total precipitation (Fig.1). On abscess axis-distances from Tbilisi (km); on ordinate - the corresponding correlation coefficients. R is the determination coefficient.

Statistical estimation of precipitation quantity according to altitude is of interest. We have estimated separately daily (◊), nightly (Δ) and diurnal (○) total precipitations (Fig.2)-on the abscess axis — altitude H m, on the ordinate-precipitation quantity in mms. It is seen from the material (Table 3) that nightly precipitation for Kakheti is far greater

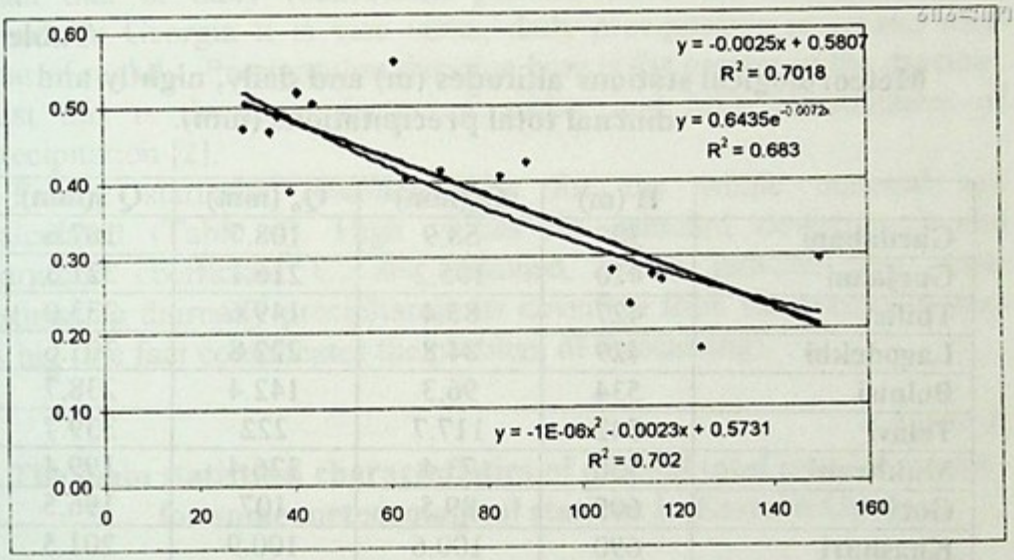

Fig.1.

Table 2.

Correlation between precipitations for meteorological stations in Tbilisi and Eastern Georgia (according to daily, nightly and diurnal total precipitations).

	Km	r_d	r_n	r_s
Telavi	61	0.19	0.59	0.56
Gurjaani	83	0.25	0.43	0.41
Lagodekhi	125	0.12	0.19	0.18
Dedoplistskaro	110	0.31	0.22	0.24
Sagarejo	44	0.31	0.45	0.50
Gardabani	39	0.37	0.32	0.39
Bolnisi	37	0.60	0.33	0.49
Manglisi	35	0.47	0.42	0.47
Mukhrani	30	0.40	0.39	0.47
Gori	63	0.36	0.35	0.40
Tskhinvali	88	0.36	0.37	0.42
Khashuri	107	0.20	0.27	0.28
Borjomi	117	0.26	0.22	0.27
Akhaltsikhe	150	0.30	0.26	0.30
Akhalkalaki	115	0.20	0.28	0.27
Pasanauri	71	0.42	0.31	0.41
Dusheti	41	0.48	0.44	0.52

Table 3.

Meteorological stations`altitudes (m) and daily, nightly and diurnal total precipitations (mm).

	H (m)	Q_d(mm)	Q_n (mm)	Q s(mm)
Gardabani	300	58.9	108.7	167.6
Gurjaani	410	105.2	216.1	321.3
Tbilisi	427	83.4	149.6	233.0
Lagodekhi	429	84.8	222.8	307.6
Bolnisi	534	96.3	142.4	238.7
Telavi	542	117.7	222	339.7
Mukhrani	550	73.4	126.4	199.4
Gori	609	89.5	107	196.5
Khashuri	690	100.6	100.9	201.5
Borjomi	789	133.7	122.9	256.7
Dedoplistskaro	800	77.8	180.2	258
Sagarejo	802	106.2	209.5	315.7
Tskhinvali	862	119.7	122.2	241.9
Dusheti	922	107	181.1	288.1
Akhaltsikhe	989	122.4	103.6	226.0
Pasanauri	1070	163.6	259	422.6
Manglisi	1194	168	165.2	333.2
Akhalkalaki	1716	140.8	112.4	253.2

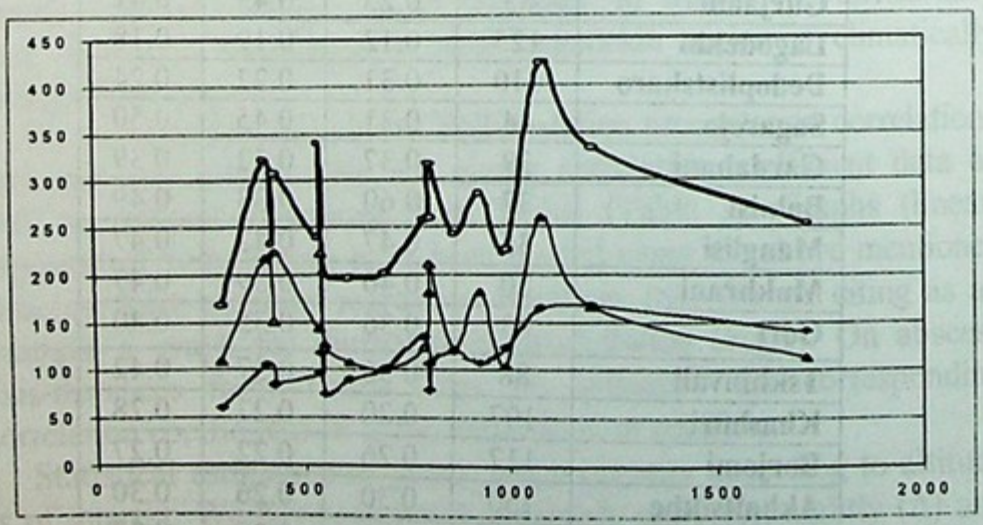

Fig.2

than that of daily (convection process effect here too), while in Southern Georgia it is vice versa, daily precipitation is greater than that of nightly. Precipitation duration here is far greater in the daytime. Just this is the main factor of aridity and little effectiveness of precipitation [2].

Finally statistical characteristics for the whole material are calculated (Table 4). High values for standard deviation σ and variation coefficient C_v are obtained, which indicate that while estimating diurnally precipitation its deviation from the average values is big (the fact complicates the problem of forecasting).

Table 4.

The main statistical characteristics of diurnal total precipitations for some meteorological stations in Eastern Georgia.

	Mean	Srandard Deviation	Min.	Max.	C_v	Count
Telavi	3.73	9.02	0	83.3	2.42	455
Gurjaani	3.52	8.66	0	80.9	2.45	455
Lagodekhi	3.37	8.64	0	87.9	2.56	455
Dedoplistskaro	2.84	7.44	0	60.2	2.62	455
Sagarejo	3.47	8.26	0	72.8	2.38	455
Gardabani	1.84	4.52	0	39	2.46	455
Bolnisi	2.62	5.82	0	49	2.22	455
Manglisi	3.66	7.09	0	55.9	1.94	455
Tbilisi	2.56	7.45	0	97.3	2.91	455
Mukhrani	2.20	5.08	0	40.7	2.31	455
Gori	2.16	4.97	0	39	2.30	455
Tskhinvali	2.66	6.08	0	64	2.29	455
Khashuri	2.20	4.82	0	38.3	2.19	455
Borjomi	2.82	4.87	0	35.5	1.73	455
Akhaltsikhe	2.48	4.39	0	24.9	1.77	455
Akhalkalaki	2.76	4.54	0	32.3	1.64	455
Pasanauri	4.63	8.90	0	88.7	1.92	455
Dusheti	3.17	6.48	0	38.8	2.04	455

Maximum precipitation for Tbilisi station -97.3mm (29.04.1982) in the Table is of interest. It is known from literature that Tbilisi region is notable for complex specificity of precipitation and Eastern Georgia`s diurnal maximum takes place here [1, 2]; This fact proves this peculiarity once more. The mentioned maximum is greater than Pasanauri maximum (88.7mm), where precipitation total quantity is far greater than Tbilisi total precipitation.

In the dominating climate region of Eastern Georgia regions with uniform climate have been singled out. In the present article correlation relations between precipitation observation data from meteorological stations functioning in each region have been stated. According to analysis of Table 1, coefficient of correlation between diurnal total precipitation as a rule is greater than 0.5. At the same time correlation coefficient value between various climate regions is very low; for example, coefficient of correlation between diurnal total precipitation for meteorological stations located in Shida Kakheti and the same data for metereological stations in any other climate regions in Eastern Georgia changes within (0.1 – 0.2).

Summary. The statistic analysis given in the present work enables us to single out new statistical series from the series of five-year precipitation observation data taking into consideration synoptical processes dominating in Georgia. We think that taking into account synoptical processes and vertical stratification created in the atmosphere, the statistic analysis of newly singled out series will enable us to create synoptical-statistic method for precipitation forecasting in Eastern Georgia.

REFERENCES

1. S. Javakhishvili. Atmosperuli naleqebi saqartvelos teritoriaze, TSU, 1981, 181, (Georgian).
2. M.S.Khvichia. Genezis osadkov I ikh rejim na territorii Gruzii. Tr.ZakNIGMI, 1971, **44 (50)**, 189, (Russian).
3. D. Alibegova, E. S. Elizbarashvili. Statisticheskaia struqtura atmospernikh osadkov vgornikh raionakh. Leningrad, 1980, 136, (Russian).

4. K. Tavartqiladze. Saqartveloshi naleqebis ganacilebis statistikuri struqtura –Hidrometeorologiis institutis Sromebi, "Mecniereba", 2002, **105**, 117, (Georgian).
5. E. S. Ulanova. Primenenie matematicheskoi statistiki v agrometeorologii dlia nakhojdenia uravnenii sviazei. Moskva, 1964, 111, (Russian).
6. I. G. Sulakvelidze. Livnevie osadki v gornikh stranakh na primere Zakavkazia. TGU, 1988, 268, (Russian).

Tbilisi State University

გ. ხვედელიძე, ა. ამირანაშვილი, ჯ. დოლიძე, დ. ჩიტალაძე, ნ. ფავლენიშვილი

ყოველდღიური ნალექების განაწილების სტატისტიკური სტრუქტურა აღმოსავლეთ საქართველოს ტერიტორიაზე

დასკვნა

ატმოსფერულ მოვლენებს შორის სხვადასხვა ინტენსივობისა და განაწილების ნალექების შესწავლა იყო და არის აქტუალური პრობლემა. ეს განსაკუთრებით საყურადღებოა თანამედროვე გაუდაბნოების ფონზე. შრომაში შერჩეულ იქნა აღმოსავლეთ საქართველოს რეგიონი მასზე განლაგებული 18 მეტეოროლოგიური სადგურით; 1982 - 86 წლების მასალა, გაზაფხულ - ზაფხულის სეზონი. დადგენილია კორელაციური კავშირები ყველა სადგურის მონაცემებს შორის, აგებულია შესაბამისი კორელაციური მატრიცა და მოხდენილია სათანადო ანალიზი დარაიონების ჩათვლით. ჩატარებული სამუშაო შესაძლებლობას იძლევა გამოყოფილ იქნას ახალი სტატისტიკური მწკრივები, რომლებიც დააზუსტებენ ნალექების სინოპტიკურ - სტატისტიკური პროგნოზის ხარისხს.

STATISTICAL DESCRIPTION OF EVOLUTION OF THE QUANTUM PENDULUM

A. Ugulava, L. Chotorlishvili, K. Nickoladze.

Accepted for publication June, 2004

ABSTRACT. **The mathematical pendulum is the simplest system having all the basic properties inherent in dynamic stochastic systems. In the present paper we investigate the mathematical pendulum with the aim to reveal the properties of a quantum analogue of dynamic stochasticity or, in other words, to obtain the basic properties of quantum chaos.**

It is shown that periodic perturbation of the quantum pendulum (similarly to the classical one) in the neighbourhood of the separatrix can bring about irreversible phenomena. As a result of recurrent passages between degenerate states, the system gets self-chaotized and passes from the pure state to the mixed one. Chaotization involves the states, the branch points whose levels participate in a slow "drift" of the system along the Mathieu characteristics. This "drift" is caused by a slowly changing variable field. Recurrent relations are obtained for populations of levels participating in the irreversible evolution process. It is shown that the entropy of the system first grows and, after reaching the equilibrium state, acquires a constant value.

1. INTRODUCTION. FORMULATION OF THE PROBLEM

Dynamic stochasticity is directly connected with the assumption that classical equations of motion may contain nonlinearities which arise when the (exponential) repulsion of phase trajectories occurs at a sufficiently quick rate. In the case of quantum consideration, the dynamics of a system is described by a wave function that obeys a linear equation, while the notion of a trajectory is not used at all. Hence, at first sight it seems problematic to find out the quantum properties of systems whose classical consideration reveals their

dynamic stochasticity. A quantum analogue of classical stochastic motion is usually called quantum chaos.

On the other hand, it is of practical interest to investigate parametrically dependent Hamiltonians $H(Q,P,l)$, where (Q,P) is the set of canonical coordinates, l is the parameter describing how the system is related to the external field. The interest in such systems is explained by their use in the study of quantum points and other problems of mesoscopic physics [1].

In most of the papers that deal with parametrically dependent systems, their authors consider the following situation. For $l=0$, the Hamiltonian $H(Q,P,0)$ is exactly integrable. As l increases, the Hamiltonian $H(Q,P,l)$ becomes nonintegrable and, for a certan value of l_0, solutions of the classical equations corresponding to $H(Q,P,l_0)$ become chaotic. In the case of quantum consideration, eigenvalues $E_n(l_0)$ and eigenfunctions $\psi_n(l_0)$ are found in the above-mentioned area of parameter values by using the method of numerical diagonalization. In that case, we show interest in the dependence of the parametrical kernel $P(n/m)=\left|<\psi_n(l_0+\delta l)|\psi_m(l_0)>\right|^2$ on a parameter displacement $\delta l << l$. The value $P(n/m)$, averaged statistically over states n, $\overline{P(n/m)}=\overline{P(n/n+r)}=P(r)$ can be interpreted as the local density of states. The introduction of $P(r)$ means that we pass from the quantum-mechanical description to the quantum statistical description [2 - 5] carried out by an intuitive reasoning.

In the problems considered in the above-listed papers, the Hamiltonian $H(Q,P,l)$ displays chaos for both parameter values $l=l_0$ and $l=l_0+\delta l$.

As different from these papers, in the present paper we investigate the situation, in which the Hamiltonian $H(Q,P,l)$ is integrable and becomes nonintegrable after adding a strictly periodic perturbation $\delta l(t)$. As the basic Hamiltonian we take the Hamiltonian of the mathematical pendulum (universal Hamiltonian).

As is known, the Schrodinger quantum-mechanical equation for the universal Hamiltonian is written in the form of the Mathieu equation. The Mathieu-Schrodinger equation for an atom, which is under the action of optical pumping in the area of large quantum numbers, was for the first time obtained by G. Zaslavsky and G. Berman [6]. These authors also performed analysis of quasiclassical states of the Mathieu-Schrodinger equation [6].

The main objective of the present paper is to investigate the behavior of the quantum mathematical pendulum in the area of dynamic stochasticity parameters. As is known [7], this area, called the stochastic layer, lies in the neighborhood of the separatrix of the classical pendulum.

We show here that with the appearance of quantum chaos the pure state passes to the mixed one. In other words, the reversible quantum process transforms to the reversible process of quantum chaos which can be described by a kinetic equation. The common feature of classical dynamic chaos and quantum chaos is, as will be shown below, the irreversibility of their states.

2. A PARAMETRICALLY DEPENDENT HAMILTONIAN

After writing the stationary Schrodinger equation

$$\hat{H}\psi_n = E_n\psi_n \tag{1}$$

for the universal Hamiltonian of the atom+pumping system

$$\hat{H} = -\frac{\partial^2}{\partial\varphi^2} + V$$

$$V = l\cos 2\varphi,$$

we come to the equation coinciding with the Mathieu equation [8, 9]

$$\frac{d^2\psi_n}{d\varphi^2} + (E_n - V(l,\varphi))\psi_n = 0, \tag{2}$$

where $E_n \to \frac{8E_n}{\hbar^2\omega'}$ are the introduced dimensionless values, l is the dimensionless amplitude of pumping, $\omega' = \frac{d\omega(I)}{dI}$ is the derivative of nonlinear oscillation frequency $\omega(I)$ with respect to the action I [9].

The Mathieu-Schrodinger equation is characterized by a specific dependence of the spectrum of eigenvalues $E_n(l)$ and eigenfunctions $\psi_n(\varphi, l)$ on the parameter l (see Fig.1). On the plane (E, l) with the spectral characteristics (so-called Mathieu characteristics [9]) of the problem, this specific feature manifests itself in the alternation of areas of degenerate $G_{\pm}$ and nondegenerate G states (see [10], Figs. 3,4). The boundaries between these areas pass through the branch points of energy therms $E_n(l)$.

Degenerate and nondegenerate states of the quantum mathematical pendulum were established by studying the symmetry properties of the Mathieu-Schrodinger equation. In [10], by using the symmetry properties of the Mathieu-Schrodinger equation and applying the group theory methods, the eigenvalues for each of the areas G_+; G_-; G were found:

$$G_- \to \psi^{\pm}_{2n+1}(\varphi) = \frac{\sqrt{2}}{2}(ce_{2n+1}(\varphi) \pm ise_{2n+1}(\varphi))$$

$$\psi^{\pm}_{2n}(\varphi) = \frac{\sqrt{2}}{2}(ce_{2n}(\varphi) \pm ise_{2n}(\varphi)); \qquad (3G_-)$$

$$G \to ce_{2n}(\varphi);\ ce_{2n+1}(\varphi);\ se_{2n}(\varphi);\ se_{2n+1}(\varphi) \qquad (3G)$$

$$G_+ \to \xi^{\pm}_{2n}(\varphi) = \frac{1}{\sqrt{2}}(ce_{2n}(\varphi) \pm ise_{2n+1}(\varphi));$$

$$\zeta^{\pm}_{2n+1}(\varphi) = \frac{1}{\sqrt{2}}(ce_{2n+1}(\varphi) \pm ise_{2n+2}(\varphi)); \qquad (3G_+)$$

Here $ce_n(\varphi)$, $se_n(\varphi)$ denote the Mathieu functions [9].

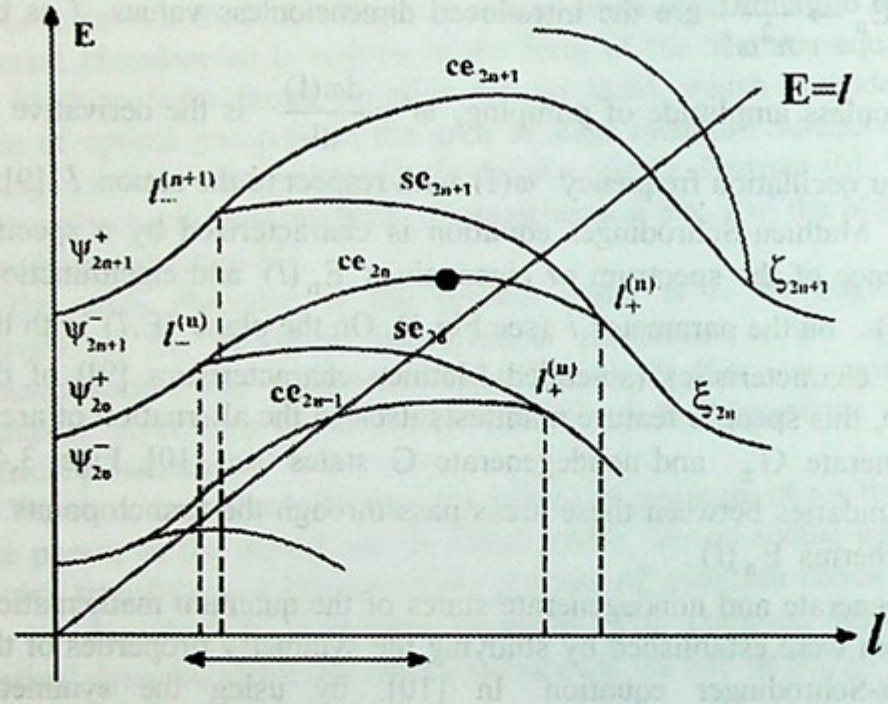

Fig.1. A fragment of the parameter-dependent energy spectrum of the quantum mathematical pendulum (1)

The wave functions $(3G_{\pm})$ and $(3G)$ form the bases of irreducible representations of the respective groups. Each of the four functions $(3G)$ forms a one-dimensional irreducible representation of the Klein group V, while the functions $\psi^{\pm}_{2n+1}(\varphi)$, $\psi^{\pm}_{2n}(\varphi)$ from $(3G_{-})$ and $\xi^{\pm}_{2n}(\varphi)$, $\zeta^{\pm}_{2n+1}(\varphi)$ from $(3G_{+})$ form the two-dimensional irreducible representations of two invariant subgroups of the group V [10].

Let us assume that the pumping amplitude is modulated by a slowly changing electromagnetic field. The influence of modulation can be taken into account by making a replacement in the Mathieu-Schrodinger equation

$$l(t) \to l_0 + \Delta l \cos \nu t, \qquad (4)$$

where Δl is the modulation amplitude expressed in dimensionless units, ν is the modulation frequency.

We assume that a gradual change of $l(t)$ may involve some N branch points on the left and on the right side of the separatrix (Fig.1):

$$\Delta l \geq \left| l_+^n - l_-^n \right|, \quad n = 1,2....N . \tag{5}$$

After making replacement (4) in the universal Hamiltonian, we obtain

$$\hat{H} = \hat{H}_0 + \hat{H}'(t),$$

$$\hat{H}_0 = -\frac{\partial^2}{\partial \varphi^2} + l_0 \cos 2\varphi , \tag{6}$$

$$\hat{H}'(t) = \Delta l \cos 2\varphi \cos \nu t . \tag{6'}$$

Simple calculations show that the matrix elements of perturbation $\hat{H}'(t)$ with respect to the wave functions (3G) of the nondegenerate area G are equal to zero

$$< ce_n \left| \hat{H}'(t) \right| se_n > \sim \Delta l \int_0^{2\pi} ce_n(\varphi) \cos 2\varphi se_n(\varphi) d\varphi = 0 , \tag{7}$$

where n is any integer number. Therefore perturbation (6') cannot bring about passages between nondegenerate levels.

The interaction $\hat{H}'(t)$, not producing passages between levels, should be inserted in the unperturbed part of the Hamiltonian. The Hamiltonian obtained in this manner can be considered as slowly depending on time.

Thus, in the nondegenerate area G the Hamiltonian can be written in the form

$$\hat{H} = -\frac{\partial^2}{\partial \varphi^2} + l(t) \cos 2\varphi ,$$

$$l(t) = l_0 + \Delta l \cos \nu t . \qquad (8)$$

As it has been mentioned above, to different areas on the plane (E,l) we can assign different eigenfunctions $(3G_-)$, $(3G)$, $(3G_+)$. Because of the modulation of the parameter $l(t)$ the system passes from one area to another, getting over the branch points.

3. PASSAGE FROM THE QUANTUM-MECHANICAL DESCRIPTION TO THE KINETIC DESCRIPTION. IRREVERSIBLE PHENOMENA

As different from the nondegenerate states area G, in the areas of degenerate states G_- and G_+, the nondiagonal matrix elements of perturbation $\hat{H}'(t)$ (6) are not equal to zero. For example, if we take the matrix elements with respect to the wave functions $\psi^{\pm}_{2n+1}(\varphi)$ (see $(3G_-)$), then for the left degenerate area G_- it can be shown that

$$H'_{+-} = H'_{-+} = \langle \psi^{+}_{2n+1} \left| \hat{H}'(t) \right| \psi^{-}_{2n+1} \rangle \sim \Delta l \int_0^{2\pi} \psi^{+}_{2n+1} \psi^{-*}_{2n+1} \cos 2\varphi \, d\varphi \neq 0 \qquad (9)$$

Note that the value H'_{+-} has order equal to the pumping modulation depth Δl.

Analogously to (9), we can write an expression for even $2n$ states as well.

An explicit dependence of $\hat{H}'(t)$ on time given by the factor $\cos \nu t$ is assumed to be slow as compared with the period of passages between degenerate states that are produced by the nondiagonal matrix elements H'_{+-}. Therefore below the perturbation H'_{+-} will be assumed to be the time-independent perturbation that can bring about passages between degenerate states.

Thus, in a degenerate area the system may be in the time-dependent superpositional state

$$\psi_{2n}(t) = C_n^+(t)\,\psi_{2n}^+ + C_n^-(t)\,\psi_{2n}^- . \qquad (10)$$

The probability amplitudes $C_n^{\pm}(t)$ are defined by means of the fundamental quantum-mechanical equation expressing the casuality principle [11]. We write such equations for a pair of doubly degenerate states:

$$\begin{cases} -i\hbar\dfrac{dC_n^+}{dt} = (E_{0n} + H'_{++})C_n^+ + H'_{+-}C_n^- \\ -i\hbar\dfrac{dC_n^-}{dt} = H'_{+-}C_n^+ + (E_{0n} + H'_{--})C_n^- \end{cases} \qquad (11)$$

Let us solve system (11). In our case it can be assumed that $H'_{++} = H'_{--}$ and $H'_{+-} = H'_{-+}$. Let us investigate changes that occurred in the state of the system during time ΔT while the system was in the area G_-, assuming that ΔT is a part of the modulation period T, $\Delta T \le T$.

For arbitrary initial values system (11) has the solution

$$C_n^+(t) = e^{\frac{i}{\hbar}Et}\left(C_+\cos\left(\frac{H'}{\hbar}t\right) + iC_-\sin\left(\frac{H'}{\hbar}t\right)\right),$$

$$C_n^-(t) = e^{\frac{i}{\hbar}Et}\left(C_-\cos\left(\frac{H'}{\hbar}t\right) + iC_+\sin\left(\frac{H'}{\hbar}t\right)\right), \qquad (12)$$

where we redenote $E \to E_0 + H'_{++}$, $H'_{+-} \to H'$. A slow dependence of the interaction $\hat{H}'(t)$ (6) on time can be taken into account in (12) if we use the replacement $H' = H'\cos\nu t$.

Let motion begin from the state ψ_{2n}^- of the degenerate area. Then as the initial conditions we take

$$C_n^-(0)=1,\quad C_n^+(0)=0. \tag{13}$$

Having substituted (13) into (12), for the amplitudes $C_n^{\pm}(t)$, we obtain

$$C_n^+(t)=i\exp\left(\frac{i}{\hbar}Et\right)\sin(\omega t),$$

$$C_n^-(t)=\exp\left(\frac{i}{\hbar}Et\right)\cos(\omega t), \tag{14}$$

where $\omega=\frac{2\pi}{\tau}=\frac{H'}{\hbar}$ is the frequency of passages between degenerate states, τ is the passage time.

Note that the parameter ω, which is connected with the modulation depth Δl, has (like any other parameter) a certain small error $\delta\omega$, which during the time of one passage $t\sim 2\pi/\omega$, leads to an insignificant correction in the phase $2\pi(\delta\omega/\omega)$. But during the time $t\sim\Delta T$, there occurs a great number of oscillations (phase incursion takes place) and, in the case $\Delta T>>\tau$, a small error $\delta\omega$ brings to the uncertainty of the phase $\sim\Delta T\delta\omega$ which may have order 2π. Then we say that the phase is self-chaotized.

Let us introduce the densitity matrix averaged over a small dispersion $\delta\omega$:

$$\rho_n^{+-}(t)=\begin{pmatrix} W_n^+(t) & iF_n(t) \\ -iF_n^*(t) & W_n^-(t)\end{pmatrix}, \tag{15}$$

where $W_n^{\pm}(t)=\overline{\left|C_n^{\pm}(t)\right|^2}$, $F_n(t)=\overline{\left|C_n^+(t)C_n^{-*}(t)\right|}$. The overline denotes the averaging over a small dispersion $\delta\omega$

$$\overline{A(\omega,t)}=\frac{1}{2\delta\omega}\int_{\omega-\delta\omega}^{\omega+\delta\omega}A(x,t)dx \tag{16}$$

To solve (16) we can write that

$$W_n^+(t) = \overline{\sin^2(\omega t)}, \quad W_n^-(t) = \overline{\cos^2(\omega t)}, \quad F_n(t) = \frac{1}{2}\overline{\sin 2\omega t} \qquad (17)$$

After a simple integration of the averaging (16), for the matrix element (17) we obtain

$$W_n^{\pm}(t) = \frac{1}{2}\left(1 \mp f(2\delta\omega t)\cos 2\omega t\right),$$
$$F_n(t) = F_n^*(t) = \frac{1}{2} f(2\delta\omega t)\sin 2\omega t, \qquad (18)$$
$$f(2\delta\omega t) = \frac{\sin 2\delta\omega t}{2\delta\omega t}.$$

At small values of time $t << \bar{\tau}$ $(\bar{\tau} = 2\pi/\delta\omega)$, insufficient for self-chaotization $(f(2\delta\omega t) \approx 1)$, we obtain

$$W_n^+(t << \bar{\tau}) = \sin^2(\omega t), \qquad W_n^-(t << \bar{\tau}) = \cos^2(\omega t),$$
$$F_n(t << \bar{\tau}) = \frac{1}{2}\sin 2\omega t.$$

Comparing these values with the initial values (17) of the density matrix elements, we see that the averaging procedure (16), as expected, does not affect them. Thus, for small times we have

$$\rho_n^{+-}(t << \bar{\tau}) = \begin{pmatrix} \sin^2 \omega t & \frac{i}{2}\sin 2\omega t \\ -\frac{i}{2}\sin 2\omega t & \cos^2 \omega t \end{pmatrix}. \qquad (19)$$

One can easily verify that matrix (19) satisfies the condition $\rho^2(t << \bar{\tau}) = \rho(t << \bar{\tau})$, which is a necessary and sufficient condition for the density matrix of the pure state.

For times even smaller than $t << \tau << \bar{\tau}$, when passages between degenerate states practically fail to occur, by taking the limit $\omega t << 1$ in (19), we obtain the following relation for the density matrix:

$$\rho_n^{+-}(t=0) = \rho_n^{+-}(t << \tau) = \begin{pmatrix} 0 & 0 \\ 0 & 1 \end{pmatrix}. \qquad (20)$$

This relation corresponds to the initial relation (13) when the system is in the eigenstate ψ_{2n}^{-}. Let us now investigate the behavior of the system at times $t \geq \bar{\tau}$ when the system gets self-chaotized.

On relatively large time intervals $t \geq \bar{\tau}$, in which the self-chaotization of phases takes place, for the matrix elements we should use general expressions (18). The substitution of these expressions for the matrix elements (18) into the density matrix (15) gives

$$\rho_n^{+-}(t) = \frac{1}{2}\begin{pmatrix} 1 - f(2\delta\omega t)\cos 2\omega t & if(2\delta\omega t)\sin 2\omega t \\ -if(2\delta\omega t)\sin 2\omega t & 1 + f(2\delta\omega t)\cos 2\omega t \end{pmatrix}. \qquad (21)$$

Hence, for times $t \geq \bar{\tau}$ during which the phases get completely chaotized, after passing to the limit $\delta\omega t >> 1$ in (21), we obtain

$$\rho_n^{+-}(t) = \frac{1}{2}\begin{pmatrix} 1 - O(\varepsilon) & iO(\varepsilon) \\ -iO(\varepsilon) & 1 + O(\varepsilon) \end{pmatrix}, \qquad (22)$$

where $O(\epsilon)$ is an infinitesimal value of order $\varepsilon = \dfrac{1}{2\delta\omega t}$.

The state described by the density matrix (22) is a mixture of two quantum states ψ_{2n}^{+} and ψ_{2n}^{-} with equal weights. The comparison of the corresponding matrix elements of matrices (22) and (21) shows that they differ in the terms that play the role of quickly changing fluctuations. When the limit is $t >> \bar{\tau}$, fluctuations decrease as $\sim \dfrac{1}{2\delta\omega t}$ (see Fig.2 and Fig.3).

Thus the system, which at the time moment $t = 0$ was in the pure state with the wave function ψ_{2n}^{-} (20), gets self-chaotized with a lapse of time $t >> \bar{\tau}$ and passes to the mixed state (22). In other words, at the

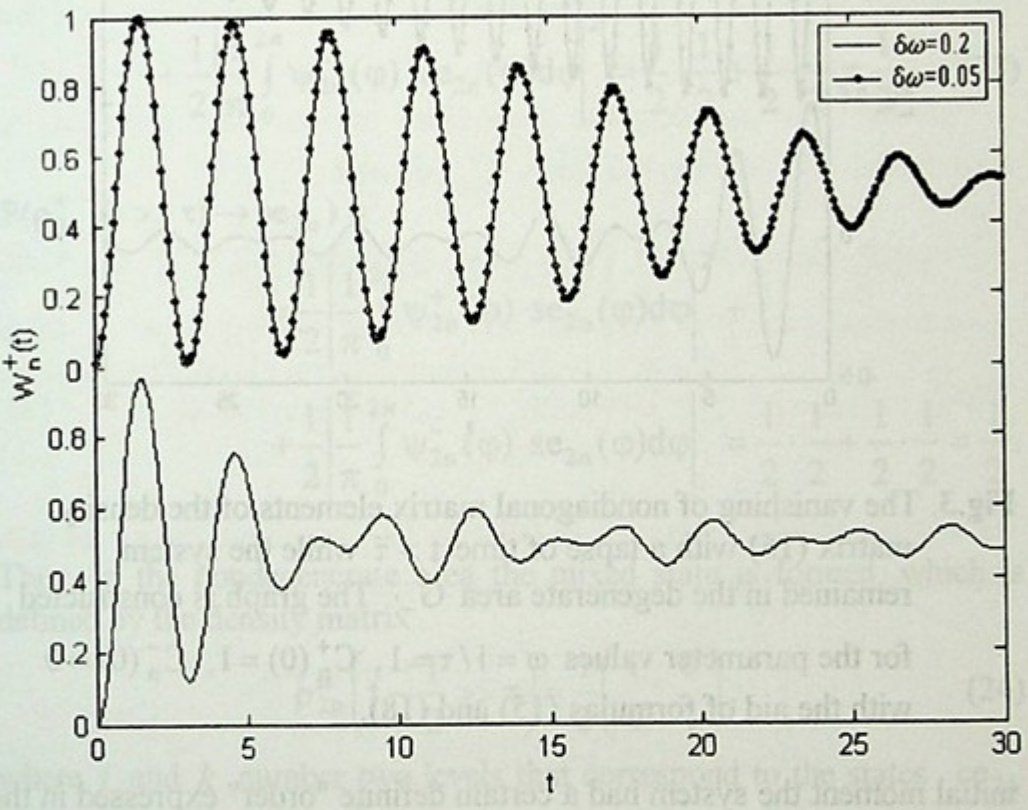

Fig.2. Time-dependence of the diagonal matrix element $W_n^+(t)$ of the density matrix (15), constructed by means of formulas (15), (18) for the parameter values $\omega = 1/\tau = 1$, $C_n^+(0) = 1$, $C_n^-(0) = 0$. As clearly seen from the Figure, the higher the dispersion value of the parameter $\delta\omega$, the sooner the stationary value $W_n^+\left(t > \bar{\tau} \sim \frac{1}{\delta\omega}\right) = \frac{1}{2}$ is achieved

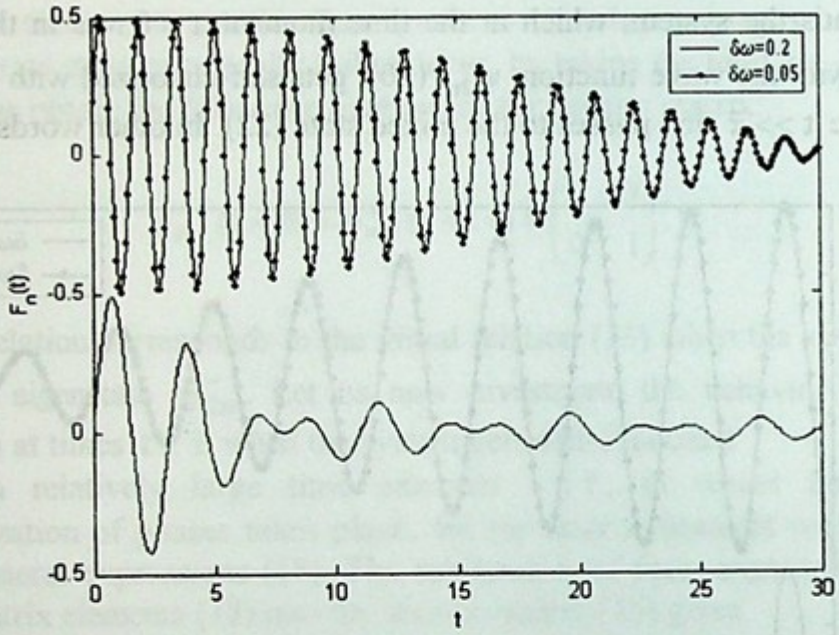

Fig.3. The vanishing of nondiagonal matrix elements of the density matrix (15) with a lapse of time $t > \bar{\tau}$ while the system remained in the degenerate area G_-. The graph is constructed for the parameter values $\omega = 1/\tau = 1$, $C_n^+(0) = 1$, $C_n^-(0) = 0$ with the aid of formulas (15) and (18).

initial moment the system had a certain definite "order" expressed in the form of the density matrix $\rho_n^{+-}(0)$ (20). With a lapse of time the system got self-chaotized and the fluctuation terms appeared in the density matrix (21). For large times $t >> \bar{\tau}$ a new "order" looking like a macroscopic order is formed, which is defined by matrix (22).

After a halfperiod the system passes to the area of nondegenerate states G (20). In passing through the branch point, there arise nonzero probabilities for passages both to the state ce_{2n} and to the state se_{2n}. Both states ψ_{2n}^+ and ψ_{2n}^- will contribute to the probability that the system will pass to either of the states ce_{2n} and se_{2n}. For the total probability of passage to the states ce_{2n} and se_{2n} we obtain respectively

$$P(\rho_{2n}^{+-}(t >> \tau) \to ce_{2n}) =$$

$$= \frac{1}{2}\left|\frac{1}{\pi}\int_0^{2\pi} \psi_{2n}^{+}(\varphi)\ ce_{2n}(\varphi)d\varphi\right|^2 +$$

$$+\frac{1}{2}\left|\frac{1}{\pi}\int_0^{2\pi} \psi_{2n}^{-}(\varphi)\ ce_{2n}(\varphi)d\varphi\right|^2 = \frac{1}{2}\cdot\frac{1}{2}+\frac{1}{2}\cdot\frac{1}{2}=\frac{1}{2}, \quad (23)$$

$$P(\rho_{2n}^{+-}(t >> \tau) \to se_{2n}) =$$

$$= \frac{1}{2}\left|\frac{1}{\pi}\int_0^{2\pi} \psi_{2n}^{+}(\varphi)\ se_{2n}(\varphi)d\varphi\right|^2 +$$

$$+\frac{1}{2}\left|\frac{1}{\pi}\int_0^{2\pi} \psi_{2n}^{-}(\varphi)\ se_{2n}(\varphi)d\varphi\right|^2 = \frac{1}{2}\cdot\frac{1}{2}+\frac{1}{2}\cdot\frac{1}{2}=\frac{1}{2}.$$

Thus, in the nondegenerate area the mixed state is formed, which is defined by the density matrix

$$\rho_{2n}^{ik}\left(t \sim \frac{T}{2} >> \tau\right) = \frac{1}{2}\begin{pmatrix} 1 & 0 \\ 0 & 1 \end{pmatrix}, \quad (24)$$

where i and k number two levels that correspond to the states ce_{2n} and se_{2n}.

As follows from (24), at this evolution stage of the system, the populations of two nondegenerate levels get equalized. It should be noted that though the direct passage (7) between the nondegenerate levels is not prohibited, perturbation (6') essentially influences "indirect" passages. Under "indirect" passages we understand a sequence of events consisting of a passage $G \to G_-$ through the branch point, a set of passages between degenerate states in the area G_- and the reverse passage through the branch point $G_- \to G$. The "indirect" passages ocurring during the modulation halfperiod $T/2$ result in the equalization (saturation) of two nondegenerate levels.

As to the nondegenerate area, the role of perturbation $\hat{H}'(t)$ in it reduces to the displacement of the system from the left branch point to the right one.

It is easy to verify that after states (24) pass to the states of the degenerate area G_+, we obtain the mixed state which involves four states $\xi_{2n}^{\pm}(\varphi)$ and $\zeta_{2n+1}^{\pm}(\varphi)$ (see Fig.1).

Let us now calculate the probability of four passages from the mixed state ρ_{2n}^{ik} (22) to the states $\xi_{2n}^{\pm}(\varphi)$ and $\zeta_{2n-1}^{\pm}(\varphi)$

$$P(\rho_{2n}^{ik} \to \xi_{2n}^{\pm}) = \frac{1}{2}\left|\frac{1}{\pi}\int_0^{2\pi}(ce_{2n}(\varphi) + se_{2n}(\varphi))\xi_{2n}^{\pm}(\varphi)d\varphi\right|^2 = \frac{1}{4},$$

$$P(\rho_{2n}^{ik} \to \zeta_{2n-1}^{\pm}) = \frac{1}{2}\left|\frac{1}{\pi}\int_0^{2\pi}(ce_{2n}(\varphi) + se_{2n}(\varphi))\zeta_{2n-1}^{\pm}(\varphi)d\varphi\right|^2 = \frac{1}{4}. \quad (25)$$

As a result of these passages, in the area G_+ we obtain the mixed state described by the four-dimensional density matrix

$$\rho_{2n,2n+1}^{+-}(t \sim T >> \tau) = \frac{1}{4}\begin{pmatrix} 1 & 0 & 0 & 0 \\ 0 & 1 & 0 & 0 \\ 0 & 0 & 1 & 0 \\ 0 & 0 & 0 & 1 \end{pmatrix}, \quad (26)$$

where the indices of the density matrix (26) show that the respective matrix elements are taken with respect to the wave functions $\xi_{2n}^{\pm}(\varphi)$ and $\zeta_{2n+1}^{\pm}(\varphi)$ of degenerate states of the area G_+.

It is easy to foresee a further evolution course of the system. At each passage through the branch point, the probability that an energy level will get populated is equally divided between branched states. We can see the following regularity of the evolution of populations for the next time periods.

After odd halfperiods, the population of any n-th nondegenerate level is defined as an arithmetic mean of its population and the

population of the nearest upper level, while after even halfperiods -- as an arithmetic mean of its population and the nearest lower level. This population evolution rule can be represented both in the form of Table 1 and in the form of recurrent relations

$$P(n,2k) = P(n+1,2k) = \frac{1}{2}\left(P(n,2k-1) + P(n+1,2k-1)\right), \qquad (27)$$

$$P(n+1,\ 2k+1) = P(n+2,\ 2k+1) = \frac{1}{2}\left(P(n+1,\ 2k) + P(n+2,\ 2k)\right),$$

where $P(n,k)$ is the population value of the n-th level after time $k\frac{T}{2}$, where k is an integer number. The creeping of populations among nondegenerate levels is illustrated in Fig.4.

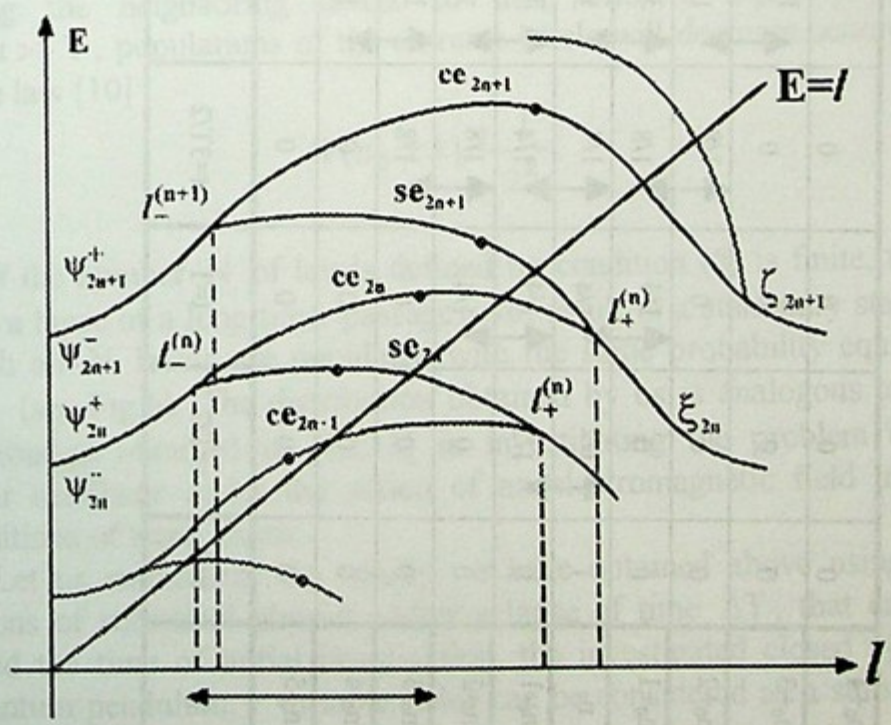

Fig.4. A fragment of the energy spectrum depending on the slowly changing parameter (4) of the quantum mathematical pendulum (6). With a lapse of time $t >> T$ the stationary state is achieved, for which all levels are populated with an equal probability

Table 1. Evolution of populations of nondegenerate levels

n_0+4	0	0	0	0	0	0	0	0
n_0+3	0	0	0	0	1/16	1/16	3/32	3/32
n_0+2	0	0	0	1/8	1/16	1/8	3/32	1/8
n_0+1	0	0	1/4	1/8	3/16	1/8	5/32	1/8
n_0	1	1/2	1/4	1/4	3/16	3/16	5/32	5/32
n_0-1	0	1/2	1/4	1/4	3/16	3/16	5/32	5/32
n_0-2	0	0	1/4	1/8	3/16	1/8	5/32	1/8
n_0-3	0	0	0	1/8	1/16	1/8	3/32	1/8
n_0-4	0	0	0	0	1/16	1/16	3/32	3/32
n_0-5	0	0	0	0	0	0	0	0
N	t=0	t=T/2	t=T	t=3T/2	t=2T	t=5T/2	t=3T	t=7/2T

This Table is a logical extrapolation of the analytical results obtained in Subsection 3. It shows how the population concentrated initially on one level n_0 gradually spreads to other levels. It is assumed that the extreme upper level $n_0 + 4$ and the extreme lower level $n_0 - 5$ are forbidden by condition (5) and do not participate in the process.

The results of numerical calculations by means of formulas (27) are given in Fig.5 and Fig.6. Fig.5 shows the distribution of populations of levels $P(n)$ after a long time $t >> T$ when the population creeping occurs among levels, the number of which is not restricted by (5). Let us assume that at the initial time moment $t = 0$, only one n_0-th level is populated with probability $P(n_0) = 1$. According to the recurrent relations (27), with a lapse of each period T "indirect" passages will result in the redistribution of populations among the neighboring levels so that, after a lapse of time $t = k\tau >> T$, populations of the extreme levels will decrease according to the law [10]

$$P(n_0 \pm k) \sim \frac{1}{2^k}.$$

If the number N of levels defined by condition (5) is finite, then, after a lapse of a long time, passages will result in a stationary state in which all N levels are populated with the same probability equal to $1/N$ (see Fig.6). The distribution obtained by us is analogous to the distribution obtained in [12,13] in investigating the problem on a linear oscillator under the action of an electromagnetic field in the conditions of weak chaos.

Let us summarize the results we have obtained above using the notions of statistical physics. After a lapse of time ΔT, that can be called the time of initial chaotization, the investigated closed system (quantum pendulum + variable field) can be considered as a statistical system.

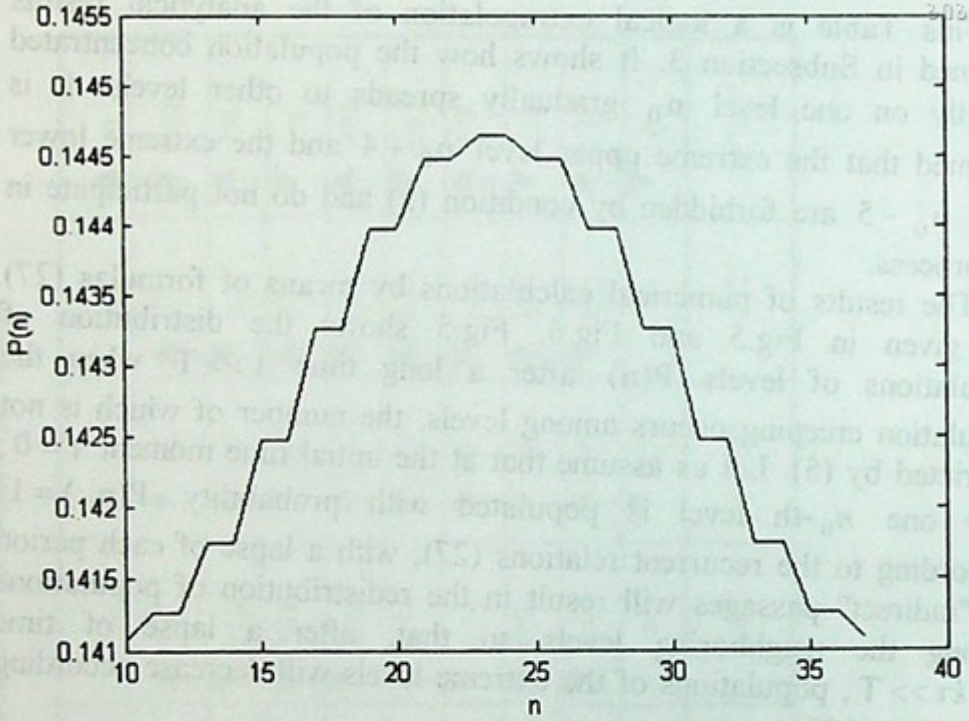

Fig.5. Results of numerical calculations performed by means of recurrent relations (27). Formation of statistical distribution of populations of levels $P(n)$ with a lapse of a large evolution time $t \approx 1000\,T$ of the system. The result shown in this figure corresponds to the case for which the level population creeping is not restricted by condition (5)

At that, the closed system consists of two subsystems: the classical variable field (6') that plays the role of a thermostat with an infinitely high temperature and the quantum mathematical pendulum (6). A weak (indirect) interaction of the subsystems produces passages between nondegenerate levels. After a lapse of time $t >> T$ this interaction ends in a statististical equilibrium between the subsystems. As a result, the quantum pendulum subsystem acquires the thermostat temperature, which in turn leads to the equalization of level populations. The equalization of populations usually called the saturation of passages can be interpreted as the acquisition of an infinite temperature by the quantum pendulum subsystem.

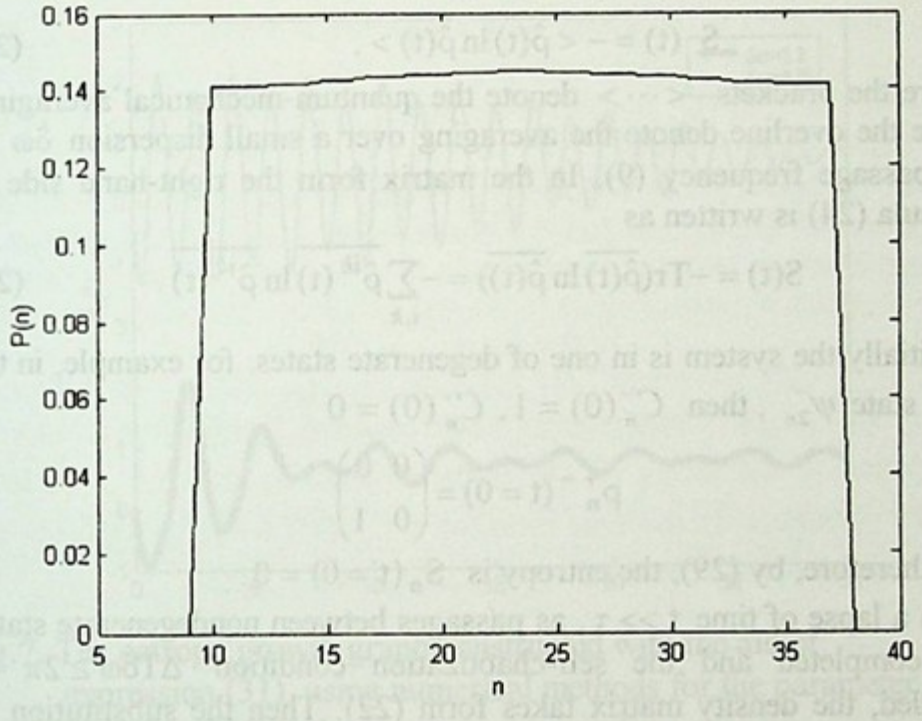

Fig.6. Results of numerical calculations performed by means of recurrent relations (27). With a lapse of a large time interval $t \sim 1000T$ the formation of stationary distribution of populations among levels takes place. By computer calculations it was found that in the stationary state all N levels satisfying condition (5) were populated with equal probability $1/N$

4. ENTROPY GROWTH OF THE QUANTUM PENDULUM SUBSYSTEM. VARIABLE FIELD ENERGY ABSORPTION

As is known, variation or constancy of entropy can be considered as a criterion of irreversibility and reversibility of processes occurring in a closed system. In the case of irreversible processes, during which the system tends to the equilibrium state, the entropy increases, while in the equilibrium state it remains constant.

Let us use this criterion to clarify the question of reversibility for our problem. As is known, the entropy of an arbitrary quantum system is defined by the operator of the density matrix $\hat{\rho}(t)$ [14]

$$S\ (t) = -<\overline{\hat{\rho}(t)} \ln \overline{\hat{\rho}(t)}>, \qquad (28)$$

where the brackets $<\cdots>$ denote the quantum-mechanical averaging, while the overline denote the averaging over a small dispersion $\delta\omega$ of the passage frequency (9). In the matrix form the right-hand side of formula (24) is written as

$$S(t) = -\mathrm{Tr}(\overline{\hat{\rho}(t)} \ln \overline{\hat{\rho}(t)}) = -\sum_{i,k} \overline{\hat{\rho}^{ik}(t)} \ln \overline{\hat{\rho}^{ik}(t)}. \qquad (29)$$

If initially the system is in one of degenerate states, for example, in the pure state ψ_{2n}^{-}, then $C_n^{-}(0) = 1$, $C_n^{+}(0) = 0$

$$\rho_n^{+-}(t=0) = \begin{pmatrix} 0 & 0 \\ 0 & 1 \end{pmatrix}$$

and therefore, by (29), the entropy is $S_n(t=0) = 0$.

With a lapse of time $t >> \tau$, as passages between nondegenerate states are completed and the self-chaotization condition $\Delta T \delta\omega \geq 2\pi$ is fulfilled, the density matrix takes form (22). Then the substitution of the density matrix (22) into the entropy formula (29) gives

$$S_n(t \sim T/2 >> \tau) = \ln 2\ . \qquad (30)$$

Thus, on a time interval from $t = 0$ to $0 \leq t \leq \Delta T$, the entropy grows

$$S_n(t >> \tau) > S_n(t=0).$$

This proves that on this time interval the process is irreversible.

Using analytical methods, we have succeeded in establishing only the asymptotic value of entropy. To investigate a complete picture of entropy change on a time interval $0 \leq t \leq \Delta T$, we use expression (15) for $\rho_n^{+-}(t)$. After substituting it into the entropy formula we obtain

$$S_n(t) = -W_n^{-}(t) \ln\left|W_n^{-}(t)\right| - W_n^{+}(t) \ln\left|W_n^{+}(t)\right| - \pi F_n(t)\ . \qquad (31)$$

Fig.7 shows the entropy as a function of time constructed with the aid of (18), (31) by numerical methods.

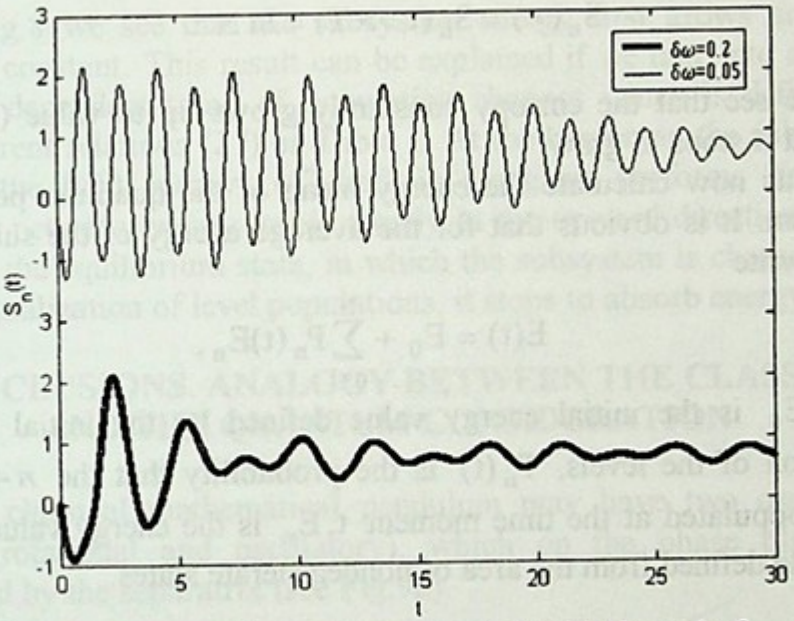

Fig.7. The entropy growth graph constructed with the aid of expression (31), using numerical methods for the parameter values $\omega = 1/\tau = 1$

To calculate the entropy value with the lapse of one period T, we substitute matrix (26) into the entropy formula (29) and thus obtain $S_n(t \sim T) = \ln 4$.

The state, in which all accessible levels of the subsystem are populated with the same probability $1/N$ (Fig.6), is the equilibrium state. The corresponding density matrix of dimension N is written as

$$\rho_{2n}^{ik}(t >> T) = \frac{1}{N}\begin{pmatrix} 1 & 0 & \cdot & \cdot & \cdot & 0 \\ 0 & 1 & 0 & \cdot & \cdot & 0 \\ 0 & 0 & 1 & \cdot & \cdot & 0 \\ \cdot & \cdot & \cdot & \cdot & \cdot & \cdot \\ \cdot & \cdot & \cdot & \cdot & \cdot & \cdot \\ 0 & 0 & 0 & 0 & 0 & 1 \end{pmatrix} \tag{32}$$

After substituting ρ_{2n}^{ik} from (32) into(29), we obtain the maximal entropy value on time intervals $t >> T$

$$S_n(\infty) = S_n(t >> T) = \ln N \ . \qquad (33)$$

Thus we see that the entropy constantly grows up to value (33) and after that it stops to grow.

Let us now calculate the energy mean of the quantum pendulum subsystem. It is obvious that for the average energy of the subsystem we can write

$$E(t) = E_0 + \sum_{n=1}^{N} P_n(t) E_n \,, \qquad (34)$$

where E_0 is the initial energy value defined by the initial $(t = 0)$ population of the levels, $P_n(t)$ is the probability that the n-th level will be populated at the time moment t, E_n is the energy value in the n-th state defined from the area of nondegenerate states.

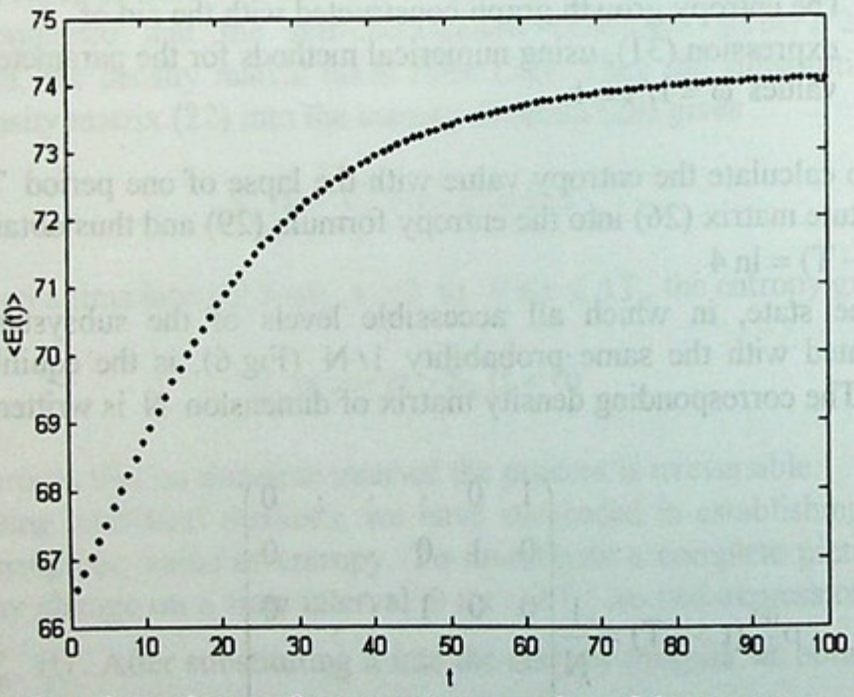

Fig.8. Time-dependence of a mean energy value of the quantum mathematical pendulum subsystem, constructed by numerical methods using formula (34). As clearly seen from the figure, the absorption of optical pumping energy takes place prior to reaching the state of statistical equilibrium

In Fig.8 we see that the subsystem energy first grows and then becomes constant. This result can be explained if we take into account the time dependent trend of population changes which is defined by the recurrent relations (27) or Table 1. At the beginning the subsystem absorbs the field energy (6') and, in doing so, performs "indirect" passages between energy levels mostly in the upward direction. Upon reaching the equilibrium state, in which the subsystem is characterized by the equalization of level populations, it stops to absorb energy.

5. CONCLUSIONS. ANALOGY BETWEEN THE CLASSICAL AND THE QUANTUM CONSIDERATION

The classical mathematical pendulum may have two oscillation modes (rotational and oscillatory), which on the phase plane are separated by the separatrix (see Fig.9a).

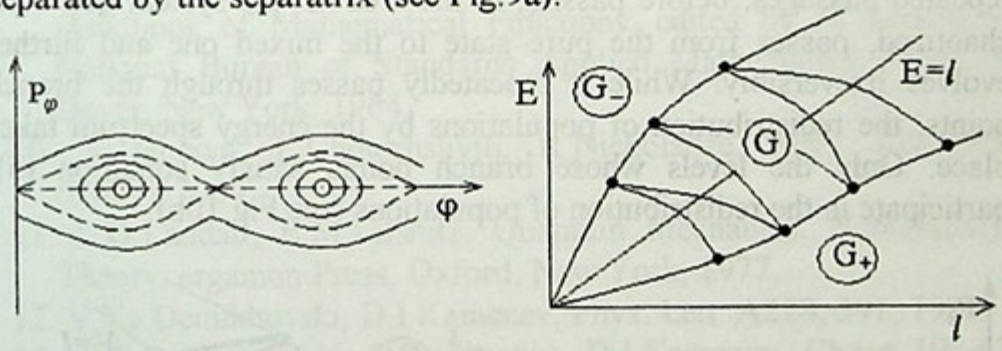

Fig.9. Analogy between the classical and quantum considerations. Unperturbed motion.

a) Classical case. Phase plane. Separatrix;
b) Quantum case. Specific dependence of the energy spectrum on the parameter (Mathieu characteristics). Degenarate $G_\pm$ and non-degenerate G areas of the spectrum

On the plane (E,l) the quantum mathematical pendulum has two areas of degenerate states -- G_- and G_+. Quantum states from the area G_- possesses translational symmetry in the pendulum phase space. These states are analogous to the classical rotational mode.

Quantum states from the degenerate area G_+ possess symmetry with respect to the equilibrium state of the pendulum and therefore are analogous to the classical oscillatory state [10]. On the plane (E,l), the area of nondegenerate states G, which lies between the areas G_- and G_+, contains the line $E=l$ corresponding to the classical separatrix (see Fig.9b). If the classical pendulum is subjected to harmonically changing force that perturbs a trajectory near to the separatrix, then the perturbed trajectory acquires such a degree of complexity that it can be assumed to be a random one. Therefore we say that a stochastic motion layer (so-called stochastic layer) is formed in the neighborhood of the separatrix [7] (see Fig.10a).

In the case of quantum consideration, the periodic perturbation (6) brings about passages between degenerate states. As a result of repeated passages, before passing to the area G the system gets self-chaotized, passes from the pure state to the mixed one and further evolves irreversibly. While it repeatedly passes through the branch points, the redistribution of populations by the energy spectrum takes place. Only the levels whose branch points satisfy condition (5), participate in the redistribution of populations (see Fig.10b).

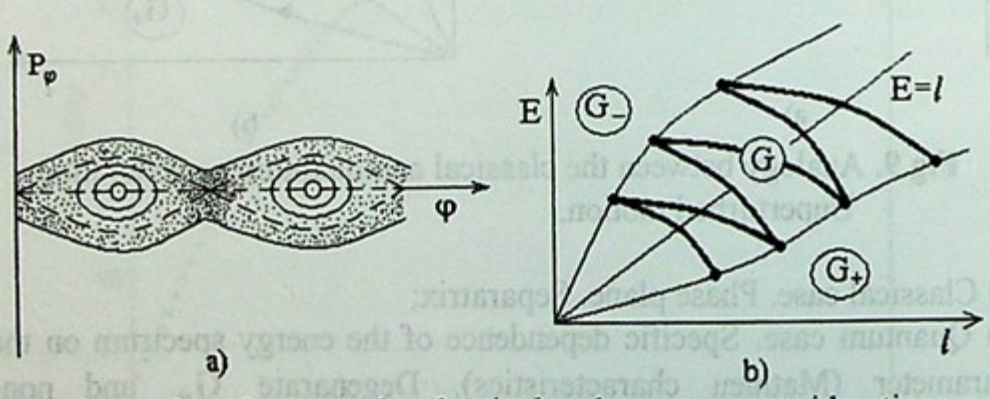

Fig.10. Analogy between the classical and quantum considerations. Perturbed motion:

a) Classical case. Stochastic trajectories in the neighborhood of the separatrix form the stochastic layer (cross-hatched area);

b) Quantum case. The mixed state was formed as a result of population of nondegenerate levels situated on both sides of the classical separatrix.

REFERENCES

1. Y.Imry. Introduction in Mesoscopic Physics. Oxford University Press, New York, 1997.
2. M.Feingold, A.Peres. Phys. Rev. **A34**, 1986, 591.
3. D.Cohen, T.Kottos. arXiv: cond-mat/0302319, **3**, 18 Mar., 2004.
4. D.Cohen, T.Kottos. Phys. Rev. Lett. **85**, 2000, 4839.
5. D.Cohen, T.Kottos. Phys. Rev. **E63**, 2001, 36203.
6. G.P.Berman, G.M.Zaslavsky. Phys. Lett. **61A,** 1977, 295.
7. R.Z.Sagdeev, D.A.Usikov, G.M.Zaslavsky. Nonlinear Physics. Hardwood, New-York, Acad. Publ., 1988.
8. A.Ugulava, L.Chotorlishvili, K.Nickoladze. Phys. Rev. **E68,** 026216, 2003.
9. H.Bateman, A.Erdelyi. Higher Transcendental Functions. **3,** MC Grow-Hill Book Company, New York-Toronto-London, 1955. Handbook of Mathematical Functions, edited by M.Abramovitz, National Bureau of Standards Applied Mathematics Series, **55,** Dover, New York, 1964.
10. A.Ugulava, L.Chotorlishvili, K.Nickoladze, Phys. Rev. **E70,** 026219 2004.
11. L.D.Landau, E.M.Lifshitz, Quantum Mechanics. Nonrelativistic Theory. ergamon Press, Oxford, New York, 1977.
12. V.Ya.Demikhovski, D.I.Kamenev, Phys. Lett. **A228,** 391, 1997.
13. G.P.Berman, V.Ya.Demikhovski, D.I.Kamenev, Chaos 10, 670, 2000.
14. S.Fujita, Introduction to Non-equilibrium Quantum Statistical Mechanics W.P.Saunders Company, Philadelphia -London, 1966.

Tbilisi State University

ა. უგულავა, ლ. ჭოტორლიშვილი, კ. ნიკოლაძე

კვანტური საქანის ევოლუციის სტატისტიკური აღწერა

დასკვნა

მათემატიკური საქანი წარმოადგენს იმ უმარტივეს სისტემას, რომელიც ამჟღავნებს დინამიურ-სტოქასტური სისტემისათვის დამახასიათებელ ყველა ძირითად თვისებას. მოცემული ნაშრომი ეძღვნება მათემატიკური საქანის კვანტურ-მექანიკურ გამოკვლევას, რომელიც მიზნად ისახავს დინამიური სტოქასტურობის კვანტური ანალოგის (კვანტური ქაოსის) ძირითადი თვისებების გამოვლინებას.

ნაშრომში ნაჩვენებია, რომ კვანტური საქანის პერიოდულმა შეშფოთებამ სეპარატრისას მახლობლობაში, ისევე როგორც კლასიკური საქანის შემთხვევაში, შეიძლება მიგვიყვანოს შეუქცევად მოვლენებამდე. გადაგვარებულ მდგომარეობებს შორის მრავალჯერადი გადასვლების შედეგად ხდება სისტემის თვითქაოტიზაცია და სუფთა მდგომარეობიდან შერეულ მდგომარეობაში გადასვლა. პერიოდული ველით გამოწვეული სისტემის ნელი დრეიფი მათიე-მახასიათებლების გასწრივ მოიცავს განშტოებათა წერტილების სასრულ რაოდენობას. კვანტური ქაოსი მყარდება ამ წერტილებით შემოსაზღრულ არეში. მიღებულია რეკურენტული თანაფარდობები იმ დონეების დასახლებებისათვის, რომლებიც მონაწილეობენ ევოლუციის შეუქცევად პროცესში. ნაჩვენებია, რომ სისტემის ენტროპია იზრდება კვანტური ქაოსის წარმოქმნის პროცესში, ხოლო შემდგომ, წონასწორული მდგომარეობის დამყარებისას, ღებულობს მუდმივ მნიშვნელობას.

ABOUT ONE CONTRADICTION IN CLASSICAL ELECTRODYNAMICS

N. Chachava, I. Lomidze, D. Karkashadze, J. Javakhishvili

Accepted for publication June, 2004

For discussion

ABSTRACT. In the article the standard problem, which arises in classical electrodynamics is considered, when the processes of energy absorption its radiation and accompanying effects are studied and interpreted. At first it concerns the processes of energy propagation in electromagnetic fields of charged particles moving in various regimes.

We consider two identical isolated systems; in each one we have charged particle moving with the same constant velocity. One particle's velocity is changed by the external force. Thus difference between energies of considered systems is equal to external force's work. From this obvious equality we have received the nonphysical result: energy of electromagnetic field of charged particle moving with constant velocity does not depend on the velocity of the movement.

This nonphysical result as usually is connected with singularity, which appears in the field of point particle. But with this reason the second result of the article cannot be explained: the energy of field induced by moving charge in definite time interval depends on observation time moment, however according to classical electrodynamics this energy is exactly determined by particle's movement in considered time interval.

Maybe this result appears because we calculate field's energy and momentum by integrating appropriate densities in some volume, however these quantities do not have proper Lorentz – transformation qualities.

INTRODUCTION

An interest to Maxwell electrodynamics principles, to results arising from them, and to their possible interpretation [1-3] has recently been renewed. First of all this interest is related with transfer processes of electromagnetic field energy under conditions of different regimes [4] of charged particles' movement. There is also a great interest to processes of energy absorption and its radiation in a strong electromagnetic field, investigation and interpretation of accompanying effects [5], a propagation of electromagnetic field in a transitional zone, non-stationary interference of electromagnetic waves [6], etc. Main attention in the cited works is focused on the study of localization and propagation of electromagnetic field energy. In addition, in a part of discussed problems the effects of so-called "tachyons" [7-9] take place, i.e. exchange of energy between sources located in points with space-like interval between them, dislocation of interference maximums' with velocity higher than light speed. Some authors noted the misbalance in an energy-momentum 4-vector during calculation of its variations caused by radiation reaction force, etc. A number of authors see roots of these difficulties in existence of singularities of point sources' (or, generally, central-symmetric fields), that complicates correct analysis of obtained results and realistic conclusion-making process

In the present article two new contradictions are found in the framework of classical electrodynamics. While deriving the first result we have used the quantity of field energy (but not its explicit form) localized in vicinity of the point charge, and that's why this contradiction may be explained by causes mentioned above. The second result appears in area of weak fields and therefore its explanation requires different ideas.

Two systems are discussed in the framework of classical electrodynamics. In the first system a charge moves with constant velocity υ_1, as for the second system it is identical to the first one until t' moment; then work A is performed on it that causes change of velocity of a charge from υ_1 to υ_2 ($\upsilon_1 || \upsilon_2$). Based on energy conservation law it is derived that starting from $t = -\infty$ moment, energy of electromagnetic field of a charge moving with constant velocity does not depend on the velocity of movement.

1. ENERGY OF LAYER

Let us consider a linear but nonuniform movement of a charge (Fig.1). Fields radiated by charge during its movement along AB interval are being localized for t moment in an eccentric spherical layer between AD and BC spherical surfaces. Calculation of energy localized in this layer gives the following (see Appendix *a*, formula (28)):

$$W_{t';\,t'+\Delta t';\,t}=\frac{2e^2}{3c}\int_{t'}^{t'+\Delta t'}\frac{\dot{\beta}^2 dt_1}{(1-\beta^2)^3}+\frac{e^2}{6c}\left[\frac{3+\beta^2}{1-\beta^2}\cdot\frac{1}{t-t_1}\right]_{t_1=t'}^{t_1=t'+\Delta t'} . \qquad (1)$$

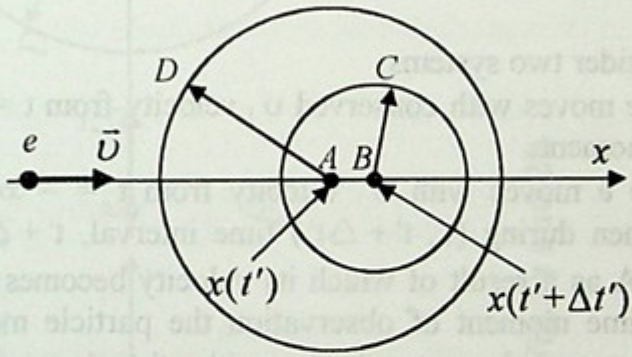

Fig.1.

$$BC=c\,(t-t'-\Delta t'),\quad AD=c\,(t-t')$$

Here $\beta=\upsilon_x(t_1)/c$.

From formula (1) for a particle moving with constant velocity we obtain:

$$W_{t';\,t'+\Delta t';\,t}(\upsilon)=\frac{e^2}{6c}\cdot\frac{3+\beta^2}{1-\beta^2}\cdot\left(\frac{1}{t-t'-\Delta t'}-\frac{1}{t-t'}\right) . \qquad (2)$$

$$\beta=\upsilon_x(t_1)/c.$$

2. WORK OF RADIATION REACTION FORCE

Charge moving with acceleration is impacted by radiation reaction force of its own field. Work of this force during (t', t'+Δt') period of

time calculated by means of the following formula (see Appendix *b*, formula (37)):

$$A_{RRF} = -\frac{2e^2}{3c}\cdot \int_{t'}^{t'+\Delta t'} \frac{\dot{\beta}^2 dt_1}{(1-\beta^2)^3} + \left[\frac{\beta\dot{\beta}}{\left(1-\beta^2\right)^2}\right]_{t_1=t'}^{t_1=t'+\Delta t'} \cdot \frac{2e^2}{3c} \quad . \quad (3)$$

Here again $\beta = \frac{\upsilon_x(t_1)}{c}$ (motion of the particle is linear).

3. LAW OF ENERGY CONSERVATION

1) Let us consider two systems:

I – a charge *e* moves with conserved υ_1 velocity from $t = -\infty$ up to t observation moment;

II - a charge *e* moves with υ_1 velocity from $t = -\infty$ up to t' moment, $t' < t$; then during $(t', t' + \Delta t')$ time interval, $t' + \Delta t' < t$, its undergone work A as a result of which its velocity becomes υ_2. From $t' + \Delta t'$ up to t time moment of observation the particle moves with constant velocity υ_2. In accordance with the law of energy conservation:

$$E_{II} - E_I = A. \quad (4)$$

On the other hand, the work done on system II consists of the work done against the radiation reaction force and work for the change of kinetic energy of the particle:

$$A = -A_{RRF.} + \frac{m_0c^2}{\sqrt{1-\beta_2^2}} - \frac{m_0c^2}{\sqrt{1-\beta_1^2}} \quad .$$

Here $\beta_1 = \upsilon_{1x}/c$, $\beta_2 = \upsilon_{2x}/c$.

2) Let's calculate E_{II} and E_I energies in formula (4) (Figs. 2*a*, 2*b*). In these Figures $AD = c(t - t')$, $BC = c(t - t' - \Delta t')$, $W_{t_1,t_2;t_3}(\upsilon)$ is the energy of fields radiated by the particle moving with *constant velocity* υ during the time interval (t_1, t_2) and localization of which is

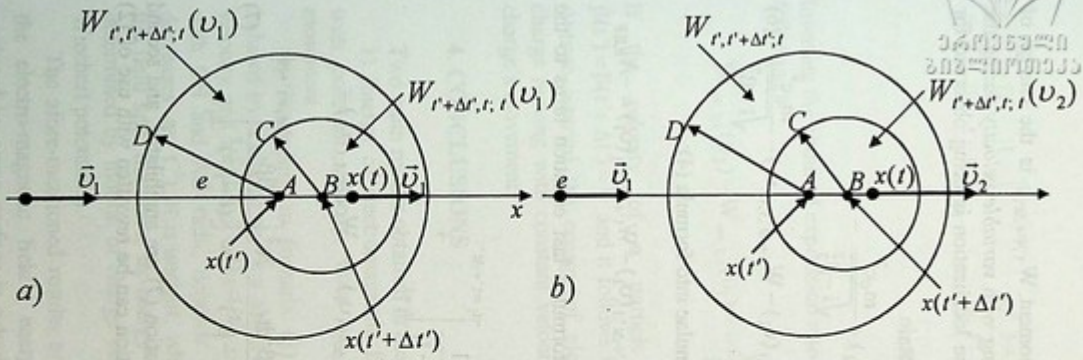
$W_{t',t'+\Delta t';t}(\upsilon_1)$
$W_{t'+\Delta t',t';\,t}(\upsilon_1)$
D
C
e
A
B
x(t)
$\vec{\upsilon}_1$
$\vec{\upsilon}_1$
x
x(t')
x(t'+Δt')
a)
$W_{t',t'+\Delta t';t}$
$W_{t'+\Delta t',t';\,t}(\upsilon_2)$
D
C
e
A
B
x(t)
$\vec{\upsilon}_1$
$\vec{\upsilon}_2$
x(t')
x(t'+Δt')
b)

Fig.2*a* and 2b

being observed for the t_3 time moment. $W_{t',t'+\Delta t';t}$ is the energy of fields radiated by the charge moving with *variable velocity* during the time interval $(t', t'+\Delta t')$ and whose localization is being observed for the time moment t.

From Figs. 2*a* and 2*b* we can obtain

$$E_{II} - E_I = W_{t',t'+\Delta t';t} + W_{t'+\Delta t',t;t}(\upsilon_2) + \frac{m_0c^2}{\sqrt{1-\beta_2^2}} -$$

$$-W_{t',t'+\Delta t';t}(\upsilon_1) - W_{t'+\Delta t',t;t}(\upsilon_1) - \frac{m_0c^2}{\sqrt{1-\beta_1^2}} \quad . (6)$$

3) Let us insert (5) and (6) formulae into formula (4):

$$W_{t',t'+\Delta t';t} + W_{t'+\Delta t',t;t}(\upsilon_2) - W_{t',t'+\Delta t';t}(\upsilon_1) - W_{t'+\Delta t',t't}(\upsilon_1) = -A_{RRF}$$

With account of (1) and (3) formulae last equation turns to the following:

$$\frac{2c^2}{3c}\int_{t'}^{t'+\Delta t'} \frac{\dot\beta^2 dt_1}{(1-\beta^2)^3} + \frac{e^2}{6c}\left[\frac{3+\beta^2}{1-\beta^2}\cdot\frac{1}{t-t_1}\right]_{t_1=t'}^{t_1=t'+\Delta t'} +$$

$$+W_{t'+\Delta t',t;t}(\upsilon_2) - W_{t',t'+\Delta t';t}(\upsilon_1) - W_{t'+\Delta t',t;t}(\upsilon_1) =$$

$$= \frac{2e^2}{3c}\int_{t'}^{t'+\Delta t'} \frac{\dot\beta^2 dt_1}{(1-\beta^2)^3} - \frac{2e^2}{3c}\left[\frac{\beta\dot\beta}{(1-\beta^2)^2}\right]_{t_1=t'}^{t_1=t'+\Delta t'} \quad . (7)$$

The integrals in both sides of equation (7) are annihilated, and second summand on the left side of equation can be rewritten with use of (2) formula in the following way:

$$\frac{e^2}{6c}\left[\frac{3+\beta^2}{1-\beta^2}\cdot\frac{1}{t-t_1}\right]_{t_1=t'}^{t_1=t'+\Delta t'} = \frac{e^2}{6c}\frac{3+\beta_2^2}{1-\beta_2^2}\frac{1}{t-t'-\Delta t'} - \frac{e^2}{6c}\frac{3+\beta_1^2}{1-\beta_1^2}\frac{1}{t-t'} =$$

$$= W_{-\infty,t'+\Delta t';t}(\upsilon_2) - W_{-\infty,t';t}(\upsilon_1) \quad .(8)$$

Inserting the obtained expression into formula (7) we get the following:

$$W_{-\infty,t;t}(\upsilon_2) - W_{-\infty,t;t}(\upsilon_1) = -\frac{2e^2}{3c}\left[\frac{\beta\dot{\beta}}{(1-\beta^2)^2}\right]_{t_1=t'}^{t_1=t'+\Delta t'} \quad . \qquad (9)$$

If the velocity of a particle is changing smoothly, then $\dot{\beta}(t') = \dot{\beta}(t'+\Delta t') = 0$ and it follows from the equation (9) that for $(-\infty, t)$ time interval the energy of electromagnetic field induced by a charge moving with constant velocity does not depend on velocity of charge's movement.

4. CONCLUSIONS

Two main results obtained in the paper are the following:

1) Energy of electromagnetic field, induced by a charge moving with constant velocity, does not depend on velocity of charge's movement.

2) According to formula (2) energy of electromagnetic field, induced by a charge moving along (A,B) section (Fig.1) with constant velocity and localized within the asymmetric layer formed by spheres with CB and AD radii, depends on observation time moment t (it decreases as t^{-2}). It is unclear, where this energy disappears, because the field and, therefore, its energy outside the layer is unambiguously determined by motion of charge beyond the (A,B) section (by Lienar-Wiechert potentials).

The afore-mentioned results are based on the standard idea, that the electro-magnetic field's energy and momentum in a volume enclosed by some surface is calculated by integrating the densities of

these quantities in the considered area. But it is known, that Lorentz transformation for energy and momentum densities generally includes the densities of flows of energy and momentum [10]. If these flows are not equal to zero, the quantities received by integrating energy and momentum densities don't have proper transformational qualities. That's why these quantities cannot be considered as the energy and momentum of the field localised in some space area.It means that if we cut some area from space filled by electro-magnetic field, we cannot consider it as an independent physical object because it doesn't satisfy Maxwell equations and its energy and momentum don't have proper transformational qualities.

We think that the reason for appearance of nonphysical results when we consider complicated nonstationary processes and try to receive energy-momentum balance by traditional method is that we just do not take into account the circumstances mentioned above.

APPENDIX A. ENERGY OF LAYER

1. The field of moving charge is described by potentials:
2.

$$\vec{E}(\vec{r},t)=\frac{e}{(1-\beta\cos\alpha)^3}\left\{\frac{1-\beta^2}{R^2}\left(\hat{\vec{R}}-\hat{\vec{x}}\beta\right)+\frac{1}{R}\frac{\dot{\beta}}{c}\left(\hat{\vec{R}}\cos\alpha-\hat{\vec{x}}\right)\right\}, \quad (10)$$

$$\vec{H}(\vec{r},t)=\frac{1}{R}[\vec{R},\vec{E}]. \quad (11)$$

In (10) and (11) formulae $[\vec{a},\vec{b}]$ is a vector product of $\vec{a}$ and $\vec{b}$ vectors, values of $\vec{E}$ and $\vec{H}$ are defined in some $M(\vec{r})$ point (Fig.3) at t moment, and values of $\vec{\beta}$ and $\vec{R}$ in the right-hand parts of formulae, are given for moment t' which is defined by the following relation:

$$t'+\frac{R(t')}{c}=t \quad (12)$$

2) Let us discuss a charge moving along the *Ox* axis (Fig. 4).

Formulas (10) and (11) are rewritten in the following way:

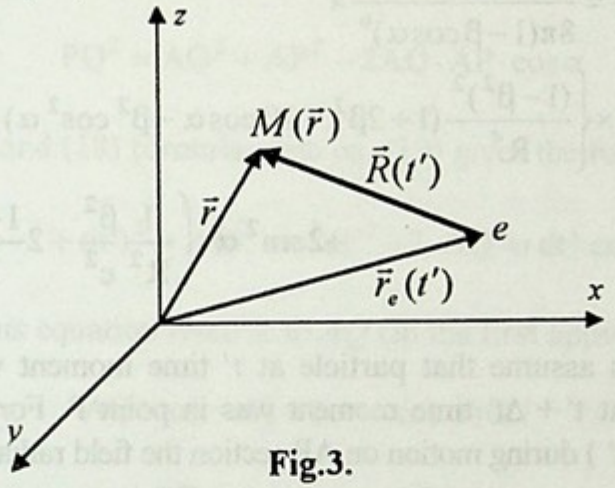

Fig.3.

$$\vec{E}(\vec{r},t)=\frac{e}{(1-\beta\cos\alpha)^3}\left\{\frac{1-\beta^2}{R^2}\left(\hat{\vec{R}}-\hat{\vec{x}}\beta\right)+\frac{1}{R}\frac{\dot{\beta}}{c}\left(\hat{\vec{R}}\cos\alpha-\hat{\vec{x}}\right)\right\}\ , \quad (13)$$

$$\vec{H}(\vec{r},t)=\frac{e}{(1-\beta\cos\alpha)^3}[\hat{\vec{x}},\hat{\vec{R}}]\left[\frac{1-\beta^2}{R^2}\beta+\frac{1}{R}\frac{\dot{\beta}}{c}\right], \quad (14)$$

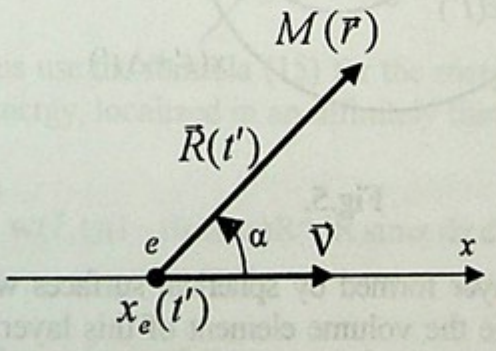

Fig.4.

where $\beta=\frac{\upsilon_x}{c}$, $\hat{\vec{x}}=\frac{\vec{x}}{|\vec{x}|}$, $\hat{\vec{R}}=\frac{\vec{R}}{|\vec{R}|}$ (Fig. 4).

Let us calculate the density of field energy:

$$w = \frac{E^2 + H^2}{8\pi} = \frac{e^2}{8\pi(1-\beta\cos\alpha)^6} \times$$

$$\times \left\{ \frac{(1-\beta^2)^2}{R^4}(1 + 2\beta^2 - 2\beta\cos\alpha - \beta^2\cos^2\alpha) + \right.$$

$$\left. + 2\sin^2\alpha \left(\frac{1}{R^2}\frac{\dot{\beta}^2}{c^2} + 2\frac{1-\beta^2}{R^3}\frac{\dot{\beta}}{c}\beta \right) \right. . \quad (15)$$

3) Let us assume that particle at t' time moment was in point A (Fig.5) and at $t' + \Delta t'$ time moment was in point P. For t time moment ($t > t' + \Delta t' > t'$) during motion on AP section the field radiated by a

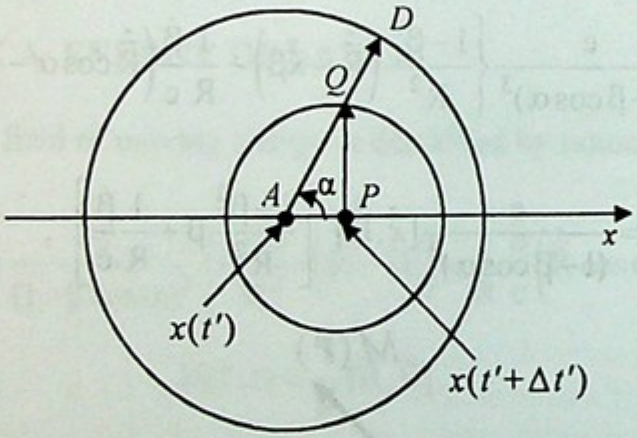

Fig.5.

charge is localized in a layer formed by spherical surfaces with AD and PQ radii. Let us calculate the volume element of this layer. According to formula (12):

$$AD = c(t - t') = R(t'), \quad (16)$$

$$PQ = c(t - t' - dt') = R + dR, \quad (17)$$

i.e.

$$dR = -c\,dt', \quad AP = \upsilon\,dt'. \quad (18)$$

Let us consider triangle ΔAPQ. According to cosine theorem:

$$PQ^2 = AQ^2 + AP^2 - 2AQ \cdot AP \cdot \cos\alpha \qquad (19)$$

Inserting (16) and (18) formulae into eq. (19) gives the following:

$$c^2(t - t' - dt')^2 = AQ^2 + \upsilon^2 dt'^2 - 2 \cdot AQ \cdot \upsilon\, dt' \cdot \cos\alpha\,.$$

Let us solve this equation relative to AQ (in the first approximation to dt'):

$$AQ = c(t - t') - (c - \upsilon\cos\alpha)\, dt'$$

Therefore

$$QD = (c - \upsilon\cos\alpha)dt' \quad . \qquad (20)$$

Let us transfer to spherical coordinates and measure radius R from point A (Fig. 5). Then we obtain:

$$dV = (c - \cos\alpha)dt' \cdot R^2 \sin\alpha\, d\alpha\, d\varphi = -(1 - \beta\cos\alpha)\, dR \cdot R^2 \sin\alpha\, d\alpha\, d\varphi \qquad (21)$$

Formula (17) was used during deriving the last equality.

4) Let us use the formula (15) for the energy density and calculate the amount of energy, localized in an infinitely thin layer drawn on Fig.5:

$$dW = -\int_0^{\pi}\int_0^{2\pi} w(\bar{r}, t)(1 - \beta\cos\alpha)R^2 dR \sin\alpha\, d\alpha\, d\varphi =$$

$$= -\frac{e^2}{4} dR \cdot \left\{ \frac{(1-\beta^2)^2}{R^2} \cdot \int_0^{\pi} \frac{(1 + 2\beta^2 - 2\beta\cos\alpha - \beta^2\cos^2\alpha)\sin\alpha d\alpha}{(1 - \beta\cos\alpha)^5} + \right.$$

$$\left. + \left(2\frac{\dot{\beta}^2}{c^2} + 4\frac{1-\beta^2}{R} \cdot \frac{\dot{\beta}}{c} \cdot \beta \right) \cdot \int_0^{\pi} \frac{\sin^3\alpha d\alpha}{(1 - \beta\cos\alpha)^5} \right\} \quad . \qquad (22)$$

The calculation of integrals in this expression gives the following:

$$I_1 = \int_0^{\pi} \frac{\sin\alpha d\alpha}{(1-\beta\cos\alpha)^5} = \frac{2(1+\beta^2)}{(1-\beta^2)^4} , \quad (23)$$

$$I_2 = \int_0^{\pi} \frac{\sin\alpha d\alpha}{(1-\beta\cos\alpha)^4} = \frac{2}{3}\frac{3+\beta^2}{(1-\beta^2)^3} , \quad (24)$$

$$I_3 = \int_0^{\pi} \frac{\sin\alpha d\alpha}{(1-\beta\cos\alpha)^3} = \frac{2}{(1-\beta^2)^2} , \quad (25)$$

$$I_4 = \int_0^{\pi} \frac{\sin^3\alpha d\alpha}{(1-\beta\cos\alpha)^5} = \frac{\beta^2-1}{\beta^2} I_1 + \frac{2}{\beta^2} I_2 - \frac{1}{\beta^2} I_3 = \frac{4}{3}\cdot\frac{1}{(1-\beta^2)^3} . \quad (26)$$

After inserting the obtained results into (22) we get the following expression:

$$dW = -\frac{e^2}{4} dR \left\{ \frac{(1-\beta^2)^2}{R^2}(2\beta^2 I_2 + I_3) + \left(2\frac{\dot{\beta}^2}{c^2} + 4\frac{1-\beta^2}{R}\cdot\frac{\dot{\beta}}{c}\cdot\beta \right) I_4 \right\} =$$

$$= -\frac{e^2}{6} dR \left\{ \frac{3+\beta^2}{R^2(1-\beta^2)} + \left(\frac{\dot{\beta}^2}{c^2} + 2\frac{1-\beta^2}{R}\cdot\frac{\dot{\beta}}{c}\cdot\beta \right) \frac{4}{(1-\beta^2)^3} \right\} . \quad (27)$$

5) Let us calculate the energy ΔW (Fig.1) localized in a layer of finite thickness. Let us remember that $dR = -cdt'$, $R = c(t-t')$, and β is taken for t' time moment. Integration of (27) expression from *t' to t'* $+\Delta t'$ time moment gives the following:

$$\Delta W = \frac{e^2}{6} \int_{t'}^{t'+\Delta t'} \left[\frac{3+\beta^2}{1-\beta^2}\cdot\frac{1}{c^2(t-t')^2} + \frac{4\dot{\beta}^2}{c^2(1-\beta^2)^3} + \right.$$

$$\left. + \frac{8}{(1-\beta^2)^2}\cdot\frac{\dot{\beta}}{c}\cdot\beta\frac{1}{c(t-t')} \right] cdt' =$$

$$= \frac{2e^2}{3c}\int_{t'}^{t'+\Delta t'} \frac{\dot{\beta}^2}{(1-\beta^2)^3}dt_1 + \frac{e^2}{6c}\left[\frac{3+\beta^2}{1-\beta^2}\cdot\frac{1}{t-t_1}\right]_{t_1=t'}^{t_1=t'+\Delta t'} \quad .(28)$$

APPENDIX B. WORK OF RADIATION REACTION FORCE

1) Four-vector of radiation reaction force acting on a non-uniformly moving charge is given by the following expression (Landau, Lifshitz, vol.2, §76 (76.2)):

$$g^i = \frac{2e^2}{3c}\left(\frac{d^2u^i}{ds^2} - u^i u^k \frac{d^2u_k}{ds^2}\right), \qquad (29)$$

where $u^i = \left(\frac{1}{\sqrt{1-\beta^2}}, \frac{\vec{\beta}}{\sqrt{1-\beta^2}}\right)$, $ds = c\sqrt{1-\beta^2}dt$, $i, k = 0,1,2,3.$

g^0 component of this four-vector has the meaning of the work done by the force acting on the charge during unit of time – a power of radiation reaction force. Let us write the equation of motion in covariant form:

$$g^i = mc\frac{du^i}{ds} = \frac{d}{ds}p^i \quad . \qquad (30)$$

Here $p^i = \left(\frac{\mathcal{E}}{c}, \vec{p}\right) = \left(\frac{m_0 c}{\sqrt{1-\beta^2}}, \frac{m\vec{\upsilon}}{\sqrt{1-\beta^2}}\right)$ – is the four-vector of momentum, ε and $\vec{p}$ are relativistic energy and three-dimensional momentum, respectively. Taking into account these notations from equation (30) we can obtain that:

$$\vec{g} = \frac{d}{ds}\vec{p} = \frac{1}{\sqrt{1-\beta^2}}\frac{1}{c}\frac{d}{dt}\frac{m_0\vec{\upsilon}}{\sqrt{1-\beta^2}} = \frac{m\vec{\beta}(\vec{\beta}\dot{\vec{\beta}})}{(1-\beta^2)^2} + \frac{m\dot{\vec{\beta}}}{1-\beta^2} = \frac{1}{\sqrt{1-\beta^2}}\frac{\vec{F}}{c},$$

$$g^0 = \frac{d}{ds}\frac{\mathcal{E}}{c} = \frac{1}{\sqrt{1-\beta^2}}\frac{1}{c}\frac{d}{dt}\frac{m_0 c}{\sqrt{1-\beta^2}} = \frac{m(\vec{\beta}\dot{\vec{\beta}})}{(1-\beta^2)^2} = (\vec{g}\vec{\beta}) = \frac{1}{\sqrt{1-\beta^2}}\frac{(\vec{F}\vec{\beta})}{c}, \qquad (31)$$

where $\bar{F}$ is the vector of three-dimensional force acting on the particle.

2) It is easy to obtain that:

$$\frac{du^i}{ds} = \frac{1}{c}\left(\frac{(\bar{\beta},\dot{\bar{\beta}})}{(1-\beta^2)^2},\ \frac{\dot{\bar{\beta}}}{1-\beta^2} + \frac{\bar{\beta}(\bar{\beta},\dot{\bar{\beta}})}{(1-\beta^2)^2} \right), \tag{32}$$

$$\frac{d^2u^i}{ds^2} = \frac{1}{c^2}\cdot\left[\frac{\dot{\beta}^2 + (\bar{\beta}\ddot{\bar{\beta}})}{(1-\beta^2)^{5/2}} + \frac{4(\bar{\beta}\dot{\bar{\beta}})^2}{(1-\beta^2)^{7/2}},\right.$$

$$\left. \frac{\ddot{\bar{\beta}}}{(1-\beta^2)^{3/2}} + \frac{3\dot{\bar{\beta}}(\bar{\beta},\dot{\bar{\beta}}) + \bar{\beta}\dot{\beta}^2 + \bar{\beta}(\bar{\beta}\ddot{\bar{\beta}})}{(1-\beta^2)^{5/2}} + \frac{4\bar{\beta}(\bar{\beta}\dot{\bar{\beta}})^2}{(1-\beta^2)^{7/2}} \right], \tag{33}$$

$$u^i \frac{d^2u_i}{ds^2} = u_i \frac{d^2u^i}{ds^2} = \frac{\dot{\beta}^2}{c^2(1-\beta^2)^2} + \frac{(\bar{\beta}\dot{\bar{\beta}})^2}{(1-\beta^2)^3}. \tag{34}$$

Let us insert expressions (33) and (34) into formula (29), and after some simplifications we obtain:

$$g^0 = \frac{2e^2}{3c}\left[\frac{(\bar{\beta}\ddot{\bar{\beta}})}{(1-\beta^2)^{5/2}} + \frac{3(\bar{\beta}\dot{\bar{\beta}})^2}{(1-\beta^2)^{7/2}} \right]. \tag{35}$$

3) From (31) and (35) formulae we can obtain the work done by the radiation reaction force (RRF):

$$A_{\text{რ.ძ.}} = \int_{t'}^{t'+\Delta t'} (\bar{F},\bar{\upsilon})dt' = \frac{2e^2}{3c} \int_{t'}^{t'+\Delta t'} \left[\frac{(\bar{\beta}\ddot{\bar{\beta}})}{(1-\beta^2)^2} + \frac{3(\bar{\beta}\dot{\bar{\beta}})^2}{(1-\beta^2)^3} \right] dt'. \tag{36}$$

If charge moves along the Ox-axis, then we can introduce notation $\beta = \upsilon_x/c$ and expression (36) can be rewritten in the following way:

$$A_{\text{ф.д.}} = -\frac{2e^2}{3c}\int_{t'}^{t'+\Delta t'}\frac{\dot{\beta}^2 dt_1}{(1-\beta^2)^3} + \frac{2e^2}{3c}\left[\frac{\beta\dot{\beta}}{(1-\beta^2)^2}\right]_{t_1=t'}^{t_1=t'+\Delta t'}. \qquad (37)$$

REFERENCES

1. A.V.Belinski, D.N.Klishko. Uspekhi Fizichesrikh Nauk, **163, 8**, 1993, 1 (Russian).
2. G.S. Smith, An Introduction to Classical Electromagnetic Rediation. New-York, Cambridge Univ. Press, 1997.
3. R. Peierls. Suprises in Theoretical Physics. Princeton Univ. Press, Princeton, New Jersey, 1979.
4. J. Javakhishvili, I.Lomidze.Bulletin of the Georgian Academy of Sciences, **148, 3,** 1993.
5. D.S. Guo, T.Aberg. J. Phys. A: Math. Gen. **21,** 1988, 4577.
6. a) J. Javakhishvili, D. Karkashadze, I. Lomidze. On the Transportation of Energy-Momentum in Nonstationary Interference and Scattering of Electromagnetic Waves, in: Proceedings of XXV-th General Assembly of IURS, B9.17, 84.
   b) J. Javakhishvili, D. Karkashadze, I. Lomidze, J. Kervalishvili, G. Khutsishvili. Bulletin of the Georgian Academy of Sciences, **158, 2,** 1998, 223.
7. M.I. Faingold. Izvestia Vuzov, Radiofizika, **XXII, 5,** 1979, 531 (Russian).
8. L.A. Vainshtein. Uspekhi Fizichesrikh Nauk, **118 , 2,** 1976, 339 (Russian).
9. G.S. Smith, Th.W. Hertel. IEEE Antennas and Propagation Magazine, **43, 3,** 2001, 49.
10. L. Landau, E. Lifshitz. Teoreticheskaia Fizika **II,** 1967 (Russian).

Tbilisi State University

ნ. ჩაჩავა, ი. ლომიძე, დ. ქარქაშაძე, ჯ. ჯავახიშვილი

კლასიკურ ელექტროდინამიკაში არსებული ერთი წინააღმდეგობის შესახებ

დასკვნა

ნაშრომში განხილულია სტანდარტული პრობლემა, რომელიც თავს იჩენს კლასიკურ ელექტროდინამიკაში ელექტრომაგნიტურ ველში ენერგიის შთანთქმისა და გამოსხივების პროცესების, მისი თანმხლები ეფექტების შესწავლისა და ინტერპრეტაციის დროს. პირველ რიგში, ეს ეხება ელექტრომაგნიტური ველის ენერგიის გადატანის პროცესებს დამუხტული ნაწილაკების მოძრაობის სხვადასხვა რეჟიმის პირობებში.

ჩვენ განვიხილეთ ორი ერთნაირი იზოლირებული სისტემა; თითოეულში გვაქვს ერთი და იმავე სიჩქარით მოძრავი დამუხტული ნაწილაკი. ერთი ნაწილაკის სიჩქარე იცვლება გარეშე ძალის მოქმედებით. იმ მოსაზრებიდან გამომდინარე, რომ სისტემების ენერგიების სხვაობა ტოლია გარეშე ძალის მიერ შესრულებული მუშაობისა, გამომდინარეობს არაფიზიკური შედეგი: მუდმივი სიჩქარით მოძრავი დამუხტული ნაწილაკის ელექტრომაგნიტური ველის ენერგია არ არის დამოკიდებული სიჩქარის სიდიდეზე.

ამ არაფიზიკური შედეგის არსებობას, ჩვეულებრივ, აკავშირებენ წერტილოვანი მუხტის ველში არსებულ სინგულარობასთან. მაგრამ იგივე მიზეზით ვერ ავხსნით სტატიაში მიღებულ მეორე შედეგს: მუხტის მიერ დროის რაღაც შუალედში გამოსხივებული ველის ენერგია, რომლის სიდიდეც კლასიკური ელექტროდინამიკის თანახმად ზუსტად არის განსაზღვრული დროის განხილულ შუალედში ნაწილაკის მოძრაობის რეჟიმით, დაკვირვების მომენტზეა დამოკიდებული.

ჩვენი ვარაუდით ამის ახსნა შეიძლება იმით, რომ ველის ენერგიისა და იმპულსის სიმკვრივეების ინტეგრებით სივრცის მოცემულ არეში მიღებული სიდიდეები საერთოდ არ წარმოადგენენ ენერგიასა და იმპულსს, თუნდაც იმის გამო, რომ ისინი არ ემორჩილებიან შესაბამის ლორენცის გარდაქმნებს.

PECULIARITIES OF SOUND PROPAGATION IN AEROGEL FILLED WITH $He^3 - He^4$ SUPERFUID SOLUTION

Sh. Kekutia. N. Chkhaidze

Accepted for publication June, 2004

ABSTRACT. **We have studied the theory of the deformation of porous elastic solid filled with a compressible $He^3 - He^4$ solution. Hypothetic experiments for the determination of the elastic coefficients of the theory were described. From the derived equations it was shown that for highly porous media (aerogel) there exist two longitudinal sound modes at low frequencies: one is the intermediate mode between the first and fourth sound and another is the second sound like mode in impure superfluids. The present article aims to establish the coupling between temperature and pressure oscillations of these modes for superfluid $He^3 - He^4$ solution in aerogel. We show that the coupling between these two oscillations is governed either by $(c/\rho)(\partial\rho/\partial c)$ or $\bar{\sigma}\rho^a\rho^S$. Therefore the coupling for these oscillations becomes more multiform than in case of $He^3 - He^4$ solution and He II in aerogel each taken separately.**

INTRODUCTION

The effect of randomness and disorder is an important theme in condensed matter physics. Disorder and impurities often essentially change the systems behavior. We know that disorder itself can bring fascinating and often unexpected new phenomena in condensed phases matter.

One example is Anderson localization in which irregularities in a metal cause localization of the wave function and make the metal insulating at low temperatures.

The second example of such phenomena is found in glasses. Systematic studies revealed that all glasses have common characteristic thermodynamic, elastic and dielectric properties, which

differ from twin crystal chemically identical to them. This characteristic glassy behavior is related to the structural disorder inherent in glasses.

The third example is the Kondo effect, in which a very small quantity of magnetic impurity in nonmagnetic metals causes logarithmic increase of metal's electrical resistivity with temperature decrease and anomalous temperature dependence of metal's susceptibility. In the case of fluids, disorder can arised into a pure fluid system by adding impurity atoms and molecules or by placing the fluid in a porous medium.

This article focuses on the effect caused by the presence of aerogel and impurities simultaneously on superfluids acoustic properties of He^4.

Recent experimental and theoretical studies of the nature of sound propagation in $He^3 - He^4$ mixtures and He II in aerogel have shown interesting results, which are quite distinct from those found with He II [1].

The greatest success of sound propagation studies in porous media is stipulated by the development of new techniques for producing impure superfluids, which exhibit unique properties. This new class of systems includes superfluid helium confined to aerogel [2], He II with different impurities (D_2, N_2, N_e, K_r) [3], superfluids in vycor glasses [4], and watergel, i.e.a frozen water "lattice" in He II [5]. These systems exhibit very unusual properties including unexpected acoustic features. Further we discuss the sound properties of these systems and show that sound phenomena in superfluids solution in aerogel are distinct from those filled in He II aerogel and in $He^3 - He^4$ superfluid mixture.

Sound propagation in $He^3 - He^4$ superfluid solution (including superfluid helium in Im-He solids) has a number of peculiarities connected with the oscillations of pressure and temperature in the acoustic wave. Whereas in pure helium II only the pressure oscillates in the first sound wave, and only the temperature oscillates in the second sound wave (neglecting the coefficient of thermal expansion, which is enormously small for helium), in a solution there are pressure, temperature and concentration oscillations in both waves. In the first sound wave the oscillation of the temperature is proportional

to the coefficient $\beta=(c/\rho)(\partial\rho/\partial c)$ and in the second sound wave the pressure oscillation is proportional to the same coefficient (c is He^3 concentration, ρ is the density of the solution), and at low He^3 concentration the quantities proportional to β cannot be neglected. Unlike pure He^4, the first sound wave in solutions contains a relative oscillation of the normal and superfluid liquids, the magnitude of which is proportional to β. In pure He^4, there are no oscillations of the total flux $\vec{J}=\rho^n\vec{V}^n+\rho^s\vec{V}^s$ in the second sound wave, whereas in the solution the deviation from the equilibrium value of $\vec{J}$ is also proportional to β [6]. Sound phenomena in He^3-He^4 mixtures have been investigated very intensively both theoretically and experimentally [7,8]. The theory of weak solutions was first developed first by Khalatnikov [9]. Also interesting phenomena are observed in aerogels.

Aerogels are low density unique class of ultra size and open cell foams. Aerogels have continuous porosity and a microstructure composed of interconnected colloidal-like particles or polymeric chains with characteristic diameters of 100 angstroms. The microstructure of aerogels is responsible for their unusual acoustic, mechanical, optical and thermal properties. These microstructures impart high surface areas to the aerogels, for example, from about 350 m^2/g to about 2000 m^2/g. The similar size of their cells and pores minimizes light scattering in the visible spectrum, and thus, aerogels can be prepared as transparent, porous solids. Further, the high porosity of aerogels makes them excellent insulators with their thermal conductivity being about 100 times lower than those of known earlier dense matrix foams. Besides this the aerogel skeleton provides the low sound velocities in aerogels. Currently, aerogels of various compositions are known, and these aerogels were generally referred to as inorganic (such as silicon aerogels) and organic (such as carbon aerogels). Inorganic aerogels, for example, silica, alumina, or zirconia aerogels, are traditionally made via hydrolysis and condensation of metal alkoxides, such as tetrametoxy silane. Organic aerogels, such as carbon aerogels, are typically made from the sol-gel polymerization of resorcinol or melamine with formaldehyde under alkaline conditions.

Therefore it is obvious that, when aerogel is saturated even with pure He II new phenomena are caused by the presence of aerogel: namely, the coupling between the temperature and pressure oscillations in sound modes is provided by $\sigma\rho^{a}\rho^{S}$ parameter (ρ^{a} is the aerogel density, σ is helium entropy) [10], which enhances the coupling between the two oscillations. For example, the propagation of heat pulses with the velocity of the first mode in He II in aerogel was observed in [11]. It is also possible to observe such unusual sound phenomena in impure superfluids as slow mode pressure oscillations and fast mode temperature oscillations. So, as is seen superfluidity of helium in restricted geometries has been the object of much theoretical and experimental interest in recent years. A porous material filled with superfluid solution simultaneously possesses the properties of elastic solid and superfluid solution and therefore it is expected observation novel sound phenomena. Then it is interesting to consider the case when novel sound phenomena are caused by simultaneously presence of impurities and aerogels. Finally the task of the article is to find the coupling between temperature and pressure oscillations in sound modes in system $He^{3}-He^{4}$ solution -aerogel.

SOUNDS COUPLING IN SUPERFLUID $He^{3}-He^{4}$ SOLUTION - AEROGEL

Sounds propagation in superfluid $He^{3}-He^{4}$ mixtures completely filling the pores was considered in [12]. By analogy with Biot [13] about dissipative terms for the equations for solid and superfluid mixture motions we derived the following equations:

$$N\nabla^{2}\vec{u}+(A+N)\operatorname{grad}e+Q^{S}\operatorname{grad}\varepsilon^{S}+Q^{n}\operatorname{grad}\varepsilon^{n}=$$

$$=\frac{\partial^{2}}{\partial t^{2}}\left(\rho_{11}\vec{u}+\rho_{12}^{S}\vec{U}^{S}+\rho_{12}^{n}\vec{U}^{n}\right)+bF(w)\frac{\partial}{\partial t}\left(\vec{u}-\vec{U}^{n}\right)$$

$$Q^{S}\operatorname{grad}e+R^{S}\operatorname{grad}\varepsilon^{S}+R^{sn}\operatorname{grad}\varepsilon^{n}=\frac{\partial^{2}}{\partial t^{2}}\left(\rho_{12}^{S}\vec{u}+\rho_{22}^{S}\vec{U}^{S}\right)$$

$$Q^{n}\operatorname{grad}e+R^{n}\operatorname{grad}\varepsilon^{n}+R^{sn}\operatorname{grad}\varepsilon^{S}=$$

$$= \frac{\partial^2}{\partial t^2}\left(\rho_{12}^n \vec{u} + \rho_{22}^n \vec{U}^n\right) - bF(w)\frac{\partial}{\partial t}\left(\vec{u} - \vec{U}^n\right), \qquad (1)$$

where ρ_{11} is the total effective density of the solid moving in the solution $He^3 - He^4$. Coefficients ρ_{12}^s and ρ_{12}^n are mass parameters of "coupling" between a solid and correspondingly, superfluid and normal components of solution or mass coefficient $\rho_{12}^{s(n)}$ describes the inertial (opposed to viscous) drag when the fluid exerts on the solid as the latter is accelerated relative to the former and vice-versa. The $He^3 - He^4$ solution densities have the following form [12,13]:

$$\rho_{22}^s = \Phi\rho^s - \rho_{12}^n - \rho_{12}^s;\ \rho_{22}^n = \Phi\rho^n - \rho_{12}^n - \rho_{12}^s;\ -\rho_{12}^s > 0;\ -\rho_{12}^n > 0.$$

Complex function F(w) describes the deviation from Poiseille flow at finite frequencies. The coefficient $b = \eta\Phi^2/k_0$ is the ratio of total friction force to the average normal fluid velocity, where η is the fluid viscosity and k_0 is the permeability. $\bar{U}^n$, $\bar{U}^s$, $\bar{u}$, are the averaged displacement of the normal fluid components, the superfluid component and solid part. The equations (1) were derived in conditions when impurities participate only in normal fluid flow. Using well known methods for measurement of generalized elastic coefficients with jacketed and unjacketed compressibility tests in the case of a homogeneous and isotropic porous matrix it was found that

$$R^{sn} = \frac{\rho^s\rho^n}{\rho^2}(1+\beta)\left(1 - \frac{\rho^s}{\rho^n}\beta\right)R - \frac{(\rho^s)^2\tilde{\sigma}^2 T\Phi}{\rho\, C_{He}} \qquad (2)$$

$$R^n = \frac{(\rho^n)^2}{\rho^2}\left(1 - \frac{\rho^s}{\rho^n}\beta\right)^2 R + \frac{(\rho^s)^2\tilde{\sigma}^2 T\Phi}{\rho\, C_{He}} \qquad (3)$$

$$R^s = \frac{(\rho^s)^2}{\rho^2}(1+\beta)^2 R + \frac{(\rho^s)^2\tilde{\sigma}^2 T\Phi}{\rho\, C_{He}} \qquad (4)$$

Biot-Willis coefficients R and Q are equal to [14]

$$Q = \frac{\Phi K_{sol}\left(1-\Phi-\frac{K_b}{K_{sol}}\right)}{1-\Phi+\Phi\frac{K_{sol}}{K_f}-\frac{K_b}{K_{sol}}}, \tag{5}$$

$$R = \frac{\Phi^2 K_{sol}}{1-\Phi+\Phi\frac{K_{sol}}{K_f}-\frac{K_b}{K_{sol}}}. \tag{6}$$

The coefficients A and N correspond to Lame coefficients in the theory of elasticity and are positive

$$\frac{2}{3}N + A = K_{sol}\frac{(1-\Phi)\left(1-\Phi-\frac{K_b}{K_{sol}}\right)+\Phi\frac{K_{sol}}{K_f}}{1-\Phi+\Phi\frac{K_{sol}}{K_f}-\frac{K_b}{K_{sol}}}. \tag{7}$$

We see that generalized elastic coefficients (2-7) of the theory are related to the directly measurement coefficients: the bulk modulus of fluid K_f, the bulk modulus of solid K_{sol}, the bulk modulus of the skeletal frame K_b and N. And finally:

$$\tilde{\sigma}^2 = \bar{\sigma}^2 + c^2\frac{\partial}{\partial c}\left(\frac{Z}{\rho}\right)\frac{\partial\sigma}{\partial T};\quad \bar{\sigma} = \sigma - c\frac{\partial\sigma}{\partial c}. \tag{8}$$

The quantity $Z = \rho(\mu_3 - \mu_4)$ is defined in terms of the chemical potentials μ_3, μ_4 for He^3 and He^4 in the solution. C_{He} is the specific heat of the solution.

We are interested in the case which was considered by Mckenna et al, [2] who developed a theory explaining the behavior of sound modes in aerogel filled with He II, taking into account the coupling between

the normal component, aerogel and its elasticity. Here the normal component is locked in a very compliant solid matrix so that the liquid and the aerogel fibers move together under mechanical and thermal gradients. It takes place at low sound frequencies, when the viscous penetration depth is bigger than the pore size so the entire normal component is viscously locked to the solid matrix. The same phenomena have been discussed and considered in superfuid $He^3 - He^4$ solution-aerogel [12]. In this case for aerogel we have:

$$Q = \frac{K_b K_f}{K_{sol}}, \quad R = K_f. \tag{9}$$

$$\Phi = 1; \quad N, K_b \square K_{sol}. \tag{10}$$

$$Q^n = \frac{\rho^n}{\rho} Q\left(1 - \frac{\rho^s}{\rho^n}\beta\right), \quad Q^s = \frac{\rho^s}{\rho} Q\left(1+\beta\right). \tag{11}$$

In order to consider low frequency limit we must exclude the friction force, the two equations content and substitute these two equations by a nonequivalent one. Because normal component of superfluid mixture is completely locked to the matrix due to the viscosity we have $\bar{u} = \bar{U}^n$.

So, we obtain two dispersion equations for two variables:

$$-(A+2N+2Q^n+R^n)k^2U^n-(Q^s+R^{sn})k^2U^s =$$

$$= -\omega^2[\ (\rho_{11}+2\rho_{12}^n+\rho_{22}^n)U^n+\rho_{12}^s U^s \tag{12}$$

$$-(Q^s+R^{sn})k^2U^n-R^s k^2U^s = -\omega^2(\rho_{12}^s U^n+\rho_{22}^s U^s \tag{13}$$

From equations (12-13), we have two longitudinal sounds, which have the following form:

$$C_{14}^2 = \frac{C_1^2 + \frac{\rho^a}{\rho^n} C_4^2}{1 + \frac{\rho^a}{\rho^n}}, \qquad (14)$$

$$C_{2a}^2 = \frac{C_2^2 + \frac{\rho^a \rho^s}{\rho^n \rho} \frac{(1+\beta)^2}{1+\frac{\rho^s}{\rho^n}\beta^2} C_a^2}{1 + \frac{\rho^a \rho^s}{\rho^n \rho} \frac{(1+\beta)^2}{1+\frac{\rho^s}{\rho^n}\beta^2}}, \qquad (15)$$

where the first sound C_1, the second sound C_2, the fourth sound C_4 and the sound velocities in empty aerogel C_a:

$$C_1^2 = \frac{K_f}{\rho}\left(1 + \frac{\rho^s}{\rho^n}\beta^2\right); \quad C_2^2 = \frac{\rho^s}{\rho^n} \frac{\tilde{\sigma}^2 T}{C_{He}\left(1 + \frac{\rho^s}{\rho^n}\beta^2\right)};$$

$$C_4^2 = \frac{\rho^n}{\rho} C_1^2 \frac{(1+\beta)^2}{1+\frac{\rho^s}{\rho^n}\beta^2} + \frac{\rho^n}{\rho} C_2^2 \left(1 + \frac{\rho^s}{\rho^n}\beta^2\right); \quad C_a^2 = \frac{K_b + (4/3)N}{\rho^a}. \qquad (16)$$

The first solution (14) is intermediate between the first and fourth sounds. It resembles the fast mode and propagates at a speed slightly lower than in mixture. Another solution (15) corresponds to the slow mode. Experimental data for silica aerogel give $C_a^2 >> C_2^2$ [2], so from this inequality and (15) it follows $C_{2a}^2 >> C_2^2$. Therefore, the velocity of slow wave is much bigger than that of temperature sound in free solutions.

From the continuity equations for mass and entropy we can derive the ratio of the density oscillation to the entropy oscillation:

$$\rho'/\sigma' = \frac{\rho}{\sigma}\frac{1+\left(\rho^n/\rho^s\right)\left(U^n/U^s\right)}{\left(U^n/U^s\right)-1}. \qquad (17)$$

The ratio of normal average displacement to the superfluid average displacement we find from equation (13)

$$\frac{U^n}{U^s} = -\frac{C^2\rho_{22}^s - R^s}{C^2\rho_{12}^s - \left(Q^s + R^{sn}\right)}. \qquad (18)$$

Then the ratio (17), in the case of aerogel takes the form:

$$\rho'/\sigma' = \frac{\rho}{\sigma\rho^s}\frac{\rho^n C^2 - \rho^s\beta\dfrac{1+\beta}{1+\left(\rho^s/\rho^n\right)\beta^2}C_1^2 - \rho^n\left(1+\left(\rho^s/\rho^n\right)\beta^2\right)C_2^2}{C^2 - \dfrac{1+\beta}{1+\left(\rho^s/\rho^n\right)\beta^2}C_1^2} \qquad (19)$$

We must calculate the value of this ratio for the first mode (14) in the approximation $C_2^2/C_1^2 << 1$. Usually, it is adopted to establish the coupling between the pressure and temperature oscillations:

$$\left(\frac{T'}{P'}\right) = \frac{\overline{\sigma}\left(\partial\rho/\partial P\right)}{\partial\sigma/\partial T}\frac{1}{\sigma\left(\dfrac{\rho'}{\sigma'}\right)-\rho\beta} =$$

$$= \frac{\rho^s\overline{\sigma}\left(\partial\rho/\partial P\right)}{\rho^n\rho\left(\partial\sigma/\partial T\right)} \times \frac{C^2 - \dfrac{1+\beta}{1+\dfrac{\rho^s}{\rho^n}\beta^2}C_1^2}{\left(1-\dfrac{\rho^s}{\rho^n}\beta\right)C^2 - \left(1+\dfrac{\rho^s}{\rho^n}\beta^2\right)C_2^2} \qquad (20)$$

that for the first mode takes the form

$$\left(\frac{T'}{P'}\right)_{14} = -\frac{\bar{\sigma}(\partial\rho/\partial P)}{\partial\sigma/\partial T}\cdot\frac{\left(\rho^S/\rho^n\rho\right)\left[\beta+\frac{\rho^a}{\rho}(1+\beta)\right]}{1+\frac{\rho^S}{\rho^n}\beta^2+\frac{\rho^a\rho^S}{\rho^n\rho}(1+\beta)^2}. \qquad (21)$$

From (21) expression it follows that in the first mode pressure oscillations are accompanied by temperature oscillations and they are stipulated by the presence of He^3 atoms and aerogel.

In pure He II $\left(\rho^a = 0; \beta = 0\right)$ we obtain the well-known result: that only the pressure oscillates in the first sound due to the size of the thermal expansion coefficient $\partial\rho/\partial T$. Because of very weak coupling between temperature and pressure oscillations in He II, such phenomena as the slow mode (basically, representing temperature or entropy oscillations [15]) as well as heat pulse propagation with the velocity of the first sound have never been observed in pure superfluids.

In order to consider sound conversion in mixtures of different impurities in superfluids we take $\rho^a = 0$ in (21). We note that He^3-He^4 solution can be considered as an example of an impure superfluid. We see that the coefficient between T' and P' is determined by β and that the pressure oscillations accompany the temperature oscillations in the plane wave. The onset of pressure oscillations in impure helium produces propagating temperature oscillations only below T_c.

The ratio (21) allows to analyze the sound propagation phenomena in superfluid He (He^3 and He^4) in aerogel ($\beta = 0$). In this case the temperature oscillations are provided by $\sigma\rho^a\rho^S$. It is easy to see that the parameters β and $\sigma\rho^a\rho^S$ are changed by linear combination of these parameters for the system He^3-He^4 solution-aerogel. So, the coupling of the first mode to the second one in superfluid He^3-He^4 solution in aerogel is defined by the linear combination of β and $\bar{\sigma}\rho^a\rho^S$ instead of β in superfluid He^3-He^4 solution and $\sigma\rho^a\rho^S$ in He II-aerogel separately.

Now we can determine pressure oscillations, which accompany the temperature oscillations in running second plane mode:

$$\left(\frac{P'}{T'}\right)_{2a} = \frac{\rho\rho^s\tilde{\sigma}^2}{\bar{\sigma}\rho^n} \times \frac{\beta - \frac{\rho^a}{\rho}\frac{\left(1-\frac{\rho^s}{\rho^n}\beta\right)(1+\beta)}{1+\frac{\rho^s}{\rho^n}\beta^2}\frac{C_a^2}{C_2^2}}{1+\frac{\rho^s}{\rho^n}\beta^2+\frac{\rho^a\rho^s}{\rho\rho^n}(1+\beta)^2}, \qquad (22)$$

From expression (22) the results can be derived, which take place both in superfluid $He^3 - He^4$ solution and in superfluid helium in aerogel. In our case these parameters participate simultaneously.

The quality, which determines the fraction oscillations of pressure and temperature, is their relative alterations ratio:

$$\left(\frac{T'/T}{P'/P}\right)_{14} = -\frac{\bar{\sigma}PC_2^2\left(1+\frac{\rho^s}{\rho^n}\beta^2\right)^2\left[\beta+\frac{\rho^a}{\rho}(1+\beta)\right]}{T\rho\tilde{\sigma}C_1^2\left[1+\frac{\rho^s}{\rho^n}\beta^2+\frac{\rho^a\rho^s}{\rho\rho^n}(1+\beta)^2\right]}, \qquad (23)$$

$$\left(\frac{P'/P}{T'/T}\right)_{2a} = \frac{\rho^s\rho T\tilde{\sigma}^2}{P\bar{\sigma}\rho^n} \times \frac{\beta - \frac{\rho^a}{\rho}\frac{\left(1-\frac{\rho^s}{\rho^n}\beta\right)(1+\beta)}{1+\frac{\rho^s}{\rho^n}\beta^2}\times\frac{C_a^2}{C_2^2}}{1+\frac{\rho^s}{\rho^n}\beta^2+\frac{\rho^a\rho^s}{\rho\rho^n}(1+\beta)^2}, \qquad (24)$$

where P and T are the equilibrium volumes of pressure and temperature. Our results show, that disorder induced by porous materials or impurities may change the coupling between oscillations of quantities in propagating sounds or alter the nature of propagation sounds in superfluid helium.

REFERENCES

1. P. Brusov, P. Brusov, G. Lawes, C. Lee, A. Matsubara, O. Ishikava, P. Majumbar. Phys. Lett. **A310,** 2003, 311.
2. McKenna, T. Slawecki, J.D. Maynard. Phys. Rev. Lett. **66,** 1991, 1878.
3. S.I. Kiselev, V.V. Khmelenko, D.M. Lee, Fiz. Nizk. Temp. **26**, 2000, 1.
4. M.N.W. Chan, K.Y. Blum, S.Q. Murphy, G.K.S. Wong, J.D. Reppy. Phys.Rev. Lett. **G1,** 1988, 1950.
5. A.M. Kokotin, L.D. Mezhov-Deglin. Fiz. Nizk. Temp. **28**, 2002, 235.
6. R.G. Arkhipov, I.M. Khalatnikov, Sov. Phys. Jepr. **6**, 1958, 583.
7. I.M. Khalatnikov. Zh. Eksp. Teor. Fiz. **23**, 1952, 263.
8. B. Eselson, M.I. Kaganov, E. Ya. Rudavski, I.A. Serbin. Sov. Usp. Fiz. Nauk. **112,** 1974, 591.
9. M Khalatnikov.Theory of Superfluidity. Benjamin, New York, 1965.
10. P. Brusov, J.M. Parpia, P. Brusov, and G. Lawes. Phys. Rev.B. **63,** 2002, 40507.
11. A. Golov, D.A. Geller, J.M. Parpia, Phys.Rev. Lett. **82,** 1999, 3492.
12. Sh. Kekutia, N. Chkhaidze. Proceeding of I. Javakhishvili Tbilisi State University.
13. M.A. Biot, J. Acoust. Soc. Am. **28,** 1956, 168.
14. M.A. Biot, D.G. Willis. J. Appl. Mech. **24,** 1957, 594.
15. Sh. Kekutia, N. Chkhaidze. Sov. Fiz Nizkikh Temp. **28, 11,** 2002, 1115.

Georgian Academy of Sciences
Institute of Cybernetics

შ. კეკუტია, ნ. ჩხაიძე

ბგერების გავრცელების თავისებურებანი ზედნადი $He^3 - He^4$ ხსნარით შევსებულ ფოროვან გარემოში

დასკვნა

ჩვენს მიერ დამუშავებული იყო კუმშვადი ზედნადი He^3-He^4 ხსნარით შევსებული ფოროვანი, დრეკადი მყარი სხეულის დეფორმაციის თეორია. ასევე აღწერილი იყო თეორიაში შემავალი დრეკადობის კოეფიციენტების განმსაზღვრელი ჰიპოტეტური ექსპერიმენტები. მიღებული განტოლებებიდან ნაჩვენებ იქნა, რომ მაღალი ფოროვნობის გარემოსათვის (აეროგელისათვის) დაბალი სიხშირის ზღვარში არსებობს ორი გრძივი ბგერითი მოდა, რომელთაგან ერთ-ერთი წარმოადგენს საშუალედო მოდას პირველსა და მეოთხეს შორის, ხოლო მეორე - ზედნად ხსნარში ტემპერატურული ბგერის მსგავსია. წარმოდგენილი სტატიის მიზანია დადგენილ იქნეს ამ ორ მოდაში ტემპერატურისა და წნევის რხევებს შორის კავშირი მინარევებიანი ზედნადი სითხით შევსებულ აეროგელისათვის. ჩვენ ვაჩვენებთ, რომ კავშირი ამ რხევებს შორის განისაზღვრება როგორც $(c/\rho)(\partial\rho/\partial c)$ პარამეტრით, რომელიც განსაზღვრავდა ანალოგიურ კავშირს ზედნად $He^3 - He^4$ ხსნარში, ასევე $\bar{\sigma}\rho^a\rho^s$ პარამეტრით, რომელიც განსაზღვრავდა იგივე კავშირს He II-ით შევსებულ აეროგელში.

INVESTIGATION OF ZnO LAYERS TREATED BY RBQE METHOD

L. Trapaidze, T. Butkhuzi, T. Khulordava, M. Sharvashidze, L. Aptsiauri, E. Kekelidze

Accepted for publication September, 2004

ABSTRACT. We investigated new quasiepitaxial ZnO layers treated by RBQE method. To state that in the process of the formation of new ZnO layers neither extraction of sulfur from the basic ZnS crystal nor inclusion in basic crystal of activated oxygen existed in the gas phase occur, the implantation of ZnO samples by S^+ ions has been carried out. In PL spectra of ZnO ($\rho \approx 10^9$ to 10^{10} Ωcm) samples obtained by implantation of S^+ ions (T = 300-350°C; in O_2) $\lambda = 390$ nm ($\lambda = 385$ nm, $\lambda = 400$ nm); $\lambda = 440$ nm; $\lambda = 460$ nm and $\lambda = 505$ nm peaks were observed. In our opinion, these peaks correspond to (V_{Zn}^{-}-V_O^{++}); V_O^{++}; AX^+; V_{Zn}^{-}; V_O^{+}, respectively. In PL spectrum of implanted ZnO layers the peak related to sulfur has been observed. Thus, the obtained ZnO serves as a protective layer.

The control of electrical and optical properties of wideband semiconductors is very problematic because of strong compensation and self-compensation caused by residual impurities and point defects. For this reason the inversion of conductivity type is problematic [1,2].

The ZnO, ZnS are very interesting materials among the wideband semiconductors [3]. The ZnO quasiepitaxial layers are obtained on the base of ZnS by RBQE method [4,5]. Quasiepitaxial layers are formed by metal component that because of diffusion comes out of the volume of basic crystal onto the surface and oxygen singlet radicals from gas phase. In our case the RBQE method enables us to obtain single crystalline layers of ZnO on the basic crystal of ZnS but generally it might be used for other binary compounds. To state that in the process of the formation of new ZnO layer neither extraction of sulfur from the basic ZnS crystal nor inclusion in basic crystal of

activated oxygen existed in the gas phase occur the implantation of ZnO samples by S^+ ions has been carried out.

By means of RBQE method the single crystal layers of ZnO were grown on the basic ZnS crystal, the *n*-type ZnS samples with $\rho=10^2$ Ωcm grown by gas phase epitaxy were used as initial basic crystals. To obtain, new single crystal layers of ZnO the treatment was carried out in the atmosphere of activated oxygen obtained by RF-discharge of 40-80 Wt. The treatment temperature was 300-900°C and duration was 45 min-6 hours. We have studied electrical and optical properties of the basic crystals and new quasiepitaxial layers.

The *n*-type ZnO ($\rho \approx 10^2$ Ωcm) samples were implanted by S^+ ions (E = 150 keV) with D = 10^{14}-10^{16} cm^{-2} doses. The density of ion current was J = 0.3 to 2μA/cm^2. The subsequent heat treatment of implanted samples was carried out within the temperature interval of 300-500°C in molecular oxygen atmosphere. Duration of treatment was 4-8 hours.

PL spectra of the obtained ZnO layers were studied. We measured PL of ZnO/ZnS quasiepitaxial layers grown at various temperatures 350°C-850°C. The PL spectra of ZnO quasiepitaxial layers grown at different temperatures are given in Fig.1.

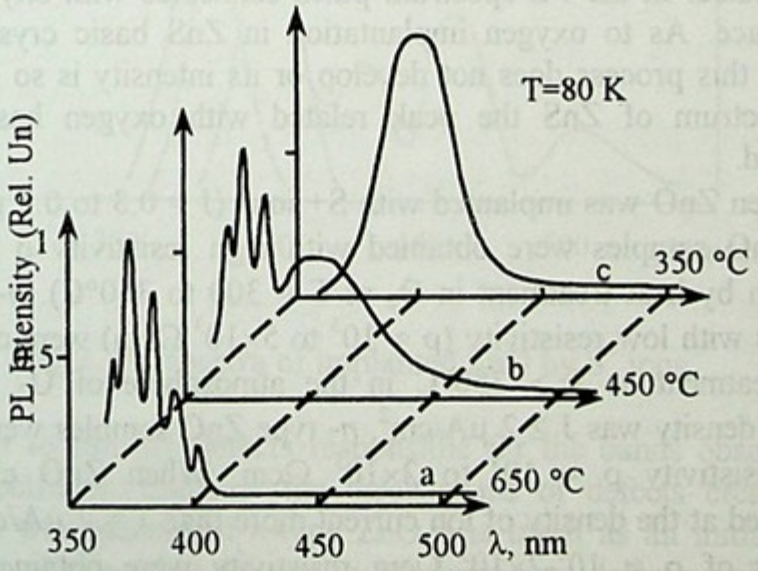

Fig.1. PL spectra of ZnO quasiepitaxial layers grown at different temperatures

At T = 650°C stoichiometric layers of ZnO ($\rho \geq 10^{13}$ Ωcm) were obtained. In the PL spectrum exciton part was observed (λ = 367 nm - A exciton, λ = 371 nm – bound exciton; λ = 374 nm; λ = 383.4 nm; λ = 392 nm and λ = 401 nm - phonon replicas of A exciton), visible part was completely vanished. During the treatment at T = 450°C a weak hole conductivity ($\rho = 10^5$-10^6 Ωcm) was observed. In the PL spectrum the exciton emission is partially covered by the emission band with maximum at λ = 390 nm. Subsequent lowering of temperature growth leads to increase of the intrinsic defect hole conductivity. At T = 350°C p-type ZnO layers with resistivity $\rho = 10^2$ Ωcm were obtained. In the PL spectrum of this crystal λ = 390 nm band completely covers the exciton part. With temperature decrease the quantity of uncontrollable impurities also decreases and the degree of monocrystallinity of the built up layers increases.

The band, connected with sulfur, was not observed in PL spectra of ZnO quasiepitaxial layers. Thus, there is no diffusion of sulfur in building layers of ZnO during the RBQE.

After removing the quasiepitaxial ZnO layers the basic ZnS crystal was studied. In the PL spectrum pikes connected with oxygen do not take place. As to oxygen implantation in ZnS basic crystal, in our opinion this process does not develop or its intensity is so low that in PL spectrum of ZnS the peak related with oxygen has not been observed.

When ZnO was implanted with S+ ions (J = 0.3 to 0.5 μA/cm^2) *n*-type ZnO samples were obtained with high resistivity $\rho \approx 10^9$-10^{10} Ωcm (in by heat treatment in O_2 at T = 300 to 350°C). *n*- type ZnO samples with low resistivity ($\rho \approx 10^3$ to 5×10^3 Ωcm) were obtained by heat treatment at T > 350°C in the atmosphere of O_2. When ion current density was J ≥ 2 μA/cm^2, *n*- type ZnO samples were obtained with resistivity $\rho \approx 10^3$ to 2×10^3 Ωcm. When ZnO crystal was implanted at the density of ion current more than J = 2 μA/cm^2 *n*- type samples of $\rho \approx 10^3$-2×10^3 Ωcm resistivity were obtained. This is caused by self-annealing of radiation defects in the process of implantation.

The temperature of heat treatment T = 300 to 350°C was found to be enough for stimulation of diffusion in the crystal after ion

implantation. The obtaining of *n*-type ZnO samples with $\rho \approx 10^9$ to 10^{10} Ωcm corresponds to the establishment of equilibrium between the crystal and molecular oxygen atmosphere at this temperature. The PL spectra of implanted ZnO samples were investigated. In PL spectra of ZnO ($\rho \approx 10^9$ to 10^{10} Ωcm) samples obtained by implantation of S^+ ions (T = 300-350°C; in O_2) λ = 390 nm (λ = 385 nm, λ = 400 nm); λ = 440 nm; λ = 460 nm and λ = 505 nm peaks were observed (Fig.2). In our opinion, these peaks correspond to (V_{Zn}^--V_O^{++}); V_O^{++}; AX^+;V_{Zn}^-; V_O^+, respectively.

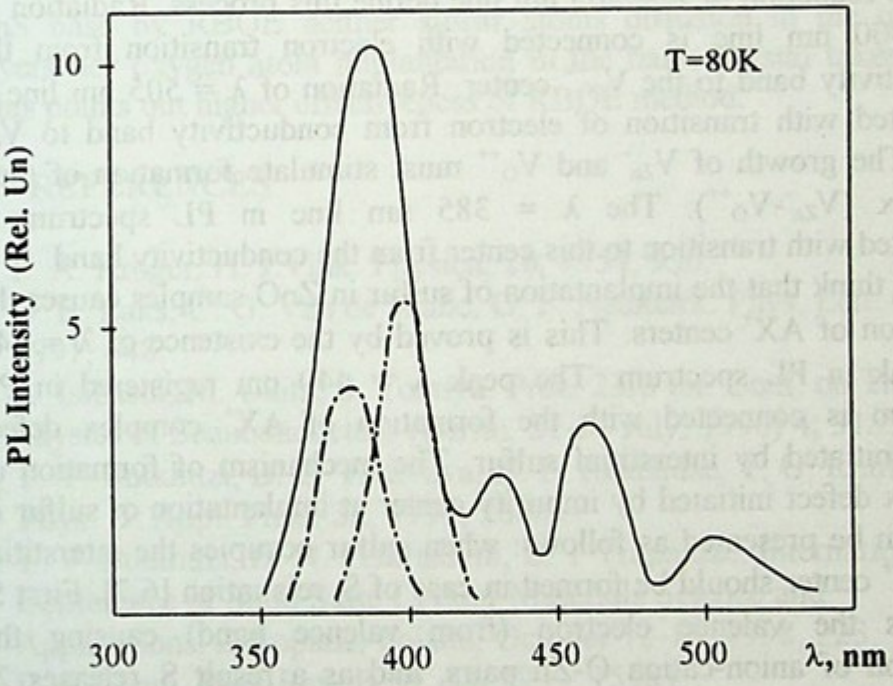

Fig.2. PL spectra of implanted ZnO by S^+ ions

In order to identify defects responsible for the bands observed in the PL spectra we consider the mechanisms of defects creation in ZnO. As it was mentioned *n*-type ZnO was taken as an initial basic crystal. It is obvious that the quality of donor type defects such as V_O, V_O^+ and Zn_i should be high in it. Creation of zinc vacancy is high in the area where defect already exists, in particular near to V_O^+. In the PL spectrum λ = 460 nm line might be connected with V_{Zn}^-. The low intensity of this line may be explained with the low electron capture

cross-section. The λ = 390 nm line is characterized with wide half width and it changes the shape according to the excitation conditions. It indicates, that the line does not have the elementary structure. We disintegrated the line and we received two elementary peaks with maxima at λ = 385 nm and λ = 400 nm wavelength. Proceeding from local electro-neutrality the recharging of one charged oxygen vacancies V_O^+ into double charged ones V_O^{++} must occur. The latter has a wide capture cross-section, and consequent peak growth must be observed in the PL spectrum. Indeed, the growth of λ = 400 nm line and the reduction of λ = 505 nm line define this process. Radiation of λ = 400 nm line is connected with electron transition from the conductivity band to the V_O^{++} center. Radiation of λ = 505 nm line is connected with transition of electron from conductivity band to V_O^+ level. The growth of V_{Zn}^- and V_O^{++} must stimulate formation of their complex (V_{Zn}^--V_O^{++}). The λ = 385 nm line in PL spectrum is connected with transition to this center from the conductivity band.

We think that the implantation of sulfur in ZnO samples causes the formation of AX^+ centers. This is proved by the existence of λ = 440 nm peak in PL spectrum. The peak λ = 440 nm registered in PL spectrum is connected with the formation of AX^+ complex defect center initiated by interstitial sulfur. The mechanism of formation of complex defect initiated by impurity center at implantation of sulfur in ZnO can be presented as follows: when sulfur occupies the interstitial site AX^+ center should be formed in case of S_i relaxation [6,7]. First S_i captures the valence electron (from valence band) causing the formation of anion-cation O-Zn pairs, and as a result S_i releases 2e into conduction band and sulfur is charged positively. Thus, sulfur implanted in ZnO acts as a donor. We think that the obtained AX^+ complex defect first captures a free hole and then a free electron from the valence band resulting in the formation of center bound exciton.

In PL spectrum of ZnO implanted by S^+, a band with maximum on λ = 440nm has been observed additionally; the case was not observed in PL spectrum of ZnO obtained on ZnS base. Thus, there is no diffusion of sulfur in new layers of ZnO during the RBQE.

An important feature of RBQE method is the fact, that on the one hand the obtained ZnO is a protective layer for ZnS, i.e. it can inhibit S and allows to extract Zn only. As a result the conductivity type

inversion in surface layers is possible. On the other hand, at fixed oxygen concentration control of concentration of Zn extraction from ZnS by temperature change is possible, which enables electrical and optical properties of new layers to vary in wider range. The obtained semiconductive ZnO layer not only inhibits S in ZnS, but prevents inclusion of oxygen occurring in gas phase in ZnS. Thus, it has been shown that it is possible by the RBQE method to achieve the conductivity type inversion with the aid of semiconductor ZnO protective layer. Thus, the obtained ZnO serves as a protective layer.

In that way, we can conclude that when obtaining ZnO layers on ZnS base by RBQE neither sulfur atoms diffusion in the obtained layers nor oxygen atom implantation in the basic crystal takes place. This points out higher effectiveness of RBQE method.

REFERENCES

1. F. A. Kroger, H. J.Vink. Physica, **20**, 1954, 950.
2. D. B. Laks, C. G. Van de Walle, G. F. Neumark. Phys. Lett. **66**, 1991, 648.
3. A. Isibashi, M. Ukita, S. Tomiya. Proc. 23rd Int. Conf. on The Physics of Semiconductors (Berlin, 21-26 July, 1996) **4,** 3155.
4. T. V. Butkhuzi, B. E. Tsekvava, N. P. Kekelidze, T. G. Khulordava.
J. Phys. D: Appl. Phys. **32,** 1999, 2683.
5. T. V. Butkhuzi, D. N. Peikrishvili, L. T Trapaidze. International Conference of Solid State Crystal-Materials Science and Applications. Zakopane, Poland, October 12-16, 1998, 223.
6. D. J. Chadi, Phys.Rev. B **59**, **23,** 1999, 15181.
7. D. J. Chadi, Phys.Rev. Lett. **72**, **4,** 1994, 534.

Tbilisi State University

თ. ბუთხუზი, თ. ხულორდავა, მ. შარვაშიძე, ლ. ტრაპაიძე,
ლ. აფციაური, ე. კეკელიძე

თუთიის სულფიდის ბაზაზე რადიკალურ სხივური ეპიტაქსიით მიღებული თუთიის ოქსიდის ფენების გამოკვლევა

დასკვნა

გამოკვლეულია თუთიის სულფიდის - ZnS ბაზაზე რადიკალური სხივური ეპიტაქსიის (რსკე) მეთოდით მიღებული თუთიის ოქსიდის - ZnO ახალი კვაზიეპიტაქსიური ფენები. იმის დასადგენად, რომ ახალი ფენების ფორმირების პროცესში ბაზური ZnS კრისტალიდან არ ხდება გოგირდის ამოსვლა და ასევე, გაზურ ფაზაში არსებული აქტივირებული ჟანგბადის ჩასვლა ბაზურ კრისტალში, მოვახდინეთ ZnO ნიმუშის S^+ იონებით იმპლანტაცია. იმპლანტირებული ZnO-ს ფლ სპექტრში დაიმზირა $\lambda = 390$ ნმ (385 ნმ და 400 ნმ); $\lambda = 440$ ნმ; $\lambda = 460$ ნმ და $\lambda = 505$ ნმ მაქსიმუმის მქონე ზოლები. ეს პიკები შეესაბამება (V_{Zn}^--V_O^{++}); V_O^{++}; AX^+; V_{Zn}^-; V_O^+ დეფექტების არსებობას. რსკე მეთოდით მიღებულ ZnO-ს ფლ სპექტრში კი გოგირდთან დაკავშირებული პიკი არ იქნა დამზერილი, რაც იმაზე მიუთითებს, რომ ბაზური კრისტალიდან არ მოხდა გოგირდის გადასვლა. მიღებულმა თუთიის ოქსიდის ფენამ დამცავი ფენის როლი შეასრულა.

POLARIZATION MEASUREMENTS IN $He^+ - N_2$ COLLISIONS

M.Gochitashvili, I.Noselidze, T.Chighvinadze , R.Lomsadze

Accepted for publication September, 2004

ABSTRACT. Emission cross-section and linear polarization of the excitation of helium atomic HeI (388.9nm) and nitrogen ionic NII (500.1-500.5nm) lines have been measured in a broad range of collision energy (1-10keV) of He^+ ions. High degree of the polarization P = - 20% was observed in the case of helium line. Such a great negative value of the degree of polarization indicates that $m_L = \pm 1$ sublevels of the excited state 3^3P of helium atom are preferably populated. Analysis of the experimental results indicates that the electron density formed in He^* during the collision is oriented perpendicularly with respect to the incident beam direction. Strong correlation is revealed between inelastic channels of the formation of excited helium and nitrogen particles.

INTRODUCTION

Ion-impact processes on molecular nitrogen N_2 have been studied extensively because of its importance in many natural and applied phenomena. From the practical point of view the collision that produces electronically excited species plays a key role in plasma physics, gas discharges, in the study of the interstellar medium and in the upper layers of the atmosphere.

Numerous works have been devoted to investigate the polarization of radiation in ion-atomic and ion-molecule processes [1-13]. Such investigations aim to determine electron alignment and polarization effects [4-9]. The polarization fraction is quantitatively discussed in terms of alignment of the orbital momentum sublevels. The cross sections of population of magnetic sublevels provide detailed information on the excitation mechanism. Due to the different populations of magnetic sublevels within a certain (nl) subshell, the radiation can be polarized and, consequently, anisotropic. Hence, from experimental point of view the information about the polarization is

important for the determination of accurate absolute and relative photon emission cross sections.

Usually in the polarization measurements the coincidences of photon and scattered particle are detected. In the above mentioned works the Lyman-α line of the hydrogen atom was mainly registered. In order to amplify the optical registration sensitivity instead of monochromator the broad bandpass filters have been used for isolating the optical lines.

In case of $He^+ - N_2$ colliding system the radiation spectrum is quite multitudinous and therefore the monochromator with high resolving power (~ 0.2 nm) is to be used. As a result the optical sensitivity became worse and it was impossible to use the coincidence scheme in measurement. The obtained results of polarization experiments allowed to make some nontrivial conclusions about the spatial distribution of the electron cloud.

In this paper, we report experimental results of the study of the excitation processes in ion-molecular collisions in a broad range of collision energy (1-10 keV). In the visible range (380 ÷ 800 nm) we have measured excitation functions and degree of linear polarization for the lines of the helium atom (λ = 388.9nm, transition $3p\ ^3P^0 \rightarrow 2s\ ^3S$)) and nitrogen ion ($\lambda$ = 500.1÷500.5nm, transition $3d\ ^3F^0 \rightarrow 3p\ ^3D$) due to the He^+-N_2 collision.

APPARATUS AND METHOD OF MEASUREMENT

The experimental setup and calibration procedure have been described in details in [13]. The ion beam extracted from the discharge source is focused, accelerated and mass selected in a 60° magnetic sector field. The beam of He^+ was passed through collision chamber. The radiation emitted as a result of the excitation of colliding particles was observed at 90° to the direction of the beam. The spectroscopic analysis of the emission was performed with visible monochromator incorporating the diffraction grating with resolution - 40 nm/mm.

Polarizer and the mica quarter-wave phase plate are placed in front of the entrance slit of the monochromator and the linear polarization of the emission is analysed. The phase plate was placed after the polarizer, was rigidly coupled to it, and applied to cancel the polarizing effect of the monochromator. The emission was recorded

by photomultiplier with a cooled cathode and operated in the current mode.

The helium ion currents in the collision chamber were of the order 0.1-0.5μA and the pressure of the gas under investigation did not exceed $6 \cdot 10^{-4}$ Torr, so that multiple collisions could be ignored. The system was pumped differentially by the oil-diffusion pump. The residual-gas pressure did not exceed $0.1 \cdot 10^{-6}$ Torr.

Particular attention was devoted to the reliable determination and control of the relative and absolute spectral sensitivity of the light-recording system. This was done by measuring the photomultiplier output signal due to the (0.0), (0.1), (0.2), (0.3), (0.4), (1.2), (1.3) and (1.4) bands in the first negative system of the ion N_2^+ ($B\ ^2\Sigma_u^+$ - $X\ ^2\Sigma_g^+$ transition) and (4.0), (4.1), (6.2), (6.3), (2.0), (3.0), (5.1) and (5.2) bands of the Meinel system ($A\ ^2\Pi_u$-$X\ ^2\Sigma_g^+$ transition) excited in collisions between the (E_e=110 eV) electrons and nitrogen molecules. The electron gun was located directly in front of the entrance slit of the collision chamber. The output signal was normalized to (0.1) band (λ = 427.8 nm), which had the high intensity in this range. The relative spectral sensitivity curve of the recording system obtained in this way was compared with the relative excitation cross sections for the same bands, averaged over the experimental data reported in ref. [14-18]. The absolute excitation cross-sections for the (0.1) band (λ = 427.8 nm) were assumed to be $5.3 \cdot 10^{-18}$ cm^2 at the electron energy of 110 eV. This value was taken from ref. [14].

The relative uncertainty in our measurements was 5%, the absolute uncertainty was 15%. The accuracy of polarization measurements did not exceed ~2%.

RESULTS OF MEASUREMENTS AND DISCUSSION

Excitation functions measured for lines of the helium atom HeI (λ=388.9nm, $3p\ ^3P \rightarrow 2s\ ^3S$) and nitrogen ion NII ($\lambda$ = 500.1÷500.5nm, $3d\ ^3F \rightarrow 3p\ ^3D$) are plotted in Fig.1. Presented curves exhibit surprising resemblance: in the whole investigated energy region both the absolute values of the emission cross sections and their energy-dependence are close to each other.

Results of polarization measurements are presented in Fig.2. As shown maximum degree of polarization is 20% for HeI (388.9 nm)

line and that is ~ 5% for NII (500.1÷500.5 nm) which is a dissociation product. It is clear from Fig.2 that degrees of polarization for the investigated emission lines change the sign at the nearly same energy ~3 keV and reach their maximum in region of 8-10 keV of the incident He^+ energy. The obtained results presented in

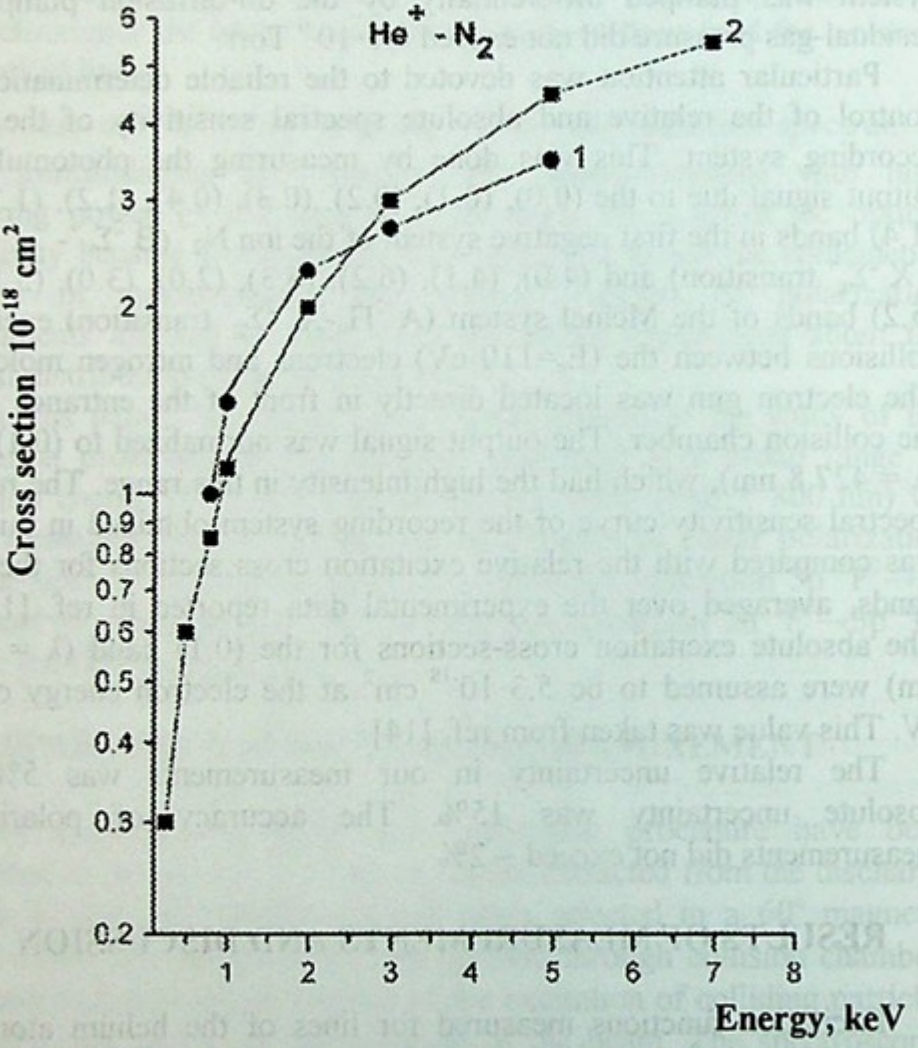

Fig.1. Energy dependence of the excitation cross section of helium atomic and nitrogen ionic lines: 1- HeI(388.9 nm), 2 -NII (500.5 nm)

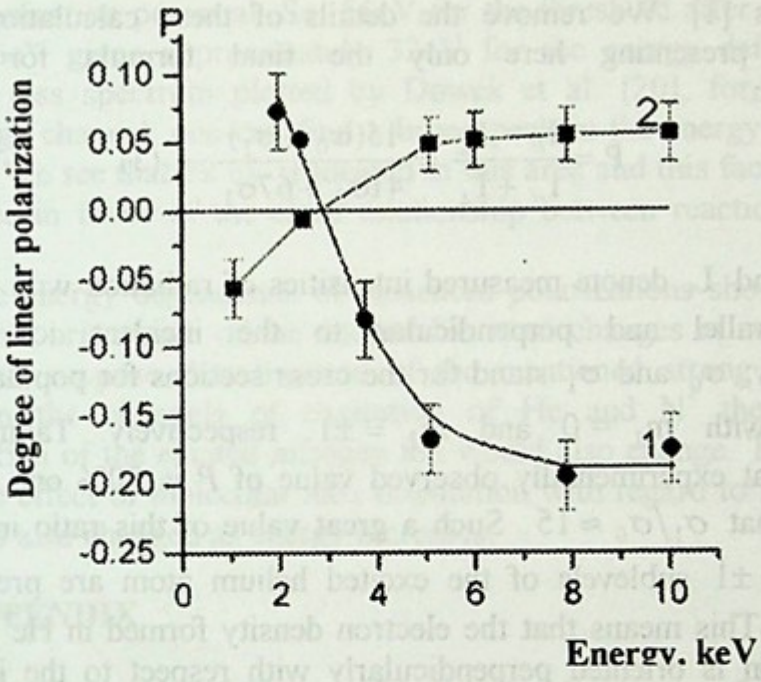

Fig.2. Energy dependence of the degree of polarization
1 - HeI(388.9nm), 2- NII(500.5nm)

Figs.1 and 2 point to the fact that there should exist a strong correlation between inelastic processes producing the excited helium atoms and nitrogen ions (dissociation products)

$$He^+ + N_2\left(X^1\Sigma_g\right) \rightarrow He^* + N^+ + N \qquad (1)$$

$$He^+ + N_2\left(X^1\Sigma_g\right) \rightarrow He + \left(N_2^+\right)^* \rightarrow He + \left(N^+\right)^* + N. \qquad (2)$$

Also we have supposed that the inelastic energy defects for these channels are close to each other.

Polarization of the emission emerging from excited ^{3}P-state of helium is connected to the relative populations of $m_L = 0$ and $m_L = \pm 1$ sublevels. Expression for the first Stock's parameter has been derived on the basis of general approach developed by Macek

and Jaecks [1]. We remove the details of these calculations into Appendix presenting here only the final formula for linear polarization:

$$P = \frac{I_{//} - I_{\perp}}{I_{//} + I_{\perp}} = \frac{15(\sigma_0 - \sigma_1)}{41\sigma_0 + 67\sigma_1}, \quad (3)$$

where $I_{//}$ and $I_{\perp}$ denote measured intensities of radiation with electric vector parallel and perpendicular to the incident ion beam, respectively; σ_0 and σ_1 stand for the cross sections for population of sublevels with $m_L = 0$ and $m_L = \pm 1$, respectively. Taking into account that experimentally observed value of P is 20% one obtains from (1) that $\sigma_1/\sigma_0 \approx 15$. Such a great value of this ratio indicates that $m_L = \pm 1$ sublevels of the excited helium atom are preferably populated. This means that the electron density formed in He^* during the collision is oriented perpendicularly with respect to the incident beam direction.

For polarization of radiation emitted by nitrogen ion N^+ (dissociation product) we have used the same technique as for derivation of (3) and the following expression has been obtained:

$$P \approx \frac{\sigma_0 + 2\sigma_1 - 3\sigma_3}{3\sigma_0 + 6\sigma_1 + 6\sigma_2 + 5\sigma_3} \quad (4)$$

We note that in case of excited N^+-ion it is complicated to trace any pronounced alignment of the radiating object. The reason is that expression (4) contains not only σ_0 and σ_1, but σ_2 and σ_3 too and the unambiguous determination of branching ratios seems to be a difficult task.

There are some additional arguments that substantiate the existence of correlation between the channels (1) and (2). Filippelli et. al in ref. [19] investigated electron impact dissociative ionization of N_2. The authors have observed the same emission line of N^+ - 500.5nm. Because of the small mass of the incident particle – electron, the threshold impact energy for the appearance of this line nearly coincides with the corresponding energetic defect less than the helium

atom ionization potential. So, 56eV for the threshold after subtraction of 24.6eV gives approximately 32eV for the energy defect. In the energy loss spectrum plotted by Dowek et al. [20], for the charge exchange channel, one can find a broad peak in the energy range of ~ 30 eV. We see that 32 eV is located in this area and this fact is indirect evidence in favor of the close relationship between reactions (1) and (2).

The energy dependence of measured polarizations shows that the electronic orientation of the excited He atom changes at nearly 3keV. One can suppose that because of the mentioned strong correlation between the channels of excitation of He and N^+ the electronic orientation of the excited nitrogen ion would also change. This implies that the effect of molecular axis orientation with regard to incident ion beam is also changed as energy increases.

APPENDIX

Here we derived the simple formula for the degree of polarization of radiation as result of the atomic particle collision process. Presented calculations are based on the pioneering work of Macek and Jaecks [1]. Below we use the following quantum numbers: L- electronic orbital quantum number, M_L-magnetic quantum number, J- full electronic momentum quantum number, *S*- electronic spin quantum number, I- nuclear spin quantum number and F – full atomic momentum (electronic + nuclear) quantum number.

In the polarization experiments number of the photon and projectile coincidences dN_c depends upon the position of the photon and particle detectors. The incoming beam axis is usually taken to be the z-axis, and the *x*-z plane is located arbitrarily. The angular coordinates of the particle detector relative to this coordinates system are denoted by θ and φ, and the coordinates of the photon detector by θ' and φ'. Number dN_c is proportional to linearly polarized light intensity which is oriented at an angle β with respect to z-axis, provided projectile particle is scattered in (θ, φ) direction.

$$dN_c = \{A_{00}\cos^2\beta + A_{11}\sin^2\beta + (A_{11} - A_{00})\cos^2\beta\cos^2\theta +$$
$$+\sqrt{2}\,\mathrm{Re}A_{01}\left[\sin 2\theta'\cos^2\beta\cos(j - j') + \sin 2\beta\sin\theta'\sin(j - j')\right] -$$

$$-\mathrm{Re}A_{1,-1}\Big[(\cos 2\beta\cos 2\theta' - \sin^2\beta)\cos 2(j-j') + \\ +\sin 2\beta\cos\theta'\ \sin 2(j-j')\Big]\Big\}d\Omega d\Omega' \quad (A1)$$

$d\Omega$ and $d\Omega'$ are the solid angles covered by the particle and photon detector, respectively. Coefficients $A_{qq'}$ are determined as:

$$A_{qq'} = \sum_{JFJ'F'M'_L M_L} U(qq'M_L M'_L JFJ'F'LL_0)\left\langle a_{M'_L} a_{M_L}\right\rangle \int_0^{\Delta t} dt e^{-(\gamma+i\omega_{JFJ'F'})t}. \quad (A2)$$

Here

$$U(qq'M_L M'_L JFJ'F'LL_0) = \quad (A3)$$

$$= \frac{(2J+1)(2J'+1)(2F+1)(2F'+1)(2L+1)}{(2S+1)(2I+1)}(-1)^{L_0+q-M_L}\sum_{\chi=0,1,2}(2\chi+1)(-1)^{-\chi}\times$$

$$\times\begin{Bmatrix} L & L & \chi \\ J' & J & S \end{Bmatrix}^2\begin{Bmatrix} J & J' & \chi \\ F' & F & I \end{Bmatrix}^2\begin{Bmatrix} L & L & \chi \\ 1 & 1 & L_0 \end{Bmatrix}\begin{pmatrix} L & L & \chi \\ -M'_L & M_L & \nu \end{pmatrix}\begin{pmatrix} 1 & 1 & \chi \\ -q & q' & -\nu \end{pmatrix},$$

q is polarization vector component of the photon; ω is the frequency of the emitted light and $1/\gamma$ is the mean life of the excited atom. The excitation amplitudes contain all information about collision dynamics and they depend on θ only. Time integration in (A2) involves detection time interval 0-Δt.

In our experiment we do not fix scattered particles. This means that expression (A1) should be integrated over coordinates θ and φ. Furthermore, in our experimental condition the photon detector is installed in direction perpendicular to the primary ion beam, i.e. $\theta' = 90^0$. As to analyzer angle β, it was taken equal to 0^0 and 90^0. Therefore only the following terms will contribute to the detected intensity

$$I \sim (A_{00}\cos^2\beta + A_{11}\sin^2\beta)d\Omega' \quad (A4)$$

In case when radiation from helium atom is observed, nuclear spin $I = 0$, so we have no hyperfine structure. Consequently, we can change

$\omega_{JFJ'F'}$ by $\omega_{JJ'}$. Further, since the mean life of excited atom $1/\gamma$ and $1/\omega_{JJ'}$ is much shorter than commonly employed resolution time, the time integral becomes:

$$\int_0^{\infty} dt \exp[-(\gamma + i\omega_{JJ'})t] = \frac{1}{\gamma + i\omega_{JJ'}} \approx \begin{cases} 0, & J \neq J' \\ 1/\gamma, & J = J' \end{cases}. \qquad (A5)$$

Now, (A1)-(A5) allow to find an exact value for the first Stocks parameter

$$P = \frac{I(\beta = 0^\circ) - I(\beta = 90^\circ)}{I(\beta = 0^\circ) + I(\beta = 90^\circ)}. \qquad (A6)$$

Let's determine degree of polarization for He atom line (388.9 nm, transition $^3p \rightarrow {}^3s$). For this case when q = 0 q′= 0,

$$U(00M_L M'_L\, JJJJ|10) = (2J+1)^4 (-1)^{-M_L} \sum_{\chi=0,1,2} (2\chi+1)(-1)^{-\chi} \times$$

$$\times \begin{Bmatrix} 1 & 1 & \chi \\ J & J & 1 \end{Bmatrix}^2 \begin{Bmatrix} J & J & \chi \\ J & J & 0 \end{Bmatrix}^2 \begin{Bmatrix} 1 & 1 & \chi \\ 1 & 1 & 0 \end{Bmatrix} \begin{pmatrix} 1 & 1 & \chi \\ -M_L & M_L & 0 \end{pmatrix} \begin{pmatrix} 1 & 1 & \chi \\ 0 & 0 & 0 \end{pmatrix},$$

and when q = 1 q′ = 1,

$$U(1\,1|M_L M'_L\, JJJJ|10) = (2J+1)^4 (-1)^{1-M_L} \sum_{\chi=0,1,2} (2\chi+1)(-1)^{-\chi} \times$$

$$\times \begin{Bmatrix} 1 & 1 & \chi \\ J & J & 1 \end{Bmatrix}^2 \begin{Bmatrix} J & J & \chi \\ J & J & 0 \end{Bmatrix}^2 \begin{Bmatrix} 1 & 1 & \chi \\ 1 & 1 & 0 \end{Bmatrix} \begin{pmatrix} 1 & 1 & \chi \\ -M_L & M_L & 0 \end{pmatrix} \begin{pmatrix} 1 & 1 & \chi \\ -1 & 1 & 0 \end{pmatrix}$$

Here ( ) and { } denote the 3-j and 6-j symbols, respectively.

Finally, we obtain the following expression for the degree of polarization for the mentioned helium emission line:

$$P = \frac{15(\sigma_0 - \sigma_1)}{67\sigma_0 + 41\sigma_1}. \qquad (A7)$$

where σ_0 and σ_1 are cross-sections of population of magnetic sublevels with $m_L = 0$ and $m_L \pm 1$, respectively.

REFERENCES

1. J.Macek, D. H. Jaecks. Phys. Rev. 1971, **A 4**, 2288.
2. U.Fano, Joseph H.Macek.. Rev. Modern Phys. 1973, **45,** 553.
3. I.C. Malcolm, H.W. Dassen, J.W. McConkey. J. Phys. B: Atom. Molec. Phys. 1979, **12**, 1003.
4. D.H.Jaecks,O.Yenen, M.Nataragan, D.Mueller. Phys. Rev. Lett. 1983, **50**, 825.
5. R.Hippler, M.Faust, R.Wolf, H.Kleinpoppen, H.O. Lutz. Phys.Rev. **A31,** 1985, 1399.
6. O.Yenen, D.H.Jaecks. Phys.Rev.**A32,** 1985, 836.
7. O.Yenen,D.H.Jaecks,P,J,Martin. Phys.Rev.**A35**, 1987, 1517.
8. R.Hippler, M.Faust,R.Wolf, H.Kleinpoppen, H.O.Lutz. Phys.Rev. **A36,** 1987, 4644.
9. C.Richter,D.Dowk, J.C.Houver. J. Phys. B. At. Mol. Opt. Phys.**24**, 1991, L213.
10. Rainer Hippler, Phys. B. At. Mol. Opt. Phys. **26**, 1993, 1.
11. B.Siegmann , R.Hippler, H.O. Lutz . J. Phys. B. At. Mol. Opt. Phys. **31,** 1998, L675.
12. H Tanuma, T Hayakawa, C Verzani, H Kano, H Watanabe, B D DePaola, N Kobayashi, J. Phys. B. At. Mol. Opt. Phys. **33**, 2000, 5091.
13. H.Merabet, R.Bruch, S. Fulling, K.Bartschat, A. L .Godunov, J. Phys. B. At. Mol. Opt. Phys. **36,** 2003, 3383.
14. M.R.Gochitashvili, R.V.Kvidzhinadze, N.R.Djaliashvili , B.I.Kikiani. JTF. **63**, 1993, 35.
15. V.V.Skubenich, I.P. Zapesochni. Geomagnetizm, Aeronomia. **21**, 1981, 481.
16. W.R. Pendleton, R.R. O'Neil. J. Chem. Phys. **56**, 1972, 6260.
17. P.N.Stanton, R.M. St.John. J. Opt. Soc. **50**, 1969, 252.
18. D.C. Cartwright. J. Chem. Phys. **58**, 1973, 178.

19. A.R.Filippelli, F.A.Sharpton, C.C.Lin, R.E.Murphy. J. Chem. Phys. **76**, 1982, 3597.
20. D.Dowek, D.Dhuicq, J.Pommier, VU Ngoc Tuan , V.Sidis, M.Barat. Phys.Rev. **A24**, 1981, 2445.

Tbilisi State University

მ. გოჩიტაშვილი, ი. ნოსელიძე, თ. ჩიღვინაძე,
რ. ლომსაძე

პოლარიზაციური გაზომვები $He^+ - N_2$ დაჯახების პროცესში

დასკვნა

გაზომილია ჰელიუმის ატომური HeI(388.9 ნმ) და აზოტის იონური NII(500.1-500.5 ნმ) ხაზების გამოსხივების წრფივი პოლარიზაციის ხარისხი დამჯახებელი იონების ფართო ენერგეტიკულ არეში (1-10კევ). ჰელიუმის ხაზისათვის დამზერილია პოლარიზაციის ხარისხის მაღალი მნიშვნელობა P = -20%, რაც მიუთითებს იმაზე, რომ დაჯახების პროცესში ადგილი აქვს აღგზნებული 33P მდგომარეობის შესაბამისი $m_L = \pm 1$ ქვედონეების უპირატეს დასახლებას. ექსპერიმენტული მონაცემების ანალიზის საფუძველზე გაკეთებულია დასკვნა, რომ აღგზნებული ჰელიუმის ელექტრონული ღრუბელი ორიენტირებულია პირვანდელი იონების მიმართულების მართობულად.

THE EFFICIENCY OF ELECTROSTATIC ENERGY ANALYZER IN ION-ATOM COLLISIONS

M.Gochitashvili, R.Lomsadze, B.Lomsadze, N.Mosulishvili, G.Sakhelashvili

Accepted for publication July, 2004

ABSTRACT. Collision spectroscopy method is used for study of inelastic processes in collisions of closed electron shell pairs. To obtain inelastic energy loss spectrum of primary scattering particles the "box" type electrostatic energy analyzer (ESA) is designed. For estimation of principal parameters K^+-Ar pair was tested as a typical example. The resolution ability of ESA is determined.

The experimental determination of absolute value of cross-section of an inelastic processes (ionization, charge exchange, excitation) occurring during ion-atom collisions is a subject of great interest. Such investigations are important for development of various branches of physics and techniques (plasma physics, astrophysics, gaseous discharge, etc.) it is also necessary for testing of theoretical models.

Complex investigation of such processes especially when it concerns the closed electron shell of colliding pairs (alkali metal ions, rare gas atoms) is connected with definite methodical difficulties. Due to the small collision parameter the scattering of primary particles at large angles take place and hence secondary recoil particles acquire large kinetic energy. This makes impossible the effective detection of particles. Moreover due to the large amount of inelastic channels their identification becomes problematic. Hence such investigations require perfect methods. Therefore taking into account the difficulty of physical task it was decided to choose the perspective of the so-called collision spectroscopy method.

Certainly there exists more sensitive methods e.g. electrical or optical spectroscopy but the circumstance that the mentioned processes might be realized without detachment of electrons or without radiation, or lifetime of excited electrons to be sufficiently

large (so-called metastable particles) the advantage was paid on a collision spectroscopy method.

This method is based on an investigation of scattering primary ion energy loss spectra resulting after collision with target gas atoms. The idea of this method schematically is explained in Fig.1.

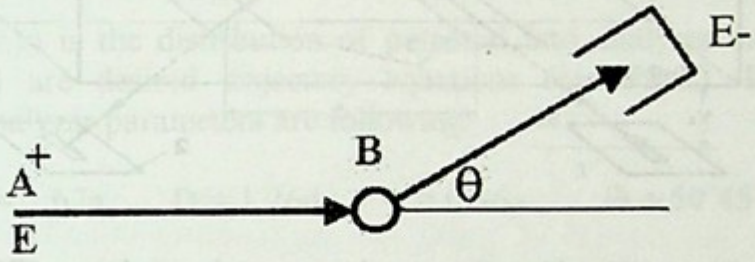

Fig.1. Schematic drawing of scattering

The fixed E-energy A^+ ions collide with B target particles, they are scatter on a definite angles and enter into the ESA.

The kinetic energy of scattered particles is measured in analyzer and therefore energy loss, that concerns the various inelastic channels are determined.

According to our task to obtain a necessary energy loss spectrum the definite condition was laid on a selection of measuring systems (analyzer). There are also a lot of types of electrostatic systems such as: analyzer with homogeneous electric field (plane condenser, capacitor), cylindrical and spherical mirror types, toroidal, parabolic etc. [1-4].

The aim of our work was to select such an analyzer which has small size, would be easy for construction, has a possibility for double focusing, large luminosity and, what is most important, optimal resolution ability $R=E/\Delta E$. Where E is energy of primary particles and ΔE minimum difference between observed peaks (shape curves) that can be distinguished by detector. In our case the "box" types dispersion electrostatic analyzer was used. Such systems compared to others have some advantage, particularly maximal localization of fields surrounding the analyzer, full screening of outer fields and minimal losses on power supply.

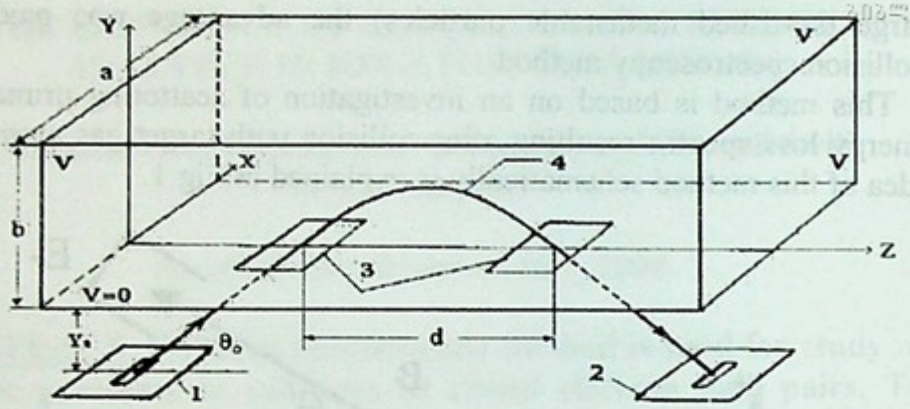

Fig.2. The "box" type electrostatic analyzer (ESA)

Schematic 3D drawing of "box" type electrostatic analyzer is shown in Fig.2. It consists of two pairs of parallel plane electrodes that are located so that its section gives right angle. The potential applied on the upper and side electrodes was equal to the acceleration potential of primary ions and on entering one the potential is zero.

According to the physical task the unique parameter selected in advance was resolution ability the value of which is equal to R = 500. It means that if energy of primary particles E = 2 keV then we can distinguish two inelastic channels from each other with 4eV difference. From this requirement we estimate all principal parameters of analyzer. The estimation of parameters and among them a potential distribution into analyzer and charge particle trajectory formed into analyzer was possible by solving the Laplace equation [5]. For simplification of solution calculations were made for that partial cases when potentials on a reflective and adjacent side electrodes were equal to each other and to acceleration potential V of entering ions into analyzer. Distribution of potentials and trajectory equation looks as below [1]:

$$\Phi(x,y) = V - \frac{2V}{\pi}\operatorname{arctg}\left(\frac{\sin \pi x}{\operatorname{sh}\pi y}\right) + 4V\operatorname{sh}\left[\pi y(2n+1)\right]\times$$

$$\times \sum_{n=0}^{\infty} \frac{e^{-\pi b(2n+1)} \sin\left[\pi x(2n+1)\right]}{\pi(2n+1)\operatorname{sh}\left[\pi b(2n+1)\right]} \qquad (1)$$

$$x''(z) = \frac{1}{2\Phi(x,y)}\left[1 + x'^2(z) + y'^2(z)\right]\frac{\partial\Phi(x,y)}{\partial x}, \quad (2)$$

$$y''(z) = \frac{1}{2\Phi(x,y)}\left[1 + x'^2(z) + y'^2(z)\right]\frac{\partial\Phi(x,y)}{\partial y}, \quad (3)$$

where $\Phi(x,y)$ is the distribution of potential into analyzer and x''(z) and y''(z) are desired trajectory equations (see Fig.2). Relations between analyzer parameters are following:

$$d = 1.67a; \quad D = 1.26d; \quad b = 0.96a; \quad \Theta = 50°45';$$

$$y = 0.25a; \quad h = 0.06d; \quad S_{opt} = 0.87R^{-1}d,$$

where d is the distance between slits, D dispersion, a width of analyzer, b height, Θ entrance angle of primary beam in analyzer, y distance from source to electrodes, R resolution ability, S_{opt} optimal width of slit, h slits height. In our case d = 60 mm. By means of obtaining parameters we made "box" type electrostatic analyzer that have been used on a mass-spectrometric setup for studying of energy loss spectra (Fig.3).

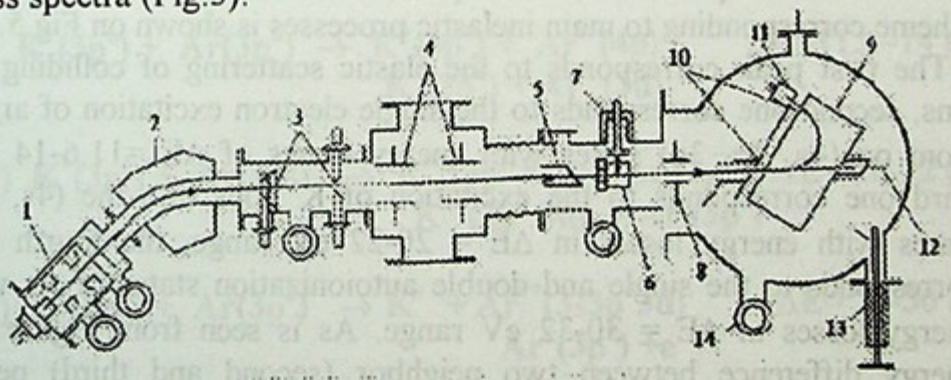

Fig.3. Experimental setup

1-ion source; 2- magnetic mass-analyzer; 3- collimating slits; 4- focusing system; 5- Faraday cup; 6- collision chamber; 7- effusion source of target particle; 8- capacitor; 9- analyzer; 10- entrance and exit slits of analyzer; 11- secondary electron multiplier; 12- collector of ions; 13- rotation system of analyzer; 14- diffusion pumps.

The primary beam extracted from surface ionization ion source (1) after focusing was accelerated to the desirable energy, formed into mass-analyzer (2), according to q/m (q–ion charge, m-mass). Collimating by slits (3) ion beam was forwarded into collision chamber (6), where it was crossed by a target particle beam and entered into electrostatic analyzer (9). Automatic change of analyzer potentials gave possibility to investigate energy loss spectra into 0-100eV ranges and the rotation of an analyzer around the center of collision chamber differential cross section of scattering in 0-20° angle ranges.

The ion signals were registered by secondary electron multiplier. Without introduction of target gas the pressure in collision chamber was kept below 10^{-6} torr and the typical pressure under operation was 10^{-4} torr. The investigation was performed in a single collision condition. The current of primary ions in collision chamber was I = 0,01 mkA.

To evaluate the resolution ability of electrostatic analyzer the test experiment of energy loss spectrum for K^+-Ar pair (as a typical example) was carried out. The spectrum of primary ions with fixed energy E = 2 keV and scattering angles Θ =3.5° are shown in Fig.4. It seems that the spectrum has sharp discrete character. The reaction scheme corresponding to main inelastic processes is shown on Fig.5.

The first peak corresponds to the elastic scattering of colliding K^+ ions, second one corresponds to the single electron excitation of argon atom on (4s, 4p, 3d) states with energy losses of ΔE =11.6-14 eV, third one corresponds to the excitation of K^+ ions into the (4s, 3d) states with energy losses in ΔE = 20-22 eV range, the fourth one corresponds to the single and double autoionization states of Ar with energy losses in ΔE = 30-32 eV range. As is seen from Figure the energy difference between two neighbor (second and third) peaks consists of 5 eV. They are well distinguishable from each other.

This result indicates that the preliminary idea concerning the creation of electrostatic analyzer with resolution ability R = 500 was solved successfully.

The obtained spectrum analysis shows that definite portion into ionization process have excitation of autoionization states. For identification of excitation states the analyze based on Gaussian distribution (dashed line in Fig.4.) was applied.

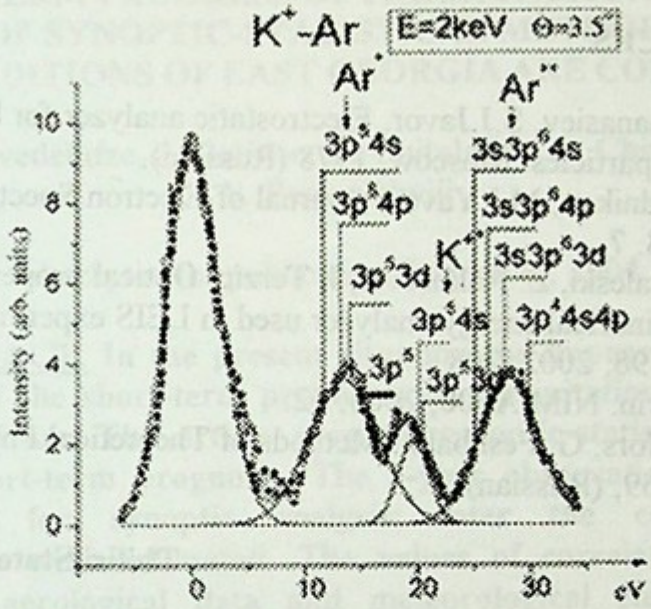

Fig.4. Energy loss spectrum

I) $K^+(3p^6) + Ar(3p^6) \rightarrow K^+(3p^6) + Ar(3p^6)$ $\Delta E=0$

II) $K^+(3p^6) + Ar(3p^6) \rightarrow K^+(3p^6) + Ar^*(4p)$ $\Delta E=11.6–14$ eV
$K^+(3p^6) + Ar^*(3d)$

III) $K^+(3p^6) + Ar(3p^6) \rightarrow K^{+*}(3p^5\,4s) + Ar(3p^6)$ $\Delta E= 20\text{-}22$ eV
$K^{+*}(3p^5\,3d) + Ar(3p^6)$

IV) $K^+(3p^6) + Ar(3p^6) \rightarrow K^+ + Ar^{**}(3s3p^63d)$ $\Delta E= 28\text{-}30$ eV
$Ar^+(3p^5) + e$

Fig.5. Reaction schemes for various inelastic processes

As is seen from Figure in a second peak the main portion has an excitation of Ar atom in 3d and 4p states, in third one the excitation of K^+ ions in a 4s and 3d states. In autoionization peak the definite portion has a single electron excitation of Ar atom in $3s3p^63d$ state.

REFERENCES

1. V.P.Aphanasiev, S.J.Javor. Electrostatic analyzer for beam of charged particles. Moscow, 1978 (Russian).
2. A.S.Berdnikov, M.I.Yavor, Journal of Electron Spectroscopy, **94,** 1998. 7.
3. N. Bundaleski, Z. Rakocevic, I. Terzic. Optical properties of the 127° cylindrical energy analyzer used in LEIS experiments. NIM **B198**, 2002, 208.
4. A.M. Ilyin. NIM **A500**, 2003, 62.
5. F.M. Mors, G. Feshbakh. Methods of Theoretical Physics. **2,** 1960, 169, (Russian).

Tbilisi State University

მ. გოჩიტაშვილი, რ. ლომსაძე, ბ. ლომსაძე,
ნ. მოსულიშვილი, გ. სახელაშვილი

ელექტროსტატიკური ანალიზატორის გამოყენების ეფექტურობა იონ-ატომურ დაჯახებათა კვლევის დროს

დასკვნა

ნაშრომში ჩაკეტილ გარსიან ნაწილაკთა წყვილების ურთიერთქმედების შედეგად მიმდინარე არადრეკადი პროცესების შესასწავლად გამოყენებულია დაჯახებითი სპექტროსკოპიის მეთოდი. პირველადი გაფანტული ნაწილაკების ენერგეტიკული დანაკარგების სპექტრის მისაღებად შერჩეულია კოლოფის ტიპის ელექტროსტატიკური ანალიზატორი. K^{+}-Ar წყვილის მაგალითზე შეფასებულია ანალიზატორის ყველა ძირითადი პარამეტრი. მას-სპექტრომეტრული ტიპის დანადგარზე ჩატარებულია დაჯახების არადრეკადი ენერგეტიკული დანაკარგების გამოკვლევა და შეფასებულია ელექტროსტატიკური ანალიზატორის გარჩევის უნარიანობა.

SHORT –TERM PROGRESS OF PRECIPITATION WITH USE OF SYNOPTIC-STATISTICAL METHODS (THE CONDITIONS OF EAST GEORGIA ARE CONSIDERED)

Z. Khvedelidze, J. Dolidze, D. Chitaladze, A. Chitaladze, N. Pavlenishvili

Accepted for publication September, 2004

ABSTRACT. **In the present situation the improvement of the accuracy of the short-term prognosis of precipitation is still very important issue. The article suggests synoptic-statistical method for the short-term prognosis. The 5-year observational material was used for synoptic analysis; later the corresponding correlations were estimated. The values of correlation between calculated aerological data and meteorological elements (total diurnal and maximal values of precipitation) appeared to be sufficient. It allows the usage of the described method in the operational practice.**

The problem of weather forecasting, particularly, the prognosis of precipitation is one of the most complicated and significant questions of the modern atmospheric science. Georgia is located at the border of the middle and subtropical latitudes, thus the diversity of weather is the result of the circular processes natural to both zones. The interaction of these circular processes with orography in different regions of the country brings about the weather conditions absolutely different from each other. Indeed, air flows aiming toward the Caucasus Range react with the complex relief which cause complicated spacious distribution of the vertical the fluxes eventually resulting in the compound spacious distribution of atmospheric precipitation.

At present the accuracy of the qualitative prognosis of atmospheric precipitation is less developed than that of the temperature and wind, especially, in the mountainous countries. On the other hand, heavy precipitation is the significant source of heavy rains, river overflows, avalanches, landslides, and snowslides. That's why the elaboration

and introduction of the new methodology in a practical meteorology is quite important and actual.

Till 60s of the last century the prognosis of precipitation was carried out by aerosynoptical method. It uses the expected changes of the circular processes in the atmosphere. The prognosis of this kind is dependant on the qualification of the specialist and thus, has subjective character. Further development of computer technology made possible the implementation of a quantitative prognosis of precipitation on the basis of the thermo-dynamical and statistical methods. However, the discussion about remarkable quantitative changes in precipitation prognosis is early. We think that the main reason of the existed situation is that modern methods of precipitation prognosis are carried out using the thermo-dynamical methods. They do not consider the regularity of alternation in time and space of the multiyear observation data and aerosynoptical methods characteristic to the certain region.

Thus, the combination of all three methods depicted above to work out the prediction methods for atmospheric precipitation could have become one of the most precise ways for prognosis.

The formation of atmospheric precipitation, first of all, has frontal character and is associated with long-scale atmospheric circulation. In the works of Georgian scientists [1-4] every synoptic process in the South Caucasus is researched and classified. The types of synoptic processes that determine weather characterized by precipitation or without it on the whole territory of Georgia or on the certain regions are recognized.

On the other hand, uneven heating of the Earth's surface causes the formation of powerful convective fluxes in the atmosphere during the warm period of the year, which in case of sufficient amount of water vapor brings about cumulonimbus clouds. Convective fluxes are characteristic to East Georgia where semi deserts, valleys, and forests are neighboring; in turn, it is the reason of uneven heating of the Earth's surface. Convective precipitation is natural to the first part of the warm period, when the upper layers of the soil are well moistened and at the same time there is a good supply of water vapor in the atmosphere. Climate in East Georgia is continental and, providing significant drop of the amount of water vapor in the second part of

warm period and thus, the possibility of the formation of cumulonimbus clouds despite convection.

Either meteorological or aerological 5-year observational data for 1982-1986 period is used to implement the probable prognostic method of precipitation. First of all, the data from 18 meteorological stations scattered on the whole territory of Georgia were collected and the database containing the diurnal and night total air temperature and precipitation data for above – mentioned time period was established.

Further, every single possible synoptic type influencing country's climate was established on the basis of diurnal synoptic analysis. Later, the initial information on the following meteorological elements: air temperature, deficit point of dew, wind velocity near the Earth's surface and on the 870, 700, 500, 300 isobaric layers of the atmosphere was obtained by air sounding in Tbilisi airport twice a day: 3:00 a.m. and 3:00 p.m. It was used to build a standard emagram. The emagram helps to calculate derived quantities like: pseudo-potential temperature, levels of condensation and convection stability or instability of the atmosphere, the thickness of stable atmospheric layer, maximal deviation of the state curve from stratification curve and its altitude form the sea level, the magnitude of convective vertical velocity at the certain level.

By the primary work-out of the prepared database [5,6] was proved that the precipitation fall-down in East Georgia can not be expected in the following cases:

- if dominating synoptic situation is anti-cyclone;
- if vertical stratification of atmosphere is stable;
- if the total deficit point of dew is more than 28°C at 850, 700, 500, 300 isobaric levels.

Correspondingly, the above-mentioned synoptic situations were selected from database for further elaboration and, at the same time, arranged in accordance to the three dominating flows: eastern – 2, western 1, and wave turbulence form south – 3.

The correlative relations between the above-mentioned elements and precipitation were calculated. In case of the larger correlations the linear equation of regression was obtained. Here is given the regression equation with four variables, daily maximum precipitation (U_1), and total precipitation (U_2) for the pointed three flows.

1. Western flow:

$U_1 = -0.0892X_{11} - 1.1083X_{15} - 0.0639X_9 + 83.7106$
$r = 0.67$; ER = 0.03
$U_2 = -116.5315X_3 - 12.4457X_7 - 3.2931X_9 + 140.3456$
$r = 0.66$; ER = 0.05

2. Eastern flow:
$U_1 = -5.5868X_7 + 2.4986X_{17} + 1.62211X_{12} + 24.2422$
$r = 0.76$; ER = 0.03
$U_2 = -1.1699X_8 + 4.9321X_{18} - 60.3906X_7 + 946.9146$
$r = 0.66$; ER = 0.07

3. Wave turbulences developed in the southern flows:
$U_1 = 0.0847X_4 + 0.0637X_{14} + 0.5151X_{20} - 80.8369$
$r = 0.52$; ER = 0.08
$U_2 = 0.3064X_4 + 0.1378X_{14} + 1.6075X_{16} - 254.7671$
$r = 0.61$; ER = 0.07,

where **r** is a correlation coefficient; ER is the mean quadratic error of the coefficient of correlation; X_3 the level of condensation (km), X_4 – pressure on the level of condensation (mb), X_7 the upper level of instability , X_8 the pressure on the upper level of instability, X_9 pressure on the level of the maximal deviation (mb), X_{11} the direction of wind on 700mb level (m/s), X_{12} wind speed on 700 mb (m/s), X_{14} the direction of wind on 500 mb level (m/s), X_{15} wind speed on 500 mb (m/s), X_{16} the deficit point of dew on 500 mb level (^{0}C), X_{17} temperature on 700 mb level (^{0}C), X_{18} the total deficit point of dew on 500 mb level (^{0}C).

Finally, the large-scale magnitudes of the coefficients of correlation create the possibility of using the described method for a short-term precipitation prognosis in the operation practice.

Tbilisi State University

REFERENCES

1. V. M. Gigineishvili, E. A. Napetvaridze, K. I.. Papinashvili. Tr. TbilNIGMI, 1, 1954, (Russian).
2. K. I. Papinashvili. Atmosfernie processi v Zakavkaze I ikh sviazs, mikrocirkulacionnimi processami nad Evraziei. Leningrad, Gidrometeoizdat, 1963, (Russian).

3. I. Javakhisvili. Atmosferuli naleqebi saqartvelos teritoriaze. TSU, 1981, (Georgian).
4. I. G. Sulakvelidze. Livnevie osadki v gornikh stranakh na primere Zakavkazia. TSU, 1988, (Russian).
5. E. S. Ulanova – Primenenie matematicheskoi statistiki v agrometeorologii dlia nakhojdenia uravnenii sviazei. Moskva, Gidrometeoizdat. 1964, (Russian).
6. J. Dolidze. Trudi ZakNIGMI, **53**; Sinopticheskie I chislennie metodi analiza I prognoza pogody. Leningrad, Gidrometeoizdat, 1973, (Russian).

Tbilisi State University

გ. ხვედელიძე, ჯ. დოლიძე, დ. ჩიტალაძე,
ა. ჩიტალაძე, ნ. ფავლენიშვილი

ნალექების მოკლევადიანი პროგნოზი სინოპტიკურ-სტატისტიკური მეთოდის გამოყენებით (აღმოსავლეთ საქართველოს პირობებში)

დასკვნა

თანამედროვე პირობებში ნალექების მოკლევადიანი პროგნოზის ხარისხის გაუმჯობესება კვლავ აქტუალურ პრობლემად რჩება. ნალექების მოკლევადიანი პროგნოზირებისათვის სტატიაში შემოთავაზებულია სინოპტიკურ-სტატისტიკური მეთოდი. სინოპტიკური ანალიზისათვის გამოყენებული იქნა ხუთწლიანი მასალა და შეფასებული იქნა შესაბამისი კორელაციური კავშირები. კორელაციის კოეფიციენტის მნიშვნელობები, დათვლილი აეროლოგიურ მონაცემებსა და მეტეოროლოგიურ (ნალექთა ყოველდღიური მაქსიმალური და ჯამური მნიშვნელობები) ელემენტთა შორის აღმოჩნდა საკმარისად მისაღები. მაღალი კორელაციური შემთხვევებისათვის მიღებული იქნა რეგრესიის წრფივი განტოლებები. მაღალი კორელაციური კავშირები საშუალებას გვაძლევს დავასკვნათ, რომ აღნიშნული მიდგომა შესაძლებელია გამოყენებული იქნას ნალექების მოკლევადიანი პროგნოზირებისას ოპერატიულ პრაქტიკაში.

CONTINUOUS ADAPTATION OF THRESHOLD BODIES ON ALGORITHM OF THE UNIFIED ENCOURAGEMENT AND INDIVIDUAL PUNISHMENT (UEIP)

Z. Gogiashvili, O. Namicheishvili, G. Shonia

Accepted for publication September, 2004

ABSTRACT. The theory of continuous adaptation without a feedback and with a feedback on algorithm of the unified encouragement and individual punishment (UEIP) is stated at threshold reservation of the binary channels used for transfer of the information, received in physical experiments. The results of machine modelling of behaviour of threshold decision body are given during adaptation on algorithm UEIP.

During continuous adaptation without a feedback on Widrow-Hoff algorithm [1] on each step of iteration the size of an increment of weights is determined by a difference between the random weighted sum of input signals and restriction overlapped on it. However other algorithms of an increment of weights may use direct comparison of a signal X_i on i-th input of threshold body with a right answer submitted from the outside X (or the decision Y in the presence of a feedback). For example, it is possible to start with a principle of encouragement and punishment, according to which changes in a vector of weights (including a threshold as one of the components) are made on each step of iteration, however in the absence of a mistake weight is increased by the size dependent on number of iteration, at detection of a mistake it decreases on the size dependent both on iteration number and value of weight. Thus, an increment of i-th weight

$$\Delta a_i(k) = a_i(k+1) - a_i(k), \qquad (1)$$

made on $(k+1)$-th step of iteration, in the absence of a mistake accepts some value β_k with the probability $1-q_i$, and in the presence of a mistake – the value $\beta_k \cdot e^{a_i(k)}$ with probability q_i:

$$\Delta a_i(k) = \begin{cases} \beta_k \text{ with probability } 1-q_i \\ -\beta_k \cdot e^{a_i(k)} \text{ with probability } q_i \end{cases}, \quad (2)$$

where $\beta_k \geq 0$. The initial weights $a_i(1)\left(i=\overline{1,n+1}\right)$ can be given arbitrary. Thus, in considered strategy the encouragement is unified, it does not depend on an input of threshold body and is determined only by the number of iteration and punishment is applied strictly individually. This strategy can be named algorithm of the unified encouragement and individual punishment (UEIP).

Expectation value of $\Delta a_i(k)$ has the following form:

$$M[\Delta a_i(k)] = \beta_k(1-q_i) - \beta_k e^{a_i(k)} q_i = \beta_k q_i \left(\frac{1-q_i}{q_i} - e^{a_i(k)} \right). \quad (3)$$

Let in the established condition

$$\left. \begin{matrix} M[\Delta a_i(k)] = 0 \\ i=\overline{1,n+1} \end{matrix} \right\}. \quad (4)$$

As before, the values of weights at which such condition is reached, we designate as $\hat{a}_i$. Then for $\hat{a}_i\left(i=\overline{1,n+1}\right)$ the following equations are obtained

$$\left. \begin{matrix} \hat{a}_i = \ln \dfrac{1-q_i}{q_i} \\ i=\overline{1,n+1} \end{matrix} \right\}. \quad (5)$$

Thus, during continuous adaptation without a feedback by algorithm (2) the increments of weights, the latter are established at the levels coordinated with criterion of a maximum a posteriori

probability if only the ratios (4) take place. Particularly this condition will be fulfilled, if the value β_k, corresponding $(k+1)-th$ step of iteration is determined by the formula

$$\beta_k = \frac{1}{k}. \tag{6}$$

It is possible to prove, that such choice is in agreement with the one developed in [2] Bayesian approach giving for a statistical estimation of weight the value $\ln \frac{1-q_i}{q_i}$

$$a_i = \ln \frac{M - n_i + 1}{n_i + 1}, \tag{7}$$

where M is the number of comparisons of a signal X_i on i-th input of decision body with a right answer submitted from the outside X, and n_i is the amount of mistakes observed at it. It is supposed, that a priori distribution of a random value $\hat{q}_i = N_i/M$ is uniform.

Really, let

$$a_i(k) = \ln \frac{k - n_i + 1}{n_i + 1}. \tag{8}$$

There is an estimation of value $\ln \frac{1-q_i}{q_i}$ on $k-th$ step of adaptation, i.e. by results of k comparisons of a signal X_i with a right answer submitted from the outside X, at the number of observed mistakes equal to n. From here it follows

$$\frac{k - n_i + 1}{n_i + 1} = e^{a_i(k)}, \tag{9}$$

$$\frac{1}{n_i + 1} = \frac{e^{a_i(k)}}{k - n_i + 1}. \tag{10}$$

Then on the following step, depending on result of comparison, we have

$$a_i(k+1)=\ln\left(\frac{(k+1)-n_i+1}{n_i+1}\right)=\ln\left(\frac{k-n_i+1}{n_i+1}+\frac{1}{n_i+1}\right). \quad (11)$$

at concurrence of signals and

$$a_i(k+1)=\ln\left(\frac{(k+1)-(n_i+1)+1}{(n_i+1)+1}\right)=\ln\left(\frac{k-n_i+1}{n_i+1}\right)-\ln\left(1+\frac{1}{n_i+1}\right) \quad (12)$$

otherwise.

Taking into account (9) and (10) in last ratios, we get:

$$a_i(k+1)=\begin{cases} a_i(k)+\ln\left(1+\dfrac{1}{k-n_i+1}\right) & \text{with probability } 1-q_i \\ a_i(k)-\ln\left(1+\dfrac{e^{a_i(k)}}{k-n_i+1}\right) & \text{with probability } q_i \end{cases}. \quad (13)$$

At $k>>n_i>>1$, using valid at $x\to 0$ ratio $\ln(1+x)=x$, we get:

$$a_i(k+1)=\begin{cases} a_i(k)+\dfrac{1}{k} & \text{with probability } 1-q_i \\ a_i(k)-\dfrac{1}{k}\cdot e^{a_i(k)} & \text{with probability } q_i \end{cases}. \quad (13')$$

Introducing the designation (6), we come to the former algorithm (2) of increment weights, which proves our statement.

Thus, in a first approximation the algorithm (2) is equivalent to estimation of weights $\ln\frac{1-q_i}{q_i}$ on a ratio $\ln\frac{k-n_i+1}{n_i+1}$ on each step of iteration. Therefore there exists (11) value M determined by the formula of number of k iterations, at which statistical estimation of $\hat{q}_i$ probabilities of a mistake q_i deviates from this probability q_i not

more, than on the given small size ε with probability close enough to unit α. Due to the fact that the ratio $\frac{1}{k} \geq \frac{1}{M}$ takes place before the achievement of this condition at $k \leq M$, the use of smaller value of a constant increment of weights $\beta = \frac{1}{M}$ instead of β_k during adaptation, cannot break convergence of the process to the established condition:

$$\beta_k \equiv \beta = \frac{1}{M}. \tag{14}$$

At continuous adaptation with a feedback on algorithm of the unified encouragement and individual punishment the established values of weights are determined by formulas

$$\left.\begin{array}{c} \hat{a}_i = \ln \dfrac{1-d_i}{d_i} \\ i = \overline{1,n+1} \end{array}\right\}, \tag{15}$$

where d_i is the probability of a mismatch of a signal X_i on $i-th$ input of threshold body with the decision Y on its output. For an estimation of deviations of these weights from values $\ln \frac{1-q_i}{q_i}$ it is necessary to start with ratio

$$\left.\begin{array}{c} q_i - Q \leq d_i \leq q_i + Q \\ i = \overline{1,n+1} \end{array}\right\},$$

where Q is the probability of a mistake of threshold body.

The process of random wandering of weights at continuous adaptation causes the appropriate statistical distribution of probability of a mistake of Q threshold element which can be considered as a function of external entrance parameters $q_1, q_2, \ldots, q_n, q_{n+1}$ and internal entrance parameters $a_1, a_2, \ldots, a_n, a_{n+1}$.

As the dependence

$$Q = Q(a_1, a_2, \ldots, a_n, a_{n+1}, q_1, q_2, \ldots, q_n, q_{n+1})$$

is known to us algorithmically [3] and as an appropriate program, it is more convenient to study statistical distribution Q using Monte Carlo method [4], treating the characteristic Q of threshold body as a random value Q^*, being the function of random arguments $a_1, a_2, \ldots, a_n, a_{n+1}$ and fixed parameters $q_i \left(i = \overline{1,n+1}\right)$. Realizations of this random value are designated by a symbol $\hat{Q}\left(0 \le \hat{Q} \le 1\right)$

Knowledge of the histogram or density $f_Q(\hat{Q})$ of distribution of a random value Q^* allows to calculate the probability that Q^* is less than some maximally admited value Q_0 :

$$P_0 = \Pr\left\{Q^* < Q_0\right\}$$

Taking close to unit value of this probability, it is possible to find the value β of the weight increments, providing the required probability P_0.

For machine modelling of threshold body behaviour during adaptation and the circle of questions outlined above we created an appropriate program. It allows to study adaptation on algorithm of the unified encouragement and individual punishment at presence of a feedback. Its input data are:

- The activator of the generator of the random numbers evenly distributed in an interval (0, 1);
- The amount of channels of threshold body (not more than 11);
- Number of the channel, which weight distribution of during the adaptation is desirable to receive;
- Number of steps of adaptation (no more than ten thousand);
- The value β, serving as a measure of an increment of weights on each step of adaptation;
- Probabilities of refusal of channels and their arbitraly given initial weights (by one card on each channel);

- Aprioristic probability of presentation to threshold body for recognition of a signal $+1$ and initial value of a threshold.

The output information contains all set of the input data, and also distributions of weight interesting for the user of the channel and probability of a mistake of threshold body (with the indication of intervals of values of these sizes and probabilities of their hit in these intervals).

In machine experiment the distributions of probabilities of a mistake of threshold body were received during adaptation on algorithm UEIP with a feedback at

$$n = 8, q_1 = 10^{-3}, q_2 = 10^{-1}, q_3 = q_4 = 5 \cdot 10^{-1}, q_5 = q_6 = q_7 = q_8 = 8 \cdot 10^{-1}$$

and $q_9 = 5 \cdot 10^{-1}$, when exact value of probability of a mistake of restoring system for optimum values of weights and a threshold makes $Q_{min} = 7{,}912 \cdot 10^{-4}$.

In all three cases the initial weights and a threshold were set zero, size β made 0.05, value of the activator of the generator of random numbers was 33, and the amount of steps of adaptation- 100, 500 and 500, accordingly.

From the results received by us it follows, that (at correct selection of initial weights, a threshold and sizes β of their increments with growth of the amount of steps of adaptation maxima probability distributions of conditions to which various probabilities of mistakes of threshold body answer, are shifted to the minimal value in the given conditions Q_{min}.

REFERENCES

1. B. Widrow, M. Hoff. Adaptive Switching Circuits // IRE Wescon Convention Record.-1960.-Pt 4.-P.96-104.
2. Z.G. Gogiashvili. Research of a threshold element for radiophysical applications Abstract of the dissertation on competition of a scientific degree of the candidate physical and mathematical sciences. Tbilisi, 1998.

3. J. Gogiashvili, K. Dalakishvili, O. Namicheishvili. Bulletin of the Georgian Academy of Sciences. 157, 1,1998, 38.
4. I.M.Sobol. Numerical methods of Monte Carlo. 1973, 311.

Tbilisi State University

ქ.გოგიაშვილი, ო.ნამიჩეიშვილი, გ.შონია

ბღურბლური ორგანოების უწყვეტი ადაპტაცია უნიფიცირებული წახალისებისა და ინდივიდუალური დასჯის ალგორითმით

ნაშრომში განხილულია უწყვეტი ადაპტაცია (უკუკავშირითა და უკუკავშირის გარეშე), რომელიც ხორციელდება ფიზიკურ ექსპერიმენტებში მიღებული ინფორმაციის გადაცემისას ბინალური არხებით. ხსენებული არხების საიმედოობის ასამაღლებლად უწყვეტი ადაპტაცია უნიფიცირებული წახალისებისა და ინდივიდუალური დასჯის ალგორითმით მიმდინარეობს.

ნაშრომში მოტანილია ბღურბლური გადამწყვეტი ორგანოს ქცევის კომპიუტერული მოდელირების შედეგები იმ შემთხვევისათვის, როცა ადაპტაციის პროცესი ამ ალგორითმით წარიმართება.

THE POSSIBLE MECHANIZM OF SEMIANNUAL VARIATIONS IN THE IONOSPHERE BY DATA OF TBILISI CITY

K. Tukhashvili, V. Kandashvili, K. Otarashvili

Accepted for publication October, 2004

ABSTRACT. The degree of ionization in the ionosphere, corresponding to a given zenith angle χ_0 is delayed by τ minute due to the sluggishness of ionosphere. Therefore the electrons concentration at a given χ_0 corresponds to $\chi_1 = |\chi_0| + \Delta\chi$ forenoon and $\chi_2 = - -|\chi_0| + \Delta\chi$ afternoon. It follows that $\Delta\chi = 1/2(\chi_1 + \chi_2)$. It is possible to calculate χ_1 and χ_2 using well-known formula $\cos\chi = \sin\varphi \cdot \sin\delta + \cos\varphi \cdot \cos\delta \cdot \cos(T-12-\tau)$. First we calculate T_0, corresponding χ_0 in case of $\tau = 0$. Therefore, it is possible to calculate $\Delta\chi$ for fixed τ. On the other hand, if we calculate $V = |d\chi/dt|$ for χ_0 it becomes clear that $\Delta\chi = V \cdot \tau$. Consequently, forenoon the more $\Delta\chi$, the more χ_1 and so less the electrons concentration. Analogically, in the afternoon the more $\Delta\chi$ the less χ_2 and thus more the electrons concentration.

The data obtained at the ionospheric observatory of Tbilisi State University during 1964-1986 years have been analyzed. It is shown that $f_0E(\cos\chi = 0.2)$ has semiannual variations; at the same time the evening values of this parameter change in phase with seasonal variation of $\Delta\chi$ and morning values – in opposite phase. The correlation coefficients are 0.91 and - 0.85, respectively.

It is shown that semiannual variations are connected with Sun-Earth geometry (V) and sluggishness of ionosphere (τ). It is also shown, that the dependence between τ and solar activity (F10.7) is linear.

1. INTRODUCTION

Semiannual variations (SAV) are the variations for a six month period. If investigated quantity has equinox maximums, it's called direct SAV, but if it has minimums, than it's inverse variation.

The SAV is different from annual variations, among them seasonal variation is the most known. Seasonal variations are caused by inclination of the earth axis to the plane of ecliptic. That's why northern hemisphere takes the maximum heat from the sun during the time of summer solstice and minimum heat at time of winter solstice. In southern hemisphere seasonal-annual wave is changed in phase just with 180^0 relatively a northern hemisphere.

Consideration on the whole complex of existed facts that almost all geophysical phenomena, which proceed at a height more than ~ 90 km, experiences the SAV [1]. Thus, rhithm of SAV contains all thickness of the upper atmosphere. It is shown in [2,3], that the velocity of solar senith angle change is also subjected to SAV. An opinion on two basic sources of SAV: electromagnetic (equatorial region) and corpuscular (middle and high latitudes) has been forwed [1]. Yonezawa dedicated numerous works to SAV [4,5]. The authors of [6] suggest a new possible mechanizm of SAV at low latitudes: the semiannual variation of the amplitude of the diurnal tide in the lower thermosphere induces the semiannual variation of quatorial electrojet in the ionospheric E layer. It induces the semiannual variation of amplitude of ionospheric equatorial anomaly through the 'fountain effect'. This process causes the semiannual variation of the low latitude N_mF2.

Till today the researchers of this question haven't applied Sun-Earth geometry and sluggishness of ionosphere to explain SAV. It is shown in this work that SAV of E layer critical frequency (f_oE) is connected with Sun-Earth geometry and sluggisness of ionosphere.

2. Theory

It is established by different experiments that variation of N_mE will be described rather well by equation $N_mE \approx \sqrt{\cos\chi}$, where χ is the Sun's zenith angle. On the other hand, it is possible to make a

good approximation to N(z)E by parabola. Critical frequency of E layer $f_oE \sim \sqrt{Nm}$ [7]. The investigation of tabulate critical frequency shows, that it is described well by the equation:

$$f_oE = (f_oE)_0 \cdot (\cos \chi)^n, \qquad (1)$$

where $n = 0.25$ as it must be for equilibrium layer of Chapman [8].

The degree of ionization in the ionosphere, corresponding a given zenith angle χ_0 is delayed by τ minutes due to the sluggishness of ionosphere [9]. Therefore the electrons concentration at a given χ_0 corresponds to $\chi_1 = |\chi_0| + \Delta\chi$ forenoon (morn.) and $\chi_2 = -|\chi_0| + \Delta\chi$ afternoon (even.); therefore $\Delta\chi = 1/2 * (\chi_1 + \chi_2)$. It is possible to calculate χ_1 and χ_2 by well-known formula in astronomy

$$\cos\chi = \sin\varphi \cdot \sin\delta + \cos\varphi \cdot \cos\delta \cdot \cos(T-12-\tau) \qquad (2)$$

first T_0 is calculated, corresponding χ_0 in case $\tau = 0$; i.e. it is possible to calculate $\Delta\chi$ for fixed τ. On the other hand, if we calculate $V = |d\chi/dt|$ [3] for χ_0, it becomes clear that $\Delta\chi = V * \tau$. Corresponding calculations are given in Table1. Consequently forenoon the more $\Delta\chi$ the more χ_1 and so less the electrons concentration . Analogically, afternoon the more $\Delta\chi$ the less χ_2 and so more the electrons concentration

The influence of sluggishness of ionosphere on the absorption radiowave is shown in [10]. Not only absorption is subjected to SAV, but other parameters of ionosphere, such as critical frequencies of E and F2 layers - f_oE and foF2.

If ionosphere hasn't sluggishness, i.e. $\tau = 0$ and following $\Delta\chi = 0$; resulting $f_oE(\cos\chi = \text{const.})$ must be just the same for every month.

If $\tau = \text{const.}$ $(\tau \neq 0)$ in expession $\Delta\chi = V * \tau$, then variation of $\Delta\chi$ must be caused by variation of V; i.e. according to above given opinion, seasonal variation of morning values of $f_oE(\chi_0)$ must being in oposite phase with seasonal variation of V, and evening one – in phase. In the Fig.1 are showed seasonal variations of V and f_oE

Table 1.

Tbilisi

Values of Dc and Vt cos c = 0.2 t = 15min

φ =	42											
Month	1	2	3	4	5	6	7	8	9	10	11	12
δ	-21	-13	-2	10	19	23	22	14	3	-8	-18	-23
Tm (0.2)morn	8.62	7.93	7.17	6.44	5.90	5.66	5.72	6.20	6.86	7.56	8.34	8.83
Te (0.2)even	15.38	16.07	16.83	17.56	18.10	18.34	18.28	17.80	17.14	16.44	15.66	15.17
P	-0.24	-0.15	-0.02	0.12	0.22	0.26	0.25	0.16	0.04	-0.09	-0.21	-0.26
Q	0.69	0.72	0.74	0.73	0.70	0.68	0.69	0.72	0.74	0.74	0.71	0.68
mor.cos(t-τ)	0.58	0.43	0.24	0.05	-0.09	-0.15	-0.14	-0.01	0.16	0.34	0.52	0.62
eve.cos(t-τ)	0.68	0.54	0.36	0.18	0.04	-0.02	-0.01	0.12	0.29	0.46	0.63	0.72
mcosχ	0.16	0.16	0.15	0.15	0.15	0.16	0.16	0.15	0.15	0.16	0.16	0.17
ecosχ	0.23	0.24	0.25	0.25	0.25	0.24	0.25	0.25	0.25	0.24	0.24	0.23
V(cosχ = 0.2)	0.548	0.647	0.723	0.742	0.717	0.695	0.701	0.735	0.738	0.689	0.590	0.515
χ_1	1.406	1.4123	1.417	1.418	1.416	1.415	1.415	1.417	1.4179	1.415	1.409	1.404
χ_2	-1.334	-1.328	-1.322	-1.321	-1.322	-1.324	-1.3232	-1.321	-1.321	-1.32	-1.332	-1.337
$\Delta\chi=1/2(\chi_1+\chi_2)$	**0.0358**	**0.0423**	**0.0473**	**0.0486**	**0.0469**	**0.0455**	**0.0459**	**0.0481**	**0.0483**	**0.0451**	**0.0386**	**0.0337**
Vτ	**0.0358**	**0.0423**	**0.0473**	**0.0486**	**0.0469**	**0.0455**	**0.0459**	**0.0481**	**0.0483**	**0.0451**	**0.0386**	**0.0337**

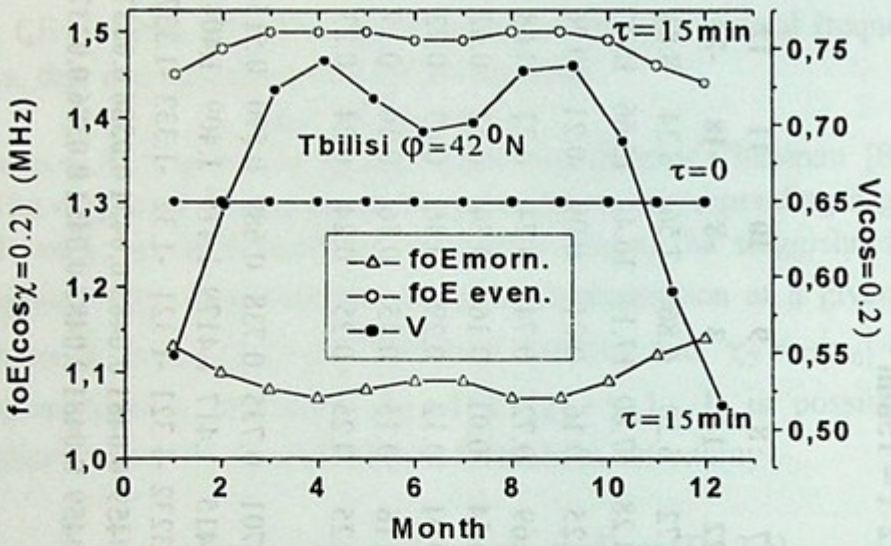

Fig.1. Seasonal variations of foE($\cos\chi = 0.2$) and sun's angular rate V($\cos\chi = 0.2$) (theoretical values)

(calculated by formula (3)) for the data: $\varphi = 42^0$, $(f_oE)_o = 4$MHz; n = 0.70; τ =15 min; cos $\cos\chi_0 = 0.2$

$$f_oE(\chi_0) = (f_oE)_o \cdot [(P + Q \cdot \cos(T_o - 12 - \tau)]^n , \qquad (3)$$

where $P = \sin\varphi \cdot \sin\delta$, $Q = \cos\varphi \cdot \cos\delta$. This confirms the above opinion.

3. EXSPERIMENTAL RESULTS

The data obtained at the ionosphere observatory of Tbilisi State University ($\varphi = 42^0$) during 1964-1986 years have been analyzed. Polynom of second power was applied for approximation of diurnal variation of f_oE instead of (3) formula. Polynom describes experimental data very good: coefficient correlation R>0.98. $\mathbf{f_oE} = \boldsymbol{at^2+bt+c}$ formula is much more simple (where **t** local time and f_oE-corresponding critical frequency) than (3). The shift of parabola's peak from 12 o'clock (τ) can be calculated comparatively easy by ***a*** and **b** coefficients.

It is necessary to exclude Sun's activity for investigated seasonal variation of f_oE. f_oE is a function of solar activity as well as of Sun's zenith angle - $f_oE(\chi, F10.7)$. To study a dependence of f_oE on the F10.7 it is necessary to fix χ. It was done as for f_oF2 in [11]. Dependence between f_oE and F10.7 is linear, as for f_oF2, but coefficient correlation is smaller than in case of f_oF2. Here it should be noted that more below, in the D region correlation between absorption of radiowave and F10.7 is very bad as it turned out when studing this question.

In Fig.2 seasonal variations of $f_oE(\cos\chi = 0.2)$ and $\Delta\chi = V \cdot \tau$ are given for F10.7 = 150. Correlation coefficients between f_oE and $V \cdot \tau$ are 0.85 (morn.) and 0.91 (even.).

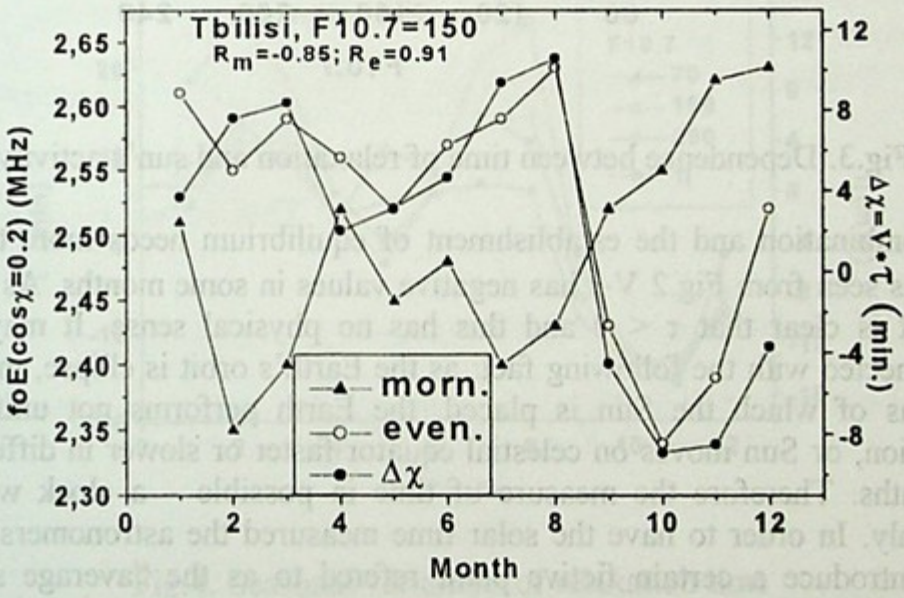

Fig.2. Seasonal variations of $f_oE(\cos\chi = 0.2)$ and $\Delta\chi$ (experimental values)

The dependence of τ on the F10.7 has been studied. It was found that τ increases linearly with increasing of F10.7 (Fig.3). It can be explained in this way: Stream of ionising quantum which incidences on the ionosphere, increases with increasing the Sun's activity. At the same time there takes place a

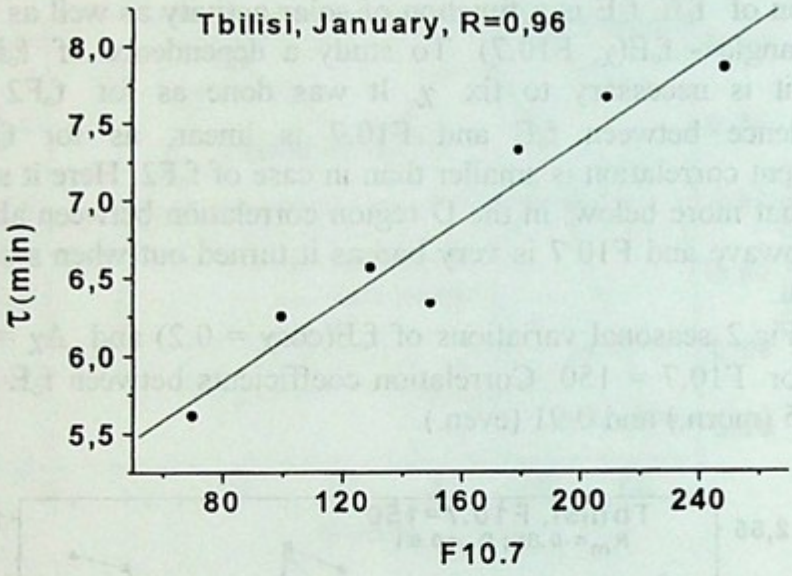

Fig.3. Dependence between time of relaxation and sun's activity.

recombination and the establishment of equilibrium needs more time. As is seen from Fig.2 V·τ has negative values in some months. As V > 0, it is clear that $\tau < 0$ and this has no physical sense. It may be connected with the following fact: as the Earth's orbit is ellipse, in one focus of which the Sun is placed, the Earth performs not uniform motion, or Sun moves on celestial equator faster or slower in different months. Therefore the measure of time in possible – a clock works evenly. In order to have the solar time measured the astronomers had to introduce a certain fictive point refered to as the "average solar body", that actually shifts the "apparent solar body". The "average solar body" moves evenly on celestial equator performing the entire annual detour and is considered by the scientists as an index for average solar time. Daily corrections of time, so-called time equation (η), are given in Astronomic Calendar. Average solar time t_m and appeared solar time t_0 are connected by equation: $t = t_0 + \eta$ [12]. Seasonal variation of monthly mean values of η and τ (for different activity) are given in Fig.4. It is clear that seasonal trends τ and η are similar. Actual measured τ is sum of appear τ (τ_0) and η: $\tau = \tau_0 + \eta$. Therefore, if τ_0 is small τ will become negative.

Table 2.

Correlation coefficient R between t and F10.7

1	2	3	4	5	6	7	8	9	10	11	12
0.96	-0.98	0.98	-0.76	0.99	0.96	1.00	1.00	0.99	0.91	-0.95	0.90

As was noted above, the dependence between τ and F10.7 is linear (Fig.3). The values of correlation coefficient of this dependence are given in Table 2. As is seen for February, April and November correlation coeficients are negative – the increase of activity causes decrease of τ, that cannot be explained the approach by given above.

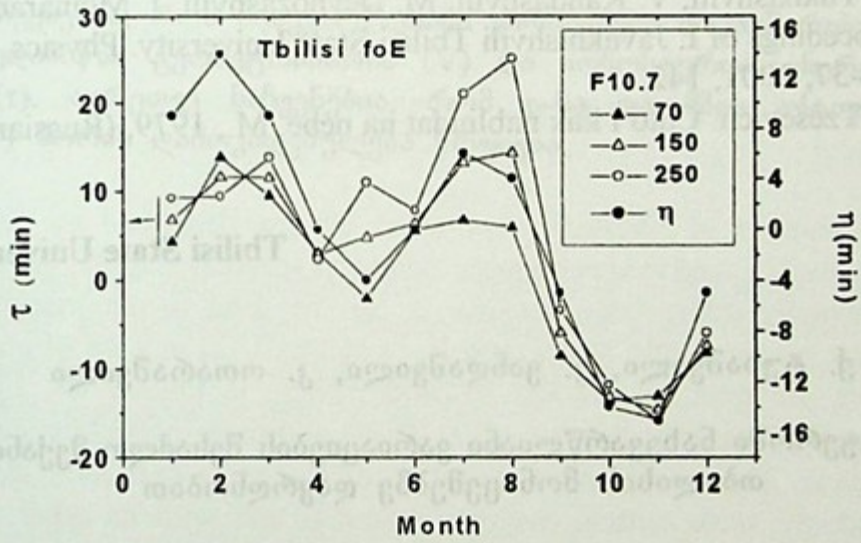

Fig.4. Seasonal variations of relaxation time (experimental values for different activity of sun by f_0E) and time equation

REFERENCES

1. G.S. Ivanov-Kholodni. Geomagnetizm i Aeronomia, **XIII, 6,** 1973, 969.
2. K. Tukhashvili. Geomagnetizm i Aeronomia, **IX, 2,** 1969, 350.
3. K. Tukhashvili. J.Georgian Physical Society. **3,** 1996, 74.

4. T. Yonezawa. J. Radio Res. Lab., **14, 71,** 1967, 1.
5. T. Yonezawa, Y. J. Radio Res. Lab., **6, 25,** 1959, 1293.
6. Ruiping Ma, Jiyao Xu, Huaizhe Liao. J. Atm. Sollar-Terr. Phys. **65,** Is.1, January 2003, 47.
7. Ja.L.Alpert.Rasprostranenie radiovoln I ionosphera. 1960, (Russian).
8. Physics of the Upper Atmosphere, Edited by Ratcliffe, M., 1963, (Russian).
9. E.V.Appleton J. Atm. Terr. Phys. **3,** 1953, 282.
10. K.Tukhashvili, G. Entzian, V. Kandashvili, M. Devnozashvili, M. Miminoshvili. Bulleten of the Georgian Academi of Sciences, **164, 2,** 2001, 267.
11. K. Tukhashvili, V. Kandashvili, M. Devnozashvili, J. Mdinaradze. Procedings of I. Javakhishvili Tbilisi State University. Physics. **36–37,** 2001, 142.
12. V. Tzesevich. Chto I kak nabliudat na nebe. M., 1979, (Russian).

Tbilisi State University

ქ. ტუხაშვილი, ვ. ყანდაშვილი, კ. ოთარაშვილი

იონოსფეროში ნახევარწლიანი ვარიაციების შესაძლო მექანიზმი თბილისის მონაცემებზე დაყრდნობით

დასკვნა

იონოსფეროში იონიზაციის ხარისხი, რომელიც შეესაბამება მზის მოცემულ χ_0 ზენიტურ კუთხეს, დაგვიანებულია τ წუთით იონოსფეროს ინერციის გამო, ამიტომ ელექტრონების კონცენტრაცია მოცემულ χ_0 კუთხეზე შეესაბამება $\chi_1 = |\chi_0| + \Delta\chi$ კუთხეს შუადღემდე და $\chi_2 = -|\chi_0| + \Delta\chi$ კუთხეს შუადღის შემდეგ; აქედან $\Delta\chi = 1/2\cdot(\chi_1 + \chi_2)$. χ_1 და χ_2 კუთხეების გამოთვლა შესაძლებელია ასტრონომიაში ცნობილი ფორმულით $\cos\chi = \sin\varphi\cdot\sin\delta + \cos\varphi\cdot\cos\delta\cdot\cos(T-12-\tau)$, ჯერ გამოითვლება რა χ_0-ის შესაბამისი T_0 დრო $\tau = 0$ შემთხვევისათვის. ე.ი. შესაძლებელია $\Delta\chi$-ს გამოთვლა დაფიქსირებულ τ–ზე. მეორეს მხრივ, თუ გამოვთვლით $V = |d\chi/dt|$ χ_0-

სთვის, ცხადი გახდება, რომ $\Delta\chi = V\cdot\tau$. გამოდის, რომ შუადღემდე რაც დიდია $\Delta\chi$, მით დიდია χ_1 და ამის გამო მცირეა ელექტრონების კონცენტრაცია. ანალოგიურად, შუადღის შემდეგ რაც დიდია $\Delta\chi$, მით ნაკლებია χ_2 და ამიტომ მეტია ელექტრონების კონცენტრაცია.

გაანალიზებულია თსუ იონოსფეროს ობსერვატორიაში 1964–1986 წლებში მოპოვებული მონაცემები. ნაჩვენებია, რომ $f_0E(\cos\chi = 0.2)$-ს აქვს ნახევარწლიანი ვარიაციები. ამასთან ერთად, ამ პარამეტრის საღამოს მნიშვნელობები იმყოფება $\Delta\chi$-ს სეზონურ ცვლილებასთან ფაზაში, ხოლო დილის მნიშვნელობები – საწინააღმდეგო ფაზაში. კორელაციის კოეფიციენტები, შესაბამისად, ტოლია 0.91 და –0.85. მოყვანილია ამ ცდისეული შედეგის ორიგინალური ახსნა.

ნაჩვენებია, რომ ნახევარწლიანი ვარიაციები დაკავშირებულია მზე-დედამიწის გეომეტრიასთან (V) და იონოსფეროს ინერციასთან (τ). აგრეთვე ნაჩვენებია, რომ τ–სა და მზის აქტივობას (F10.7) შორის დამოკიდებულება წრფივია.

MODIFIED METHOD OF HYPERSPHERICAL FUNCTION FOR THREE-PARTICLE SYSTEM IN 3D SPACE WHEN PAIR INTERACTION BETWEEN PARTICLES IS $\left(a/r^2 + b/r\right)$

A.Lomidze

Accepted for publication October, 2004

ABSTRACT. **Three-particle system has been investigated by modified hyperspherical function method between particles by pair interaction $\left(a/r^2 + b/r\right)$. For hyperradial wave function there has been obtained the system of infinitely coupled equations solved analytically by diagonal approximation. In the same approximation analytical expressions of binding energy have been obtained.**

A number of physical phenomena can be described by singular potentials [1], and inverse square potential (critical singular potential) is especially interesting, because it can be used as an independent singular potential and power singular potentials [2] in a lot of physical spheres. In spite of this the research sphere is limited by: 1) Two particle system in $D \geq 1$ space; 2) Three and more particle systems in 1D space. Therefore the investigation of this three-particle system independently with critical singular potential and with its other power singular potential in 2D and 3D space extends knowledge and the sphere of its utilization and gives more precise definition about this potential. The results will be useful for the scientists, experts and specialists which are also working in the 2D space of development of science and technological spheres.

The problem of three-particles for pair inverse square interaction using modified hyperspherical function method has been studied in 2D space [3] and 3D space [4], respectively.

Two particles in correspondence with solution of Schordinger equation in 3D space when potential of interaction is the algebraic sum of square inverse potential and Coulomb potential, or when it is as follows:

$$\left(\frac{a}{r^2}+\frac{b}{r}\right) \qquad (1)$$

has been studied in 3D space analytically [5], when $b < 0$.

The object of this work is to study theoretically three-particle system in 3D space. We use the modified method of hyperspherical function when pair interaction between particles is as in (1).

The aim of this paper is the following. In Section I, we discuss exact solution of Schrodinger equation for three-particle system in 3D space when pair interaction between particles is as (1). In Section II, we discuss the same system with same interaction when we used the modified method of hyperspherical function [3, 4]. In Section III, our main conclusions are summarized.

1. APPROXIMATE ANALYTICAL SOLUTION OF SCHRODINGER EQUATION FOR THREE-PARTICLE SYSTEM

Considering the three-particle system in 3D space which correspons to Schrodinger equation using hyperspherical function method is given in [4]. For Schrodinger equation we have got coupled differential equations system:

$$\left(\frac{\partial^2}{\partial\rho^2}-\left[\chi^2+\frac{(K+2)^2-0{,}25}{\rho^2}\right]\right)\chi_{RL}^{l_1l_2}(\rho)=$$

$$\sum_{K'l_1'l_2'M'} W_{KK'LL'MM'}^{l_1l_2l_1'l_2'}(\rho)\chi_{K'L'}^{l_1'l_2'}(\rho)\,, \qquad (2)$$

where

$$\chi^2=-\frac{2\mu}{\hbar^2}E\,, \qquad (3)$$

and $W_{KK'LL'MM'}^{l_1l_2l_1'l_2'}(\rho)$ is defined by expression:

$$W_{KK'LL'MM'}^{l_1l_2l_1'l_2'}(\rho)=$$

$$= \frac{2\mu}{\hbar^2}\left[J^{l_1 l_2 l_1' l_2'}_{KK'LL'MM'} + \sum_{\bar{l}_1 \bar{l}_2} {}^{i}\langle \bar{l}_1 \bar{l}_2 \,|\, l_1 l_2 \rangle^{j}_{KL} \; {}^{i}\langle \bar{l}_1' \bar{l}_2' \,|\, l_1' l_2' \rangle^{j}_{KL} J^{\bar{l}_1 \bar{l}_2 \bar{l}_1' \bar{l}_2'}_{KK'LL'MM'} + \right.$$

$$\left. + \sum_{\bar{\bar{l}}_1 \bar{\bar{l}}_2} {}^{i}\langle \bar{\bar{l}}_1 \bar{\bar{l}}_2 \,|\, l_1 l_2 \rangle^{j}_{kL} \; {}^{i}\langle \bar{\bar{l}}_1' \bar{\bar{l}}_2' \,|\, l_1' l_2' \rangle^{j}_{KL} J^{\bar{\bar{l}}_1 \bar{\bar{l}}_2 \bar{\bar{l}}_1' \bar{\bar{l}}_2'}_{KK'LL'MM'} \right]. \qquad (4)$$

In angular integral of (4) expression, e.g. for 1 and 2 particles are:

$$J^{l_1 l_2 l_1' l_2'}_{KK'LL'MM'} = \int \Phi^{*\, l_1 l_2}_{KLM}(\Omega_i) U_{12} \Phi^{l_1' l_2'}_{K'L'M'}(\Omega_i) d\Omega, \qquad (5)$$

where $\Phi^{l_1 l_2}_{KLM}(\Omega)$ are eigenvalues $K(K+4)$, of eigenfunction for square of K orbital moment, and create full collection of orthonormal basic functions that are following:

$$\Phi^{l_1 l_2}_{KLM}(\Omega) = N^{l_1, l_2}_{K} \cos^{l_1}\alpha \sin^{l_2}\alpha \, P_n^{l_1+1/2, l_2+1/2}(\cos 2\alpha) \times$$

$$\times Y_{l_1 m_1}(x) Y_{l_1 m_1}(y), \qquad (6)$$

where

$$N^{l_1 l_2}_{K} = \left[\frac{2n!(K+2)\Gamma(l_1 + l_2 + 2 + n)}{\Gamma(n + l_1 + 3/2)\Gamma(n + l_2 + 3/2)} \right]^{1/2}$$

and

$$n = \frac{K - l_1 - l_2}{2}. \qquad (7)$$

l_1 და l_2 are orbital moments of Jacoby coordinates.

We consider only one equation from equation's system (2), when $K = K'$.

Total potential of system that is between particles by pair interaction is:

$$U_{123}(\bar{x}, \bar{y}) = a_{12} r_{12}^{-2} + a_{13} r_{13}^{-2} + a_{23} r_{23}^{-2} + b_{12} r_{12}^{-1} + b_{13} r_{13}^{-1} + b_{23} r_{23}^{-1} \quad (8)$$

Solution of Schrodinger equation for the same particle system (2) when it is in extension angular integral (see (5)) and terms of integral, for example 1 and 2, will be:

$$J_{12} = \int \Phi^*_K(\Omega)\left(a_{12}r_{12}^{-2} + b_{12}r_{12}^{-1}\right)\Phi_K(\Omega)d\Omega \qquad (9)$$

and expression (9) is solved analytically.

With account of obtained results and zero approximation (2), solution of Schrodinger equation has been gotten as:

$$\left(\frac{\partial^2}{\partial\rho^2} - \left[\chi^2 + \frac{(K+2)^2 - .25}{\rho^2}\right]\right)\chi_K(\rho) = \left(\frac{1}{\rho^2}W_1 + \frac{1}{\rho}W\right)\chi_K(\rho), \qquad (10)$$

where

$$\left(\frac{1}{\rho^2}W_1 + \frac{1}{\rho}W\right) = \left[J_{12} + \langle 00\,|\,00\rangle_2\langle 00\,|\,00\rangle_2 J_{13} + \right.$$
$$\left. + \langle 00\,|\,00\rangle_2\langle 00\,|\,00\rangle_2 J_{23}\right] \qquad (11)$$

After the solution of Schrodinger equation (10) for energetical levels of the system we have:

$$E = -\frac{\hbar^2}{2m}\left(\frac{W}{2N+2\lambda}\right)^2 \qquad (12)$$

and for radial components of wave function it is:

$$\varphi(\rho) = (2\chi)^{\lambda+1/2}\left[\frac{\Gamma(N+1)}{2\lambda}\right]^{1/2}\frac{1}{\left[\Gamma(N+2\lambda)\right]^{3/2}}\rho^{(\lambda-1/2)} \times$$
$$\times \exp(-\chi\rho)\, L^{2\lambda-1}_{N+2\lambda-1}(2\chi\rho), \qquad (13)$$

where

$$\lambda = \frac{1}{2} + \sqrt{(K+2)^2 + W_1}\ ;\ -N = \lambda + W/(2\chi). \qquad (14)$$

2. SOLUTION OF SCHRODINGER EQUATION FOR THREE-PARTICLE SYSTEM USING THE MODIFIED METHOD OF HYPERSPHERICAL FUNCTION WHEN PAIR INTERACTION BETWEEN PARTICLES IN 3D SPACE IS AS (1)

When K = K'= 0 we have expression (10). For solution of this equation we can use modified method of hypersperical function [3].

The main idea of the MMHF is that wave function Ψ represents the product of two functions, where the first is the main hyperspherical function and the second is the correlation function- $\zeta = \exp(f)$ that is defined by singularity and clustering properties of the wave function and it is equal to

$$f = -\sum_{i=1}^{3} \gamma_i r_i, \tag{15}$$

where r_i is the distance between the particles and γ_i is determined according to physical considerations.

Taking into account the relation between three different sets of Jacobi coordinates [7], the expression (15) can be presented as following:

$$\sum_{i=1}^{3} \gamma_i z_i = \rho(G_1 \cos\alpha + G_2 \sin\alpha), \tag{16}$$

where: $G_1 = \gamma_1 + \gamma_2 \cos(\phi_{23} + \phi_{31}) - \gamma_3 \cos\phi_{31}$;

$$G_2 = \gamma_2 \sin(\phi_{23} + \phi_{31}) - \gamma_3 \sin\phi_{31}. \tag{17}$$

If we substitute expression (15) into (10), and after transformation by hyperradial differential equation we obtain:

$$\left(\frac{\partial^2}{\partial\rho^2} + \left(\frac{5}{\rho} - W_2'\right)\frac{\partial}{\partial\rho} + \frac{W_4' + W_3'}{\rho} - \frac{2\mu}{\hbar^2}\frac{J}{\rho} + \right.$$

$$\left. + \left(\chi^2 + W_6'\right) - \frac{2\mu}{\hbar^2}\frac{K(K+4) + J_1}{\rho^2}\right)\psi(\rho) = 0, \tag{18}$$

where:

$$W_2' = (G_1 - G_2) * \frac{4}{15}; \qquad W_4' = 3W_2';$$

$$W_6' = G_1^2 + G_2^2; \qquad W_3' = G_1\left(\frac{4}{15} - \frac{3\pi}{8}\right) - \frac{42}{105}G_2; \qquad (19)$$

J_1 is the sum of the first members and J is the sum of second members in expression (9) (and same expressions for particles 13 and 23).

Taking into account the asymptotic behavior of the equation (18), let us seek a solution as the following:

$$\psi(\rho) = \exp(-\delta\rho)\rho^{\sigma}\varphi(\rho), \qquad (20)$$

where:

$$\sigma = -1 + \sqrt{9 + \frac{2\mu}{\hbar^2}J_1}; \qquad \delta = \frac{\sqrt{W_2'^2 - 4\left(\chi^2 + W_6'\right)} - W_2'}{4}. \qquad (21)$$

When substituting expression (20) into the equation (18), then for $\varphi(\rho)$ we obtain the equation of hypergeometrical function:

$$\left(r\frac{\partial^2}{\partial\rho^2} + (-r + 2\sigma + 3)\frac{\partial}{\partial\rho} + \frac{3W_2' + W_3' - 3\delta - V_C}{2\delta + W_2'} - \sigma\right)\varphi(\rho) = 0, \qquad (22)$$

where:

$$r = (2\delta + W_2')\rho, \qquad (23)$$

and

$$V_C = \frac{2\mu}{\hbar^2}J \qquad (24)$$

If we take into account that three-body system is bonded then solution of the (8) equation is represented as the following type of hypergeometrical function:

$$\varphi(\rho) = C_1 F(a, b, r), \qquad (25)$$

where: $b = \sigma + 5;$

$$a = \frac{(W_4' + W_3' - 2\delta\sigma - 5\delta - \sigma W_2' - V_c)}{2\delta + W_2'} = -N\,; \quad N = 1,2.... \qquad (26)$$

For binding energy we received:

$$E_N = -\frac{\hbar^2}{8\mu}\left\{\left[\left(\frac{4(W_4' + W_3' - V_c) - W_2'(2\sigma + 5 - 3N)}{2\sigma + 5 - N}\right)^2 - W_2'^2\right] + 4W_6'\right\} \qquad (27)$$

3. CONCLUSIONS AND ANALYSES

The dependence of binding energy of three body system on the global quantum number N obtained as a solution results in the expressions (12) and (27) that is given in the Table 1.

Table 1. Dependence of the binding energy of the three-body system in 3D space on the global quantum number N

N	Binding energy -E (*a*.u.), by expression (12)	Binding energy -E (*a*.u.), by expression (27)
0	0.3156439	0.304168
1	0.1264723	0.123532
2	0.067679	0.066523
3	0.042062	0.041494
4	0.0286507	0.028331
5	0.0207633	0.020566
6	0.0157354	0.015605
7	0.0123351	0.012244
8	0.0099287	0.009863

(In these results we assume that correlation parameters are the same for all particles. Interaction constants are the same for all particles too and satisfy the conditions: $a_{ij} < 0$, and $b_{12} = b_{13} < 0$, $b_{23} > 0$. If the conditions (14) and (21) are satisfied their variation doesn't give any qualitatively new results).

The Table shows that the binding energy of three-body system depending on the global quantum number N calculated from (12) and (27) formulae is exactly the same.

We can say that the use of MMHF doesn't give any quantity variation.

If we compare the MMHF with the results of $1/r^2$ potential, we can say that the MMHF for (1) potential doesn't give qualitative variation, because the potential contains 1/r.

REFERENCES

1. W.M.Frank, D.Land, R.M.Spector. Rev. Mod. Phys. **43,** 1971, 36. D. Amin, Phys. Today 35, 35(1982); Phys. Rev. Lett. 36, 323 (1976); A. Khare and S. N. Behra, Pramana. J. Phys. **14,** 1980, 327; S. Colemann, "Aspects of Symmetry" selected Erice Lectures Cambridge Univ. Press, Cambridge, 1988.
2. N.F. Johnson, L.Quiroga. Analytic rezults for N particles with 1/r2 interaction in two dimensions and an external magnetic field. cond-mat/9504025; Shi-Hai Dong, Zhong-Qi Ma, Giampiero Esposito. Phys.Lett. **12**, 1999, 465. quant-ph/9902081; Avinash Khare, Rajat K. Bhaduri. J.Phys. **A27**, 1994, 2213. hep-th/9310103; B. Basu-Mallick, S. Kumar. Phys.Lett. **A292,** 2001, 36. hep-th/0109022; C. A. Piguet, D. F. Wang, C. Gruber. SU(m|n) supersymmetric Calogero-Sutherland model confined in harmonic potential. cond-mat/9608015; T. James Liu, D. F. Wang. Integrable SU(m|n) supersymmetric electronic models of strong correlations. cond-mat/9602093; Saugata Ghosh. Long Range Interactions in Quantum Many Body Problem in One-Dimension: Ground State. quant-ph/0401116; Pijush K. Ghosh, Kumar S. Gupta On the Real Spectra of Calogero Model with Complex Coupling. Phys.Lett. A323 (2004) 29-33. hep-th/0310276.
3. A.Lomidze, Sh.Tsiklauri. Proceedings of I. Javakhishvili Tbilisi State University. Physics. **38,** 2002, 154.
4. A.M. Lomidze, Sh.M. Tsiklauri. Bulletin of the Academy of Sciences of the Georgia. **159, 1,** 1999, 52.

5. L.D.Landau, E.M.Lifshitz. Quantum Mechanics.I. 1948.
6. A.Lomidze, Sh.Tsiklauri. Three-electron quantum dot with inverse square potential between particls in 2D space. Georgian Electronic Scientific Journal: Computer Sciences and Telecommunication 1, 2002,49.
7. R.I.Jibuty, N.B.Krupennikova. The Hyperspherical Functions Method in Few – Body Quantum Mechanics. Tbilisi, 1984, (Russian).

Tbilisi State University

ა. ლომოძე

მოდიფიცირებული ჰიპერსფერული ფუნქციათა მეთოდი სამ ნაწილაკიანი სისტემისათვის 3D სივრცეში, როცა ნაწილაკებს შორის წყვილურ ურთიერთქმედებას აქვს სახე $\left(a/r^2+b/r\right)$

დასკვნა

მოდიფიცირებულ ჰიპერსფერულ ფუნქციათა მეთოდით გამოკვლეულია სამნაწილაკოვანი სისტემები, ნაწილაკებს შორის $\left(a/r^2+b/r\right)$ წყვილური ურთიერთქმედების გათვალისწინებით.

ჰიპერრადიალური ტალღური ფუნქციებისათვის მიღებულია უსასრულო გადაჯაჭვულ განტოლებათა სისტემა, რომელიც დიაგონალურ მიახლოებაში ამოხსნილია ანალიზურად. ამავე მიახლოებაში მიღებულია ბმის ენერგიის ანალიზური გამოსახულება.

EXCITONS IN ZnSe/CdSe QUANTUM DOTS MOLECULES

T.Chelidze, T.Sichinava, T. Kereselidze

Accepted for publication July, 2004

ABSTRACT. **We theoretically investigated electron-hole states in isolated and vertically coupled flat quantum dots. The dependence of exciton binding energy on interdot distance has been studied. The obtained results show very high value of exciton binding energy at a wide range of interdot distance.**

INTRODUCTION

Semiconductor quantum dots (QDs) are solid-state nanostructures, which allow confinement of carriers in all directions within dimensions smaller than their de Broglie wavelength [1]. Quantum confinement results in a characteristic discrete energy spectrum and δ-like density of states. Confinement in nanostructures with some of the linear dimensions is small compared to the exciton radius providing a possibility of enhancement of both binding energy and the oscillator strength of exciton.

Coupling between quantum dots (QDs) is now a matter of great importance. In the "artificial molecules" formed by two or more coupled QDs interdot coupling can be tuned far out of the regimes accessible in natural molecules, and single-particle tunneling and Coulomb interactions can be varied in a controlled way.

In the present work electron-hole Coulomb interaction is calculated in the two-fold stack of ZnSe/CdSe QDs. 2D-like QDs formed by Cd fluctuation [2] are considered. In quantum structures of this type lateral sizes few times exceed the bulk exciton effective radius therefore only vertical confinement is considered. Realistic potential of Pöschl-Teller type was used as a single particle potential for describing space confinement in vertical direction. Coulomb interaction between electron and hole is defined by direct diagonalization method.

CALCULATIONS AND RESULTS

Let us first consider single sheet of QDs. In the 2D-like QDs formed by Cd fluctuation with very low height to width ratio the vertical motion of carriers is mainly governed by confinement effects while their lateral motion obeys Coulomb attraction between them.

The potential energy of interaction of two opposite elementary charges – electrons and holes placed in a thin semiconductor layers (with dialectical constant ε_1) the thickness of which is less than the radius of electron-hole pair of bulk embedded between the material with dielectric constant ε_2 is given in the formula [3]:

$$V = \frac{e^2}{\varepsilon_1}\left[\frac{1}{\sqrt{\rho^2 + (Z_2 - Z_1)^2}} + \frac{\varepsilon_1 - \varepsilon_2}{\varepsilon_1 + \varepsilon_2}\frac{1}{\sqrt{\rho^2 + (Z_2 + Z_1)^2}}\right]. \qquad (1)$$

Here cylindrical coordinates are used.

In our case $\varepsilon_1 \approx \varepsilon_2$, therefore the second term if the brackets in eq.1 are negligible, besides this the thickness of the embedded layer is counted to be much less than characteristic distance of in-plane motion. That is why in the first approximation may be assumed that $V_0 = -\frac{e^2}{\varepsilon_1 \rho}$. The rest of the potential, which will be accounted by means of direct diagonalization is:

$$V' = \frac{e^2}{\varepsilon_1}\left[\frac{1}{\rho} - \frac{1}{\sqrt{\rho^2 + (z_e - z_h)^2}}\right]. \qquad (2)$$

In the first approximation when z-dependent Coulomb term is neglected the wave function is given by the formula:

$$\Psi_{pqnm} = \phi_p^e(z_e)\phi_q^h(z_h)\chi_{nm}(\rho, \varphi). \qquad (3)$$

$\chi_{nm}(\rho,\varphi)$ is the solution of two dimensional Coulomb problem describing electron-hole lateral motion:

$$\chi_{nm}(\rho,\varphi) = C_{nm} e^{im\varphi} (2k_n\rho)^{|m|} e^{-k_n\rho} F(-n+|m|, 2|m|+1, 2k_n\rho),$$

$$k_n = \frac{e^2}{\hbar\varepsilon_1 (n+1/2)} \sqrt{2\mu}, \qquad (4)$$

where n is the main quantum number, $m = 0, \pm 1 \ldots \pm n$; e and $\hbar$ are elementary charge and Planck constants, μ reduced effective mass of the electron-hole pair; F is the confluent hypergeometric function; C_{nm} normalizing constant. $\phi^{e(n)}_{p(q)}(z_{e(h)})$ are the electron (hole) single particle wave functions which describe their vertical motion. Corresponding to (3) energies are given by the formula:

$$E_{pqn} = \varepsilon^e_p + \varepsilon^h_q - \frac{e^4\mu}{2\varepsilon_1{}^2\hbar^2(n+1/2)^2}, \qquad (5)$$

where $\varepsilon^{e(h)}_{p(q)}$ are eigenvalues corresponding to $\phi^{e(n)}_{p(q)}(z_{e(h)})$. As to small dot vertical size separation between $\varepsilon^{e(h)}_{p(q)}$ shells much exceeds the Coulomb term, under each $\varepsilon^e_p + \varepsilon^h_q$ the energy levels corresponding to different main quantum number of in-plane motion are grouped. These levels are (2n+1)-fold degenerated. Taking into account z coordinate in Coulomb interaction causes their shift and splitting.

To take into account variation of Cd concentration in QDs formed by Cd segregation and interdiffusion vertical confinement is expressed by the potential (Fig.1):

$$U(z) = \frac{-U_0}{ch^2\alpha z} \qquad (6)$$

Here U_0 is the maximum band off set between the QD and barrier material realized in the center of QD layer. $1/\alpha$ is a measure of dot size and is defined from the emission spectra of single QDs.

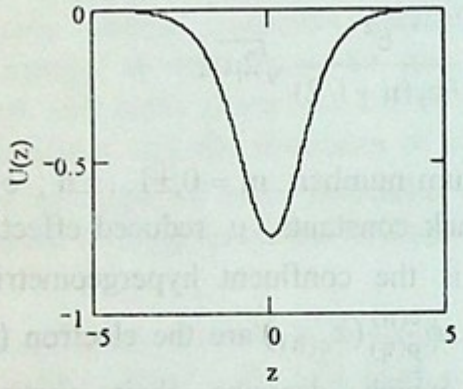

Fig.1. z-direction confinement potential in eV for single QDs

The expressions for eigenvectors $\phi^{e(h)}_{p(q)}(z_{e(h)})$ and eigenvalues $\varepsilon^{e(h)}_{p(q)}$ can be found elsewhere [4]. In our case for ZnSe/CdSe quantum dots only one electron and only one hole levels are possible inside the well. For potential barriers of electrons and holes - U_{0e} and U_{0h} 0.750eV and 0.230eV are taken; effective masses are $0.13m_0$ for electrons and $0.45m_0$ for holes.

As was mentioned we calculated z-dependent Coulomb energy by direct diagonalization of Hamiltonian matrix

$$H_{ll'} = \langle l | (H_0^e + H_0^h - H_c) | l' \rangle \qquad (7)$$

$|l\rangle$ denotes the states of electron-hole system described by wave functions (3). $H_0^{e(h)}$ and H_c are single particle Hamiltonian and Coulomb term. respectively. In our calculations six lowest energy states of electron-hole relative lateral motion are found to yield good convergence. In Figure.2 exciton energies in 2D ZnSe/CdSe QDs without (on the left) and with accounting (on the right) z-dependent Coulomb term are given. As is seen accounting z-dependent term in

Coulomb potential causes strong shift and splitting of energy levels. Calculated value of exciton binding energy in ZnSe/CdSe QDs is increased up to 100meV for 1nm dot vertical size and significantly exceeds the binding energy of exciton in bulk CdSe crystal (15mev).

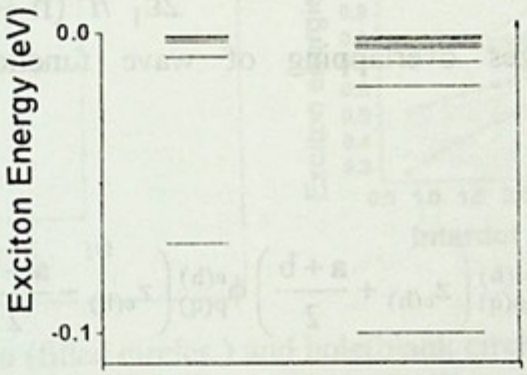

Fig. 2. Exciton energies with (right hand side) and without (left hand side) accounting z-dependent Coulomb term

For the stacks of QDs single particle potential is (Fig. 3b))

$$U(z) = \frac{-U_0}{ch^2\alpha\left(z-\frac{a+b}{2}\right)} + \frac{-U_0}{ch^2\alpha\left(z+\frac{a+b}{2}\right)} \qquad (8)$$

z = o is taken between the centers of QDs, a and b are dots vertical size and the distance between them. If neglecting z coordinate in the Coulomb term again the wave function of electron-hole system is given as:

$$\Phi_{pqnm} = \left[\phi_p^e\left(z_e - \frac{a+b}{2}\right) \pm \phi_{ps}^e\left(z_e + \frac{a+b}{2}\right)\right] \times$$

$$\times\left[\phi_q^h\left(z_h - \frac{a+b}{2}\right) \pm \phi_q^h\left(z_h + \frac{a+b}{2}\right)\right]\chi_{nm}(\rho,\varphi), \qquad (9)$$

Because of coupling of QDs in z direction single particle wave functions are presented as symmetric and antysymmetric combination

of functions centered in neighboring dots(fig.3c)). Corresponding energies are expressed as:

$$E_{spn} = \varepsilon_p^e \pm \Delta_e + \varepsilon_q^h \pm \Delta_h - \frac{e^4 \mu}{2\varepsilon_1^2 \hbar^2 (n+1/2)^2} \qquad (10)$$

$\Delta_{e(h)}$ characterizes overlapping of wave functions centered in neighboring dots:

$$\Delta_{e(h)}(a,b) =$$

$$= \varepsilon_{p(q)}^{e(h)}(a) \int \phi_{p(q)}^{e(h)}\left(z_{e(h)} + \frac{a+b}{2}\right) \phi_{p(q)}^{e(h)}\left(z_{e(h)} - \frac{a+b}{2}\right) dz_{e(h)} \qquad (11)$$

In Fig.3a) electron and hole single particle energies corresponding to symmetric and antisymmetric wave functions are given. The energy of electron-hole system if neglecting their interaction is the sum of electron and hole energy. So, in our case, when only one single particle energy level is possible in the single dot, there is QD molecule there are four energy levels: two with positive *z*-parity corresponding to the both carriers in symmetric or antisymmetric state; and two with negative total parity corresponding to the electron in symmetric and hole in antysymmetric state, and vice versa (Fig.3d)).

a)

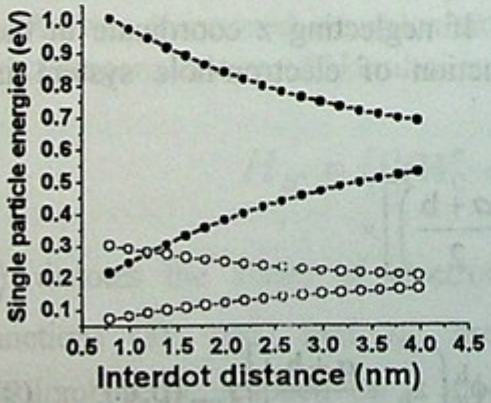

b)

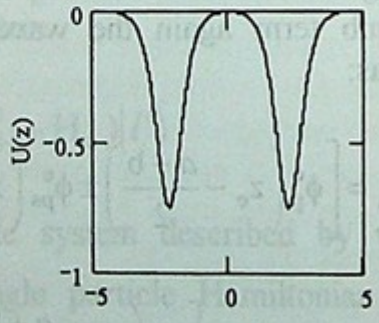

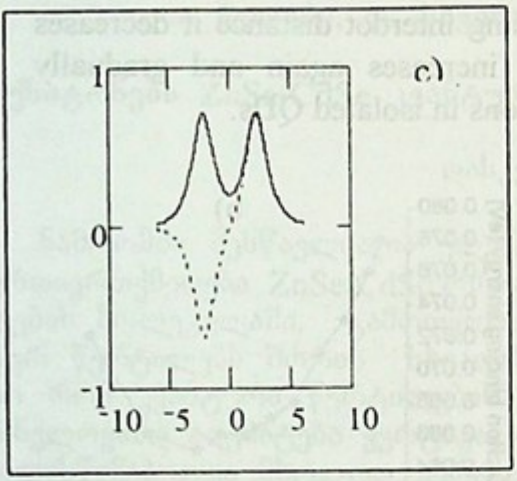

Fig.3. a) – electron (filled circles) and hole(blank circles) single particle energies as a function of interdot distance; b) - shape of confinements potential in quantum dot molecule; c) - single particle wave functions; d) energies of electron-hole pair excluding Coulomb interaction between them as a function of interdot distance

When accounting the Coulomb interaction in the first approximation, that is the last term in (10), under each of four energy levels group energy levels describing electron-hole lateral motion appear (not shown here).

We took into account z coordinate in Coulomb term by diagonalization (4) matrix with $|l\rangle$ corresponding to (6) and (5) as single particle potential. z-dependent Coulomb interaction mixes the states with the different main quantum number of in-plane motion and owing the same total z-parity. In Fig.4.a) the obtained energies of excitons as a function of interdot distance are given. The solid lines correspond to the states with even z-parity, dotted lines to the states with odd z-parity. For simplicity only two lower energy states of "bonding" and "antybonding" behavior of positive and negative parity are presented. With increasing the distance between dots low energy level approaches to the lowest energy level of exciton confined in isolated dot (labeled by E_{exc}), the high energy levels tend to the sum of the energies of non-interacting electron and hole ($\varepsilon^e+\varepsilon^h$). Exciton binding energy is very high again (Fig.4.b)). For $a = 1$nm and

b=1.2nm it is 0.078eV. With increasing interdot distance it decreases to 0.065eV for b= 4.2 nm, then increases again and gradually approaches the binding energy of excitons in isolated QDs.

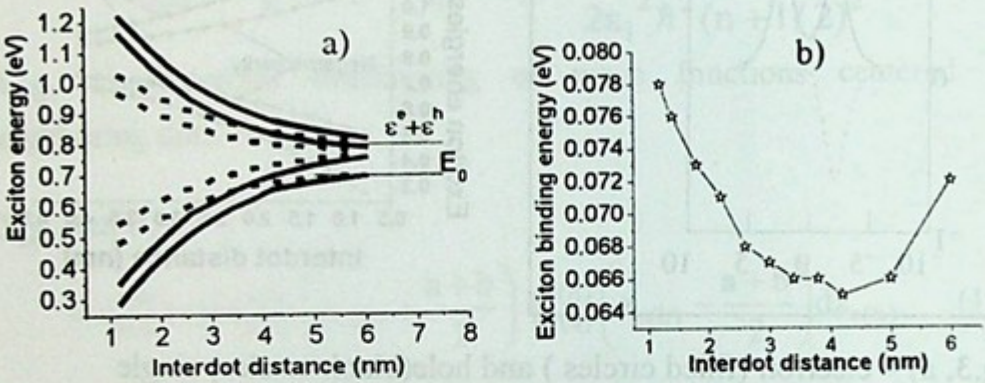

Fig.4. a) - Energies of excitons of positive total parity (solid lines labeled and negative total parity (cyrcles) as a function of interdot distance; b) - exciton binding energy as a function of interdot distance

ACKNOWLEDGMENTS

The work is supported by NATO Reintegration Grant FEL.RIG 980760.

REFERENCES

1. D. Bimberg, M.Grundmann, N.N. Ledentsov. Quantum dot.Heterostuctures. New York 1999.
2. T. Passow, H. Heinke, T. Schmidt, J. Falta, A. Stockmann, H. Selke, P. L. Ryder, K. Loenardi, D. Hommel. Phys. Rev. **B 65,** 2001, 193311.
3. A. B. Chaplik, M. B. Entin. Soviet Phys. J. Exper. Theor. Phys. **61**, 1971, 2496.
4. L. D. Landay, E. M. Lifshits Quantum mechanics. Moscow. 1989, 767.

Tbilisi State University

თ. ჭელიძე, თ. სიჭინავა, თ. კერესელიძე

ექსიტონები ZnSe/CdSe კვანტური წერტილების მოლეკულაში

დასკვნა

ნაშრომში შესწავლილია ელექტრონულ-ხვრელური კულონური ურთიერთქმედება ZnSe/CdSe ორგანზომილებიან კვანტური წერტილების მოლეკულაში. გამოთვლილია ექსიტონების ენერგია კვანტურ წერტილებს შორის სხვადასხვა მანძილებისათვის. იმის გამო რომ კვანტური წერტილების ჰორიზონტალური ზომები მნიშვნელოვნად აღემატება ვერტიკალურს, სივრცული შეზღუდვა გათვალისწინებულია მხოლოდ ვერტიკალური მოძრაობისათვის. კვანტურ წერტილებში Cd-ის განაწილების გასათვალისწინებლად როგორც შეზღუდვის პოტენციალი გამოყენებულია პოლშ-ტელერის ტიპის რეალისტური პოტენციალი. ჰორიზონტალური მიმართულებით ელექტრონულ-ხვრელური წყვილის მოძრაობა აღწერილია ორგანზომილებიანი კულონის ამოცანის ფარგლებში. ვერტიკალური მიმართულებით ელექტრონულ-ხვრელური ურთიერთქმედება გათვალისწინებულია ძლიერი ბმის მიახლოებაში. გამოთვლებმა აჩვენეს, რომ ექსიტონის ბმის ენერგია მკვეთრად იზრდება მოცულობითი ექსიტონის ბმის ენერგიასთან შედარებით (0.015 ევ). კერძოდ, 1 ნმ ზომის კვანტური წერტილებისათვის და მათ შორის 1.2 ნმ მანძილისთვის იგი შეადგენს 0.078 ევ-ს. წერტილებს შორის მანძილის ზრდა 4.2 ნმ-მდე ამცირებს ბმის ენერგიას 0.065 ევ-მდე. მანძილის შემდგომი ზრდისას ბმის ენერგია ისევ იზრდება უახლოვდება რა ექსიტონის ბმის ენერგიას იზოლირებულ კვანტურ წერტილში.

QUANTIZATION OF SINE-GORDON EQUATION SOLITON AND φ4 KINK EQUATION USING EIKONAL APPROACH

T. Gvarjaladze, A. Lomidze, S. Chkhaidze

Accepted for publication November, 2004

ABSTRACT. We offer nonperturbed scheme of S-G equation soliton and briser, φ4 equation of kink-antikink couple for obtaining of the spectrum of bound state in eikonal approach using Glauber method. Correspondingly, analytical expression of profile functions have been obtained. This gives the possibility to express scattering amplitude on briser by meson of the theory and on kink-antikink couple of their constituent solution, antisoliton and kink-antikink scattering amplitudes without using potential.

It is known that collective excitons of particle systems having nonlinear potential (due to strong self-influence of the scalar field) are considered as physical solitons [1].

According to the hypothesis the soliton like particles are quantum corpuscles of such field. [2].

At first from the activity function by means of variation principle for the classical nonlinear fields, Euler-Lagrange equation is obtained, where soliton like solutions are nonperturbed. Thus, we gradually imagine the quantization of the classical field by means of nonperturbation method, particularly eikonal approach.

In this approach, when the scattering is observed only on the small angles, the field inside interaction area is equal to the field, which is elastic scattered, and this one far from scattering is the diffraction field of Fraungofer. In conditions of ermitivity of the scattering potential the inside field gives the binding states i.e. negative energies $E < 0$, if imaginary part of wave vector is $ImK = i\chi$, $\chi > 0$ [3]. If the "black" $ReK = 0$ is scattered, an interaction is nonelastic and the inside field is the absorbed one. If $Re\ K \neq 0$, then the absorbed part corresponds to the field of the binding state of system [4].

To the solutions of sine-Gordon (S-G) equations solitons and antisolitons – Skyrme [5] gave a topological charge +1 and –1

respectively, which agrees with the phase shift, while studying their intercollision [App.A].

A couple solution of soliton and antisoliton i.e. briser is neutral according to the topological charge; it itself is antiparticle and, that is why the meson corresponds to it.

Soliton is surrounded with briser clouds and most part of time it spends in the state of exchange of vacuum with mesons of theory. The meson is the briser of small radius. The free soliton (antisoliton) is absorbed by the vacuum briser and soliton of briser is irradiated. According to the classical theory this process is stochastic and corresponds to the interaction of classical solution field, to its own meson one.

According to nonstochastic approach, the description is possible in the conditions of small deviation from balance position and during small scale of physical system.

In the future approach, using the multitime method, one excludes the secular members in the formal asymptotic setting. This dictate the expression of nonlinear potential $U(\Phi)$ in the evaluative equation of Euler-Lagrange, which doesn't reveal any stochastic behaviour. The trajectories in the phase space are smooth, the field $\eta = \langle\Phi\rangle$, where $\langle\cdot\rangle$ means the vacuum average value, Φ is the descriptive field of physical system, which generally may be stochastic. The trajectories on the rotation points of the separatrice are not smooth – the physical system here is still stochastic.

Then one is deriving linearity near η, but it breaks the symmetry of task to the transformation of rotational and translational permanent groups. This leads us to elementary excitation – Goldstone boson type mode with zero energy. New $\Phi - \langle\Phi\rangle \equiv x$ field will change them into the Higgs bosons. The field equation gets the expression of Klein-Gordon linear equation:

$$\Box x + U''(\eta)x = O(x^2) .$$

The solutions of these equations are mesons.

If the constant g of an interaction is small and the Hamiltonian of interacting fields was renormalized, it would be possible to use the perturbation theory. That time the mesons were described by free

fields and their quantum transitions on the classical solitons of mesons or on kink between the conditions of scattering link were due to their interaction.

Faddeev and Takhtajian [2] solved S-G classical equation by means of determination of action-angle variables. In these variables classical Hamiltonian was brought to the sum of free-coupled particles, taking into account a coupled soliton-antisoliton (briser) solution. Hamiltonian depended on variables of activity and not on angles. That is why, the following steps of quantization are trivial. Unfortunately, it's problematic to find these variables. This task may be solved using the method of reverse scattering.

Dashen et al. [6] made quantization of S-G and φ4 systems. The lower energetic level is S-G or φ4.According to this its mass consists of classical part which is followed by quantum correction. In the correction of high order divergence was neglected by counter members; they made quantization of briser in the same way. The setting of the field in the approach of the given soliton solution breaks the symmetry of the tasks in relation to continuous group. Crist and Lee [7] solved the problem of emerged zero modes (which appeared because of breaking continuous rotational and continuous translational symmetries) by introducing collective coordinates as implicit form.

The solutions of the field of quantum theory are correct using the theory of perturbation [5]. The precision of quantum correction with the members of the fourth order from the point of view of the relativity of masses is due to particularity of S-G. In the case of kink it is not so. Though the correction of soliton mass is not precise, the precision of their relativity is unexpected. The existence of the theory of mesons points that an interaction is strong. It is known that if we use the normalized theory of interaction for not small meanings of g, it's impossible to use the theory of perturbation successfully.

In the conditions of strong interaction for the solution of the task of scattering different methods are used. Of them Glauber method of eikonal approach is one of the widespread approaches [8]. It uses the function of profile $\Gamma(\rho)$ (ρ is a target parameter), which allows us to count the scattering amplitude more precisely, than in the Born approach, or using Shvinger's variation functional.

QUANTIZING OF SOLITON TYPE FIELDS

According to the given approach the central subject is a finding of conditions of the scattering of meson on the soliton.

Let us discuss a model of self-acting complex scalar field $\Phi(\bar{r},t)$. The acting functional is:

$$S[\Phi(\bar{r},t)]=\int\left[\frac{1}{2}|\Phi_t|^2-\frac{1}{2}|\Phi_x|^2-\frac{1}{g^2}U(g|\Phi|)\right]dtd^3r, \qquad (1)$$

where g is a bound constant. The Euler-Lagrange equation has a form [5]:

$$\frac{\delta S}{\delta\Phi}=-\Box\Phi(\bar{r},t)-U_{|\phi|}\frac{\Phi(\bar{r},t)}{g|\Phi(\bar{r},t)|}=0 \qquad (2)$$

It means that the nonlinearity of the potential $U[\Phi(\bar{r},t)]$ is selected so that the equation has soliton like solution, but soliton like particle is described by a pseudoscalar field $\Phi(\bar{r},t)$.

It's assumed in the eikonal approach that transferred impulse is in the perpendicular plane of the particle spreading z, along the radial coordinate ρ. Let's write a field in the cylindric coordinates (z,ρ) of this approach:

$$\Phi(\bar{r},t)=\frac{\langle\Phi(z,t)\rangle}{g}+\left\{\Gamma_R(\rho)+i\Gamma_I(\rho)e^{i\omega t}\right\}e^{ikz}, \qquad (3)$$

where $\{\ \}e^{ikz}$ is scattered field, $\langle\cdot\rangle$ is classical field and $\Gamma_R(\rho)+i\Gamma_I(\rho)=1-e^{ix(\rho)}$ is the profile function. Inserting the expression (3) into the equation (2), we shall get three following equations:

$$(-\partial_{,zz}+\partial_{,tt})\langle\Phi\rangle=\partial_{,\Phi}u\langle\Phi\rangle, \qquad (4)$$

$$(-\partial_{,\rho\rho}+V)\Gamma_R(\rho)=0, \qquad (5)$$

$$(-\partial_{,\rho\rho} + V)\Gamma_1(\rho) = \omega^2\Gamma_1(\rho), \qquad (6)$$

where $x(\rho) = -\frac{iE}{k}\int_{-\infty}^{\infty} dz' V(\bar{\rho}, z')$ [App.B]. The last equations describe bound conditions in the scattering in the point z = 0. From the equation (4), we shall find V, becouse we have known $x(\rho)$ and $\Gamma_R(\rho)$.

From (6) the law of dispersion is obtained:

$$\omega^2 = m^2 + k^2 \qquad (7)$$

SOLITON

If $U\langle\Phi(\bar{r},t)\rangle = \frac{m^2}{g^2}\left(1 - \cos\langle\Phi(\bar{r},t\rangle\right)$, then we shall get S-G equation from (4) one:

$$\left(\partial_{\bar{t}\bar{t}} - \partial_{\bar{z}\bar{z}}\right)\langle\Phi\rangle + \sin\langle\Phi\rangle = 0. \qquad (8)$$

Here the variables are changed:

$$mt \to \bar{t}, \quad mz \to \bar{z}, \quad g\Phi \to \langle\Phi\rangle. \qquad (9)$$

The soliton solution of this equation is

$$\langle\Phi(\bar{z},t)\rangle = 4\,\mathrm{arctge}^{(\bar{z}+v\bar{t})}. \qquad (10)$$

This means, that the first member or classical field of three equations has the form:

$$\frac{\langle\Phi(\bar{z},t)\rangle}{g} = \frac{4}{g}\,\mathrm{arctge}^{\gamma m(z+vt)}, \qquad (11)$$

where $\gamma \equiv (1-v^2)^{-1/2}$.

Let us appeal equations (5) and (6). Assume that

$$x(\rho) = 2\text{arctge}^{\rho}. \tag{12}$$

Let us appeal the new variables

$$\rho = mz = \bar{z}. \tag{13}$$

The profile function will have a form:

$$\Gamma(\rho) = 1 - \cos(2\text{arctge}^{\rho}) - i\sin(2\text{arctge}^{\rho}) = 1 + th\rho - i\sec h\rho .. \tag{14}$$

Equation (5) gives that for a zero mode $\omega_0 = 0$ $\Gamma_R(\rho) = 1 + th\rho$ we shall get

$$\left(-\partial_{,\rho\rho} + V(\rho)\right)(1 + th\rho) = 0. \tag{15}$$

The frequency of normal oscillation is determined inserting $V(\rho) = 1 - 2\sec h^2\rho$ and $\Gamma_I(\rho) = -\sec h\rho$ in the equation (6).

$$(-\partial_{,\rho\rho} + 1 - 2\sec h^2\rho)\sec h\rho = \frac{\omega_1^2}{m^2}\sec h\rho \tag{16}$$

i.e. we can rewrite $\omega_1 = 0$ and equation (16) for nonreflective potential $-2\sec h^2\rho$

$$(\partial_{\rho\rho} + 2\sec h^2\rho)\sec h\rho = \frac{\omega_2^2}{m^2}\sec h\rho . \tag{16'}$$

φ4 kink

For two hole potential

$$U\langle\Phi(z,t)\rangle = \frac{m^2}{g^2}\left[\frac{1}{4}\left(\Phi^2(z,t) - 1\right)^2\right]$$

The classical field $\langle\Phi\rangle$ will satisfy the equation:

$$\left(\partial_{\bar{t}\bar{t}} - \partial_{\bar{z}\bar{z}}\right)\langle\Phi\rangle = \frac{m^2}{g^2}\left(\langle\Phi\rangle^3 - \langle\Phi\rangle\right) \tag{17}$$

The nonstationar solution of this equation is kink:

$$\langle\Phi(z,t)\rangle = th\left(\frac{\bar{z}}{\sqrt{2}} + v\bar{t}\right) \tag{18}$$

i.e. the classical field will have a form:

$$\frac{\langle\Phi(z,t)\rangle}{g} = \frac{1}{g}th\left(\frac{\gamma m}{\sqrt{2}}(z+vt)\right). \tag{19}$$

Then appealing to the new variabels $\rho = mz/\sqrt{2} = \bar{z}/\sqrt{2}$. If $x(\rho)$ soliton solution has the form (10)

$$x(\rho) = 4arctge^{\rho}, \tag{20}$$

we shall have

$$\Gamma(\rho) = \sec^2\rho - ish\rho\sec h^2\rho. \tag{21}$$

The equation (5), which describes a zero mode will get a form:

$$\left(-\frac{1}{2}\partial_{,\rho\rho} + V(\rho)\right)\sec h^2\rho = 0. \tag{22}$$

From this we get $V(\rho)$:

$$V(\rho) = 3th^2\rho - 1 \tag{22'}$$

For the normal mode ω_1, from equation (6) we shall get Shrodinger type equation of scattering form:

$$\left(-\frac{1}{2}\partial_{,\rho\rho}+(3th^2\rho-1)\right)sh\rho\sec h^2\rho=\frac{\omega_1}{m^2}sh\rho\sec h^2\rho\,, \qquad (23)$$

then we shall see that discrete mode

$$\omega_1^2=\frac{3}{2}m^2\,, \qquad (24)$$

which agrees with results of [6].

As we discuss the scattering on the small angles ($\cos\vartheta\approx 1$) and assume that the scattering has azimuthal symmetry, that's why of profile functions we shall get the amplitudes of scattering

$$f(\vartheta)=ik\int_0^{+\infty}d\rho\rho\Gamma(\rho)J_0(k\rho\vartheta)\,, \qquad (25)$$

where $J_0(k\rho\vartheta)$ is Bessel function of zero order, and their quadrates will give a differential section of the scattering.

QUANTIZATION OF BRISER

The equation of S-G

$$\overline{\Phi}=\sin\overline{\Phi}\,, \qquad (26)$$

in the descriptive coordinates $\sigma = x + vt$, $\rho = x - vt$ is written

$$\frac{\partial^2\overline{\Phi}}{\partial\sigma\partial\rho}=\pm\sin\overline{\Phi}\,. \qquad (27)$$

Between the solutions of this equation is soliton $\overline{\Phi}_s$, antisoliton $\overline{\Phi}_A=-\overline{\Phi}_s$ and a couple of soliton-antisoliton $\overline{\Phi}_{SA}\equiv\overline{\Phi}_V$ i.e. briser.

To form a briser soliton let is use the theorem of Baclund transformation:

$$\operatorname{tg}\frac{\overline{\Phi}_V-\overline{\Phi}_o}{4}=\frac{1}{U}\operatorname{tg}\frac{\overline{\Phi}_A-\overline{\Phi}_S}{4}. \qquad (28)$$

For briser a parameter U is imaginary U = iv

$$\overline{\Phi}_v(x,t)=4\operatorname{arctg}\left\{\frac{1}{v}\frac{\sin\left[vt/\left(1+v^2\right)^{1/2}\right]}{\operatorname{ch}\left[x/\left(1+v^2\right)^{1/2}\right]}\right\}. \qquad (29)$$

It is clear that, in briser soliton and antisoliton may be apart each other only in the limit distance.

In the v = 0 account system $\Phi_v(x,t)$ is a still wave, but in the system of pair mass center its components: soliton and antisoliton oscillate in relation to each other with the period

$$T=\frac{2\pi v}{\left(1+v^2\right)^{1/2}}, \qquad (30)$$

Accounting this (29) may be written as [5,6]:

$$\overline{\Phi}_v(x,t)=4\operatorname{arctg}\left\{\left(T^2-1\right)^{1/2}\frac{\sin\left[mt/\overline{T}\right]}{\operatorname{ch}\left[mx\left(\overline{T}^2-1\right)^{1/2}/\overline{T}\right]}\right\}, \qquad (31)$$

where $\overline{T}\equiv\frac{mT}{2\pi}$.

An assumable Skyrme's charge of briser is zero, but brizer consists of two different named topological unified charges. At the meeting of these particles the charge disappears i.e. annihilates. The other particle emerges. This is Frenkel's exciton i.e. an exciton of small radius. Quantization of doublets using WKB method was made by Dashen et al.[3].

Taking into consideration a meson of theory – briser we have found above the bound conditions on S-G soliton and kink of its elastic scattering.

The consideration of eikonal approach according to Glauber having a form of multiorder scattering allows us to consider bound conditions of briser on the complex objects – briser, φ4 doublet, the soliton and antisoliton, kink and antikink.

Briser will not have topological charge of Skyrme. It is itself antiparticle. That is why the meson corresponds to it.

Thus we think, that briser is a meson of theory. It is special, because it has a mass

$$M_B = \frac{16}{\gamma_o m} \sin \frac{n\gamma_o}{16}, \text{ where } n = 1,2...,N. \tag{32}$$

We shall make quantization using Glauber's method. Really we are accounting briser structure.

From (5) let us appeal the following equation:

$$(-\partial_{,\rho\rho} + V)G_R(\rho) = 0, \tag{33}$$

From (6) we shall get

$$(-\partial_{,\rho\rho} + V)G_I(\rho) = \omega^2 G_I(\rho), \tag{34}$$

where according to Glauber, the profile function of a pair is

$$G^S(p) = \Gamma_S\left(\rho + \frac{1}{2}\bar{r}\right) + \Gamma_{AS}\left(\rho - \frac{1}{2}\bar{r}\right) - \Gamma_S\left(\rho + \frac{1}{2}\bar{r}\right)\Gamma_{AS}\left(\rho - \frac{1}{2}\bar{r}\right), \tag{35}$$

In the system of mass center ρ is a distance in briser between soliton and antisoliton. If we insert Γ_S and Γ_{AS} from (14) and (14') meanings we have

$$G^S(\rho)=\frac{2\mathrm{sh}\frac{1}{2}r}{\mathrm{ch}^2\rho+\mathrm{sh}^2\frac{1}{2}r}\left(\mathrm{sh}\frac{1}{2}r-i\mathrm{ch}\rho\right), \qquad (36)$$

For a pair of φ4 kink and antikink we have

$$G^K(\rho)=\frac{4}{\left(\mathrm{ch}^2\rho+\mathrm{sh}^2\frac{1}{2}r\right)^2}\left(2\mathrm{sh}^2\rho\mathrm{ch}^2\frac{1}{2}r-i3\mathrm{ch}^3\rho\mathrm{sh}\frac{1}{2}r\right). \qquad (37)$$

The offered scheme of quantization is true in the eikonal approach, but contrary the need of setting of potential (accounting the member of second order) is not necessary.

APPENDIX A

The quantitative experiments of Skyrme topological charge showed, that soliton and antisoliton attract each other, but solitons (antisolitons) do not. We have analogous results in the case of kinks and antikinks

If we take a mark "+" then 2π soliton satisfies limit conditions $<\varphi>\to 0$ if $z\to -\infty$ and $<\varphi>\to 2\pi$, when $z\to +\infty$, i.e. 2π soliton undergoes to interpolation from 0 to 2π.

$$<\varphi(\infty,t)>-<\varphi(-\infty,t)>=2\pi-0.$$

4π soliton totally undergoes to interpolation from 2π to 4π and so on.

If we have antisoliton ("-" mark), then $<\varphi>\to 2\pi$, when $z\to-\infty$ and $<\varphi>\to 0$ if $z\to+\infty$, i.e. it undergoes to interpolation from 2π to 0. According to this Skyrme gave to soliton and antisoliton topological charge, respectively.

In the case of φ4 kink interpolation occurs from $-\pi$ to $+\pi$. That is why, topological charge of Skirme for kink will be +1 and for antikink

–1. Skirme supposed about equivalence of S-G and MT models, which are proved by Coleman.

In the MT model fermion charge is

$$Q=\int_{-\infty}^{+\infty} J_o dx = \int_{-\infty}^{+\infty} \overline{\Psi}\gamma_o \Psi dx .$$

Fermion has Q = 1 and antifermion - Q = -1. In the bound (linked) position Q = 0. From the theorem of Coleman it yields that

$$-\frac{\sqrt{\lambda}}{2\pi m} E^{\mu\nu}\partial_\nu \Phi = \overline{\Psi}\gamma^\mu \Psi \equiv J^\mu ,$$

where charge can be written by means of S-G fields.

$$Q = \int_{-\infty}^{+\infty} -\frac{\sqrt{\lambda}}{2\pi m} E^{01}\partial_x \Phi dx = \frac{\sqrt{\lambda}}{2\pi m}\int_{-\infty}^{+\infty} \partial_x \Phi dx .$$

This is topological charge of S-G model.

APPENDIX B

Let us note that the method does not need the knowledge of potential [9], and it is used successfully to study elastic scattering of pions on protons, deutons and some complex nucleus.

We know that the meson of theory is briser. We have to solve the equation of Klein-Gordon, which describes it. In the stationary case it has a form

$$\nabla^2 \psi + \left[(\omega - V)^2 - M^2\right]\psi = 0 .$$

This expression can be written simply in the form of Shrodinger equation if we use the values $K^2 \equiv \left(\omega^2 - M^2\right)$, $U \equiv V(2\omega - V)$, where M is a mass of briser. If we are searching for the solution in the

form flat wave $\varphi(r)e^{ikz}$, then in the eikonal approach $\partial_z\phi << ik\partial_z\phi$ we get the equation of diffusion type more exactly of diffraction type $ik\partial_z\phi = \omega V\phi$.

From this expression we have

$$\psi = e^{ikz+\chi(\rho)}.$$

The Shrodinger equation of scattering form

$$\left[\nabla^2 + k^2 - U(\vec{r})\right]\Psi = 0$$

could be initially transformed into Lippmann-Schwinger, which in the asymptotic region $\vec{r} \to \infty$ will get a form

$$\psi = e^{ikz} - \int d^3r' \frac{1}{4\pi}\frac{e^{ik\vec{r}}}{r} e^{-ik\frac{\vec{r}\vec{r}'}{r}} U(\vec{r})\Psi(\vec{r}).$$

So, equation (3) is a modified form of Lippmann-Schwinger equation in the eikonal approach.

REFERENCES

1. R.K.Dodd, J.C.Eilbeck, J.D. Gibbon, H.C. Morris. Solitons and Nonlinear Wave Equations. Academic Press., Inc.1982.
2. L.D.Faddeev, L.D. Takhtajian. Teoreticheskaia i Matematicheskaia Fizika. **71,** 1974, 160; Uspekhi Matematicheskikh Nauk. **29,** 1974, 249.
3. M. Wadati, T. Kamijo. Prog. Theor. Phys. **52,** 1974, 397.
4. Luc Valentin. Physique Subatoinique: Noyax et Particules., **2,** Hermann, Paris, 1982.
5. R.Rajaraman. Solitons and Instantons (in Quantum Field Theory). 1982, North-Holland Pabl. Co., Amsterdam, New York, Oxford, 414.
6. R.F.Dashen, B.Hasslasher, A.Neveu. Phys.Rev. **D10,** 1974, 4114; **D10,** 1974, 4130; **D11,** 1975, 3431; **D12,** 1975, 2443.
7. N. H. Crist, T. D. Lee. Phys. Rev. **D12,** 1975, 1606.

8. R. J. Glauber. Lectures in Theoretical Physics. Ed. M.C. Britten et all., 1. 1959.
9. H.M.Pilkuhn. Relativistic Particle Physics. Springer-Verlag N.Y. Heiderberg, Berlin, 1979.

Tbilisi State University

თ. გვარჯალაძე, ა. ლომიძე, ს. ჩხაიძე

სინუს-გორდონ განტოლების სოლიტონის და φ4 განტოლების კინკის დაკვანტვები ეიკონალის მიახლოების გამოყენებით

დასკვნა

შემოთავაზებულია არაპერტურბაციული სქემა S-G განტოლების სოლიტონისა და ბრიზერის, φ4 განტოლების კინკის და კინკი-ანტიკინკი წყვილის ბმული მდგომარეობების სპექტრის მისაღებად ეიკონალის მიახლოებაში გლაუბერის მეთოდის გამოყენებით. შესაბამისად, მიღებულია პროფილის ფუნქციების ანალიზური გამოსახულებები, რაც შესაძლებლობას იძლევა გამოისახოს თეორიის მეზონის გაბნევის ამპლიტუდა ბრიზერზე და კინკი-ანტიკინკი წყვილზე მათი შემადგენელი სოლიტონის, ანტისოლიტონის და კინკის და ანტიკინკის გაბნევის ამპლიტუდებით პოტენციალის გამოყენების გარეშე.

PHOTOLUMINESCENCE OF EPITAXIAL FILMS OF $Ga_xAL_{1-x}P$ DOPED BY VARIOUS CONCENTRATIONS OF ZINC AND TELLURIUM

S. Gotoshia

Accepted for publication November, 2004

ABSTRACT. **The effect of zinc and tellurium ligature on photoluminescence spectra has been studied in a large quantity of epitaxial films $Ga_xAl_{1-x}P$. It was found that inclusion of zinc or tellurium in large quantities in $Ga_xAl_{1-x}P$ films causes the attenuation of the green luminescence and photoluminescence origination in the red area of spectrum simultaneously. We were the first to reveal this phenomenon in this system. As the reason of the formation of these two parallel processes we consider technological defects as well as recombination and annihilation processes proceeding on acceptor and donor levels of zinc and tellurium, respectively. The dependence of changes of intensity of the green luminescence on the quantity of acceptor and donor impurities has been expressed graphically.**

$Ga_xAl_{1-x}P$ are very interesting and promising semiconductor materials in optoelectronic instrumentmaking industry. These mixed crystals are notable for the forbidden gap increase with aluminum addition to GaP and at the same time for a shift to short wavelengths of yellow luminescence characterizing GaP. As a result it is possible to receive a green luminescence in this system. Optical properties of this system are insufficiently explored, so we continue the purposeful study of the above semiconductors in the mentioned direction.

The aim of the given work is to study photoluminescence in epitaxial films of various types to determine photoluminescence mechanisms and conditions in the films, where green luminescence is optimal. It is important to study the influence of Te and Zn ligatures included in various concentrations in $Ga_xAl_{1-x}P$ on photoluminescence spectra.

Many epitaxial films of various kind and origin were at our disposal. They all were synthesized with liquid-phase epitaxy. Graphite boat was used as a reactor. Epitaxy process was produced at 970^0C temperatures. Deposition was carried out on both *n*-type and *p*-type GaP substrates surfaces, orientation of which was mainly (001). There were undoped films giving n-type conductivity; *n*-type films doped with tellurium impurity and that of *p*-type doped with zinc impurity.

Recording of photoluminescence spectra was made with the same laboratory setup by which we were recording Raman spectra [1]. Double diffraction spectrometer DFS-24 served as a spectrometer. Registration was carried out by photon counting and synchronous detection methods. Photomultiplier FEU-79 served as a signal detector. We produced photoluminescence excitation by 514.5, 488.0Å wavelengths of argon ion laser radiation and 441.6Å of helium-cadmium laser radiation. All measurements were carried out at room temperature. Epitaxial film thickness was about 10-16 μmc though we had thicker films too.

Fig.1 shows photoluminescent spectra of undoped, tellurium-doped and zinc-doped $Ga_{0.68}Al_{0.32}P$ (by 488.0 nm excitation). The green luminescence characteristic peak is seen in all the three samples. Green luminescence of undoped film is observed at 540.0 nm. When doping with a few quantity of tellurium the green luminescence is shifted to long waves and observed at 542.0 nm; but in case when films are doped with a few quantity of zinc the green luminescence is shifted to longer waves and the characterizing peak is at 545.0 nm. In all the three cases there is no long wave luminescence - a red luminescence near 1.94-1.97 eV` in the photoluminescence spectrum; the fact probably denotes comparatively good quality of films, negligible quantity of defects and deep levels. In connection with this it should be noted that in $Ga_{0.68}Al_{0.32}P$ the green luminescence intensity of undoped films is slightly greater than that of doped films with a few quantity of tellurium, while introduction of a few quantity of zinc causes sharper increase of the green luminescence.

All epitaxial films of various types studied by us without exception show green photoluminescence, the intensity of which is being changed over the great range according to film composition

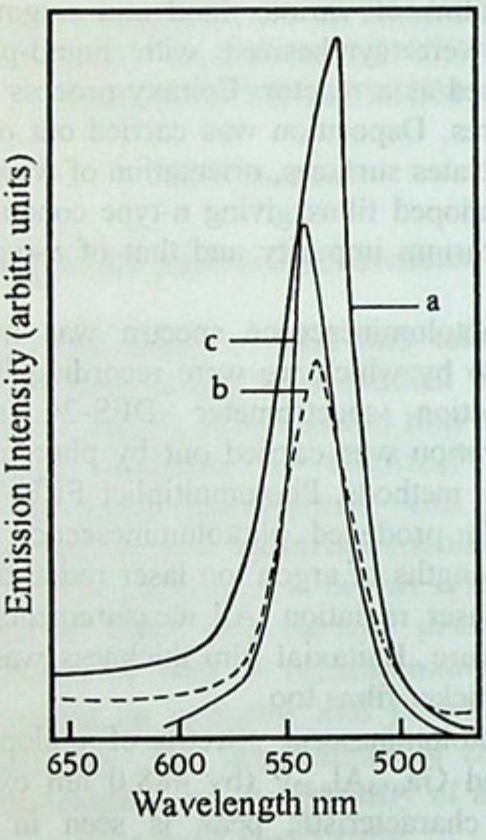

Fig.1. PL spectra for undoped (a), tellurium-doped (b) and zinc doped (c) $Ga_{0.68}Al_{0.32}P$ with 488.0 nm excitation

(x-value), carrier concentration in certain compositions, types of these impurities and degree of structural perfection of these mixed crystals. For example, in mixed crystals $Ga_{1-x}Al_xP$ that are doped with 20 mg zinc, the intensity of green photoluminescence is decreased by the ratio of about 111:11:25:1, when aluminum concentrations are changing in succession of x = 0.06, 0.32, 0.5, 0.68, accordingly. Thus green luminescence is great when a few quantity of aluminum is introduced in GaP and then it falls with aluminum concentration increase. The halfwidth of the peak characterizing the green luminescence is 25- 30 nm. The energetic position of green luminescence peak changes sharply with mixed crystal composition change. This relation is shown in Fig.2.

We have studied films of various compositions but in view of studying the concentration dependence of acceptor ligature of zinc we have selected films of three various compositions: $Ga_{0.66}Al_{0.34}P$, $Ga_{0.42}Al_{0.58}P$, $Ga_{0.35}Al_{0.65}P$. Each of these compositions was doped by zinc ligature in the following quantity: 5, 10, 20, 30, 40, 60, 90 and 100 mg.

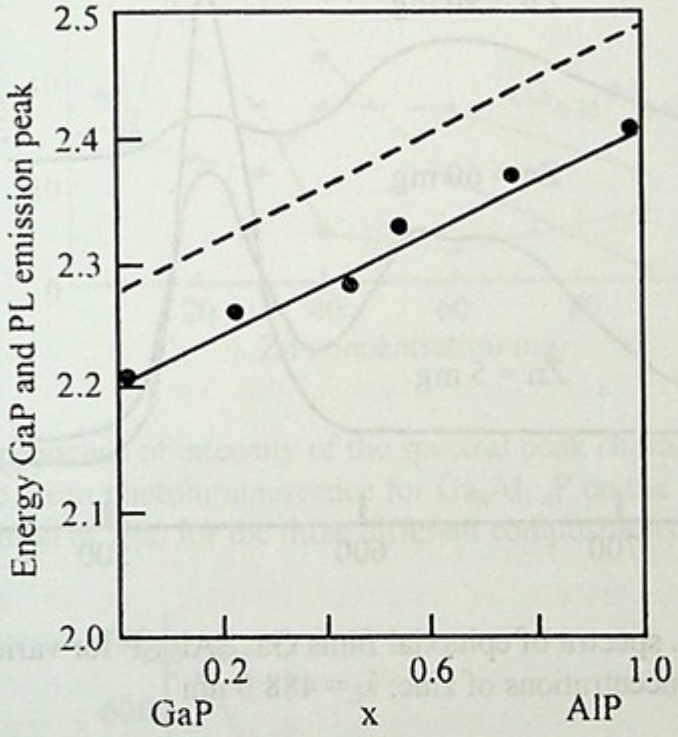

Fig.2. Dependence of the energy of the spectral peak characterizing the green photoluminescence for $Ga_xAl_{1-x}P$ on epitaxial film composition

Fig.3 shows photoluminescence spectra of $Ga_{0.66}Al_{0.34}P$ mixed crystal, when 5, 60 and 90 mg zinc is included in the film. The spectra show clearly gradual attenuation of green luminescence, the corresponding peak of which is at 545.0 nm. Simultaneously red luminescence is originated at 1.973 eV. The green luminescence changes according to composition and Fig.2 shows this process. The position of red luminescence peak is practically invariable.

Fig.3 shows that for composition $Ga_{0.66}Al_{0.34}P$ the intensity of green luminescence decreases after addition a great amount of zinc

(above 40 mg). In case when zinc amount does not exceed 40 mg (not shown in Fig.3) the intensity of green luminescence increases a little, reaches maximum and then decreases above 40 mg.

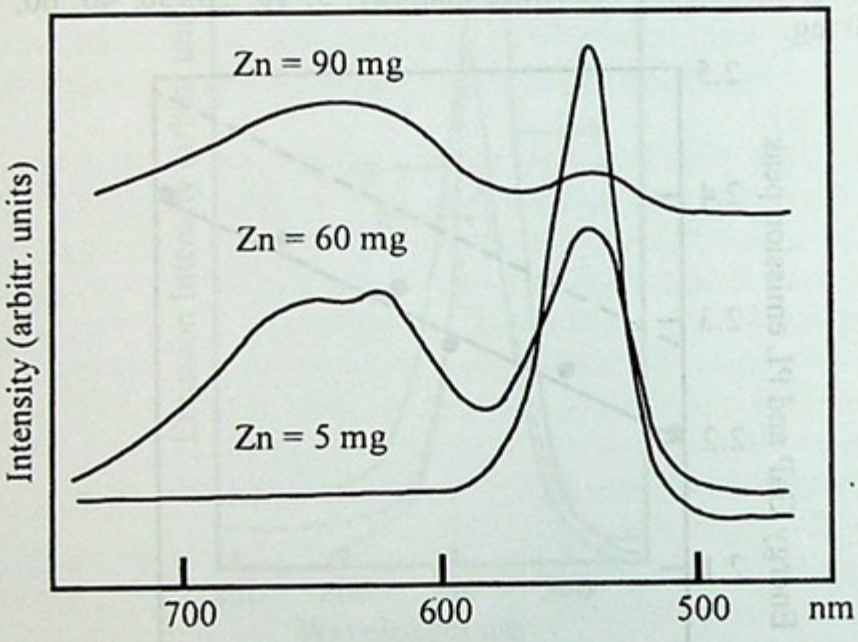

Fig.3. PL spectra of epitaxial films $Ga_{0,68}Al_{0,32}P$ for various concentrations of zinc; λ_L= 488.0 nm

For composition $Ga_{0.42}Al_{0.58}P$ the increase of zinc ligature amount causes monotonous attenuation of green luminescence and origination of red luminescence. In case of $Ga_{0.35}Al_{0.65}P$ at increase of zinc amount green luminescence decreases for a while, then increases in a certain interval of growth of zinc amount and afterwards decreases again when amount of zinc increases. These results are shown in Fig.4.

It turned out for Zn-doped films (to 40 mg) that green luminescence intensity decreases in parallel with increase of aluminum concentration. The experimental fact is shown in Fig.5.

We have studied three films of various compositions during tellurium-doping: $Ga_{0.68}Al_{0.32}P$, $Ga_{0.46}Al_{0.54}P$, $Ga_{0.35}Al_{0.65}P$. Each composition was doped by four various quantities of tellurium: 1, 4, 10 and 20 mg.

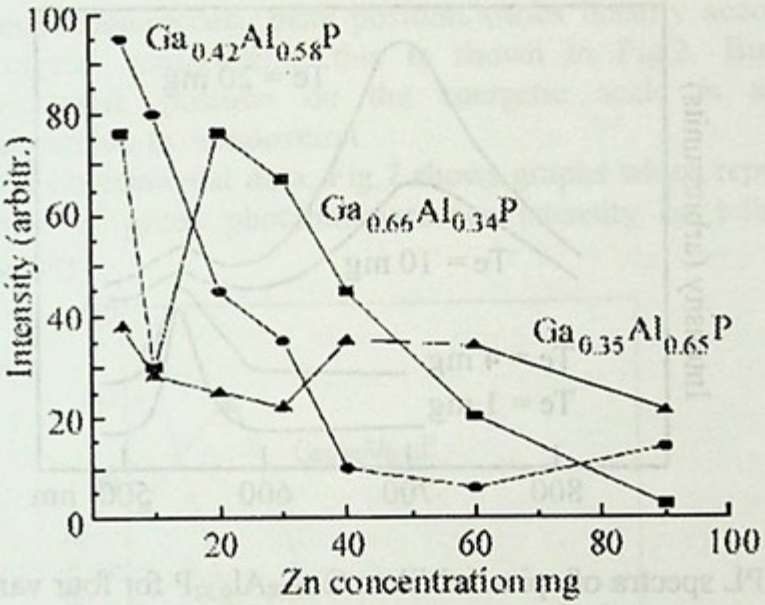

Fig.4. Dependence of intensity of the spectral peak characterizing the green photoluminescence for $Ga_xAl_{1-x}P$ on the concentration of zinc for the three different compositions of films

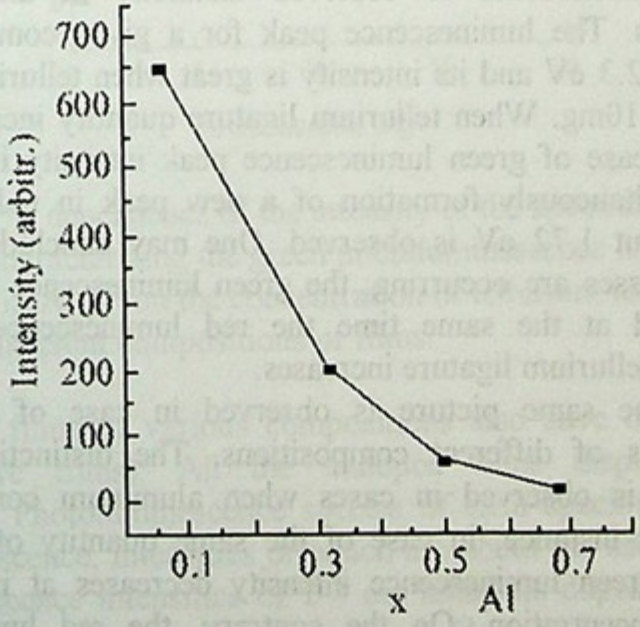

Fig.5. Dependence of the green luminescence intensity on aluminum quantity in the films $Ga_xAl_{1-x}P$

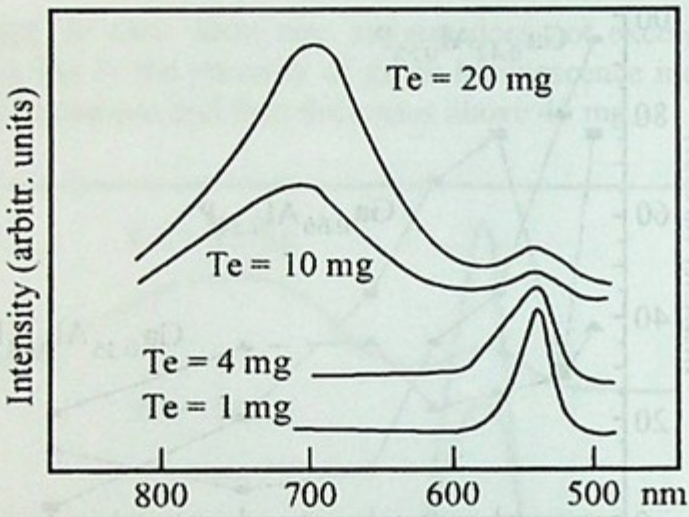

Fig.6. PL spectra of epitaxial films $Ga_{0,68}Al_{0,32}P$ for four various concentrations of tellurium; λ_L=488.0 nm

Fig.6 shows photoluminescence spectra for $Ga_{0.68}Al_{0.32}P$ composition when the ligature concentration varies according to tellurium quantity mentioned above. The spectra show clearly that the green luminescence is observed distinctly at all tellurium concentrations. The luminescence peak for a given composition is situated near 2.3 eV and its intensity is great when tellurium doping occurs up to 10mg. When tellurium ligature quantity increases (10, 20 mg), decrease of green luminescence peak intensity is observed clearly. Simultaneously formation of a new peak in red region of spectrum about 1.72 eV is observed. One may conclude that two parallel processes are occurring: the green luminescence disappears gradually and at the same time the red luminescence is being originated as tellurium ligature increases.

Almost the same picture is observed in case of two other epitaxial films of different compositions. The distinction among compositions is observed in cases when aluminum concentration increases. For instance, in case of the same quantity of tellurium ligature the green luminescence intensity decreases at increase of aluminum concentration. On the contrary, the red luminescence becomes more distinct for large compositions of aluminum.

The green luminescence peak position varies linearly according to mixed crystal composition; this is shown in Fig.2. But red luminescence peak position on the energetic scale is almost invariable according to composition.

Based on experimental data, Fig.7 shows graphs which represent a dependence of green photoluminescence intensity on tellurium ligature quantity.

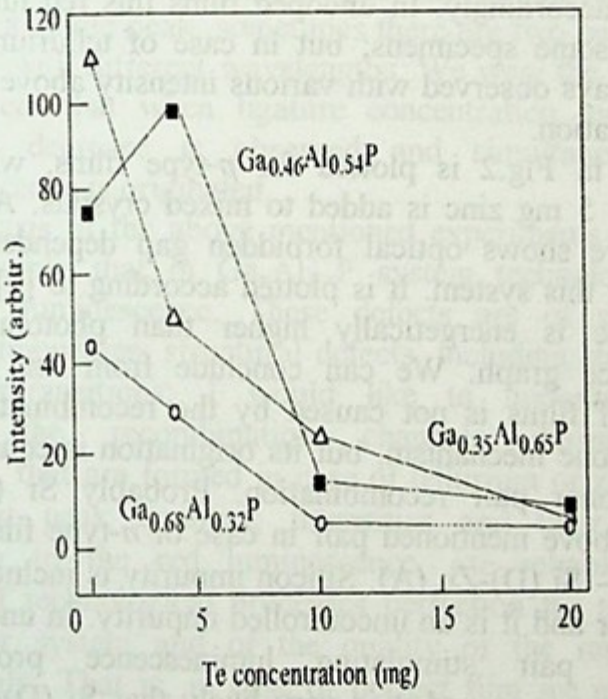

Fig.7. The dependence of the intensity of the spectral peak characterizing the green photoluminescence for $Ga_xAl_{1-x}P$ on the concentration of tellurium for the three different compositions of films

Undoped films of various compositions also have been studied (about twelve films). All the undoped films display electric conductivity. Photoluminescence spectra of each specimen give the green luminescence, intensities of which are about the same as green photoluminescence intensities of 1-4 mg tellurium-doped films. The red luminescence is noted only in some films and as in case of tellurium-doped films, the green luminescence attenuation process

in undoped films proceeds simultaneously with the red luminescence origination.

As to red luminescence peaks, their energetic position almost does not change with mixed crystal composition change. It must be noted that long wave luminescence peaks in undoped, tellurium-doped and zinc-doped films are arranged at various wavelengths. Partially these are 1.76 eV, 1.797-1.72 eV and 1.81-1.97 eV in energetic units accordingly. In undoped films this red luminescence is observed in some specimens; but in case of tellurium and zinc doping it is always observed with various intensity above carriers of certain concentration.

The graph in Fig.2 is plotted for *p*-type films, when during epitaxy process 5 mg zinc is added to mixed crystals. At the same time this Figure shows optical forbidden gap dependence on the composition for this system. It is plotted according to [2]. Evidently this dependence is energetically higher than photoluminescence peak dependence graph. We can conclude from this that green luminescence of films is not caused by the recombination of free carriers, zone-zone mechanism, but its origination is connected with the acceptor-donor pair recombination. Probably Si (A)-Te (D) serves as the above mentioned pair in case of *n*-type films while in case of *p*-type – Si (D)-Zn (A). Silicon impurity is included in films from the reactor and it is an uncontrolled impurity. In undoped films donor-acceptor pair stimulating luminescence probably are uncontrolled impurities and it is very likely that Si (D)-C (A) pair plays that part.

It is more complicated to explain the mechanisms causing red luminescence. There are different opinions. Some consider recombination radiation on Si (D)-Si (A) as a red luminescence mechanism. According to other's opinion the luminescence cannot be produced by donor-acceptor pair recombination and they consider a possible mechanism causing red luminescence, defects near heterotransition region, which are produced because of distinction between GaP and AlP lattices (before they were thought identical due to incorrect measurement).

As we partially mentioned above, on the basis of our experiments we have not detected red luminescence in films of some composition, type and containing certain carrier concentration,

whereas the green luminescence of great intensity is observed easily; moreover, we were the first to study photoluminescence dependence on carrier concentration in $Ga_{1-x}Al_xP$ system and to reveal that when electron or hole concentration is changed in this system by tellurium or zinc-doping, after a certain concentration in both cases the green luminescence slowly decreases until saturation of a certain level and simultaneously the red luminescence is originated. It should be noted that in films of a certain composition the red luminescence is presented by a single peak, sometimes there are two peaks of the red luminescence with different wavelengths. We were the first to reveal for this system that when ligature concentration increases green luminescence decrease is observed and simultaneously a red photoluminescence is originated.

On the basis of the above mentioned experiments and facts we can say certainly that in $Ga_xAl_{1-x}P$ system technological defects cause a red luminescence. These defects are of several types: uncontrolled impurities; structural defects, including stresses formed during heterotransitions; I would like to underline the third mechanism, the recombination channels during the red luminescence, that are formed in case of tellurium or zinc-doping. It is clear, that peak quantity, intensities and their half widths corresponding to the red luminescence, are reliable and exact parameters of technological processes perfection for the mentioned semiconductor system and of the quality of the resultant films, correspondingly. That is, in case of perfect film we must not have the red luminescence; and then the green luminescence achieves maximum. The fact proving nonexistence of composition gradient through the total thickness of the film will be minimal magnitude of the green luminescence peak halfwidth.

Thus we have showed directly that explanation of the red luminescence by defects formed due to the incompatibility of two different lattices is wrong and it is necessary to account those recombination channels which are formed from deeper impurity levels and which are connected to specially introduced zinc or tellurium acceptor or donor levels, correspondingly.

As the films under investigation were synthesized on GaP substrate, we consider it reasonable to eliminate the version according to which the red luminescence we had revealed in ternary

epitaxial films, was generated from GaP. It is known that GaP is characterized by luminescence in red and yellow areas according to the impurity included in it. Fig.8 shows PL spectra excited by 488.0 nm wavelength for S-doped, Te-doped and Zn-doped GaP. Table1 shows wavelengths of maxima corresponding to wide bands characterizing the PL. The wavelengths of maximums corresponding to red luminescence bands characterizing the films $Ga_xAl_{1-x}P$ are presented in the same Table. It is seen from the Table that the red luminescence of substrate and films are at different wavelengths. The fact proves that the red PL observed in films characterizes the films $Ga_xAl_{1-x}P$.

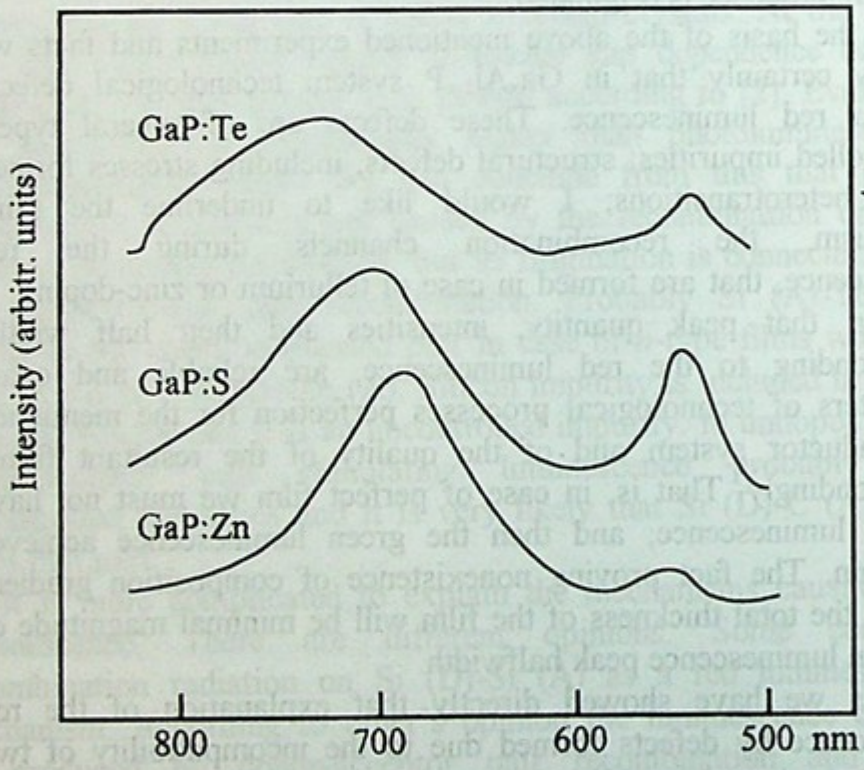

Fig.8. PL spectra with 488.0 nm excitation for zinc-, tellurium- and sulfur–doped GaP

REFERENCES

1. S. V. Gotoshia. Bulletin of the Georgian Academy of Sciences, **159**, 1999, 241.
2. H. Sonomura, T. Nanmori, T. Miyauchi Appl. Phys. Lett., **24**, 1974, 77.

Georgian Academy of Sciences
Institute of Inorganic Chemistry
and Electrochemistry

ს. გოთოშია

სხვადასხვა კონცენტრაციის ცინკითა და ტელურით ლეგირებული ეპიტაქსიალური ფირების $Ga_xAl_{1-x}P$ ფოტოლუმინესცენცია

დასკვნა

ეპიტაქსიალურ ფირებში $Ga_xAl_{1-x}P$ აქამდე არ იყო შესწავლილი დონორული თუ აკცეპტორული მინარევების კონცენტრაციული დამოკიდებულება ამ ფირების მახასიათებელ ფლ-იის სპექტრებთან. ამ შრომაში პირველად ჩვენ შევისწავლეთ აკცეპტორული ცინკისა და დონორული ტელურის კონცენტრაციული ზეგავლენა სამი სხვადსხვა შემადგენლობის $Ga_xAl_{1-x}P$ ფირების ფლ-იის სპექტრებზე. აღმოვაჩინეთ, რომ როდესაც ცინკისა თუ ტელურის ლიგატურის კონცენტრაციები იზრდება, შესამჩნევად ეცემა ლუმინესცენციის ინტენსიობა სპექტრის მწვანე უბანში და ამავე დროს ღვივდება წითელი ლუმინესცენცია. შევისწავლეთ აგრეთვე არალეგირებული ფირებიც. ასეთი ფირებისა და ლეგირებული ფირების ფლ-იის სპექტრების შედარებით მივედით დასკვნამდე, რომ თუ მწვანე ფლ-იის გამომწვევი მექანიზმია რეკომბინაცია დონორულ-აკცეპტორულ წყვილებზე, წითელი ლუმინესცენცია ძირითადად წარმოქმნილია ტექნოლოგიური დეფექტებით; ამავე დროს მიზანშეწონილია, გავითვალისწინოთ ცინკითა და ტელურით წარმოქმნილი სხვა რეკომბინაციული არხებიც.

THE USE OF LASER RAMAN SPECTROSCOPY FOR STUDY SEMICONDUCTOR FUNDAMENTAL PROPERTIES AND DIAGNOSTIC ANALYTICAL METHOD

S. Gotoshia

Accepted for publication November, 2004

ABSTRACT. In the present paper the use of a new direction-laser Raman spectroscopy first introduced in Georgia by the author for the purpose of studying semiconductor materials' fundamental properties is discussed. The importance of this direction and future trends of using it in other sciences is given in brief as well. The history and elements of theoretical principles are discussed shortly. The dynamics of technical evolution of Raman spectroscopy from early prismatic spectrometers with excitation of mercury lamps to modern laser Raman systems is given in chronological order. Within the limits of confined volume of the present paper I tried as far as possible to draw a clear picture of a single, double, triple Raman spectrometers and the function of systems and accessory combinations concerned with them; of advantage and expediency of their use in the various fields of scientific research. One of laser Raman systems constructed first by the author in Georgia, on which the experimental material has been performed is discussed in details. In the following two chapters the examples of using laser Raman spectroscopy in fields of studying and analyzing of semiconductor fundamental properties discussed in short are as follows: study of behavior of solid mixed semiconductors $ZnSe_xTe_{1-x}$, $GaAs_xP_{1-x}$; identification and quantitative analysis of ternary semiconductors GaAsP and GaAlAs synthesized during ion implantation of GaP and GaAs surfaces with phosphorous and aluminum.

The invention of lasers, especially in visible area of spectrum, gave such a powerful incentive to renascence of Raman effect that it is difficult to find nowadays an advanced scientific center, which would not use laser Raman spectroscopy (LRS) in the field of investigation or analysis. For biologists and chemists this method has the same

significance as infrared spectroscopy and even more informative in some cases. This time we consider the role of Raman spectroscopy in some areas of semiconductor study and only slightly touch upon an importance of using this method in chemical, biological, pharmaceutical and medical areas. Examples of using LRS in semiconductors will be presented in the given work on the basis of original works of the author.

When radiation passes through a transparent material, some part of the beam is scattered in all directions in this material. In 1928 the Indian physicist Raman revealed that the abovementioned part of scattered light differs from an incident beam. The mentioned part includes radiation of the wavelengths, which differ from incident wavelengths of excitation radiation. This shift of wavelengths depends on the structure of scattering molecule.

Today the theory of Raman scattering (RS) has been fully formed. It is stated that at RS the mechanism causing shifted wavelengths is the very quantum energetic levels as those at infrared (IR) absorption. That is the difference between excitation wavelength and those of scattered light corresponds to middle infrared area. Indeed, to compare RS and IR spectra for the same material, one can see similarity or identity. In brief, in IR spectroscopy those vibrations are active, whose molecular dipole moments alter according to vibrations; at RS those vibrations are active (becomes apparent in spectra), whose molecular polarization alters according to vibrations. Thus, RS and IR spectroscopy are not rivals, but mutually complementary from the point of view of information.

From the view of utilization in some cases to IR spectroscopy must be given priority, but sometimes RS is indispensable; thus, for example, when studying aqueous solutions. For RS experiments glass or quartz cuvettes are used; while in IR spectroscopy hygroscopic cuvettes made from alkali-haloid compounds are used, which are instable towards water and aggressive solutions. Thus, RS is of great importance in studying of biological and inorganic compounds and water pollutant objects. We shall not speak any more of more specific advantages of RS. We shall mention only a circumstance that sometimes hampers the use of RS. This is photoluminescence (PL) caused by impurities; though sometimes it is possible to avoid luminescence using corresponding experimental techniques.

A BRIEF THEORY OF RAMAN SCATTERING

To receive Raman spectrum (RS) the matter under study must be irradiated by laser intense monochromatic wavelength in ultraviolet, visible or near infrared regions of spectrum. During irradiation the scattered radiation must be measured by a corresponding spectrometer by a certain angle towards incident laser beam. In most cases this angle is 90°. In general Raman lines make 0.001% of intensity of excitation laser spectral line; as a result, detection and measurement of Raman spectrum is a complicated problem. This is no concern of resonance Raman scattering (RRS), Raman scattering enhanced by surface (SERS), resonance Raman scattering enhanced by surface (SERRS) and other effects of Raman scattering, which are characterized by much more powerful intensities. It should be underlined that today SERS is one of the powerful analytical methods for biologists, electrochemists and ecologists.

The scattered radiation is of three kinds, namely, Stokes, anti-Stokes and Relay radiations. The wavelength of the latter is the same as excitation laser wavelength and its intensity is far greater than two others. For example, Fig.1 shows Raman scattering spectrum for organic solvent CCl_4. To excite the spectrum, argon laser radiation of wavelength $\lambda_0 = 488.0$ nm, i.e. of wave number $\nu_0 = 20492$ sm^{-1} was utilized. In Fig.1 figures written above the peaks are Raman shifts calculated from the expression $\nu = (\nu_R - \nu_0)$ cm^{-1}. The Figure shows that a Raman spectrum is an aggregate of spectral lines positioned symmetrically to the right and left of the spectral line of an excitation laser. Anti-Stokes radiation is characterized by greater wave number than wave number of excitation line, while Stokes radiation peaks' wave numbers are less than that of excitation laser. It should be noted that Raman shift is identical for Stokes and anti-Stokes radiations. This shift is of the same value despite the fact with which laser wave number is being excited a RS spectrum of a given compound. Hence, Raman displacements of CCl_4 presented in the picture will be of the same value in spite of the fact, which laser -argon, krypton, YAG-Nd or helium-neon, will be used to record spectra.

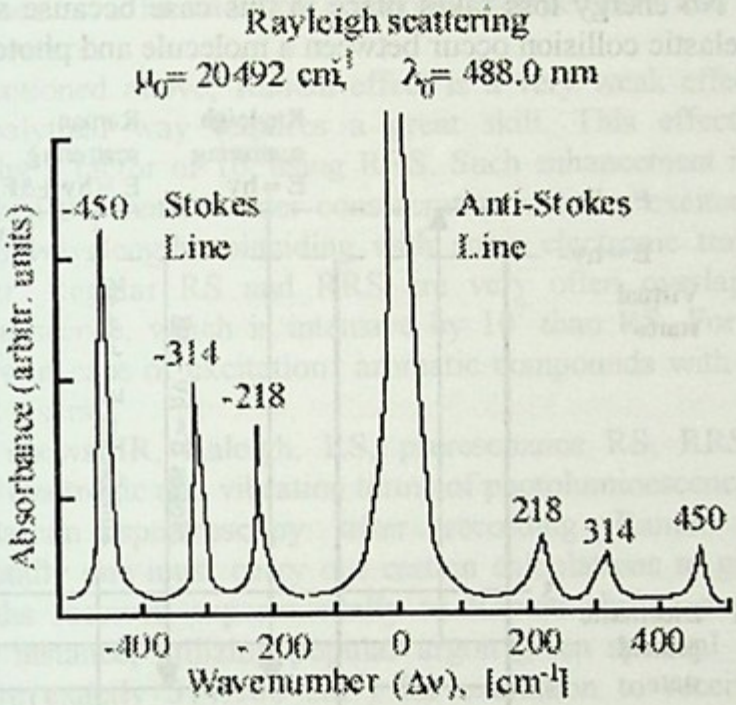

Fig.1. Raman scattering; relaxation spectrum of CCl_4

Anti-Stokes radiation is less in intensity in comparison with Stokes scattering and in practice in general only Stokes scattering is used while recording spectra. As for spectrum abscissa where Raman shifts are plotted, simply cm^{-1} are written instead of wave number. The sign minus is not written in case of Stokes scattering.

In usual or normal Raman spectroscopy excitation spectrally of a substance under investigation occurs with such a wavelength of laser radiation, which is far from any absorption peak of this substance.

Fig.2 shows Rayleigh and Raman (Stokes, anti-Stokes) scattering mechanism: the first thick arrow shows energy change in a molecule when it interacts with photons of an incident beam. Molecule energy increase is equal to photon energy $h\nu$. The second narrow arrow shows the change, which would be in case if a molecule met radiation when being on the first vibration level of the main electron state (as a rule only a few part of molecules are in such position). The two arrows in the middle part of the diagram show the changes causing Raleigh

scattering. No energy loss takes place in this case because at Raleigh scattering elastic collision occur between a molecule and photon.

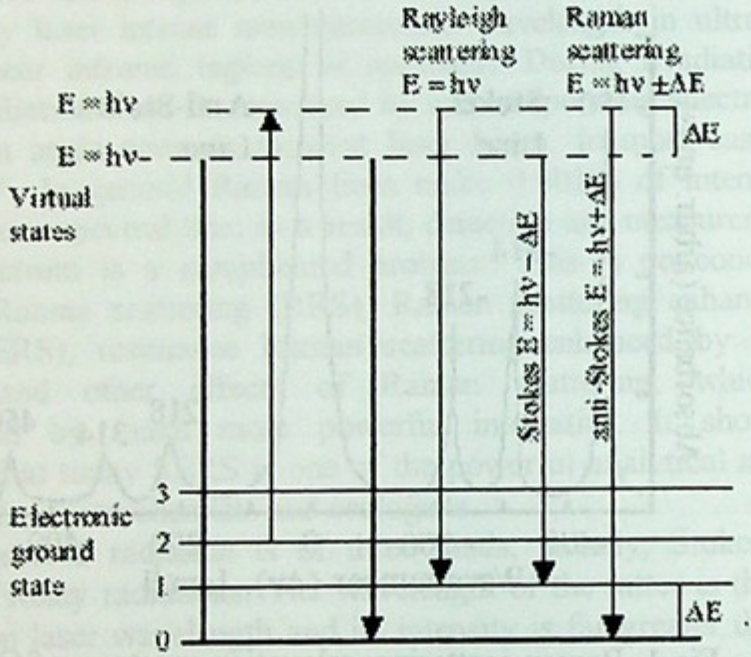

Fig.2. Relaxation of excited molecules and atoms

Energy change stimulating Stokes and anti-Stokes radiations as a result of inelastic scattering is presented on the right side of the scheme. The two latter radiations differ from Rayleigh scattering in frequencies corresponding to $+\Delta E$ energies, which are the first vibration level of the main electron state (if molecule bonds are active in IR region, then the energy absorbed by them will be $+\Delta E$. Thus, Raman shift and IR-absorption peak frequencies will be the same).

The relative population of these two energy states is such, that Stokes scattering dominates over anti-Stokes. Besides, Rayleigh scattering is more probable than RS because energy transfer to molecule in the ground state and reemission by returning the same molecule to the ground state is more probable process. It should be noted that at room temperature the intensity of anti-Stokes spectral lines is weaker than that of Stokes. The reason is that in these circumstances only a few parts of molecules are in the first excited vibration state. The ratio of intensities of Stokes and anti-Stokes

spectral lines is a function of compound temperature and increases with temperature.

As mentioned above, Raman effect is a very weak effect and its use in analytical way requires a great skill. This effect may be enhanced by a factor of 10^3 using RRS. Such enhancement is attained in case when the matter under consideration is being excited by laser beam with wavelength coinciding with some electronic transition of this matter. Regular RS and RRS are very often overlapped with photoluminescence, which is intensive by 10^7 than RS. For example, this occurs in case of excitation aromatic compounds with visible or ultraviolet lasers.

Fig.3 shows IR, Raleigh, RS, preresonance RS, RRS and the scheme of electronic and vibration terms of photoluminescence.

In Raman spectroscopy after recording Raman spectrum experimentally one must carry out certain calculations to go on from wavelengths received experimentally to Raman shifts expressed in cm^{-1}. For instance, utilizing popular argon green spectral line 514.5 cm^{-1} (more exactly 514.308 cm^{-1}) for excitation to receive Raman spectrum, wave number is calculated as follows:

$$\nu = 1/\lambda_0[nm] \times 10^7[nm]/[sm] = 1/514.308 \times 10^7 = 19444\ sm^{-1}$$

In this concrete case Raleigh scattering will take place at the same frequency, which has the green line of excitation argon and this frequency afterwards will be subtracted from all the scattered frequency, which will be fixed experimentally on the Stokes or anti-Stokes side. One receives Raman spectrum with the abscess expressed in cm^{-1}, and ordinate-in scattered light intensities.

Reverse transfer is possible too; for example, if Raman peak is observed at 3000 cm^{-1}, the corresponding wavelength is calculated as follows:

$$\lambda_{RS} = 1/\nu_0 - \nu_{RS}[cm^{-1}] \times E^7[nm]/[cm] = 1/19000 - 3000 \times E10^7 = 608.12\ nm$$

Thus excitation with green spectral line stimulates reemission of yellow spectral line in the result of Stokes scattering.

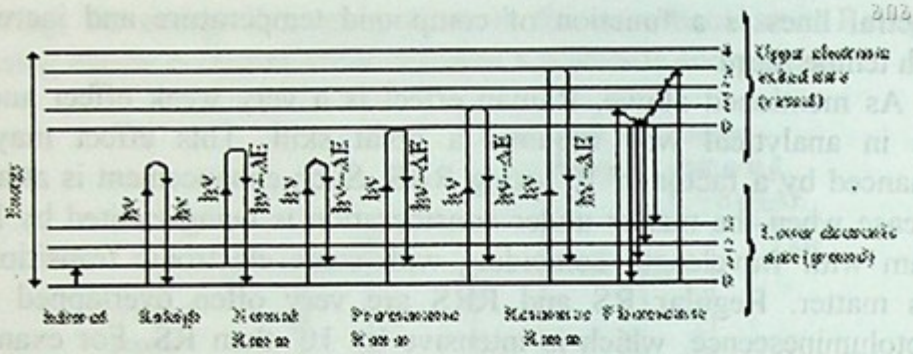

Fig.3. Relaxation patterns

It should be noted that those calculations are needed especially for home made, lab-type laser Raman-systems, as my laser-systems are. Modern expensive Raman spectrometers produced by foreign firms need not such manipulations due to complete automation and computerization.

EXPERIMENTAL LASER RAMAN SYSTEMS FOR RECORDING RAMAN SPECTRA FOR SOLIDS AND LIQUIDS

Nowadays there are foreign firms in the world, which put on sale laser Raman spectrometers of different category and function. These spectrometers are of different classes and their analytical or fundamental research possibilities are different. Recently almost all the firms produced Raman spectrometers, the price of which was about US $100000. There are today (and were) far expensive spectrometers. Just because of such a high price of those laser systems a lot of laboratories and researchers had to give up this method despite wish and necessity. Recently some firms in the world began to produce cheaper laser Raman spectrometers, especially for purpose of physical-chemical-pharmaceutical analyses. Such Raman systems cost about US $20000-30000. Perhaps these prices too are not available for most researchers, especially from such countries as Georgia.

A lot of researchers chose independent way to solve this problem - constructed a lab-type cheaper laser Raman-systems with semi-manufactured blocks.

According to the development of laser Raman-spectroscopy in Georgia and according to own scientific interests we too chose the same way.

Depending on the fact which semi-manufacture nomenclature is available it is possible to construct laser Raman-systems, which enables one to solve the scientific and analytical problems enclosed in the list of theoretical and practical ability of constructed laser Raman system.

We would like to share the experience with persons interested in, which they can use in their practical activity in case when their scientific or analytical activity demands using laser Raman spectroscopy and their financial means are not sufficient to purchase expensive laser Raman systems. It is necessary to add here that the same Raman-systems are fit for photoluminescence study too.

Any laser Raman-system consists of three main parts: exciting laser, single, double or triple spectrometer; sensitive signal detector with amplifier and registration systems. A container for specimen under consideration must be added to this complex, which gives us the possibility to study a specimen by various configurational scheme of Raman scattering. Besides these basic blocks, Raman spectrometer contains other accessories: optical, mechanical, cryogenic and other blocks or details.

Raman spectrometers depending on the basic principles of their construction are divided into some categories, which show the dynamics of LRS evolution. We do not touch on spectrometers with prisms as dispersion elements. They belong to history now. Though a good experimenter is able to use them to solve certain problems. The most widespread and integrated in laser epoch today is a double spectrometer with diffraction gratings, which are cut on lathe (replicas). The following stage of evolution is setting holographic gratings on double dispersion spectrometers; this gave experimenters opportunity to decrease sharply the quantity of stray light in spectrometers and get free from grating ghosts. Simultaneously the coefficient of light transfer decreased lightly in such spectrometers. The best triumph of Raman spectroscopy technique is considered thriple dispersion spectrometer with cut or holographic gratings set. These spectrometers are of specific importance to study such fine effects in semiconductors or in all other materials, which need to

resolve spectral fine structure. After some time Raman spectrometer with Fourier Transform (FT-RS), semiconductor diode laser or YAG-Nd laser excitation was developed. This type of spectrometers has made revolution both in analytical and fundamental research area. The reason is that it is possible to record the spectra of such materials by this system, Raman spectra of which were impossible to record or were recorded by specially elaborated technique as these compounds, for example, aromatic compounds (petroleum, kerosene), dyes, impurities in semiconductors and etc., are luminescing strongly. It should be mentioned that in the former Soviet Union, the author of the given paper constructed the infrared Raman spectrometer with garnet laser excitation for the first time but on the basis of double diffraction (dispersion) spectrometer as early as in 1970 in Moscow Institute of Physics (FIAN) in collaboration with the laboratory of Academician Prokhorov. It was not a FT-RS but we have constructed it just to study luminescing narrowband semiconductors GaAs, InP, CdTe, narrowband mixed semiconductors obtained on basis of the mentioned semiconductors and impurities in semiconductors. In the last period from the time that holographic super notch filters' production achieved the highest level, laser Raman systems with set of single diffraction spectrometer and holographic notch filters sat on sale in international spectroscopic market. Such Raman systems are far small in volume, light, comparatively cheap and for fulfillment of certain tasks have some advantages even over a triple Raman spectrometer. In this system the notch filter serves as the first stage monochromator and in case of a good super notch filter it is possible to approach the exciting laser wavelength by $100cm^{-1}$. In triple spectrometer this value is about 10 cm^{-1}, but in turn, the coefficient of light transfer is far great for a single spectrometer. A novelty in Raman spectroscopy, which is conveyed by the use of CCD detectors as detectors should be underlined specially. In such complex instead of a spectrometer a spectrograph is used and laser Raman system becomes multi-channel device. With such configuration sensitivity increases many times, which has resolving practical importance in analytical sciences.

So, the criteria for purchase or construction a spectrometer type is based on the target of the task. There is a better variant too: if one has 1500000 (perhaps it will not suffice), it is possible to purchase several Raman systems of various types and then purposes of a problem will

not be confined. These are the basic types of Raman systems, which exist nowadays. We do not touch on a lot of branches and details. Now we present a model and a brief description of one of the laser Raman systems, which we have constructed first in Georgia and carried out investigation of some semiconductor materials.

Table 1

The laser wavelength, corresponding to quantum energies and types used by us

Lasers	Laser Type	Wavelength (nm)	Energy (eV)
He-Ne	gas	632.8	1.958
Argon ion	gas	514.5	2.408
		501.7	2.469
		496.5	2.495
		488.0	2.539
		476.5	2.600
		457.9	2.705
Cripton ion	gas	647.1	1.914
		568.2	2.180
		530.9	2.33
		520.8	2.379
		476.2	2.601
He-Cd	gas	441.7	2.805
Copper	metal vapour	510.6	2.428
		578.2	2.144
YAG:Nd	solid	1064.0	1.17
Die	solution	540.0-690.0	2.296-1.797

Fig.4 shows the scheme of a laser Raman system constructed by us. The exciting source is argon, krypton, helium-neon, helium-cadmium, cuprum lasers. Those wavelength, which characterize the abovementioned lasers' radiation and we use for Raman spectra excitation, are given in Table 1. These lasers mainly are of standard, fabric production. At the same time we have also home made laboratory type lasers as follows: krypton and argon lasers. Argon and krypton lasers constructed by us have the following parameters: krypton laser radiation is single-mode with wavelengths 530.9, 568.2, 647.1 nm, integral power about two watt, with vertical polarization

radiation. Argon laser is characterized with the following parameters: single-mode, with wavelength of radiation 457.9, 476.5, 488.0 496.5, 501.7, 514.5 nm; at integral power about 3 Wt, vertically polarized radiation. Argon and krypton lasers of laboratory types constructed by us enable us to vary widely experimental conditions. This circumstance is promoted by the fact, that two high voltage rectifiers of laser active element and magnetic solenoid constructed by us work autonomicaly in current change mode.

To obtain spectra we use double diffraction spectrometer DFS-24, with diffraction replica 1200 str/mm. For these gratings the maximum concentration of light comes about on yellow region of spectra; therefore there are optimal conditions to receive Raman spectra for some of excitation wavelengths of lasers used by us, whereas for others there is a compromise situation.

To create optimal conditions for all the laser exçitation wavelengths we have constructed three various types of Raman spectrometers in correlation with radiation of lasers exciting the optical system. We are not going to speak of these systems.

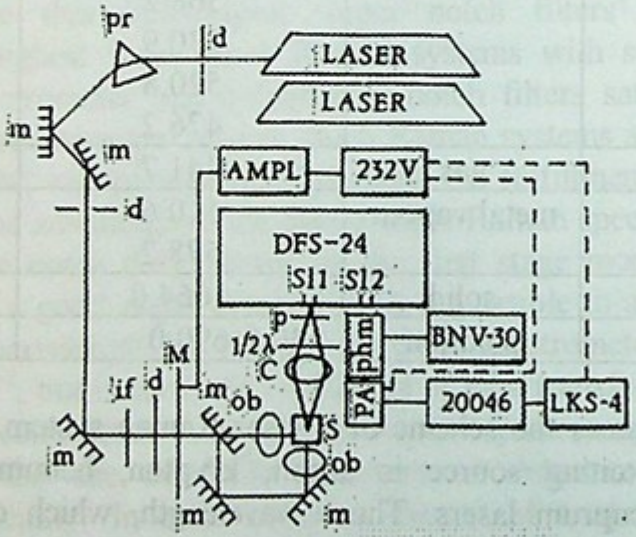

Fig.4. General scheme of home-made laser Raman-system constructed by us

Laser emission through diaphragm (d), prism (p), interference filter (if), mirrors (m) and objective (ob) is filtered from laser background, plasma lines; highly collimated monochromatic emission

in desired direction is formed according to planned scattering configuration focusing on the semiconductor (s) to be studied. Irradiation scattered in the semiconductor is collected by the condenser (c) and through the polarizator (p) is focused on the monochromator entrance slit (sl.1). Photoluminescence or Raman scattering signal from the exit slit (sl.2) falls on the photomultiplier (phm) and after amplifying and sorting photoluminescence or Raman scattering spectra are recorded by the recorder LKS-004. Detection and amplification signals of weak intensity of Raman scattering is done by two methods: a) synchronous detection-with the aid of modulator and lock-in-amplifier Uniphan 232B; or b) photon counting-with the aid of radiometer 20046.

In the visible area we use photomultiplier FEU-79 or FEU-136 with well-selected parameters. In case of need cathode of FEU-79 is cooled at about -100^0 C. Towards this purpose we have constructed low-temperature cryostats of three different types working on different principles. By cooling cathodes of FEU-79 in these cryostats we are able to increase noise to signal ratio nearly to eight which is of great importance when registering Raman-spectra.

Besides abovementioned laser Raman spectroscopy we have constructed low temperature cryostats of various types and construction, which give possibility to study PL and Raman spectra at nitrogen and helium temperatures both in fixed temperature and temperature change mode. These optical compact cryostats we have created especially for Raman spectroscopic investigations taking into consideration that in the process of RS measurements direction of excitation laser beam, crystallographic axis of specimen under investigation-semiconductor and collection angle of scattered radiation form differed configurations in various configuration schemes of measuring.

To study the effect of pressure having a uniaxial direction on Raman spectra of semiconductors and PL, we have constructed a special cryostat for our Raman systems, which works at nitrogen temperature.

Besides low temperature cryostats, we have constructed also a high temperature cryostat, which gives us the possibility to study semiconductors from 18^0C to 600^0C.

Thus, the Raman system we have constructed enables us to carry out large-scale fundamental research of solids (crystals, mixed solid solutions, amorphous, glass, pouders, small crystals, fine-dyspersated materials) and analytical works with very wide scale of spectral excitations, under influence of stress having a uniaxial direction and in the range of temperature from 10^0K to 300^0K. These investigations may be conducted both on transparent crystals and thin films.

It should be noted that the described system enables one to carry out investigations and analytical works in Raman spectroscopy on liquids as well, which chemists, biologists, pharmaceutics, medics, agricultural workers, geologists, etc are interested in.

In the following part of this paper the experimental material, which we have done on abovementioned Raman systems in some brunch of semiconductor study is discussed.

RAMAN SPECTROSCOPY OF MIXED SEMICONDUCTORS

Mixed crystals are one of basic materials of semiconductor microelectronic devices. For instance, light emitting diodes and laser diodes are being prepared on their basis. The main criteria of utilizing of such materials is that that all their physical chemical properties depends upon their composition; hence one can prepare devices with previously planned properties on their basis. The main property possibly is the dependence of forbidden band on composition.

The first mixed crystals complex we have studied is GaAsP from A^3B^5 group known in optoelectronic instrument making. As it is known, on the basis of this material light emitting diodes of a good quality in red, orange and yellow spectral ranges are being prepared. Laser diodes are prepared in the same manner. These materials were studied earlier by laser Raman spectroscopy [1]. In the mentioned paper these materials were investigated by volume excitation, with 632.8 nm of helium-neon laser and 106.0 nm of garnet laser radiations. It should be noted one of the most important methodical circumstances in Raman spectroscopy: when such semiconductor as GaAs (it is one of components of crystals under observation), is studied with RS, the spectrum of plazmon-phonon interaction is added to phonon spectrum. Plazmon influence on phonon spectrum is more when excitation is bulk and electroactive impurities are in great

quantity in semiconductors (the quantity of free electrons is great). We have studied three epitaxial films of various compositions, exactly such films, on the basis of which light emitting diodes are produced in the abovementioned three spectral ranges. Thus, concentration of electrons in these films is great, about 10^{19} cm^{-3} orders. Because of this we studied these films by surface reflection method with argon laser excitation with 488.0 nm radiation. In such experimental conditions we are far from interfering photoluminescence. Besides, as 488.0 nm radiation penetration skin-layer is small in mixed crystals under research, about 150.0 nm, plazmon influence on phonon spectrum is less. Thus, we have the possibility to study these crystals in natural conditions with relations to diagnostics and at the same time to decrease eminently or annihilate interfering factors, which are characterizing bulk excitation.

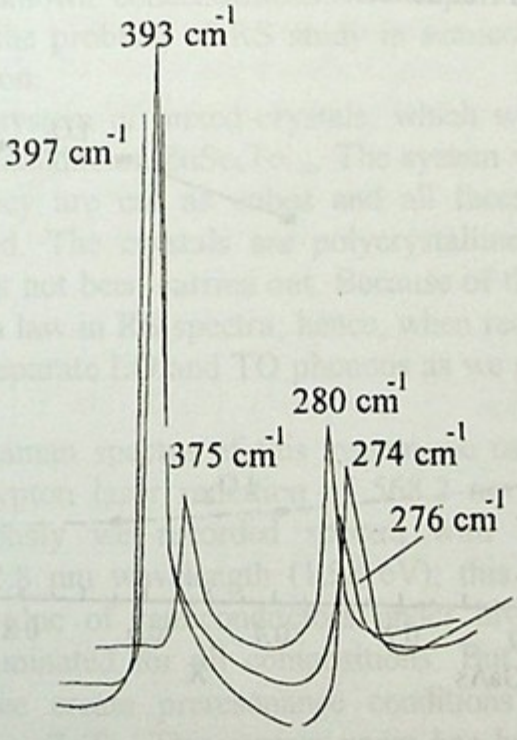

Fig.5. RS spectra of $GaAs_{0.6}P_{0.4}$, $GaAs_{0.35}P_{0.65}$ and $Ga\ As_{0.15}P_{0.85}$; $\lambda_L = 488.0$ nm

The mixed crystals $Ga_xAs_{1-x}P$, which have been studied, are epitaxial films. These films are grown epitaxially on GaP substrate of

(001) orientation. Fig.5 shows RS spectra of GaAs, $GaAs_{0.6}P_{0.4}$, $GaAs_{0.35}P_{0.65}$, Ga $As_{0.15}P_{0.85}$ and GaP. For excitation of these spectra we have used argon laser radiation of wavelength 488.0 nm.

All crystals under investigation are of cubic symmetry and belong to T_d point symmetry. Therefore, according to selection rules only LO phonons must be active in Raman spectra of the studied surface (001). The spectra in Fig.5 prove this. The figure shows that in Raman spectra of mixed films two categories of LO phonons are observed- LO_1 and LO_2 in contrast to GaAs and GaP. The first, LO_1 shows longitudinal vibrations of atoms of GaAs-like sublattice, and the second, LO_2 shows longitudinal vibrations of atoms of GaP-like sublattice. Table 3 shows the frequencies of observed phonons. On base of these data the schemes in Fig.6 are plotted, which show dependence of composition of this mixed semiconductor on longitudinal phonon frequencies.

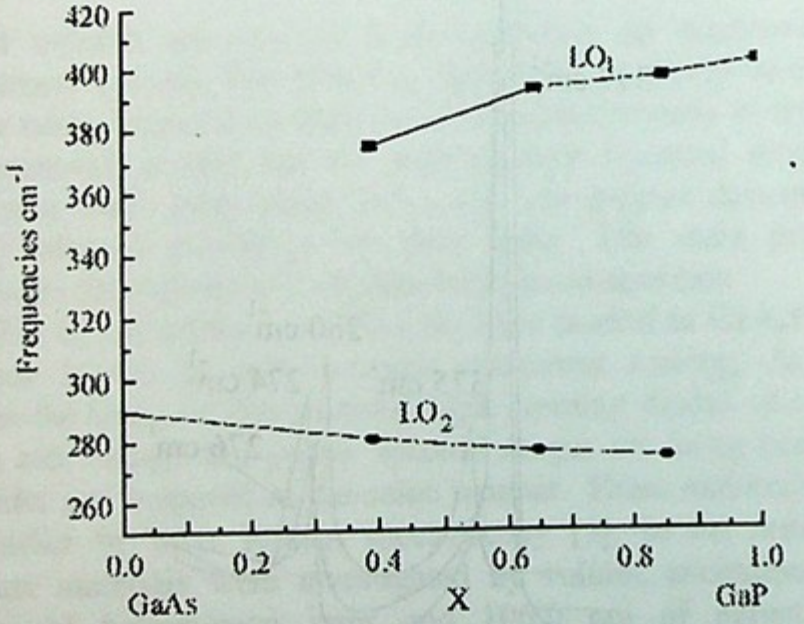

Fig.6. Dependence of composition x of mixed semiconductors $GaAs_xP_{1-x}$ on longitudinal phonon frequencies

Table 2

Semiconductors	LO_1 (cm^{-1})	LO_2 (cm^{-1})
GaP		402
$GaP_{0.85}As_{0.15}$	274	397
$GaP_{0.65}As_{0.35}$	276	393
$GaP_{0.39}As_{0.61}$	280	375
GaAs	290	

It is known that mixed crystals according to their behavior are divided into two classes [2]: single-mode behavior and two-mode behavior. The dependences presented in Fig.6 show that mixed crystal $GaAs_xP_{1-x}$ belongs to two-mode crystals. These graphics work for estimation of unknown concentrations. We shall illustrate this later, when we touch the problem of RS study in semiconductors modified by ion implantation.

The second system of mixed crystals, which we have studied, is A^2B^6 group semiconductor $ZnSe_xTe_{1-x}$. The system we have studied is bulk crystal. They are cut as cubes and all faces of the cube are optically polished. The crystals are polycrystalline and orienting of these crystals has not been carried out. Because of this it is impossible to hold forbidden law in RS spectra; hence, when recording spectra we are not able to separate LO and TO phonons as we did in the previous case.

To obtain Raman spectra of this system we used almost volume excitation of krypton laser radiation of 568.2 nm wavelength (2.18 eV). Simultaneously we recorded spectra with helium-neon laser radiation of 632.8 nm wavelength (1.98 eV); this is far away from forbidden gap value of semiconductors under investigation. In this case RRS is eliminated for all compositions. But when exciting by krypton laser we create preresonance conditions during recording spectrum for pure ZnTe. This system never has been investigated in such conditions. To clarify our argumentation, we present Fig.7, which shows the dependence of composition x of this system upon forbidden gap magnitude E_0 [3]. As it is seen, the dependence has a minimum. Because of this for this compositions krypton laser quantum energy 2.18 eV is more than forbidden band width for

compositions near minimum, while ZnTe and some compositions are fully transparent for this radiation. To create more equal conditions, for exciting the spectra we have used radiation wavelength of dye laser 589.8 nm (2.102 eV). Fig.8 shows two Raman spectra of ZnTe: one 632.8 nm and the second wavelength excitations 589.8 nm. The spectra show clearly the distinction: in spectra recorded in resonance conditions we were able to fix multiple 2LO phonons. One cannot attain this by increasing intensity of radiation of helium-neon laser or spectrometer sensibility, because revelation of multiple phonons lays in physical mechanism in this case. This mechanism is phonon cascade mechanism and its realization occurs when excitation laser quantum energy and semiconductor forbidden gap width achieve a certain ratio. At this time preresonance or resonance situation takes place, but it is impossible to detect this effect in all types of semiconductors. Fig.9 shows Raman spectra of mixed crystals we have studied; when excitation occurred by 589.8 nm wavelength of dye laser radiation. Table 3 shows the observed phonon frequencies. On the basis of these data we have plotted LO, TO and 2LO phonons' concentration dependence (Fig.10). The graphs differ diametrically from schemes discussed and studied at first. The schemes for the second system show that the system $ZnTe_xTe_{1-x}$ belongs to single-mode behavior crystals.

Table 3

Semiconductor composition x	LO (cm^{-1})	TO (cm^{-1})	2LO (cm^{-1})
ZnTe	203	170.7	409.5
$ZnTe_{0.9}Se_{0.1}$	207.3	173.5	415
$ZnTe_{0.8}Se_{0.2}$	210	176	423.2
$ZnTe_{0.7}Se_{0.3}$	215.7	177	436.9
$ZnTe_{0.6}Se_{0.4}$	221.3	179.7	450.5
ZnSe	250	205	

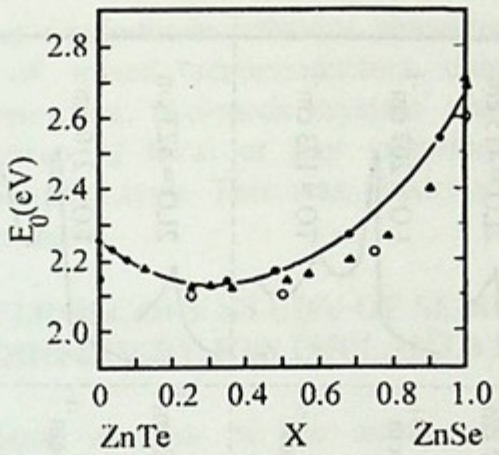

Fig.7. Lowest band gap E_0 of $ZnSe_xTe_{1-x}$ as a function of x at room temperature

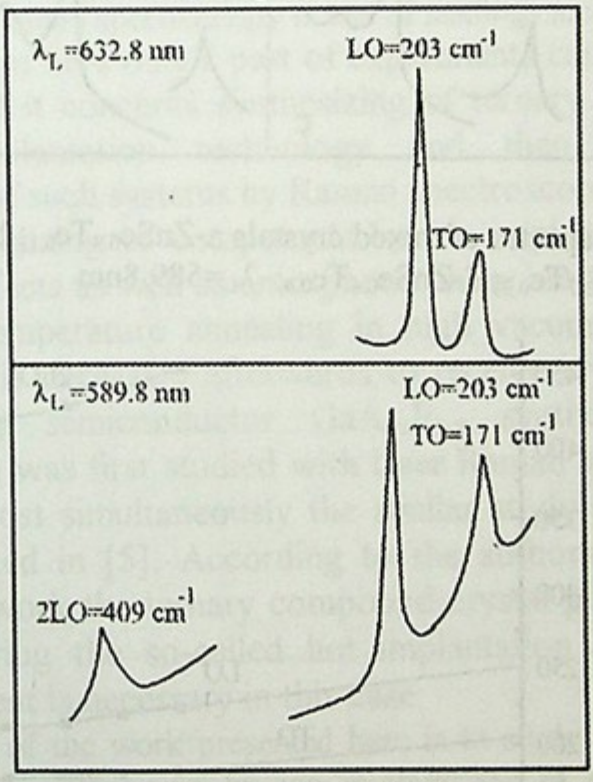

Fig.8. Raman spectra of ZnTe a-λ = 632.8nm and b-λ = 589.8nm excitation

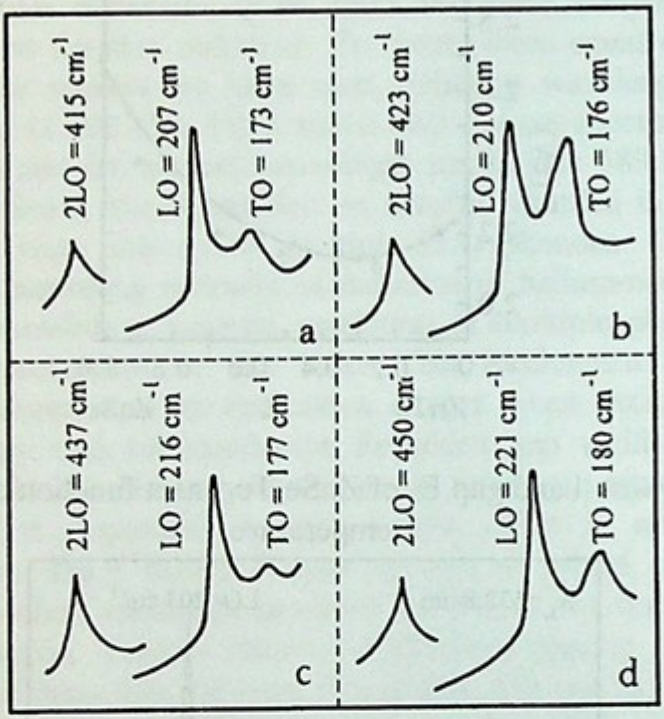

Fig.9. Raman spectra of mixed crystals a-$ZnSe_{0.9}Te_{0.1}$; b-$ZnSe_{0.8}Te_{0.2}$; c-$ZnSe_{0.7}Te_{0.3}$; d-$ZnSe_{0.6}Te_{0.4}$; λ_L=589.8nm

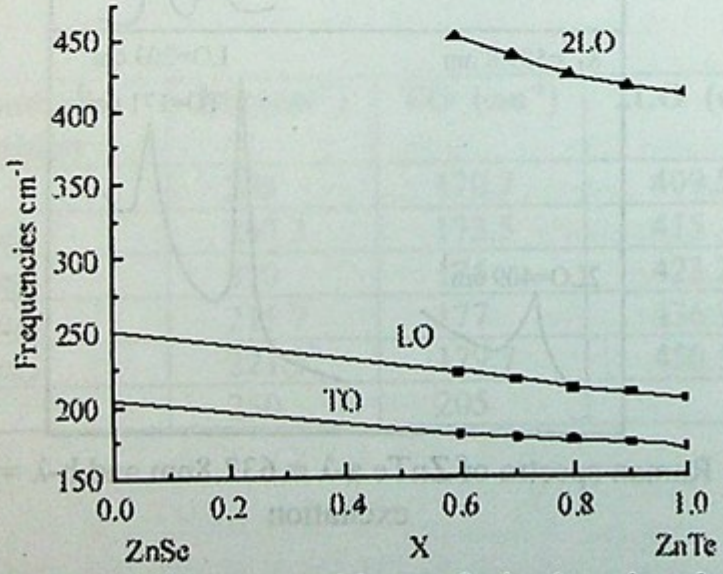

Fig.10. Dependence of composition x of mixed semiconductors $ZnSe_xTe_{1-x}$ on LO, TO and 2LO phonon frequencies

In this case at single-mode behavior characteristic phonons LO, TO and 2LO of mixed semiconductors change monotonously according to composition; two-mode crystals' characteristic property consists in formation of local or gap vibrations and therefore in graphical form of other type. This was illustrated in the process of study of the first system.

RAMAN SPECTROSCOPY STUDY OF SEMICONDUCTORS MODIFIED BY ION IMPLANTATION

Ion implantation is one of the actual methods of modern semiconductor complex micro technology; at present the fabrication of a device occurs rare without this method. Nowadays a lot of physical diagnostics are elaborated for monitoring of ion implanted surfaces and Raman spectroscopy is one of leadings among them.

We present here only a part of experiments carried out in this direction and it concerns synthesizing of ternary mixed crystals by ion implantation technology and then identification-diagnostics of such systems by Raman spectroscopy.

At synthesizing of compounds by ion implantation a lot of radiation defects as well as amorphous phase are formed. That is why high temperature annealing in high vacuum or inert gas atmosphere is necessary afterwards to receive crystalline phase. The ternary semiconductor $GaAs_xP_{1-x}$ synthesized by ion implantation was first studied with laser Raman spectroscopy by us [4]. Almost simultaneously the similar study of the question was presented in [5]. According to the authors of the above-mentioned work the ternary compound crystal phase is obtained directly during the so-called hot implantation and no further heat treatment is necessary in this case.

The aim of the work presented here is to study the technological conditions of synthesizing by ion implantation of crystalline mixed ternary semiconductors $GaAs_xP_{1-x}$ and $Ga_xAl_{1-x}As$ using laser RS.

We implanted polish surfaces of GaAs with 70 KeV phosphorous and 100 KeV aluminum ions, with 1.8×10^{17} ion/cm^2 and 2.8×10^{16} ion/cm^2 doses. The orientations of surfaces were (111) in the first case and (001) in the second relatively. GaAs substrate was located at the

room temperature at the time of phosphorous implantation and at 400° C at the time of aluminum ion implantation.

As we showed in [6], single-phase amorphous ternary semiconductor α–$GaAs_xP_{1-x}$ is formed when implanting GaAs by phosphorous at room temperature. The amorphous phase is formed during the hot implantation too, when implanting at 450°C. Fig.11 shows Raman-spectra of standard GaAs of (111) orientation and of α-GaAsP formed by phosphorous implantation. According to the selection rules LO phonon characteristic peak is seen in the Raman-spectra of the crystalline GaAs at 290 cm^{-1} frequency and TO phonon characteristic peak at 268 cm^{-1}. While amorphous compound Raman-spectra are characterized by two wide bands: one corresponds to Ga-As bond vibration and the second-to Ga-P bond vibration.

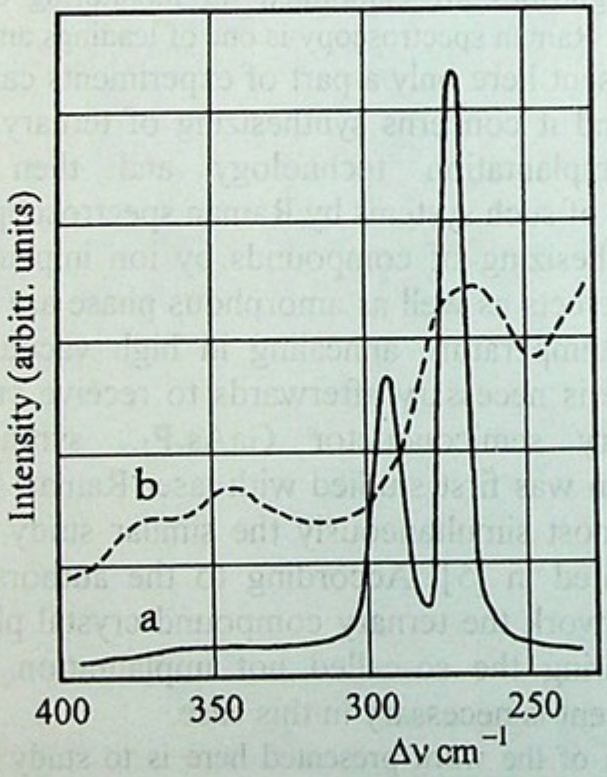

Fig.11. Raman spectra of standard GaAs of (111) orientation (a) and of α-GaAsP (b) formed by phosphorous implantation

We used the thermal annealing in the high vacuum to recover the crystal structure. Before annealing we coated the surface of implanted GaAs with about 1000 A thickness protective layer of SiO_2 to avoid the phosphorous and arsenic evaporation from the crystalline surface. We carried out annealing at 500, 700 and 850^0 C during an hour. The general picture of Raman spectra recorded after annealing at the above temperatures, is represented in Fig.12. It is clearly seen that as a result of annealing, α-$GaAs_xP_{1-x}$ transforms gradually into a crystalline state and at the 850° C nearly entirely recovering of crystalline phase takes place, although a small amount of radiation defects is still felt. This fact is confirmed by narrowing of wide bands typical for amorphous phase with rising of annealing temperature and formation of new peaks at 370 cm^{-1} and 345 cm^{-1} frequencies, respectively. We referred these peaks to LO_2 and TO_2 phonons vibration of ternary compound GaAsP.

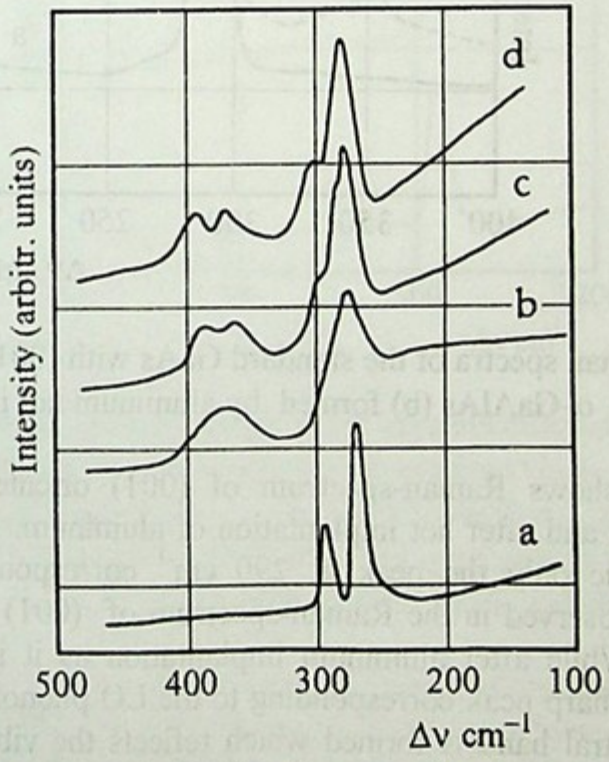

Fig.12. Raman spectra indicating the crystallization process of α-GaAsP: a-the spectrum of the standard GaAs with orientation (111); b, c, d-the spectra of crystals received after quenching at 500, 700, 850^{0}C, respectively

The synthesizing of the mentioned ternary compound is confirmed by formation of a peak at the 278 cm $^{-1}$ shifted by 12 cm^{-1} from the LO phonon of the standard GaAs. This peak relates to the LO_1 phonon vibration of the synthesized crystalline GaAsP.

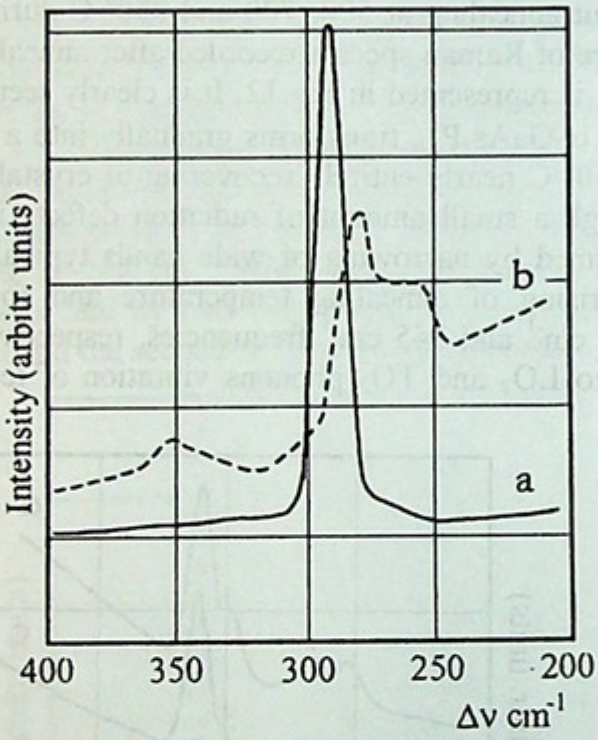

Fig.13. Raman spectra of the standard GaAs with (001) orientation (a) and α-GaAlAs (b) formed by aluminum hot implantation

Fig.13 shows Raman-spectrum of (001) oriented GaAs before implantation and after hot implantation of aluminum. According to the selection rule only the peak at 290 cm^{-1} corresponding to the LO phonon is observed in the Raman-spectrum of (001) oriented surface of GaAs. While after aluminum implantation as it is seen from the picture the sharp peak corresponding to the LO phonon disappears and a wide spectral band is formed which reflects the vibration of Ga-As bond; simultaneously near 360 cm^{-1} a wide band of low intensity is formed which reflects the Al-As bond vibration. The two experimental facts indicate that amorphous α-Ga_xAl_{1-x} is formed at the hot implantation too. Besides the Raman-spectra show that a low-intensity

sharp peak is formed at 284 cm^{-1}, which is shifted from the LO phonons of the crystalline GaAs by 6 cm^{-1}. Therefore the peak corresponds to the low amount of crystalline GaAlAs formed due to the hot implantation. Thus at the hot implantation of GaAs, α-GaAlAs is formed together with a few amount of crystalline phase.

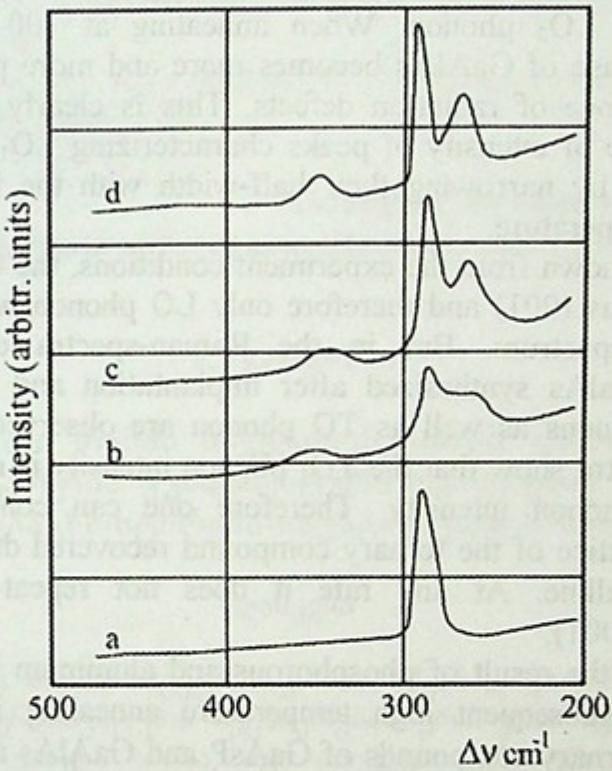

Fig.14. Raman spectra indicating the crystallization process of α-GaAlAs: (a) the spectrum of standard GaAs with (001) orientation; (b) the spectrum of α-GaAlAs synthesized by hot aluminum implantation; (c,d) the spectra of crystals received after quenching at 500, 700°C, respectively

In this case just as in the case of phosphorous implantation for crystal lattice recovering we have used high-temperature annealing in vacuum at 500, 700 and 850°C. The Raman-spectra reflecting the received results are presented in Fig.14. It is seen that at 500°C annealing characteristic wide band of α-$Ga_xAl_{1-x}As$ is sharply splitting into two narrow peaks with frequencies 281 cm^{-1} and 263 cm^{-1} respectively. These frequencies are shifted by 6 cm^{-1} and 5 cm^{-1} from

the characteristic frequencies of LO and TO phonons of standard GaAs, they characterize the vibration of GaAs sublattice of crystalline GaAlAs and belong to the LO_1 and TO_1 phonons, respectively. In the same time a new peak formation occurs at 360 cm^{-1} which we ascribe to the AlAs sublattice vibration in the crystalline GaAlAs that is expressed by LO_2 phonon. When annealing at 700 and 850^0 the crystalline phase of GaAlAs becomes more and more perfect because of disappearance of radiation defects. This is clearly reflected by a sharp increase of intensity of peaks characterizing LO_1, TO_1 and LO_2 phonons and by narrowing their half-width with the increase. of the annealing temperature.

As it is known from the experiment conditions, the GaAs substrate orientation was (001) and therefore only LO phonon was observed in the Raman-spectrum. But in the Raman-spectra of the ternary compound GaIAs synthesized after implantation and annealing LO_1 and LO_2 phonons as well as TO phonon are observed. At the same time the spectra show that the TO_1 phonon intensity is much more less than LO_1 phonon intensity. Therefore one can conclude that the crystalline lattice of the ternary compound recovered due to annealing is polycrystalline. At any rate it does not repeat the substrate orientation (001).

Thus, in the result of phosphorous and aluminum implantation of GaAs with subsequent high temperature annealing in the vacuum crystalline ternary compounds of GaAsP and GaAlAs are synthesized. We have stated, that the perfect crystalline phases of the mentioned compounds are got as a result of subsequent thermal treatment regardless of the fact at what temperature the ion implantation occurrs, at room or high temperature.

Thus, it is clear from this work how multiform and interesting is the utiliziation laser Raman spectroscopy in semiconductor science of materials and microelectronics dealing with study of fundamental properties as well as analysis.

REFERENCES

1. N. D. Strahm, A. L. McWhorter. Proceedings of the International Conference on Light Scattering Spectra of Solids, Ed, George B. Wright, New York, 1969, 455.

2. L. F. Chang, S. S. Mitra. Adv. Phys., **20,** 1971, 359..
3. A. Ebina, M.Iamamoto, T, Takahashi. Phys. Rev., **B6,** 1972, 3786.
4. S.V. Gotoshia, L.K. Vodopianov, V.S. Vavilov, V.S. Spitsin. Materiali II Vsesoiuznoi konferentsii po spektroskopii RS, Moscow 1978, 103.
5. I.I. Novak, V.V. Baptizmanski, N.S. Smirnova, A.V.Suvorov, FTT, **20,** 1978, 2134.
6. S. Gotoshia. L. Gotoshia, Bulletin Of the Georgian Academy of Sciences, **150,** 1999, 234.

Georgian Academy of Sciences
Institute of Inorganic Chemistry and Electrochemistry

ს. გოთოშია

ლაზერული რამან სპექტროსკოპიის გამოყენება ნასევარგამტარების ფუნდამენტური თვისებების შესწავლისა და დიაგნოსტირება-იდენტიფიკაციის მიზნით

დასკვნა

ლაზერული რამან-სპექტროსკოპია ამჟამად წარმოადგენს თანამედროვე ფუნდამენტური მეცნიერების ერთ-ერთ აქტუალურ მიმართულებას. გარდა ამისა, იგი ითვლება ერთ-ერთ უპირველეს დიაგნოსტიკურ-ანალიზურ მეთოდადაც. ჩვენს საუკუნეში თითქმის არ არსებობს მოწინავე, ფინანსურად შეძლებული სამეცნიერო ცენტრები და უნივერსიტეტები. რომლებიც კვლევათა და ანალიზის სხვადასხვა სფეროში არ იყენებდნენ ამ მეთოდს. 1928 წელს აღმოჩენილი ამ ფიზიკური მეთოდისათვის ინდოელ მეცნიერს რამანს 1930 წელს მიენიჭა ნობელის პრემია.

ამ მეთოდის ფართო მასშტაბით გამოყენება ძირითადად შეზრუდულია იმის გამო, რომ თანამედროვე რამან-სისტემები (რამან-სპექტრომეტრი, შესაბამისი ლაზერები და საჭირო აქსესუარები) მსოფლიო ბაზარზე საკმაოდ ძვირია. ალბათ, გასაგებია თუ რა სიძნელეებთანაა დაკავშირებული ამ მიმართულების განვითარება საქართველოში მისი სამეცნიერო ცენტრების უკიდურესი სიღარიბის გამო.

ამ შრომის ავტორმა აღნიშნული პრობლემა გადალახა თვითნაკეთი ლაბორატორიული ტიპის ლაზერული რამან-სისტემების კონსტრუირებით, რომლებიც თავიანთი პარამეტრებით არაფრით არ ჩამოუვარდება საშუალო დონის უცხოური ფირმების მიერ წარმოებულ ლაზერულ რამან-სისტემებს. ეს სისტემები, რომლებიც ამ შრომის ავტორმა შექმნა, პირველია საქართველოში და სწორედ ერთ-ერთი მათგანია დეტალურად აღწერილი წარმოდგენილ ნაშრომში.

ლაზერული რამან-სპექტროსკოპიის მეთოდით შევისწავლეთ A3B5 ჯგუფის შერეული ნახევარგამტარების GaAsP და A2B6 ჯგუფის ნახევარგამტარების $ZnSexTe1_{-x}$ მოდური სტრუქტურა. $ZnSexTe1_{-x}$ სისტემის რეზონანსული აღგზნების პირობებში შესწავლამ საშუალება მოგვცა დაგვეფიქსირებინა ამ სისტემის როგორც პირველი რიგის LO და TO ფონონები, ასევე ჯერადი 2LO ფონონი. აღმოჩნდა, რომ თუ ეს სისტემა მიეკუთვნება ერთმოდიანი ქცევის კრისტალებს, მეორე სისტემა, GaAsP ტიპური წარმომადგენელია ორმოდიანი ქცევის კრისტალებისა.

ლაზერული რამან-სპექტროსკოპია გამოვიყენეთ იონური იმპლანტაციით მოდიფიცირებული ნახევარგამტარების ზედაპირების შესწავლისა და მონიტორინგის მიზნით. კერძოდ, GaAs-ის ზედაპირის ფოსფორისა და ალუმინის იონებით იმპლანტაციის შედეგად მივიღეთ სამმაგი შერეული ნახევარგამტარები GaAsP და GaAlAs შესაბამისად. ამ ნაერთების იმპლანტაციურ სინთეზს ვაწარმოებდით როგორც ოთახის ტემპერატურაზე, ასევე ცხელი იმპლანტაციის პირობებში. GaAs-ის კრისტალური სტრუქტურის დარღვევისა და შემდგომ ინერტულ არეში მაღალტემპერატურული გამოწვის შედეგად კრისტალური სტრუქტურის აღდგენის დინამიკის მონიტორინგს ვატარებდით ლაზერული რამან-სპექტროსკოპიის მეთოდით. დავადგინეთ, რომ აღდგენილი სტრუქტურა შეესაბამებოდა სამმაგ ნახევარგამტარებს GaAsP და GaAlAs, ამავე შრომაში შესწავლილი სამმაგი შერეული ნახევარგამტარის GaAsP (რომელიც სინთეზირებული იყო ჩვეულებრივი თხევადფაზური ეპიტაქსიით) მოდური სტრუქტურის მრუდები გამოვიყენეთ კალიბრაციულ მრუდებად და მათი საშუალებით შევაფასეთ იონური იპლანტაციით სინთეზირებული სამმაგი ნახევარგამტარების კონცენტრაციები.

CONTENTS

შინაარსი

გამომცემლობის რედაქტორი ნ. მუზაშვილი
ტექრედაქტორი თ. ფირცხელანი
კორექტორი ნ. ჩახაია

ხელმოწერილია დასაბეჭდად 23.12.04
საბეჭდი ქაღალდი 60×84
პირ. ნაბეჭდი თაბახი 16,75
სააღრ.-საგამომც. თაბახი 12,51
შეკვეთა №10 ტირაჟი 150

ფასი სახელშეკრულებო

თბილისის უნივერსიტეტის გამომცემლობა,
0128, თბილისი, ი. ჭავჭავაძის გამზ., 14.

გამომცემლობა „მერიდიანი“,
თბილისი, აკ. წერეთლის გამზ., 112.